Investigation of a transgenic model of Alzheimer's Disease, the TASTPM mouse, using magnetic resonance spectroscopy and matrix assisted laser desorption imaging

A thesis submitted to The University of Manchester for the degree

of

Doctor of Philosophy (PhD)

In the Faculty of Medical and Human Sciences

2010

Duncan Matthew Forster

Division of Imaging Science and Biomedical Engineering

CONTENTS

Word Count - 48400

List of Figures

Fig.17 *Comparison of spectra from 18 month wild type (top) and TASTPM mice showing differences in succinate signal (1) at 2.41ppm, also showing the glutamate C4 pseudo triplet (2) and a GABA triplet (3)*
Fig.18 *Comparison of spectra from 18 month wild type (top) and TASTPM mice showing differences in MI signal (1) at 4.06ppm, also showing the creatine peak at 3.93ppm (2) and lactate quartet at 4.12ppm (3)*
Fig.19 *Comparison of spectra from 12 month wild type (top) and TASTPM mice showing differences in choline signal (1) at 3.20ppm, also showing the phosphocholine peak at 3.23ppm (2), the glycerophosphocholine peak at 3.24ppm (3) and the creatine peak at 3.03ppm (4). These spectra have been offset in frequency for clarity*
Fig.20 *Example of integration of spectrum, integrated peaks, functional groups represented from left to right: $C=CCH_2C=C$, CH_2CO and $CH_2C=C$*
Fig.21 *Peak assignments for lipid integrals. 1 – C18/19 cholesterol methyls, 2 – triglyceride terminal methyls, 3 – CH_3, 4 – $(CH_2)_n$(used as reference peak), 5 - CH_2CH_2CO, 6 - $CH_2C=C$, 7 - CH_2CO, 8 – $CH=CH-CH_2-CH=CH$, 9 - $CH_2NH_3^+$, 10 - $N^+(CH_3)_3$, 11 - CH_2OR, 12 - $(CH_3)_3$, 13 - $CH_2OPO_2^-$, 14 - CH_2OCOR, 15 - CH_2OCOR, 16 - $CH=CH$, 17 – chloroform (undeuterated)*
Fig.22 *$CH=CH-CH_2-CH=C$ levels in TASTPM and wild type mice, error bars represent S.E.M.*
Fig.23 *CH_2OR levels in TASTPM and wild type mice, error bars represent S.E.M.*
Fig.24 *Example images showing voxel placement. Left image shows coronal slice, right image shows axial slice*
Fig.25 *Image from RARE T1/T2 sequence showing areas from which T1 and T2 values were obtained. 1 – thalamus, 2 – hippocampus, 3 - cortex*
Fig.26 *Example spectrum from a 13 month old TASTPM mouse with peak assignments. 1 – NAA, 2 – Glx, 3 – Creatine, 4 – Choline containing compouns, 5 – Taurine, 6 - NAA aspartyl protons, 7 – MI, 8 – amino acid alpha protons, 9 – glycine coresonates with MI at 3.55ppm. Example has 3Hz line broadening*
Fig.27 *Example spectrum from a 13 month old wild type mouse with peak assignments. 1 – NAA, 2 – Glx, 3 – Creatine, 4 – Choline containing compouns, 5 – Taurine, 6 - NAA aspartyl protons, 7 – MI, 8 – amino acid alpha protons, 9 – glycine coresonates with MI at 3.55ppm. Example has 3Hz line broadening*
Fig.28 *Example of the fit obtained using QUEST to quantify a spectrum from a 17 month TASTPM mouse*
Fig.29 *Example of the fit obtained using QUEST to quantify a spectrum from a 19 month wild type mouse*
Fig.30 *Average coefficients of variation for the different age groups in TASTPM mice*
Fig.31 *Average coefficients of variation for the different age groups in wild type mice*
Fig.32 *Creatine ratios to selected metabolites for all age groups, values are given ± S.E.M.*
Fig.33 *Glutamate ratios to selected metabolites for all age groups, values are given ± S.E.M.*

Fig.51 *MALDI Imaging results from frozen brain sections from TASTPM mice. Trypsin concentrations on sections **1** - 500ng/µl, **2** - 50ng/µl, **3** - 500pg/µl, **4** - 5ng/µl. Scaling bars indicate intensity of signal, from low intensity (blue) to high intensity (white). Magnification x 5*

Fig.52 *MALDI Imaging results from dewaxed formalin-fixed TASTPM brain sections, 1 hour trypsin digest. Treatment of sections **1** - 1mg/ml Aβ 1-40 + trypsin (40ng/µl), **2** - 200µg/ml Aβ 1-40 + trypsin (40ng/µl), **3** – 40µg/ml Aβ 1-40 + trypsin (40ng/µl), **4** – trypsin (40ng/µl) zonly. Scaling bars indicate intensity of signal, from low intensity (blue) to high intensity (white). Magnification x 5*

Fig.53 *MALDI Imaging results from dewaxed formalin-fixed TASTPM brain sections, 24 hour trypsin digest. Treatment of sections **1** - 1mg/ml Aβ 1-40 + trypsin (40ng/µl), **2** - 200µg/ml Aβ 1-40 + trypsin (40ng/µl), **3** – 40µg/ml Aβ 1-40 + trypsin (40ng/µl), **4** – trypsin (40ng/µl) only. Scaling bars indicate intensity of signal, from low intensity (blue) to high intensity (white). Magnification x 5*

Fig.54 *MALDI Images showing distribution of unknown ion m/z 4811 in TASTPM brain sections containing thalamic hypointensity regions. ImagePrep (top), manual spray (bottom). Scaling bars indicate intensity of signal, from low intensity (blue) to high intensity (white). Magnification x 5*

Fig.55 *Mass spectra from THI regions showing intensity of signal for unknown peptide 4811. ImagePrep (top), manual spray (bottom).*

Fig.56 *Overall spectra from ImagePrep (top) and manual spray (bottom) comparison*

Fig.57 *MALDI Images of 12 month old TASTPM brain sections showing an optical image with the THIs depicted as white spots, and the distribution of the 4811 ion (coloured spots) and its localisation to the THI regions. Another ion found localised to the THI regions, though apparently in much lesser concentration, m/z 7635 is also shown. Scaling bars indicate intensity of signal, from low intensity (blue) to high intensity (white). Magnification x 5*

Fig.58 *Zoom of relevant section of mass spectrum showing highest intensity of unknown ion 4811*

Fig.59 *MALDI Images of 18 month old TASTPM brain sections showing an optical image with the THIs depicted as white spots, also the distribution of the 4811 and 7635 ions and their localisation to the THI regions. Scaling bars indicate intensity of signal, from low intensity (blue) to high intensity (white). Magnification x 5*

Fig.60 *Zoom of relevant section of mass spectrum showing highest intensity of unknown ion 4811*

Fig.61 *Graph showing maximum peak intensities for detection of 4811 peptide in TASTPM and wild type mice*

Fig.62 *MALDI Images of 12 month old wild type brain sections showing an optical image with the small THIs depicted as white spots, also the distribution of the 4811 ion and its localisation to the THI regions. Scaling bars indicate intensity of signal, from low intensity (blue) to high intensity (white). Magnification x 5*

Fig.63 *Zoom of relevant section of mass spectrum showing highest intensity of unknown ion 4811*

Fig.64 *MALDI Images of 18 month old wild type brain sections showing an optical image with the small THIs depicted as white spots, also the distribution of the 4811 ion and its localisation to the THI regions. Scaling bars indicate intensity of signal, from low intensity (blue) to high intensity (white). Magnification x 5*

Fig.65 *Zoom of relevant section of mass spectrum showing highest intensity of unknown ion 4811*

Fig.66 *MALDI Images of 12 month old TASTPM (bottom 3) and wild type (top 3) brain sections showing an optical image with the THIs (where present) depicted as white spots, also the distribution of the 4811 and 7635 ions and their localisation to the THI regions. Scaling bars indicate intensity of signal, from low intensity (blue) to high intensity (white). Magnification x 5*

Fig.67 *MALDI Images of 18 month old TASTPM (bottom 3) and wild type (top 3) brain sections showing an optical image with the THIs (where present) depicted as white spots, also the distribution of the 4811 ion and its localisation to the THI regions. Also shown is a visualisation of amyloid plaques detected by the presence of Aβ 1-40 in the TASTPM sections. Scaling bars indicate intensity of signal, from low intensity (blue) to high intensity (white). Magnification x 5*

List of Tables

Abbreviations

^{1}H MRS – proton magnetic resonance spectroscopy
Aβ – Amyloid beta peptide
Aβ 1-40 – Amyloid beta peptide, 40 amino acid parent peptide
Ach – acetylcholine
AD – Alzheimer's disease
ADAS-Cog – Alzheimer's Disease Assessment Scale – Cognitive Subscale
ADAM – a disintegrin and metalloprotese
alpha-cyano – α-cyano-4-hydroxycinnamic acid
ApoE4 – apolipoprotein E4
APP – amyloid precursor protein
BACE – β-site APP-cleaving enzyme
BBB – blood-brain barrier
CID – collision-induced dissociation
CHESS – chemical shift selective excitation
Cho – choline-containing compounds
CO – cytochrome oxidase
CoV – coefficient of variation
Cr – creatine
DCl – deuterated hydrochloric acid
EDE – endothelin-converting enzyme
FAD – familial Alzheimer's disease
FID – Free induction decay
FTD – fronto-temporal dementia
GABA – γ-aminobutyric acid
GFAP – glial fibrillary acidic protein
Glx – glutamate and glutamine
GPC – glycerophosphocholine
GSK3 – glycogen synthase kinase 3
HLSVD – Hankel-Lanczos singular value decomposition
IDE – insulin-degrading enzyme
LCM – laser capture microscopy
LC-MS – liquid chromatography – mass spectrometry
LDL – low density lipoprotein
LOAD – late-onset Alzheimer's disease
LRP-1 – low density lipoprotein receptor-related protein-1
LTL – lateral temporal lobe
MALDI MS – Matrix-assisted laser desorption ionisation mass spectrometry
MCI – Mild cognitive impairment
MI – myo-inositol
MMSE – mini-mental state exam
MRI – magnetic resonance imaging
MRS – magnetic resonance spectroscopy
MS – mass spectrometry
M_{xy} – net magnetisation in the xy plane
M_z – net magnetisation in the z plane

m/z – apparent molecular weight determined by MALDI mass spectrometry
NAA – N-acetyl aspartate
NaOD – deuterated sodium hydroxide
NBV – normalised brain volume
NEP – neprilysin
NFT – neurofibrillary tangles
NMDA – N-methyl-D-aspartate
NMR – nuclear magnetic resonance
NSAID – Non-steroidal anti inflammatory drugs
PET – positron emission tomography
ppm – parts per million
PRESS – point-resolved spectroscopy
PS1 – presenilin 1
PS2 – presenilin 2
QUEST – quantitation based on quantum estimation
RF – radiofrequency
ROS – reactive oxygen species
sinapinic acid – 3,5-dimethoxy-4-hydroxycinnamic acid
SNR – signal to noise ratio
SORL 1 – sortilin-related receptor
TASTPM – Transgenic mouse model of AD carrying human mutant APP and PS1 genes
TE – echo time
TFA – trifluoroacetic acid
THI – thalamic hypointensity
TOF – time of flight
TR – repetition time
TSP – trimethylsilylproprionate
VD – vascular dementia
WBNAA – whole brain NAA
WBV – whole brain volume

Abstract
The University of Manchester
Duncan Matthew Forster
Doctor of Philosophy (PhD)
Investigation of a transgenic model of Alzheimer's Disease, the TASTPM mouse, using magnetic resonance spectroscopy and matrix assisted laser desorption imaging
2010

There is currently no definitive biomarker for Alzheimer's Disease (AD), confirmation of diagnosis is only possible post-mortem. Magnetic resonance spectroscopy (MRS) has potential in aiding diagnosis, an MRS scan can be performed during an MRI scan, only adding around 10 minutes to scan time. Use of data from the two scans may allow more accurate diagnosis of AD. This thesis investigates a transgenic mouse model of AD, the TASTPM mouse using *in vitro* and *in vivo* MRS as well as matrix assisted laser desorption ionisation mass spectrometry imaging (MALDI MS Imaging). The first aim of the study was to search for a biomarker of AD that may allow better diagnosis or further our understanding of the pathology of the disease. The second aim was to evaluate the TASTPM mouse as a model of AD for use in preclinical testing of amyloid lowering agents. The third aim was to investigate a thalamic pathology in the TASTPM mice using MALDI MS Imaging. Metabolically, we found differences between the brains of TASTPM mice and their wild type base strain in both *in vitro* and *in vivo* scans. These differences may be exploited in the preclinical testing of novel amyloid lowering therapies. We also found similarities with human AD and other mouse models, lower N-acetylaspartate, lower glutamate and higher *myo*-inositol are all observed in human AD, as well as the TASTPM mice *in vivo*. We also found further evidence of impaired neuronal energy metabolism in TASTPM mice, such as lower succinate. Cerebral hypometabolism is a symptom of human AD. The TASTPM mouse seems to be a fairly good approximation of the human disease, sharing several traits. In our investigation of the thalamic pathology, we discovered a peptide which was strongly localised to the regions of the pathology and isolated it, but were unable to identify it, the work in this area will continue.

Declaration

I hereby declare that no portion of the work referred to in this thesis has been submitted in support of an application for another degree or qualification of this or any other university or other institute of learning.

Acknowledgements

Firstly I would like to thank my supervisor, Professor Steve Williams for giving me the opportunity to better myself in this way. His help and guidance during the last four years have been invaluable to me, along with his patience when I was initially struggling with one or two concepts! His ability to explain complex concepts in a way I could understand has helped immeasurably, thank you Steve.

Secondly I would like to thank my lab manager, Karen Davies for her patience and tireless assistance with my work. She has helped make the lab feel like a home away from home, I always looked forward to chewing the fat on Monday about the weekend football results, always nice to meet a Man Utd fan with perspective!

I would also like to thank some of the good people at GlaxoSmithKline, especially Dr Mike James and Dr Peter Marshall for their help and expertise with the industrial part of my project. Mike made me feel welcome from the start and Pete took over when Mike left, giving me all the support I needed and generally cultivating a friendly atmosphere.

I would also like to thank Dr Danielle Graveron-Demilly for allowing me to go to Lyon to write up this thesis and Federico Di Cesare for making my time in Lyon a very positive experience.

I would also like to thank Dave Da Costa, because otherwise I'll never hear the end of it!

Lastly I would like to thank the people I have shared the lab with, Dr Inna Linnik, Dr Tolga Turgut and Dr Darragh Downey for putting up with me over the years!

Chapter 1. Introduction

1.1. Aims of Thesis

Alzheimer's disease (AD) is a progressive, irreversible neurodegenerative disease associated with β-amyloid (Aβ) neuritic plaques, neurofibrillary tangles and neuronal and synaptic degeneration (Selkoe, 2001; Blennow et al., 2006). There is a need to develop a biomarker for AD, to aid in drug development, treatment monitoring, diagnosis and patient monitoring. An ideal biomarker must be easy to measure, non-invasive, related to disease progression and specific for AD. There is currently no definitive biomarker for AD. Magnetic resonance imaging (MRI) observation of AD patients has found atrophy, increasing in severity with disease progression (Frisoni et al., 2010), however brain atrophy is not specific to AD. A proton magnetic resonance spectroscopy (^{1}H MRS) scan could be performed during the same session as an MRI scan, only adding approximately 10 mins to scan time. If a ^{1}H MRS biomarker could be found, a more robust diagnosis could potentially be made. Disease progression could also be monitored more closely. A metabolic biomarker for AD could also be invaluable in treatment monitoring. If the ^{1}H MRS spectrum from an AD patient could be normalized by application of a therapeutic agent, this could give an early, non-invasive indication of drug efficacy. Our ^{1}H MRS work with the transgenic mouse strain TASTPM will be carried out with this in mind, specifically to look for a robust biomarker of disease progression in the mice that could be exploited during the drug discovery process and possibly give us a better understanding of human AD.

Significant age dependent thalamic pathology has been observed in TASTPM mice (Evans et al., 2007), any insights gained into this phenomenon may be invaluable. The work will complement longitudinal MRI investigations carried out by GlaxoSmithKline in collaboration with University of London, as well as other pathophysiological studies of TASTPM mice. Hopefully this will give further insight into the relevance of amyloid deposition in the pathology of AD. The TASTPM mouse has potential as a transgenic model of AD to be used in

drug discovery. Again, we aim to identify a specific, robust disease-related neurometabolic difference between the TASTPM mouse and its wild type base strain, which may allow the model to be validated for testing disease modifying therapies. It could then become a valuable tool for evaluating new therapies. This could potentially speed up drug discovery in AD research, allowing new drugs on to the market faster and improving the standard of care and quality of life for AD patients (and their carers) everywhere.

The thalamic pathology observed in the TASTPM (and other) mice is worthy of further investigation, due to the presence of observable neurodegeneration, and thus a similarity with human AD. Therefore matrix assisted laser desorption ionisation (MALDI) Imaging experiments will be initiated on TASTPM brains, to look for protein and/or peptide moieties specific to the thalamic lesions and attempt to identify any differences observed. Any proteomic information gleaned from this process may provide valuable insight into the underlying pathology behind the lesion.

This chapter contains an introduction to Alzheimer's disease with a description of the biochemical and pathological which accompany the disease, followed by a review of current and potential therapies. The magnetic resonance methods used in the thesis are introduced with a description of the underlying physical principles followed by a review of applications in Alzheimer's disease. The use of mouse models to study the disease is reviewed and the strain used in this work –the TASTPM mouse – is described. Finally there is a description of an *in vitro* imaging technique (MALDI) which is used to investigate neuropathology in the TASTPM model in this thesis.

1.2.1. Alzheimer's Disease

AD is the leading cause of dementia among the elderly. It is characterised by progressive cognitive decline and memory loss, eventually leading to death. Death normally occurs within 7-10 years of the clinical diagnosis of symptoms.

As medical science advances, the population in general are living to a more advanced age. Consequently, the problem of AD (and other forms of dementia) is likely to become much more significant as time goes on, and will ultimately lead to huge cost implications for society. Currently, there is no definitive biomarker for AD and therefore, examination of biopsy or autopsy tissue is currently the only way to ensure a correct diagnosis of AD.

The aim of this introduction is to give an overview of the current understanding of AD, current therapies and potential novel drug targets, followed by an overview of the use of cerebral ^{1}H MRS, its potential uses in the study of AD and the reasons for carrying out the proposed project.

1.2.2. Amyloid β Peptide and the Amyloid Cascade Hypothesis

There are many hypotheses about the causes underlying the pathogenesis of AD. The amyloid cascade hypothesis is currently the most widely accepted of these hypotheses. Central to this hypothesis is amyloid precursor protein (APP). which is a membrane bound protein residing on chromosome 21 (Kang et al., 1987). APP is widely expressed in tissues throughout the body. Metabolism of APP is carried out by the secretase enzymes, α, β and γ. The amyloidogenic pathway is mediated by β and γ-secretases, whereas the non-amyloidogenic pathway involves α and γ-secretases (Blennow et al., 2006). α-Secretase activity is mediated by a disintegrin and metalloprotese (ADAM), the main form is ADAM-10 (Lammich et al., 1999). The enzyme responsible for β-secretase activity is β-site APP cleaving enzyme (BACE) (Vassar et al., 1999). γ-Secretase activity is mediated by a membrane bound protein complex comprised of presenilin, nicastrin, Aph-1 and Pen-2, in which presenilin is thought to form the active site (Kimberly et al., 2003; Chyung et al., 2005). Firstly cleavage by α or β-secretase occurs, releasing the majority of the extracellular domain of APP in soluble form as α-APP or β-APP (Newman et al., 2006). The remainder of the protein is then cleaved by γ-secretase. In the non-amyloidogenic pathway p3 peptide is released. In the amyloidogenic

pathway amyloid β (Aβ) protein is released (Fig.1). The most common forms of the protein are 40 and 42 amino acid residues in length ($A\beta_{40}$ and $A\beta_{42}$), of the two $A\beta_{42}$ appears to accumulate more rapidly into amyloid plaques (Jarrett et al., 1993). The $A\beta_{42}$ protein is widely thought to be central to the pathology of AD, mainly as familial mutations leading to early onset AD almost invariably increase prevalence of $A\beta_{42}$ in the CNS (see below for more detail and references).

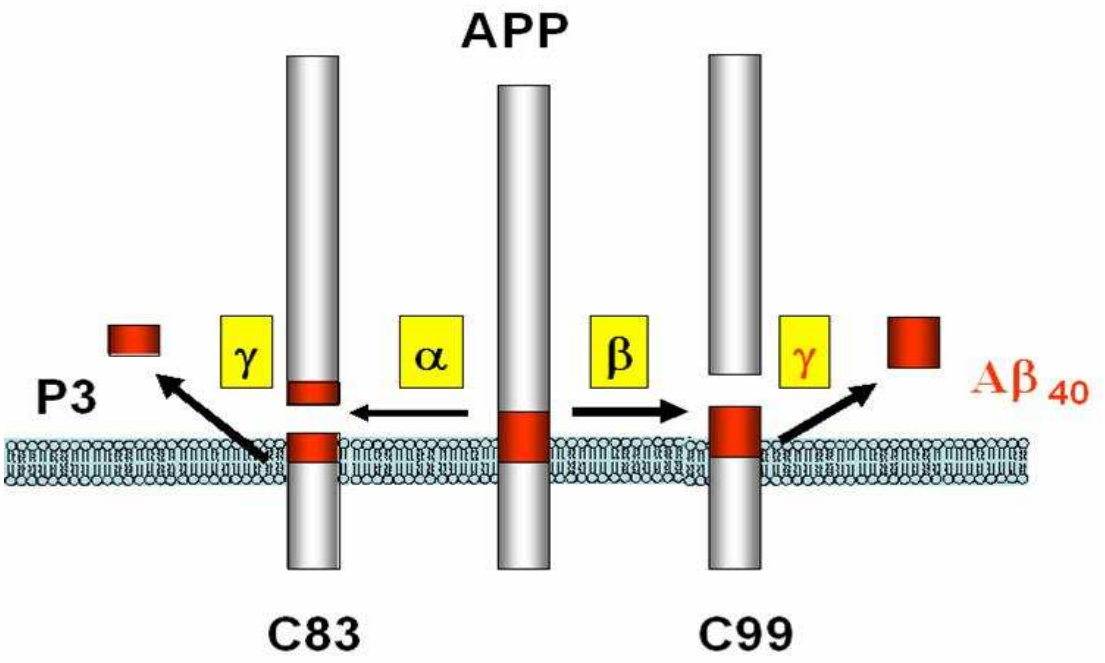

Fig.1 *Diagram representing the cleavage of APP, first by either α- or β-secretase, release of the resulting extracellular domain, then further cleavage by γ-secretase, releasing either P3 or Aβ, depending upon whether initial cleavage was by α- or β-secretase (diagram sourced from http://www1.tu-darmstadt.de/fb/ch/Fachgebiete/OC/AKSchmidt/Research.htm)*

The amyloid cascade hypothesis states that an imbalance in the production and degredation/clearance of Aβ in the brain is the initiating event in a cascade ultimately leading to neuronal degeneration, dementia and death (Hardy and Selkoe, 2002). This hypothesis is supported by the fact that causal mutations in familial AD are located on the genes for APP (Goate et al., 1991) and the

presenilin genes (part of the γ-secretase complex)(Esler et al., 2000). When Aβ builds up it is thought to undergo a conformational change to high β-sheet content, leading to aggregation initially as soluble oligomers, then larger, insoluble fibrils and plaques (Blennow et al., 2006). The Aβ plaques were initially thought to be the cause of the neurotoxicity, but a study (Dahlgren et al., 2002) suggested that soluble Aβ oligomers might be to blame, since oligomeric species were shown to inhibit neuronal viability to a much greater degree than fibrillar species. Other studies have suggested that oligomers interfere with hippocampal long term potentiation (memory) and synaptic plasticity (Walsh and Selkoe, 2004).

Aβ clearance is mediated by both enzymatic degradation and a balance between efflux and influx to and from the CNS (Blennow et al., 2006). Some of the enzymes responsible for Aβ degradation are neprilysin (NEP), insulin-degrading enzyme (IDE), endothelin-converting enzyme (ECE 1 and 2) and plasmin (Ledesma et al., 2000; Eckman and Eckman, 2005). Plasmin levels have been found to be reduced in the brains of AD patients, especially in the hippocampus (Ledesma et al., 2000). NEP levels have been found to decrease with age in both normal subjects and AD patients (Hellstrom-Lindahl et al., 2006). Membrane bound (but not cytosolic) IDE concentration and activity were found to be significantly reduced in the hippocampus of mild (or moderate) cognitive impairment (MCI) patients at high risk of developing AD (Zhao et al., 2007). The IDE levels continued to decrease during conversion from MCI to AD, the occipital cortex was also examined but no such effect was seen (Zhao et al., 2007). ECE 2 gene expression was found to be significantly downregulated in AD patients (Weeraratna et al., 2007). Clearance of Aβ from the brain by efflux at the blood-brain barrier (BBB) appears to be mediated largely by low density lipoprotein (LDL) receptor-related protein-1 (LRP-1) (Shibata et al., 2000).

1.2.3 The Role of Tau

Tau is a protein found in neurons which binds to microtubules and assists in microtubule assembly and stability (Iqbal et al., 2005). In AD tau becomes hyperphosphorylated (Grundke-Iqbal et al., 1986; Kopke et al., 1993), leading to sequestration of normal tau and other microtubule-associated proteins by the hyperphosphorylated tau (Alonso et al., 1994; Alonso et al., 1997). As a consequence microtubules disassemble (Iqbal et al., 1986; Alonso et al., 1997) and axonal transport is disrupted, normal neuronal and synaptic function are thus compromised, leading to loss of synapses and death of neurons (Iqbal et al., 2005). Loss of functional tau may also increase expression of tau protein by way of a compensatory mechanism. Hyperphosphorylated tau also polymerises by association with normal tau, resulting in the formation of paired helical fragments and neurofibrillary tangles (NFT) (Fig.2) (Alonso et al., 1996). These formations are not directly toxic to the neuron but as the disease progresses they may grow to a size whereupon the affected cell is physically choked to death (Iqbal et al., 2005). The end product of both these processes is dementia.

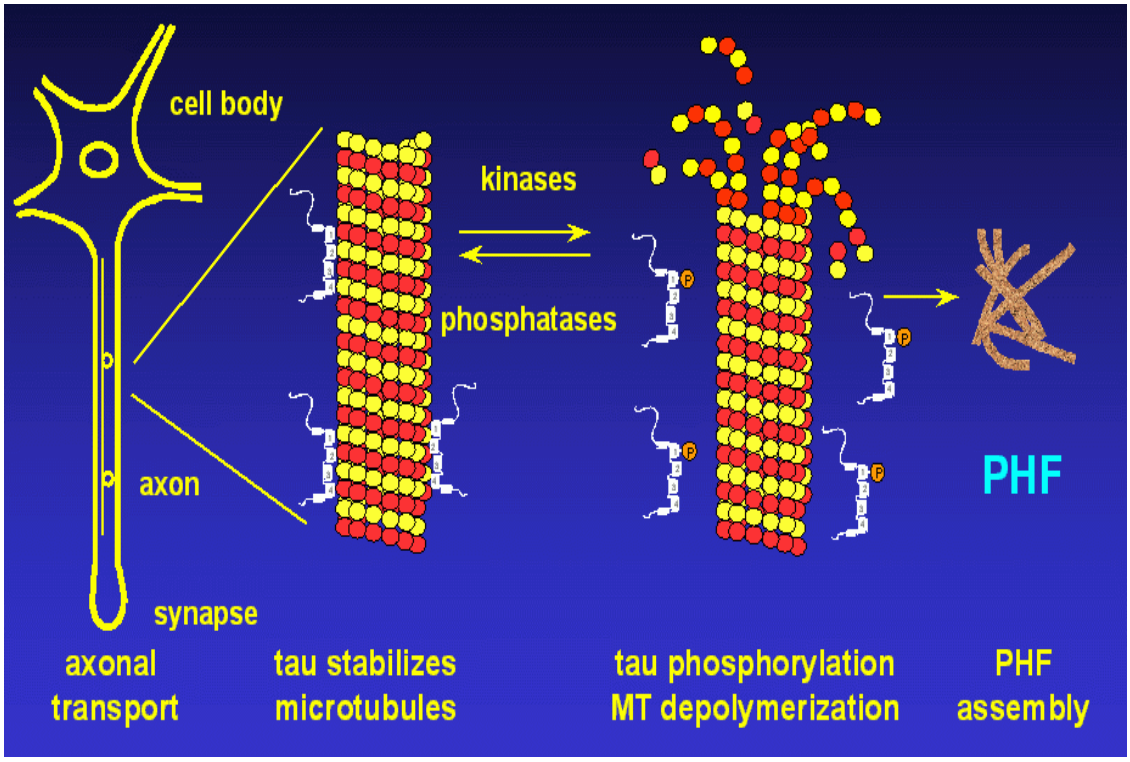

Fig.2 *Diagram illustrating the hyperphosphorylation of tau protein, microtubule depolymerisation and aggregation of phosphorylated tau into paired helical fragments, the precursor to neurofibrillary tangles (Diagram sourced from http://www.mpasmb-hamburg.mpg.de/mandelkow2/taubilder.htm)*

In AD tau levels in the brain are around eightfold higher than in age-matched controls, with the increase being in the form of the abnormally phosphorylated protein (Khatoon et al., 1992). Whether the hyperphosphorylation of tau and subsequent tangle formation are one of the causes of AD or a consequence of the disease is not currently known.

An *in vitro* study using cultured neuronal cells transfected with a mutant tau fragment showed that abnormal tau aggregation was cytotoxic, a toxicity that could be prevented by inhibition of aggregation or by proteolysis (Wang et al., 2007).

A possible link between tau hyperphosphorylation and reduced glucose metabolism has been postulated. O-glycosylation, a process regulated by glucose metabolism, has been shown to correlate negatively with tau hyperphosphorylation. A four-fold decrease in O-glycosylation was observed when compared to non-hyperphosphorylated tau (Liu et al., 2009).

1.2.4. Symptoms and Disease Progression

AD is a slowly progressive disease characterised by increasing impairment of episodic memory with instrumental signs including aphasia, apraxia and agnosia (Blennow et al., 2006). Other general cognitive symptoms also manifest themselves, such as impaired judgement, orientation and decision making (Blennow et al., 2006). The initial neurodegenerative changes occur in the medial temporal lobe, with the entorhinal cortex and hippocampus among the first areas affected (Braak et al., 1999).

The underlying pathology and neurodegeneration behind AD has been estimated to begin between 20 and 30 years before symptoms allow clinical diagnosis (Blennow et al., 2006). In this phase, it is thought that plaque and tangle load increase to a certain threshold level where symptoms start to appear. The initial observable phase of AD is often described as mild cognitive impairment (MCI).

MCI is a term used to describe subclinical complaints of memory impairment in the elderly. There is thought to be a high risk of patients with MCI progressing to AD (Ritchie and Touchon, 2000). MCI can be seen as a precursor for dementia, however some people with MCI may remain stable for many years or even return to normal over time (Gauthier et al., 2006). Amnestic (memory impaired) MCI is thought to be a potential intermediate stage between normal aging and AD (Gauthier et al., 2006). Pathologically speaking it may in many cases just be the early stages of AD where symptoms start to become

detectable. A study found that approximately 12% of patients with MCI progressed to clinical dementia each year (Petersen, 2004).

There is considerable research currently ongoing into potential neural compensatory mechanisms which allow pre-clinical AD patients to remain cognitively normal while much of the neurodegeneration leading to AD takes place (Smith et al., 2007). Potential compensatory mechanisms include upregulation of neurotransmitters such as Ach, use of redundant memory systems and recruitment of other neural networks as ones in current use are damaged (Smith et al., 2007). In a recent study using positron emission tomography (PET) 5-HT_{1A} receptor binding was found to be significantly higher in patients with MCI compared with controls, whereas AD patients had significantly lower receptor binding (Truchot et al., 2007). This provides further evidence of potential compensatory mechanisms prior to the onset of clinically detectable AD.

1.2.5. Familial Predisposition

Familial AD (FAD) is caused by mutations in the genes coding for APP and presenilin 1 and 2 (PS1 and PS2). The known APP mutations (chromosome 21) are all located either immediately before the β-secretase cleavage site, after the α-secretase cleavage site or on the C-terminal side of the γ-secretase site (Selkoe, 2001). In APP mutations have increased overall Aβ production or increased $Aβ_{42}$:$Aβ_{40}$ ratio as a consequence (Selkoe, 1994). Onset of symptoms with the APP mutation can be as early as age 50 (Selkoe, 2001). The PS mutations – PS1 (chromosome 14q) and PS2 (chromosome 1) seem to selectively increase the ratio of $Aβ_{42}$:$Aβ_{40}$ (Scheuner et al., 1996), while some seem to reduce $Aβ_{40}$ production along with other PS-dependent actions (Shen and Kelleher, 2007). New evidence is emerging that most PS mutations result in an overall loss of function and a reduction in overall Aβ production (loss of function), but somehow favour release of $Aβ_{42}$ over $Aβ_{40}$ (gain of function)

(Wolfe, 2007). In PS mutation FAD symptoms may manifest as early as in the patients 30's (Selkoe, 2001).

The apolipoprotein E4 (ApoE4) ε4 allele is a genetic risk factor for late onset AD (LOAD) (Strittmatter et al., 1993). The frequency of the ε4 allele has been found to be significantly greater in LOAD patients compared with age matched controls (Strittmatter et al., 1993). ApoE4 has been shown to be a ligand for LRP-1 and may affect Aβ clearance across the BBB, according to a study done in transgenic mice (Shibata et al., 2000).

Another genetic candidate linked with increased risk of LOAD is sortilin-related receptor, also known as LR11 or SORLA (SORL1). Six single nucleotide polymorphisms in SORL1 have been linked with LOAD in well-defined samples from different populations (Katzov, 2007). In younger patients with AD, plaque and tangle load are strongly correlated with dementia severity, whereas with increasing age this correlation disappears (Prohovnik et al., 2006), which could be of clinical significance.

1.2.6. Brain Hypometabolism

Cognitive decline and AD have been linked with metabolic deficiencies in the brain. PET studies have found reduced cerebral glucose metabolism in AD patients, in areas central to AD, such as the posterior cingulate (Herholz et al., 2007). A multicentre PET study found that monitoring regional cerebral glucose metabolism allowed differentiation between AD and other dementias, as well as MCI (Mosconi et al., 2008). A PET study showed that ApoE4 ε4 allele carriers had reduced glucose metabolism in the lateral temporal lobe (LTL) and the superior temporal gyrus compared with non-carriers (de Leon et al., 2001). Glucose metabolism in the LTL was also found to decline faster over time in ε4 carriers than in non-carriers (de Leon et al., 2001). Anomalies in glucose metabolism have been observed in patients with MCI, with reductions in areas such as the hippocampus and middle temporal cortex (Drzezga et al., 2003).

The severity of these reductions has been found to correlate with progression from MCI to AD over the course of a year (Drzezga et al., 2003).

The posterior cingulate cortex in AD patients has been shown to have reduced cytochrome oxidase (CO) activity (Valla et al., 2001), CO is a mitochondrial enzyme essential for aerobic energy metabolism. This reduction appears to be progressive, greater in women and linked to disease duration (Valla et al., 2001).

Two mitochondrial markers, CO-1 and lipoic acid were increased in the neuronal cytoplasm of AD patients compared with controls, lipoic acid was also found in autophagic vacuoles and lipofuscin of neurons in AD patients (Moreira et al., 2007). These data suggest that mitochondria undergo increased autophagic degredation in AD sufferers. This may be due to either increased turnover or mitochondrial numbers within neurons may be reduced, leading to reduced respiration and cellular dysfunction.

A recent study has shown expression of subunits of the mitochondrial electron transport chain to be significantly lower in the posterior cingulate cortex, hippocampus and entorhinal cortex in AD patients, compared with controls (Liang et al., 2008). These regions are some of the first affected by AD, these differences may be a causal factor in the reduced glucose metabolism seen in AD.

Reproducible defects have been observed in mitochondria from the brains of AD sufferers, with deficiencies in two enzymes of the tricarboxylic acid cycle – pyruvate dehydrogenase and α-ketoglutarate dehydrogenase (Gibson et al., 1998) and in CO (Cottrell et al., 2001). Mitochondrial function is reliant upon structural integrity and there is considerable evidence of mitochondrial damage in AD (Zhu et al., 2004; Moreira et al., 2007). Damaged mitochondria are less able to utilise oxygen in the respiratory process and thus produce more reactive

oxygen species (ROS), leading to oxidative damage (see next section) (Zhu et al., 2007).

There is thus strong evidence linking defects in energy metabolism with symptoms of AD.

Glucose hypometabolism has also been observed in a transgenic mouse model of AD, which has been shown to be independent of amyloid deposition and to correlate with memory impairment (Dodart et al., 1999).

Reduced cerebral energy usage may well be a factor in causing the symptoms of AD, it may also contribute to, or be a symptom of both neuronal dysfunction and eventual neuronal death. This is discussed later in the context of the findings presented in this thesis.

1.2.7. Oxidative Stress and Inflammation

Oxidative stress has long been thought to play a role in AD neurodegeneration. This is borne out by evidence of elevated protein and lipid oxidation in AD brains (Hensley et al., 1995; Lovell et al., 1995), along with evidence of decreased antioxidant activity in AD patients (Gsell et al., 1995). There are a number of postulated sources of the observed oxidative stress, some of these are iron (and other redox-active metals) redox cycling, mitochondrial dysfunction and inflammation. Iron has been found to accumulate in both amyloid plaques and NFTs, this iron was found to be redox-active (Smith et al., 1997). $A\beta_{42}$ has been demonstrated to increase the solubility of iron, allowing it to remain in its redox-active form longer and potentially generate more reactive oxygen species (ROS) via the Fenton reaction (Khan et al., 2006). Aβ produces hydrogen peroxide *in vitro* via a mechanism which reduces iron or copper (Huang et al., 1999). *In vitro* testing has also shown that the neuronal toxicity of Aβ can be attenuated by pre-treatment with an iron chelator and restored by incubation with excess free iron (Rottkamp et al., 2001). NFTs have also been

shown to produce hydrogen peroxide when in the presence of redox metals (iron or copper) (Sayre et al., 2000).

It is postulated that Aβ deposition actually occurs due to oxidative stress and this has a protective effect against neuronal damage. In both *in vitro* and *in vivo* testing oxidative stress has been shown to increase production of APP and Aβ by neuronal cells (Yan et al., 1995). Oxidative damage has been demonstrated to be greatest in the early stages of AD, increases in Aβ deposition correlating with decreases in oxidative damage (Nunomura et al., 2001). Histologically a negative correlation has been seen between amyloid burden and oxidation levels, it has been postulated that the high levels of zinc within amyloid plaques interact with Aβ to give robust antioxidant properties (Cuajungco et al., 2000).

Inflammation in AD is mediated by both microglia (cerebral macrophages) and astrocytes (Akiyama et al., 2000a). The activated forms of both cell types have been found to be associated with Aβ (Eikelenboom and Veerhuis, 1996; Mrak et al., 1996). *In vitro* Aβ enhances ROS production and release from microglia (Klegeris and McGeer, 1997). Microglia are involved in the removal and breakdown of Aβ in the brain, however it appears that soluble Aβ is taken up and does not cause activation of the microglia, whereas the aggregated form is phagocytosed and does result in activation (Akiyama et al., 2000a).

1.2.8. The Presenilin Hypothesis

An alternative to the amyloid cascade hypothesis has recently been put forward. It proposes that a loss of PS function in AD may be the primary event triggering neurodegeneration, for detail on supporting evidence see (Shen and Kelleher, 2007). This hypothesis is potentially important as if it is true then some of the new potentially disease modifying therapies in development may actually worsen the disease rather than having a beneficial effect.

1.2.9. Intraneuronal Aβ as a possible risk factor

Recent studies have suggested an important role of intracellular Aβ in the pathogenesis of AD. In an APP/PS1 model (APP/PS1KI), correlation between intraneuronal Aβ accumulation and loss of hippocampal CA1 neurons has been demonstrated (Casas et al., 2004). No such correlation was seen with extracellular Aβ deposits. Reduced short- and long-term synaptic plasticity and poor performance in working memory tests were also observed in these mice (Bayer et al., 2008). Co-incidence of intracellular Aβ build up and behavioural changes has also been shown elsewhere (Knobloch et al., 2007). In various AD mouse models, behavioural changes have been seen to occur prior to significant Aβ plaque deposition (Bayer and Wirths, 2008). These findings indicate the potential for an important role of intracellular Aβ in the pathogenesis of AD, possibly as the disease-triggering event.

1.2.10. Other Potential Risk Factors

Old age and genetic predisposition are the only well researched risk factors for AD, however a number of physiological and psychosocial factors may also play a role. Vascular and dietary factors such as hypertension, obesity, diabetes mellitus, heart disease, cerebrovascular disease, hyperlipidaemia, heavy alcohol consumption, cigarette smoking and high saturated fat intake are all thought to increase risk of AD (Qiu et al., 2007). In contrast, light to moderate alcohol consumption has been associated with a reduction in the risk of dementia (Stampfer et al., 2005). High fish intake has also been linked to reduced risk of dementia, which is thought to be related to increased plasma levels of docosahexaenoic acid (Schaefer et al., 2006).

There is evidence to suggest a poor education increases the risk of developing AD (Karp et al., 2004). Longitudinal lifestyle studies have linked social disengagement with increased AD risk, whereas subjects with greater engagement in mentally and/or physically stimulating activities seemed to be at reduced risk of the disease (Fratiglioni et al., 2004).

Elevated occupational magnetic field exposure has been associated with an increased risk of AD (Davanipour et al., 2007). In this study AD (and suspected AD) patients and controls were classified by occupation as having low, medium or high magnetic field exposure. High exposure was classified as average exposure over 10 milligauss (or regular intermittent exposure over 100 milligauss). Medium exposure was classified as average exposure between 2 and 10 milligauss (or regular intermittent exposure over 10 milligauss). The study found that subjects with medium or high exposure were 2.1 times as likely to have AD, in the high exposure group alone, subjects were found to be 2.9 times as likely to have AD (Davanipour et al., 2007).

1.3. Current Therapies

1.3.1. Acetylcholinesterase inhibitors

Due to consistent findings of damage to cholinergic neurons in the basal forebrains (associated with memory and attention) of AD sufferers, enhancing cholinergic transmission is thought to have potential in alleviating symptoms (Terry and Buccafusco, 2003). The acetylcholinesterase inhibitors (rivastigmine, donepezil and galantamine) are the drugs of choice for this purpose, increasing acetylcholine (Ach) levels by preventing its metabolism in the synaptic cleft (Blennow et al., 2006). Modest improvements in cognitive symptoms have been observed with these drugs. A mean treatment effect of 2.7 points on the Alzheimer's Disease Assessment Scale – Cognitive Subscale (ADAS-Cog) and 1.4 points on the mini-mental state exam (MMSE) (Birks, 2006). Due to their mechanism of action these treatments only temporarily alleviate some of the symptoms of AD however, and are not thought to be disease modifying.

1.3.2 Memantine

The major excitatory neurotransmitter in the brain is glutamate. Glutamate and the N-methyl-D-aspartate (NMDA) receptor are important in the processes of learning and memory. In AD increased glutamatergic activity can result in sustained low-level NMDA receptor activation, potentially impairing neuronal function and leading to excitotoxic effects (Areosa et al., 2005). Memantine is a non-competitive antagonist at the NMDA receptor which is thought to reduce overstimulation of the receptor caused by abnormally high glutamate levels. The intent is to restore normal physiological function and reduce potential for excitotoxicity (Wilcock, 2003). Memantine has been shown to have beneficial effects in patients with moderate to severe AD (MMSE score <15), however there are currently no data to suggest that it will have beneficial effects in mild AD (Areosa et al., 2005). Although memantine may be neuroprotective, it is not specific for AD and the current trials are too short to assess potential disease modifying effects (Areosa et al., 2005).

1.4.1. Potential Novel Therapies

Due to a better understanding of AD pathology and of the underlying processes, a number of potential new therapeutic targets have been developed many of which could potentially have disease-modifying activity. In addition, based on epidemiological studies, several drugs/chemicals already in use are being investigated for any possible clinical benefit. Some of the novel therapies being investigated are described below.

1.4.2. Potential Aβ Therapies

1.4.3. Targeting Aβ Production

All three secretases are potential targets for pharmacological intervention. β-Secretase knockout mice have been proved to be viable and have reduced Aβ production (Cai et al., 2001; Luo et al., 2001). Thus if an inhibitor for β-site APP-cleaving enzyme (BACE), the enzyme responsible for β-secretase

cleavage of APP (Hussain et al., 1999; Vassar et al., 1999; Yan et al., 1999) can be synthesised it could be of great benefit in lowering Aβ and slowing amyloid pathology in AD. So far it has proven to be a difficult pharmacological target, but it is likely that effective β-secretase inhibitors will be developed within a few years (Golde, 2006). Another problem is that β-secretase knockout mice while overtly normal, may have a harmful phenotype (Dominguez et al., 2005). Disruptions in hippocampal synaptic plasticity and in cognitive and emotional tests have been reported (Laird et al., 2005). Thus there could be problems with long term β-secretase inhibition and it remains to be seen whether any inhibitors which are produced are well tolerated.

Inhibitors targeting PS have been developed and have entered into phase I clinical trials (Siemers et al., 2005). There are potential problems with these compounds too, as γ-secretase doesn't just cleave APP, it is important in other areas such as the notch signalling pathway. Blocking γ-secretase could thus have toxic effects due to disruption of notch signalling (De Strooper et al., 1999). Non-steroidal anti inflammatory drugs (NSAIDs) have potential use in selectively modulating γ-secretase action, shifting cleavage away from the $A\beta_{42}$ form to shorter peptides (Weggen et al., 2001). A selective $A\beta_{42}$ lowering agent R-flurbiprofen is currently undergoing clinical trials (Black et al., 2006).

Whereas inhibitors of β and γ-secretases are sought, an inducer of α-secretase activity could also be of therapeutic benefit. Metalloprotease disintegrins have been shown to be responsible for α-secretase cleavage of APP, namely ADAM-10 and ADAM-17 (Buxbaum et al., 1998; Fahrenholz et al., 2000; Kojro and Fahrenholz, 2005). In an APP transgenic mouse model upregulation of α-secretase activity was found to decrease production of Aβ peptides and formation of plaques, as well as alleviating cognitive symptoms (Postina et al., 2004). ADAM-10 and ADAM-17 are involved in a number of signalling pathways and long term upregulation may not be without its side effects.

1.4.4. Targeting Aβ Aggregation

In its soluble, non-aggregated form Aβ is not thought to be toxic (Golde, 2006). Which particular species of Aβ is the main contributor to neurotoxicity is unknown, but it is quite possible that many different Aβ aggregates interact and contribute to overall neurotoxicity (Walsh and Selkoe, 2004). Nevertheless preventing Aβ aggregation (and lysing already aggregated formations) is likely to have disease modifying effects. A compound which seems to have a promising future is curcumin, a component of the curry spice turmeric. Curcumin has been shown to inhibit formation of Aβ oligomers and fibrils *in vitro* (Yang et al., 2005). *In vivo*, curcumin crosses the blood brain barrier, binds plaques and reduces amyloid load in a mouse model (Yang et al., 2005). On top of this curcumin has anti-inflammatory, cholesterol lowering, antioxidant and metal chelating properties, all of which have the potential to be protective against AD neuropathology (Ringman et al., 2005).

1.4.5. Enhancing Aβ Clearance

A number of enzymes are known to be involved in degradation of monomeric Aβ, including insulin degrading enzyme (IDE), neprilysin (NEP) and endothelin converting enzyme (ECE) (Eckman and Eckman, 2005). Transgenic overexpression of IDE and NEP has been shown to lower brain Aβ levels and reduce or prevent plaque formation in APP transgenic mice (Leissring et al., 2003). Due to their mechanism of action, upregulation of these proteases would likely be more useful in prevention of AD rather than treatment of the disease once it is established.

Increasing efflux of Aβ from the brain through the BBB to the circulation is another potential way of lowering brain amyloid burden. One transporter which has been studied and is involved in the transport of Aβ across the BBB is p-glycoprotein (Lam et al., 2001). There are known pharmacologic activators of this protein and these may have therapeutic benefit in prevention or treatment

of AD, but more research and proof of concept studies are needed (Golde, 2006).

1.4.6. Immunotherapy

A study using APP transgenic mice has revealed that immunisation against $A\beta_{42}$ attenuates Aβ plaque formation in young animals and reduced the extent and progression of AD like neuropathologies in older animals where plaque build up was already significant (Schenk et al., 1999). The first active immunisation trial in humans was stopped due to 6% presentation of patients with meningioencephalitis (Nicoll et al., 2003; Orgogozo et al., 2003). This was unexpected and whilst the precise mechanism is unknown, one hypothesis is that it was caused by an autoreactive T-cell response against Aβ (Nicoll et al., 2003). However a cohort of 30 patients who participated in the study were followed up for 1 year and it was found that those patients who produced antibodies against Aβ showed slower rates of decline in cognitive function and daily living activities compared to patients who produced no such antibodies (Hock et al., 2003). Tests used included MMSE, Disability Assessment for Dementia and the Visual Paired Associates Test of delayed recall. These results indicate that the presence of antibodies against Aβ can slow the progress of AD. An MRI study of cerebral volumes in the patients who produced antibodies and showed slower rates of decline in cognitive function compared to the placebo group gave unexpected results (Fox et al., 2005). The antibody responders had significantly greater overall brain volume decrease, along with greater ventricular enlargement and a nonsignificant greater hippocampal volume decrease (Fox et al., 2005). This indicates a dissociation between brain volume loss and cognitive function in the antibody responders in this study (Fox et al., 2005). Potential reasons for this include removal of deposited Aβ and associated cerebral fluid shifts however, further work is required to fully elucidate the reason. Due to these (and other) results work continues into both active and passive immunisation methods targeting Aβ. The

details of these are beyond the scope of this report, for a review see (Weiner and Frenkel, 2006).

A study *in vitro* found that opsonisation of Aβ with anti-Aβ antibodies enhances Aβ clearance but also increases release of toxic inflammatory mediators (Strohmeyer et al., 2005). This means care should be taken with immunotherapy as there may be a balance to be struck between Aβ clearance and release of toxic mediators causing side effects, as seen above.

1.4.7. Potential Tau Modifying Therapies

1.4.8. Tau Production

Mice expressing a repressible human tau variant were shown to develop progressive NFTs, neuronal loss and memory impairments. The neuronal loss and memory decline were stabilised by suppression of the transgenic tau, but NFTs continued to accumulate (Santacruz et al., 2005). These results suggest potential therapeutic benefit could be achieved by decreasing tau expression while also questioning the role of NFTs in related toxicity. Tau knockout mice survive and seem to have a relatively mild phenotype for a complete deficiency in what is thought to be an essential protein (Harada et al., 1994), thus tau could potentially be downregulated without serious side effects. New agents targeting tau production are predominantly in the conceptual stage (Golde, 2006).

1.4.9. Tau Phosphorylation

As tau phosphorylation is under the control of multiple kinases (Golde, 2006), inhibition of any one is unlikely to have a significant therapeutic impact. An agent which could inhibit multiple kinases may be of some benefit. In a study using a mixed kinase inhibitor treatment was found to reduce soluble aggregated hyperphosphorylated (64kDa) tau and delay or prevent typical motor impairments in JNPL3 tau transgenic mice (Le Corre et al., 2006).

Partially inhibiting multiple kinases may be advantageous in the inhibition of tau induced neurodegeneration. Preclinical study has been carried out with lithium and another inhibitor of glycogen synthase kinase 3 (GSK3) in tau transgenic mice. The study showed reduced levels of both phosphorylated tau and aggregated, insoluble tau. This reduction correlated with a reduction in the level of axonal degeneration (Noble et al., 2005). Although further studies are needed, it can be seen that there is potential in modulating tau phosphorylation for the treatment of AD.

1.4.10. Other Tau Targets

Other potential strategies to reduce tau related toxicity in AD include the inhibition of tau aggregation and tau chaperone upregulation. Both of these targets need further research before suitable inhibitors can be identified (Golde, 2006). One interesting compound is the microtubule binding agent paclitaxel, usually used as an anticancer agent. This compound was found to restore fast axonal transport and increase microtubule numbers in the spines of tau deficient mice while also having a beneficial effect on observed motor impairments (Zhang et al., 2005).

1.4.11. Alternative Strategies

The exact mechanism of neuronal death in AD is still unknown, both chronic inflammation and oxidative stress are thought to be contributing factors (Akiyama et al., 2000b). Thus a wide range of compounds which may influence these processes are under investigation for their potential efficacy in treating AD (Golde, 2006). Due to the potential role of redox active metals in AD pathology, the use of metal chelating therapy could be disease modifying and some promising results have already been reported (Crouch et al., 2007).

Summary

While our knowledge of the pathology of AD is expanding all the time, we still do not know the root cause of the neurodegeneration. In spite of this, there are now several inviting drug targets such as tau and Aβ. Up until now we have been relying on purely symptomatic treatments, the new targets present a strong possibility of disease-modifying therapies being on the market in the near future.

Disease-modifying treatments will be most effective if AD can be diagnosed as early as possible. The effects of the disease-modifying therapies will need to be monitored during treatment to assess efficacy. For these reasons we need a reliable biomarker of AD, preferably one that is non-invasive, ^{1}H MRS has the potential to provide this biomarker by monitoring differences in cerebral metabolite levels, for this reason ^{1}H MRS forms the basis of much of this thesis.

1.5. Nuclear Magnetic Resonance and MRS Theory

The following references were consulted in writing this piece (Gadian, 1995; de Graaf, 1998)

1.5.1. The Basis of NMR

Nuclear magnetic resonance takes advantage of a property of certain atomic nuclei known as spin. Examples of nuclei which possess spin are hydrogen (^{1}H), carbon-13 (^{13}C), and phosphorus (^{31}P). Hydrogen is the nuclei this thesis is concerned with so this will be the focus of this section. Hydrogen has a spin quantum number ½. In the absence of an applied magnetic field, the spinning hydrogen nuclei take up random orientations (Fig.3). When hydrogen nuclei are placed in a static magnetic field B_0, they take up one of two orientations with respect to the applied magnetic field, parallel or antiparallel (Fig.3).

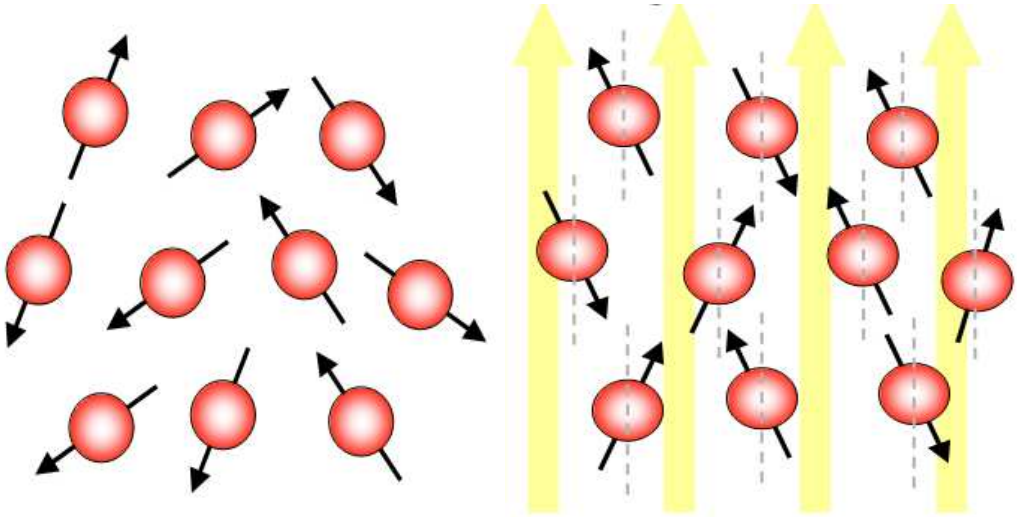

Fig.3 *The left hand side of the diagram shows protons in the absence of magnetic field, with spins in random directions. The right hand side of the diagram illustrates the behaviour of the spins in the presence of an applied magnetic field, oriented parallel or antiparallel to the field (Diagram sourced from http://physiology-physics.blogspot.com/2010/06/understanding-basic-principles-of.html)*

The two spin states are at different energy levels, the difference is proportional to the strength of B_0 and is given by the equation:

$$\Delta E = h\nu_0$$

Where *h* is the Planck constant and ν_0 is the resonant frequency, given by:

$$\nu_0 = (\gamma/2\pi)B_0$$

where B_0 is the magnitude of the applied magnetic field and γ is the gyromagnetic ratio of the nucleus (42.58MHz/T in the case of hydrogen)

The distribution of nuclei in the two spin states is given by the Boltzmann distribution:

$$n2/n1 = e(-\Delta E/kT)$$

where n1 is the number of nuclei at the lower energy level, n2 is the number of nuclei at the higher energy level, k is the Boltzmann constant and T is temperature in Kelvin. In practical situations, the difference between the two spin populations is very small, for example, around 1 part in 42000 for a 7T magnet.

The spinning protons precess around the axis of the applied field B_0, the frequency of precession is proportional to the field strength and is given by the equation:

$$\omega_0 = \gamma B_0$$

ω_0 is known as the Larmor frequency. The application of a radiofrequency (RF) pulse, B_1 at the Larmor frequency will cause the protons to absorb energy, inducing transitions between energy states. This causes the net magnetization to tilt away from the B_0 direction (z axis). The angle of the tilt θ is given by the equation:

$$\theta = \gamma B_1 t_p$$

Where t_p is is the time that the RF pulse is applied for. Prior to the RF pulse, the net magnetisation in the xy plane is zero, thus no signal is observed. After B_1 is turned off the net magnetisation has been tilted away from the z axis, toward the xy plane. This magnetisation then rotates around B_0 at frequency ω_0, inducing an electromotive force in the receiver coil. Following the RF pulse, signal decreases as magnetisation in the xy plane returns to zero with a time constant T2*. The signal generated by this process is known as a free induction decay or FID (Fig.4)

The FID is a time dependent signal, it can be converted by a mathematical manipulation known as Fourier transformation to a spectrum of frequency and amplitude (Fig.4).

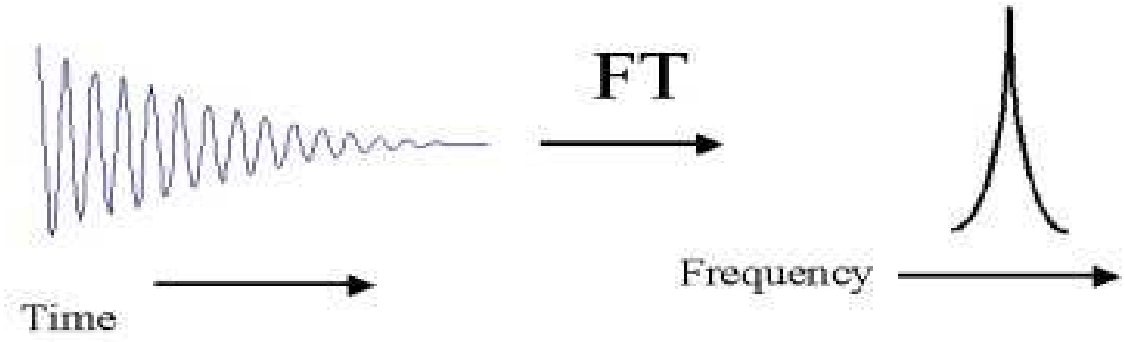

Fig.4 *An FID on the left, in the time domain, converted by Fourier transform to an amplitude signal in the frequency domain (image sourced from http://chemistry.umeche.maine.edu/CHY431/NMR/NMR-4.html)*

1.5.2. Magnetic Resonance Spectroscopy (MRS)

NMR signal is dependent on a number of physical and chemical effects, including chemical shift, spin-spin coupling and relaxation.

1.5.3. Chemical shift

The applied magnetic field B_0, causes the electrons around nuclei to generate their own magnetic field, opposing B_0. This effect is known as shielding. The magnetic field produced is proportional to B_0 and is also sensitive to the chemical environment surrounding the nuclei. Due to this, nuclei in different chemical environments produce signals with differing frequencies. The net magnetic field the protons experience is given by the equation:

$B_{eff} = B_0(1-\sigma)$

Where σ is the shielding constant and is dependent on the chemical environment of the nuclei. Shielding can arise from electrons surrounding the nucleus in question, but may also arise from electrons on different atoms in the same molecule. The separation of resonance frequencies from a reference frequency is called the chemical shift (δ). Chemical shift is usually measured relative to a reference compound and is expressed in the dimensionless units of parts per million (ppm). If the reference compound is either added to, or intrinsic to the sample it is called an internal reference, when it is unfeasible to

add a reference compound, an external reference may be used. Internal references are preferable as the reference compound will be contained in the same material as the sample. This is more desirable as the local magnetic field experienced by a nucleus is altered by shielding produced by the surrounding medium, this is known as bulk shielding. In the case of an internal reference, bulk shielding effects should be equal, and so not responsible for any differences observed. In the case of an external reference, differences in bulk shielding must be taken into account.

1.5.4. Spin-spin Coupling

Neighbouring nuclear spins often interact with each other, causing resonances produced by the nuclei to split into two or more components. This phenomenon is known as spin-spin coupling, the separation of the components is given by the coupling constant, J in Hz. Spin-spin coupling can be an interaction between nuclei which share a direct bond, or nuclei which are separated by more than one bond. J tends to decrease as the number of separating bonds increases.

Spin-spin coupling can produce first- and second-order spectra. In first order spectra the frequency difference between the nuclear resonances involved is much greater than the magnitude of J. In nuclei on an equivalent group (i.e. the protons of a CH_3 group) the spin-spin coupling produces no observable splitting. In basic terms for first-order spectra, if a nucleus is coupled to one nucleus of spin ½ the resulting resonance will be a doublet with relative intensities 1:1. If the nucleus is adjacent to 2 spin ½ nuclei, the resonance will split into a triplet, with relative intensities 1:2:1 and if the nucleus is adjacent to 3 spin ½ nuclei the resonance will split into a quartet with relative intensities of 1:3:3:1. In second order spectra the frequency difference and J are not far apart, in this case splitting can be more complicated and difficult to interpret. More information on spin-spin coupling can be found in (Gadian, 1995).

1.5.5. Relaxation

At equilibrium, net magnetisation along the z (B_0) axis is equal to M_0, at the same time the net magnetisation in the xy plane M_{xy} is zero. After an excitatory RF pulse, some of the net magnetisation is shifted into the xy plane (Fig.5). Relaxation describes the processes by which magnetisation returns to its equilibrium state.

The return of magnetisation along the z axis (M_z) to its equilibrium value is known as spin-lattice relaxation. This process is characterised by the time constant T1, or the longitudinal relaxation time.

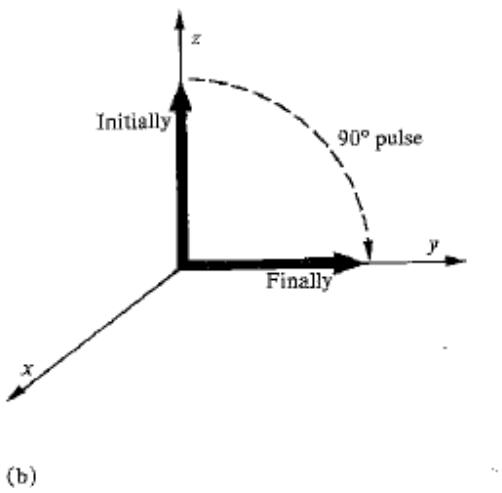

Fig.5 *Initial transfer of magnetisation from the M_z to the M_{xy} plane, magnetisation returns to the M_z direction, the time taken is dependent on the time constant T1 (diagram sourced from Gadian, 1995)*

The loss of magnetisation in the xy plane (M_{xy}) (in addition to the loss through T1 relaxation) is called spin-spin relaxation (Fig.6). This comes about by the gradual dephasing of M_{xy} caused by interactions between neighbouring nuclear spins and inhomogeneities in B_0. Spin-spin relaxation is characterised by the time constant T2, or transverse relaxation time.

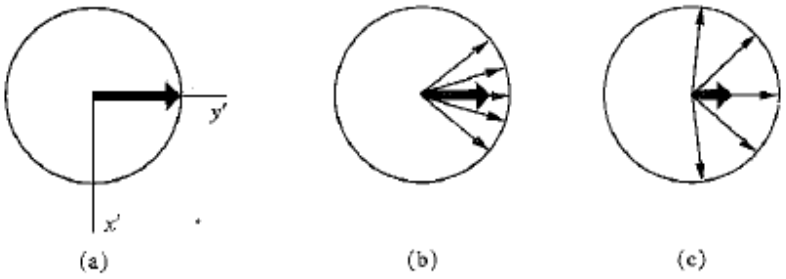

Fig.6 *a – As magnetisation is initially switched from M_z to M_{xy}, all the spins are in phase and the signal is strong. b and c – gradually the spins lose phase with each other as they precess at slightly different frequencies until net $M_{xy} = 0$*
(diagram sourced from (Gadian, 1995)

1.5.6. MRS Pulse Sequences

Spectroscopy pulse sequences consist of a combination of timed radiofrequency pulses and pulsed magnetic field gradients designed to produce a signal from a specific region of interest (or voxel), while editing out signal from the surrounding regions. Separate pulse sequences have been developed with the sole purpose of suppressing the signal from water, as water signal is ~10^5 times more abundant than the signal from metabolites. MRS experiments generally combine a spectroscopy sequence with a water suppression sequence to obtain the best possible spectrum.

1.5.7. PRESS

PRESS, or point-resolved spectroscopy (Bottomley, 1987) uses the following pulse sequence:

90^0 – *TE*1/2 – 180^0 – (*TE*1 + *TE*2)/2 – 180^0 – *TE*2/2 – Acquire

As can be seen in Fig 7, the three RF pulses are slice selective, along the x, y and z-axes respectively.

The 90^0 – 180^0 pulses generate an echo at *TE*1/2 from the 180^0 pulse from the spins inhabiting the column selected by the two slices, this echo is not collected. The collected echo is formed *TE*2/2 following the second 180^0 pulse, this echo corresponds to the voxel defined by the intersection of the three selected slices, in which spins have been excited by all three RF pulses.

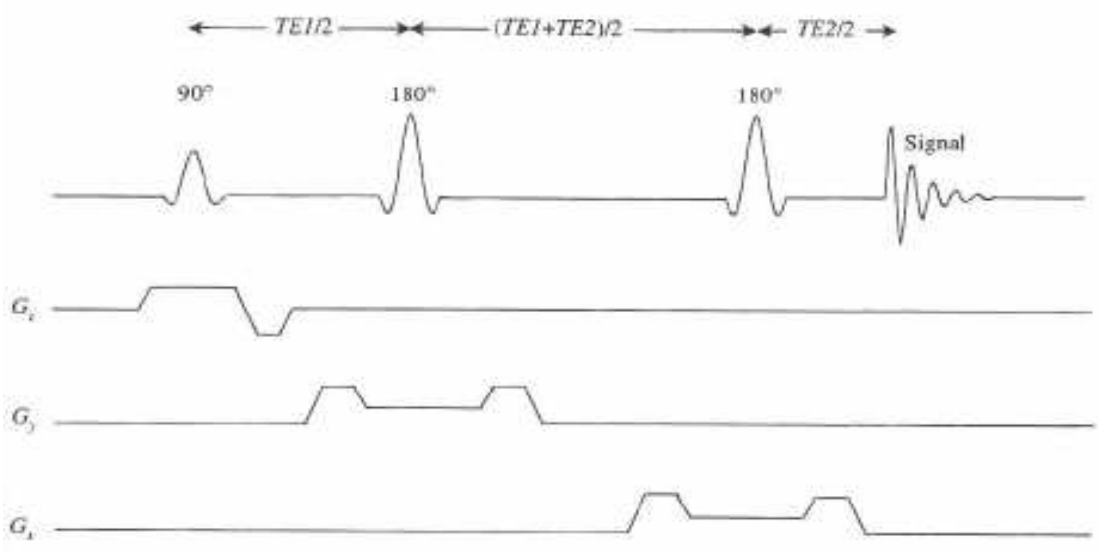

Fig.7 *PRESS pulse sequence (Bottomley, 1987) showing RF pulses, gradients in the three planes, G_x, G_y and G_z and echo generation. TE is the time between the original 90^0 pulse and the echo generated following the second 180^0 pulse.*
(diagram sourced from (Gadian, 1995)

Slice selection is achieved by use of gradients and RF pulses of specific frequencies. A gradient is applied, along the x-, y- or z-axis which alters B_0 depending upon the position along the axis. An RF pulse of a certain frequency or band of frequencies will then only excite protons which have resonance frequencies which coincide with the RF pulse. Protons in other slices will not be excited, as their resonance frequencies are different due to the presence of the gradient. Signal from spins in regions which only experience one or two RF pulses can be removed by spoiler gradients.

The PRESS sequence gives a relatively high signal detection and good SNR. One potential problem with the sequence is that TE is required to be quite long in order to accommodate the RF pulses and spoiler gradients, thus it is not optimal for detection of metabolites with short T2 values or complex coupling patterns as there is significant signal loss at longer TE. Modern magnet and gradient systems overcome these problems so that PRESS can be used at short echo times for detection of coupled spin systems.

1.5.8. Water Suppression

Metabolite concentrations in the brain are several orders of magnitude smaller than the concentration of water in the brain. Due to this, water signal will overwhelm the signal from metabolites of interest if nothing is done about it.
Water suppression is carried out in order to decrease the amplitude of the water peak in the spectrum, allowing easier visualisation of metabolite signals.
One method of water suppression is chemical shift selective excitation (CHESS), this involves excitation at the frequency of water, followed by a crusher gradient to dephase the resulting magnetization (Haase et al., 1985). This results in a system where there is a large reduction (>1000-fold) in water magnetisation, but the components which resonate at different frequencies are unaffected.

The CHESS sequence only gives good water suppression over a relatively narrow range of water T1 values and RF (B_1) values. Thus alternative sequences were developed using multiple suppression pulses with optimised flip angles and delays. The result is effective water suppression over a range of T1 and B_1 values. One of these methods is called volume localized, solvent attenuated, proton NMR VAPOR (Griffey and Flamig, 1990; Tkac et al., 1999), and it is our method of choice for water suppression.

1.5.9. Data processing method

Interpretation of an *in vivo* ^{1}H MRS spectrum must be done with care. Many factors must be taken into account in order to obtain accurate metabolic information.

Strong overlapping of metabolite peaks occurs, low SNR, broad background resonances originating from macromolecules and lipids with short T2 values, line broadening and peak overlap caused by magnetic field inhomogeneities and the residual water signal must all be taken into account during quantification. This precludes manual peak integration. Various semi- and fully automated methods have been developed, for a review see (Poullet et al., 2008).

There are two types of method involved in MRS quantification – interactive and noninteractive (Vanhamme et al., 1997). Noninteractive methods are computationally efficient and potentially fully automatic, however very little prior knowledge can be imposed on these models (Vanhamme et al., 1997). Interactive methods incorporate more user-involvement and allow inclusion of prior knowledge, but can be less computationally efficient (Vanhamme et al., 1997). Prior knowledge is the only way of increasing the accuracy of fitted model parameters for a given dataset (de Graaf, 1998). Prior knowledge can also reduce unknown model parameters, reducing calculation time (de Graaf, 1998).

For the *in vivo* part of this thesis we have chosen to use a time-domain method of quantification. This offers several advantages, the time-domain is the measurement domain in MR, consequentially missing initial and/or final data points do not greatly hamper quantification so such points may be omitted (Higinbotham and Marshall, 2001). Time-domain methods also allow automatic processing of water (de Beer et al., 1992) and background signals (Ratiney et al., 2005).

The method we used is known as QUEST (quantitation based on quantum estimation) (Ratiney et al., 2005). This is part of a software package known as jMRUI. This method is based upon extensive prior knowledge, in our case obtained by quantum mechanical simulation. The metabolite basis set will be created using a program called NMR SCOPE (Graveron-Demilly et al., 1993).

The quantification process involves initial zero-order phasing to correctly phase the water peak, followed by use of Hankel-Lanczos singular value decomposition (HLSVD) to remove the residual water peak, then (if necessary) first-order correction to phase the peaks of interest. Quantification can then be carried out using the pre-generated metabolite basis set to obtain metabolite levels based on peak amplitudes.

1.6.1. ^{1}H MRS in Alzheimer's Disease

There is increasing evidence suggesting that the symptoms of AD only manifest themselves in a clinically detectable way once the underlying pathology of the disease has progressed significantly (Golde, 2003). There is evidence from imaging studies that brain atrophy and neuronal dysfunction may precede the onset of symptoms by years or even decades (Fox et al., 2001). One study using an amyloid imaging agent recently showed significant amyloid deposition in cognitively normal subjects (Fagan et al., 2006).

The lack of a definitive biomarker is a problem for both clinical diagnosis of AD and also drug discovery in animal models. ^{1}H MRS is a non-invasive method and is sensitive to changes in metabolite concentrations *in vivo* of around 1mM (Brooks et al., 1999). Using ^{1}H MRS, differences in metabolite levels in both pathologic and healthy brain tissue can thus be assessed and potentially quantified *in vivo*. The non-invasive nature of ^{1}H MRS is a considerable advantage, along with the fact that it does not involve any ionising radiation, as with some other scanning techniques.

MRS metabolic studies were initially carried out using ^{31}P MRS as it is less complex than ^{1}H MRS. ^{1}H MRS has been used in cerebral studies as it allows non-invasive monitoring of several potentially important CNS metabolites. ^{1}H MRS is more technically complex than ^{31}P MRS as large signals from both water and fats need to be suppressed. In addition the chemical shift range of the various metabolites of interest is relatively narrow, leading to interpretive difficulties (Gadian, 1995). Advancements in solvent suppression techniques and spectral editing, as well as improvements in field homogeneity have allowed spectroscopy to be carried out even at clinical field strengths (1.5T). The fact that the brain generates very little signal from fats is also a great advantage of using ^{1}H MRS in the brain, as opposed to other tissues where the fat signal presents a problem (Gadian, 1995).

The high sensitivity of the ^{1}H nucleus when compared with other nuclei is another advantage of ^{1}H MRS as it potentially allows detection of low concentrations of metabolites. The signal from metabolites at low concentrations can however, be masked by signals from metabolites at higher concentrations. Due to this, the higher sensitivity of the ^{1}H nucleus is exploited by trading signal-to-noise ratio for spatial resolution. Smaller volume elements can therefore be used and adequate signal-to-noise ratios obtained (Gadian, 1995).

A parameter known as echo time (TE) is the delay between radiofrequency excitation and detection of the signal (echo). As different metabolites have different T_2 relaxation times, altering the TE alters the appearance of the spectrum. Short echo times (20-40ms) give spectra containing contributions from a large set of different metabolites, thus they contain more information. This information can be difficult to obtain however, as the spectra are often difficult to interpret. Longer echo times (120-300ms) give spectra with a flatter baseline and only containing contributions from creatine, choline, N-

acetylaspartate, *myo*-inositol, lactate and lipids. Information is generally easier to obtain from these spectra.

1.6.2. Major Detectable Metabolites

Several major metabolites can be detected by *in vivo* ^{1}H MRS, the main metabolites seen are: N-acetylaspartate (NAA), choline (Cho) compounds, myo-inositol (MI), creatine and phosphocreatine (Cr) and glutamate/glutamine (Glx) (Gadian, 1995). A brief overview of each of these metabolites is given below. Following that their potential significance with respect to AD will be discussed.

NAA (chemical shift [δ] = 2.02 and 2.6 ppm) is present in the brain at concentrations of about 10mM, thus it is the second most prevalent free amino acid derivative in the central nervous system after glutamate (Demougeot et al., 2004). NAA concentrations in all other body tissues are minute. Studies using lesioning (Koller et al., 1984), immunohistochemical analysis (Moffett et al., 1991) and NMR/HPLC (Urenjak et al., 1992) have shown that NAA is mainly confined to neurones in the adult brain. Loss of NAA has been attributed to either loss of neurones or neuronal damage. Various studies have found that NAA concentration in the brain correlates with either overall neuronal loss or temporary neuronal dysfunction (Demougeot et al., 2004). A strong correlation has been shown between estimates of NAA concentration *in vitro* and data derived from MRS estimates in rats (Burri et al., 1990). The exact function of NAA in the brain is still being investigated. One report has linked NAA with myelination processes in adult humans (Bhakoo and Pearce, 2000).

Significant correlation between left occipitoparietal white matter NAA/Cr and intellectual performance has been seen in young healthy volunteers (Jung et al., 1999a). A stronger association has also been made between NAA concentration and performance in neuropsychological timed tests (Jung et al., 1999b).

Choline compounds (δ = 3.2ppm). Choline itself is a precursor in the synthesis of both cell membrane phosphatidylcholine and the neurotransmitter acetylcholine (Ach), in the case of Ach it is rate-limiting. The MRS peak for choline measures mobile forms of choline, including choline, Ach, glycerophosphorylcholine (GPC) and phosphocholine. Due to its immobility, phosphatidylcholine is invisible to MRS (Valenzuela and Sachdev, 2001). Choline concentration has been shown to increase with age (Moats et al., 1994). Elevated choline levels may mark cellular proliferation (neoplasia) or myelin breakdown (Lazeyras et al., 1998).

Myo-inositol (δ = 3.6 and 4.0 ppm) is a sugar alcohol with a structure similar to that of glucose, its function is uncertain (Valenzuela and Sachdev, 2001). Of the visible peak for MI, approximately 70% comes from free MI and 15% from MI phosphate (Ross, 1991). Potential functions of MI include osmoregulation, acting as an intracellular messenger and acting as a detoxification agent in the brain/liver (Ross, 1991). Elevated MI could represent gliosis, cytoskeletal abnormalities or membrane dysfunction (Lazeyras et al., 1998).

Creatine and phosphocreatine (δ = 3.0 and 3.9 ppm). Cellular ATP/ADP ratios are buffered by the phosphocreatine-creatine equilibrium reaction, which acts as a reserve for high energy phosphates (Miller, 1991). As a consequence the combined Cr signal reflects the state of energy use and storage within a system. The Cr signal can be used as a reference metabolite in quantification of other neurochemicals (Valenzuela and Sachdev, 2001). Cr has been shown not to vary significantly between different people or between normal subjects and AD patients (Moats et al., 1994). White matter disease causes decreased Cr levels (Oppenheimer et al., 1995), whereas Cr levels increase in the grey matter with age (Chang et al., 1996).

Glutamate/glutamine (δ = 2.1-2.4 ppm). Glutamate is the most abundant neural amino acid, with approximate concentrations in the brain of 12mM. The function of glutamate is as an excitatory neurotransmitter. Glutamine is thought to be important to normal cerebral function, acting as a detoxifying agent and regulating the excitatory activity of its precursor (glutamate) (Ross, 1991). The chemical structures of glutamate and glutamine give a highly coupled and complex MRS spectrum with low individual peak intensities (Ross, 1991).

1.6.3. Metabolic Differences in AD Detected by ^{1}H MRS

The use of ^{1}H MRS in studying AD has produced some interesting results. ^{1}H MRS of perchloric acid exctracts from post-mortem AD brains showed increases in MI and aspartate, among others. It also showed decreases in NAA and phosphoethanolamine (Klunk et al., 1996). While *in vivo* techniques cannot detect the same number of metabolites as spectra from extracts, potentially useful information has been gathered.

The most striking feature of the various *in vivo* ^{1}H MRS studies in AD subjects has been a decrease in NAA in AD sufferers. Reduction in NAA has been seen in a number of different neurological disorders (Jessen et al., 2000). Due to this efforts must be made to focus on areas of the brain known to be the site of neuronal injury in AD, for instance the medial temporal lobe, which is the earliest site of neuronal loss (Braak and Braak, 1991). Exact brain locations studied have varied, but reduced NAA has been found in parieto-occipital regions (Huang et al., 2001; Waldman and Rai, 2003), hippocampus (Dixon et al., 2002; Ackl et al., 2005), medial temporal lobes (Chantal et al., 2004), posterior cingulate (Kantarci et al., 2000), occipital cortex (Shonk et al., 1995), anterior temporal lobes (Frederick et al., 2004) and parietal lobes (Schuff et al., 2002) among others. NAA decrease has been shown in over 20 papers as correlating with AD pathology. This reproducibility is encouraging, as is the magnitude of the observed decrease of around 10-15% in various studies observing different brain regions and using different protocols. NAA depletion

seems to be greater in grey matter than white matter. Furthermore, in AD atrophy of various regions of the brain is known to occur. In a study which corrected for hippocampal atrophy, reduced NAA levels were still observed in AD subjects compared with controls (Schuff et al., 1997).

The other major finding of the continued research has been elevation of MI levels in AD subjects. Increases have been seen in various brain regions, including the parietal lobe grey matter (Ackl et al., 2005; Zhu et al., 2006), occipital lobes (Dixon et al., 2002), medial temporal lobes (Kantarci et al., 2000), occipital cortex (Shonk et al., 1995) and parieto-occipital region (Waldman and Rai, 2003). However, a study using spectral acquisition and data evaluation techniques similar to Shonk et al. 1995 found reduced NAA but no change in MI (Heun et al., 1997). Elevated MI in AD could represent reactive gliosis following neurodegeneration (Lazeyras et al., 1998). Also, severe deficits in phosphoinositide signalling are thought to occur in AD (Pacheco and Jope, 1996). Abnormal activation of phospholipase C and associated metabolic dysfunctions could also play a role in the increased MI signal seen in AD (Kanfer et al., 1998).
Study of changes in MI may be confounded by the presence of other diseases which also affect the brain, such as hepatic encephalopathy (Kreis et al., 1992), diabetes mellitus (Kreis and Ross, 1992) and metachromatic leucodystrophy (Kruse et al., 1993).

Choline levels do not appear to be affected by AD. Creatine signal (which also seems fairly constant in AD subjects compared with controls), along with water is often used to quantify levels of MI and NAA seen in spectra.

One study in the cingulate region points to reduced ratios of glutamate and glutamine (Glx) to creatine in AD subjects (Antuono et al., 2001). Decreased glutamate could lead to less efficient neuronal signalling, which could be a factor contributing to the symptoms seen in AD. Glx ratios in AD sufferers were

also seen to be correlated with MMSE scores (Antuono et al., 2001), this could aid in the diagnosis of the disease, this will be discussed in more detail later. A potential flaw with this study however; is that the data were obtained from clinically diagnosed probable AD sufferers, and not histologically verified cases. Also the number of patients included in the analysis was small; therefore further work is needed before any final conclusions can be drawn.

1.6.4. Potential Uses of ^{1}H MRS in AD

The data obtained so far by ^{1}H MRS have a number of potential uses. Use of metabolite ratios in diagnosis of AD, preferably at an earlier stage than with current clinical practice is a possibility. Some correlation has been seen between metabolite ratios and cognitive test scores, this could be a useful marker of disease progression. Prediction of progression from MCI to AD may also be possible, as well as differentiating between different forms of dementia. If definitive biomarkers of the disease and their role in the disease are verified, they may be of use in treatment monitoring. Transgenic animal models of AD with similar metabolic profiles to human AD sufferers could be of great benefit in drug discovery if they can be validated.

1.6.5. Diagnosis

A number of studies have demonstrated differences in metabolite ratios between AD subjects and age matched controls. Decreased NAA and increased MI are the most common findings (Miller et al., 1993; Moats et al., 1994; Rose et al., 1999; Catani et al., 2001; Jessen et al., 2009). Absolute concentrations and creatine ratios have both been used in these studies. These findings have been largely reproducible between laboratories, with some exceptions (Stoppe et al., 2000). The potential diagnostic applications of these differences could be very useful. If they can be used to reliably diagnose AD it could allow earlier diagnosis and better treatment. The location of the volume(s) of interest varies between studies. If different laboratories could obtain spectra from the exact same regions and demonstrate genuinely reproducible results it

could go a long way toward providing proof that ^{1}H MRS can be used as a diagnostic tool in AD.

1.6.6. Disease Progression

Disease progression measured by cognitive test performance could also potentially be monitored by ^{1}H MRS. Significant correlation between MMSE score and NAA/MI, MI/Cr and absolute NAA has been reported (Rose et al., 1999). This study also showed a correlation between metabolite levels and brain atrophy (measured by comparing cerebrospinal fluid and grey matter compositions of the spectroscopy voxel). Similar results for NAA (but not always MI) have been reported to correlate with MMSE score elsewhere (Huang et al., 2001; Waldman and Rai, 2003). Another study, measuring NAA content of the whole brain (WBNAA) found it to be a good predictor of MMSE score (Falini et al., 2005). The same study found that normalised brain volume (NBV) was a good marker of overall brain damage, but found only moderate correlation between NBV and WBNAA. Verbal fluency in AD subjects was reported to positively correlate with parietal MI/NAA (Ackl et al., 2005). Correlation was found between both NAA/Cr and MI/NAA with MMSE in a single voxel study, the study also indicated that a single voxel MRS examination only added about 10 mins to a routine MRI scan (Doraiswamy et al., 1998).

If ^{1}H MRS can be reliably used to chart disease progression it could prove very valuable, especially in treatment monitoring of any new potentially disease modifying therapy.

1.6.7. Differentiation –AD/MCI

MCI is a term used to describe subclinical complaints of memory impairment in the elderly. There is thought to be a high risk of patients with MCI progressing to AD (Ritchie and Touchon, 2000). ^{1}H MRS measurements have potential use

in differentiating between the two and predicting likelihood of progression from MCI to AD. In the case of differentiation there is some disagreement between studies. One study showed significantly lower NAA/Cr ratios in AD subjects compared with MCI subjects (Kantarci et al., 2000), whereas another showed increased MI/H_2O ratios in AD subjects compared with MCI subjects (Chantal et al., 2004). A third paper found no significant difference in metabolite ratios between the two (Catani et al., 2001). Clearly more work is required to evaluate whether or not exploitable differences exist in ^{1}H MRS detectable neurometabolite profiles between AD and MCI.

Prediction of progression from MCI to AD has potential clinical benefit, especially when disease modifying drugs become available as patients at high risk could be started on appropriate therapy before full onset of symptoms. One study gathered data on subjects with MCI then followed them up on average 3 years later. It found that NAA/Cr ratio in the occipital cortex predicted dementia at 100% sensitivity and 75% specificity. Positive predictive value was 83% and negative predictive value was 100%, with an overall, cross validated accuracy of 88.7% (Modrego et al., 2005). Another study found that Cho/Cr ratios declined in stable MCI patients compared with patients who progressed to clinical AD (Kantarci et al., 2006). These results show some promise, however due to the lack of correlation between results, and the different protocols used in the studies no conclusions can be drawn. Add this to the difficulties experienced in using ^{1}H MRS to differentiate between MCI and AD and it is clear further work is required to determine whether there is a practical use for the technique in this particular area.

1.6.8. Differentiation – AD/Other Dementias

^{1}H MRS has potential uses in differentiating between different forms of dementia, which may be of use in choosing the correct therapy. Differentiation between vascular dementia (VD) and AD seems possible and appears to be a

matter of location in the brain. One study found fairly similar changes in metabolite ratios between AD and VD, but the distribution of metabolic differences was different. AD followed a temporo-parietal pattern, whereas VD followed a global, subcortically pronounced pattern (Herminghaus et al., 2003). The same study also found a difference in Cho/Cr ratios (Cho was referred to as trimethylamines in the paper), with increases in VD not seen in AD. Another study differentiated the two diseases by claiming that similar changes in metabolites are seen between the two diseases, but in VD it is predominantly the white matter affected, whereas in AD it is the grey matter (Jones and Waldman, 2004). This study also showed a higher MI/NAA ratio in AD from mesial parieto-occipital spectra, using a short echo time. Another study also showed significant differences in the mesial parieto-occipital lobes between VD and AD, showing correlation with MMSE for AD but not VD (Waldman and Rai, 2003). A further study found differences in the posterior cingulate gyrus in NAA/MI, MI/Cr and Cho/Cr between AD and VD (Martinez-Bisbal et al., 2004).

Differentiation between AD and frontotemporal dementia (FTD) was achieved using ^{1}H MRS. The differences were seen in the frontal lobe, with an altered metabolic profile seen in FTD but not in AD. Using these data a linear discriminant analysis correctly differentiated 92% of FTD patients from AD patients (Ernst et al., 1997).

The results of another study indicate that ^{1}H MRS metabolic profiles could be used to differentiate between AD, VD, FTD and dementia with lewy bodies. This paper indicates that further testing with longitudinal studies and therapeutic trials is necessary in order to be confident of accurate differentiation (Kantarci et al., 2004).

1.6.9. Treatment Monitoring

In a treatment monitoring study using the anticholinesterase donepezil on AD patients, changes were observed by ^{1}H MRS *in vivo*. Treatment caused an

increase in NAA and NAA/Cr ratio in the parietal lobe. ADAS-Cog scores were found to correlate with changes in both NAA and NAA/Cr in the left parietal lobe after 3 months of treatment. Parietal NAA/Cr ratio was also found to be predictive of treatment response, patients with lower initial NAA/Cr benefited more from the treatment (Jessen et al., 2006). One potential weakness of this study is that no placebo group was included for ethical reasons. This means changes seen might be unrelated to cholinergic treatment.

Another study used a different anticholinesterase, rivastigmine, and showed an increase in NAA/Cr ratio in the frontal cortex only. Some improvements in cognitive test scores were seen but these were not statistically significant. No effect on MI/Cr levels was seen (Modrego et al., 2006). As anticholinesterase treatment only produces modest and transient benefit in AD patients these results are not surprising.

A third study using the selective muscarinic (M1) cholinergic agonist xanomeline showed a decreased in the Cho/Cr ratio caused by xanomeline treatment (Satlin et al., 1997). This study was limited in that only a small number of subjects were included (10 xanomeline, 2 placebo) and no age-matched control subjects without AD were included.

Despite some weaknesses, these three studies are relatively encouraging for the potential use of ^{1}H MRS in treatment monitoring. However, the levels of the metabolites of interest can potentially be modified at many points in their metabolic pathways. Thus any changes seen may not be caused by a disease modifying effect of treatment, but by an interaction of the drug with the metabolite at an unrelated point in its metabolism, this would be a global effect, not restricted to a specific region. The reproducibility of the spectroscopic measurements used must also be extensively tested to ensure that changes seen are caused by the drug administered. As MRS systems and techniques improve effects of treatments on other metabolites which may play a role in

neurodegeneration may also be possible. These include glutamate and the endogenous antioxidant glutathione.

In monitoring both treatment and disease progression MRI scans can be used to observe volumetric changes in the brain as a measure of disease progression, with atrophy occurring as the disease progresses (Fearing et al., 2007), most notably in the medial temporal lobe, including the hippocampus, entorhinal cortex and the amygdala (Petrella et al., 2003). The addition of ^{1}H MRS to this protocol adds only about 10 mins to scan time and allows assessment of both brain structure and chemistry. Using the two in tandem could make interpretation of results easier and/or more accurate. As neuronal dysfunction is likely to occur before neuronal death, metabolic changes detectable by ^{1}H MRS may occur before observable brain volume loss in disorders such as AD. An observable increase in NAA (or slowing of decline) along with clinical markers of delayed disease progression may support a claim for neuroprotective properties of a drug. Interpretation of volume measures may also be difficult if neuronal loss is counterbalanced with gliosis or subtle oedema (Doraiswamy et al., 2000).

1.7. Magnetic Resonance Imaging in AD

MRI has been used extensively to study AD patients. Common findings include atrophy of cortical grey matter, temporal lobes and hippocampi, along with ventricular enlargement (Wahlund, 1996; Xanthakos et al., 1996). Some correlation between MMSE and hippocampal/temporal lobe atrophy has also been found (Wahlund, 1996; Xanthakos et al., 1996).

Medial temporal lobe structures, including the hippocampus, parahippocampal gyrus and amygdala have been investigated using volumetric MRI (Jack et al., 1997). Volumes were found to decrease with age in AD patients and age-matched controls, however the volumes of the structures were significantly

smaller in AD patients than controls. Loss of hippocampal volume was also shown to correlate with disease progression (Jack et al., 1997).

Overall brain atrophy has been shown to be greater in AD patients than age-matched controls (Fox et al., 1996a) with no overlap between groups. Accelerated hippocampal volume loss has also been shown to correlate with onset of AD symptoms (Fox et al., 1996b). Although atrophy has been observed, rates and sites of atrophy corresponding to a diagnosis of AD have not been sufficiently validated for MRI to be used as a diagnostic tool (Frisoni et al., 2010).

Amyloid plaques often contain iron (Smith et al., 1997), this means the plaques can have paramagnetic properties. This is a potential reason that some plaques are visible to MRI without the use of contrast agents (Benveniste et al., 1999).

1.8. Investigation of Animal Models

The development of transgenic mouse models of AD is a way of studying disease mechanisms and testing potential new therapeutics. Many different transgenic mice have been developed in order to study AD pathogenesis. These have human mutant variants of the genes coding for APP, the presenilins and tau expressed singly and in various combinations. Most of these mice develop amyloid plaques in their lifetimes (Higgins and Jacobsen, 2003). Pathological changes seen in these mice include deficits in synaptic transmission (Hsia et al., 1999), learning deficits (Holcomb et al., 1998), impaired long-term potentiation (Moechars et al., 1999) and reduced brain volume (Van Broeck et al., 2008).

To date, three different types of AD mouse model have been studied using ^{1}H MRS. These are the APP, APP-PS1 and PS2APP. In APP mice, mutated human amyloid-β precursor protein (APP) is expressed. The APP-PS1 mouse coexpresses mutated human presenilin 1 (PS1) and APP. The PS2APP mouse

overexpresses mutated human presenilin 2 (PS2) and APP. Presenilin 1 and 2 are thought to be part of the catalytic site of γ-secretase, an enzyme involved in the pathogenesis of AD (Esler et al., 2000). APP is a membrane bound protein which is cleaved by β- and γ-secretases to give amyloid-β protein, this protein aggregates in the CNS and is thought to be the main causal factor behind the neuronal damage seen in AD.

The three mice strains all develop amyloid plaques, the APP at 10 months, the PS1-APP at 3 months and the PS2APP at 8 months. All three strains have also shown memory deficits which correlate with AD symptoms. ^{1}H MRS studies have been performed on all 3 strains of mice. The APP mice were found to have decreases in NAA/Cr, glutamate/Cr and glutathione/Cr in the cerebral cortex compared with wild type. An increase in the amino acid taurine/Cr was also seen. Taurine is known to be predominantly present in the glia (Dedeoglu et al., 2004). This scenario seems similar to the human situation, with taurine replacing MI as a marker of glial proliferation. No attempt was made during the study to test for correlation between plaque load and neurochemical changes.

For PS2APP mice, age dependent reductions in NAA/Cr and glutamate/Cr, were observed. There was no concurrent increase in either taurine or MI. The NAA and glutamate levels were found to correlate well with plaque load in the frontal cortex. At 20 months a diagnostic test obtained results with 92% sensitivity and 82% specificity in differentiating PS2APP mice from wild type (von Kienlin et al., 2005).

The APP-PS1 mice have been the most extensively studied with ^{1}H MRS. In a study looking at APP-PS1 mice of varying ages, a reduction in NAA/Cr and glutamate/Cr was observed with advancing age (Marjanska et al., 2005). This effect has also been seen in wild type mice, but to a much lesser extent and with a later age of onset (von Kienlin et al., 2005). There is some concordance between the 3 mouse AD models and the human condition in the reduction of

NAA levels. The APP-PS1 mice also showed a dramatic, age dependent increase in MI/Cr levels (Marjanska et al., 2005). This differs from the other two mouse models. This increase was attributed to microglial activation in these mice. Thus, according to current evidence, the APP-PS1 mouse most closely resembles the human condition in that it mimics the decrease in NAA as well as the increase in MI. Activated microglia accumulate around amyloid plaques in both humans and APP-PS1 mice. Concern is expressed by the authors of the study that the increase in MI may be a consequence of plaque load rather than genotype, which could limit the use of this model (Marjanska et al., 2005).

In a study using multivariate data analysis, MI/Cr was found to be important for group separation (transgenic/wild type) in younger mice, while NAA/Cr, glutamate/Cr and macrolipids were more important in older animals (Oberg et al., 2007). This study only used animals up to 9 months old. In a study comparing memory differences (measured by the object recognition test) with metabolite levels from brain extracts, measurable memory deficits were first observed at 35 weeks. At this point the mice were sacrificed and NMR spectra acquired from extracts from various brain regions. Increased MI was found in all tested brain regions, a small decrease in NAA was found in the temporal cortex (Woo et al., 2010). It would appear that increased MI precedes NAA decrease in this model, except in the temporal cortex, one of the areas in which pathology surfaces in early human AD.

Of the 3 strains APP-PS1 appears to be the most attractive model to be used in drug discovery. Due to the similarities in the ^{1}H MRS profile of the APP-PS1 mice and human AD subjects, disease-modifying therapies could potentially be investigated using these mice, and thus accelerate the process of developing new therapies. This in turn would result in new therapies being available to AD patients much sooner.

In summary, ^{1}H MRS has many potential applications in the study and treatment of AD. The changes in NAA and MI seen are now fairly widely accepted and as techniques/instrumentation improve other metabolites may be studied in more detail. The potential use of ^{1}H MRS as a diagnostic tool and in monitoring disease progression/therapy is demonstrated, however further development and optimisation is required. The use of animal models for drug discovery is an increasingly important area of research, particularly for the novel therapeutic targets currently under investigation. Use of these animal models allows disease-modifying actions to be studied in detail before clinical trials begin in humans.

1.9. TASTPM Mouse

The TASTPM mouse was developed from two transgenic mouse strains. The first was TAS-10, overexpressing hAPP695swe (Swedish familial mutant APP) under the control of the neuronal promoter Thy-1. The second is TPM, overexpressing the PS1 M146V mutation, also under the control of Thy-1. Both mice have C57BL/6 mice as the background strain (Howlett et al., 2004). TAS-10 mice were backcrossed onto C57BL/6 and the resulting offspring were crossed with TPM mice to produce heterozygote double mutant mice (TASTPM) (Howlett et al., 2004). Thus the TASTPM expresses both human mutant APP and PS1 genes, both under the control of the neuronal promoter Thy-1 (Howlett et al., 2004). These mice begin to develop cerebral $A\beta_{42}$ deposits as early as 3 months of age, female TASTPM mice exhibit more immunolabelled Aβ deposits than their male counterparts. They also exhibit an age-dependent cognitive impairment as measured by the object recognition test, indicating that these mice could not distinguish between familiar and novel objects. The observed impairment can be detected from 6 months of age (Howlett et al., 2004). Dystrophic neurites were observed by electron microscopy in the cortex of TASTPM from 6 months of age. This suggests an age-related degenerative change (Howlett et al., 2004). The dystrophic neurites were invariably associated with extracellular Aβ deposits, suggesting that the

observed neuronal toxicity involves Aβ or something associated with it (Howlett et al., 2004).

In a study examining Aβ deposition in TASTPM mice (Howlett et al., 2008), Aβ deposition was observed from 2-4 months of age. The amyloid plaques were found to contain both human Aβ and endogenous rodent amyloid. $A\beta_{42}$ was found to be more prevalent than $A\beta_{40}$ in these plaques. Inflammatory cells were found in close proximity to amyloid deposits, from 2-4 months of age glial fibrillary acidic protein (GFAP) positive astrocytes were found associated with plaques and microglia and astrocytes were found surrounding plaques (Howlett et al., 2008).

Histopathologically, neuronal loss in the brains of TASTPM mice, particularly in the cell layers of the hippocampus, appears very similar to that occurring in the human AD brain (Howlett et al., 2008). Hyperphosphorylated tau was also observed from 4 months of age and increased with age, this tau appeared to be associated with dystrophic neuritis (Howlett et al., 2008). In a study on brain volume changes in TASTPM and C57BL/6 (WT) mice numerous differences were observed (James et al., 2007). An overall increase in brain volume was observed in both strains, but the increase was greater in the TASTPM mice and appeared to be continuous. The volume increase levelled off after 11 months in the WT. In absolute terms the majority of TASTPM brain regions increased in volume over time (James et al., 2007).

When normalised to whole brain volume (WBV) several brain regions could be seen to be affected by the genetic difference over time. The hippocampal formation reduced in size over time in WT mice, while it increased relative to WBV in TASTPM mice (James et al., 2007). The normalisation process suggests that the transgenes elicit one of two responses. The first group includes the corpus callosum, corticospinal tract, hypothalamus, midbrain-hindbrain and fornix system. In this group TASTPM brain regions are smaller

than WT, which suggests a negative early effect of the transgenes. These regions still increase in volume with age along similar lines to the WT. The second group includes the thalamus, cerebellum, cerebral cortex and caudoputamen. In this group regions are initially larger in TASTPM than WT, but reduce in size more rapidly with age (except for the cerebellum and cerebral cortex). The early increase in size in this second group is indicative of the effect of early Aβ deposition and inflammatory processes, leading to grey matter loss with age and thus a decrease in size (James et al., 2007). Early volume increases could also be a result of large amounts of intracellular APP being present, increasing cell size. Later volume loss could be offset by increased gliosis.

In most areas of the TASTPM brain Aβ deposition is accompanied by astro- and microgliosis (Howlett et al., 2008). Significant thalamic pathology has been observed in TASTPM mice by MRI, micro-CT and histology (Evans et al., 2007). The pathology (which is visible on MRI scans as signal hypointensity in the thalamus) starts to become visible at around 7 months. Although Aβ deposits are found in all areas of the brain with histology, only in the thalamus are they co-localised with calcium and ferrous iron deposits (Evans et al., 2007). The thalamic plaques are also the only plaques visible with MR and CT, suggesting that the observed signal loss may be caused by a process unique to the thalamus or connected regions (Evans et al., 2007). Similar thalamic pathology has been observed in other transgenic mouse models of AD (Dhenain et al., 2009). There are several possible reasons for this, one is potential haemodynamic disruption. It has been shown in rats that transient middle cerebral artery occlusion leads to Aβ and APP deposition in the ventroposterior medial and ventroposterior lateral nuclei of the thalamus (van Groen et al., 2005).

1.10. MALDI Imaging

The thalamic hypointensity detected in the TASTPM mouse has not been extensively characterised by histology and, in particular, there has been no proteomic analysis of the lesions. In this thesis Matrix-assisted laser desorption/ionization mass spectrometry (MALDI MS) is used to probe peptides present in the hypo-intense regions to try to identify any peptide/protein markers of the lesions.

Mass spectrometry (MS) measures the mass to charge ratio of charged particles. It is used to determine the mass of molecules and also to determine their elemental composition and chemical structure, in this case we are mainly interested in peptides and proteins. The specific type of mass spectrometer which is interfaced to the MALDI instrument we used is a time of flight (TOF) mass spectrometer. This instrument determines mass to charge ratio by time measurement, ions are accelerated by an electric field of known strength, resulting in the kinetic energy of ions with the same charge being equal. The velocity of the ion is dependent on the mass to charge ratio (with heavier molecules travelling at slower speeds). The time taken for the ion to reach a detector at a known distance is measured and allows the mass of the ion to be determined if the charge is known.

MALDI is a technique which works by co-crystallising the sample of interest (typically small molecules, peptides or proteins) with an organic compound, called a matrix. The matrix facilitates ionisation of molecules from the sample when it is bombarded with a laser (e.g. N_2, Nd-YAG) (Karas et al., 1987; Karas and Hillenkamp, 1988). The ions generated then enter the TOF mass spectrometer.

The most commonly used matrices are α-cyano-4-hydroxycinnamic acid (alpha-cyano) and 3,5-dimethoxy-4-hydroxycinnamic acid (sinapinic acid). Matrix compounds are dissolved in a mixture of water and an organic solvent

such as acetonitrile or ethanol, Trifluoroacetic acid is often added to provide protons to aid ionisation.

In MALDI MS the sample to be analysed is mixed with matrix in a ratio of around 1:1 and deposited on a target plate. The mixture is allowed to dry, during which time the matrix co-crystallises with sample molecules. The sample is then bombarded with short laser pulses, resulting in desorption and ionisation of the sample molecule. Intact, protonated molecules from the sample are then analysed, usually in a TOF mass analyser, allowing the mass of the parent molecule to be deduced.

MALDI imaging involves profiling and imaging the distribution of endogenous components e.g. proteins, directly from thin tissue sections. Thin sections of tissue (10 – 20 µm thick) are cut in a cryostat and mounted on indium tin oxide coated glass slides. Matrix is then applied to the slide in a homgenous manner (e.g. airspray deposition) to get an even coating. The slide is then placed in the MALDI TOF instrument and the laser irradiates discrete spots over the surface of the tissue, covering the surface of the section at intervals which define the resolution of the image that will be generated. In this way, distribution of proteins/peptides throughout the tissue can be visualised in two dimensions. MALDI imaging was used in this thesis to evaluate TASTPM brain sections, looking for different amyloid fragments and any variations in comparison to wild type mice.

Summary

Thus, it can be seen that further study on the TASTPM mouse, and specifically its neurobiology may lead to: discovery of a novel biomarker of AD; validation of the TASTPM mouse as an AD model for preclinical testing; or insight into the pathological processes behind the neurodegeneration.

The experimental part of the thesis is presented in four chapters, followed by a final conclusion. The first two experimental chapters deal with an extraction study carried out on the brains of the TASTPM mice, performing MRS on the aqueous and organic fractions respectively. The third chapter discusses a spectroscopic study performed *in vivo* on the brains of the TASTPM mice. The fourth chapter discusses the MALDI investigation carried out on the brains of TASTPM mice.

Chapter 2. Longitudinal *in vitro* ^{1}H MRS of chloroform-methanol extracts from the brains of TASTPM mice

2.1. Introduction

There is a need to develop a biomarker for AD to aid in drug development, treatment monitoring, diagnosis and patient management. An ideal biomarker must be easy to measure non-invasively, related to disease progression and specific for AD. There is currently no such definitive biomarker for AD. Magnetic resonance imaging (MRI) observation of AD patients has found atrophy, increasing in severity with disease progression (Frisoni et al., 2010), however brain atrophy is not specific to AD. A proton magnetic resonance spectroscopy (^{1}H MRS) scan could be performed during the same session as an MRI scan, only adding approximately 10 mins to scan time. If a ^{1}H MRS biomarker could be found, a more robust diagnosis could potentially be made. Disease progression could also be monitored more closely. A metabolic biomarker for AD could also be invaluable in treatment monitoring. If therapeutic intervention caused normalisation of the ^{1}H MRS spectrum from an AD patient this could give an early, non-invasive indication of drug efficacy.

Decreased N-acetylaspartate (NAA) and increased myo-inositol (MI) has been noted in the brains of AD patients (Shonk et al., 1995; Dixon et al., 2002; Ackl et al., 2005). NAA is thought to be a neuronal marker (Urenjak et al., 1992), MI is thought to be a marker of gliosis or microglial activation (Lazeyras et al., 1998), based on observations on cultured glial tumour cells (Brand et al., 1993). Some of these results have suggested ^{1}H MRS might be used for both diagnosis of AD and distinguishing between different dementias. AD was differentiated from frontotemporal dementia (FTD) by analysing spectra acquired from midfrontal grey matter, decreased NAA was found in FTD but not AD (Ernst et al., 1997). This regional differentiation may be present in the early stages of neurodegeneration, but may be lost as the diseases progress and neurodegeneration spreads throughout the brain (Kantarci et al., 2004; Garrard

et al., 2006). NAA/Creatine was found to be lower in white matter of patients with vascular dementia than AD (Kattapong et al., 1996). Several studies have shown positive correlation between neuropsychological cognitive test scores and NAA/Cr, MI/Cr and NAA/MI ratios (Rose et al., 1999; Jessen et al., 2000; Huang et al., 2001; Kantarci et al., 2002), suggesting ^{1}H MRS could be used to monitor disease progression. Decreased NAA can be seen in many neurological disorders, especially those involving neurodegeneration. Differentiation has been achieved by examining different regions. This may only be useful in early stage disese, before neurodegeneration becomes widespread. If another metabolic marker for AD could be discovered it could make differentiation using ^{1}H MRS easier and more accurate.

Understanding the underlying pathology behind AD has improved greatly in recent years. This is due in part to the study of mouse models of the disease, improving our understanding of deposition of Aβ and links to neurodegeneration (Moechars et al., 1999; Bayer and Wirths, 2008). Improvements in mouse models have also occurred, leading to models which are a closer approximation of human AD (Howlett et al., 2004; Bayer et al., 2008). The most widely accepted current hypothesis about AD pathology is the amyloid cascade hypothesis (Hardy and Selkoe, 2002). This states that an imbalance in the production and degradation/clearance of amyloid beta peptide (Aβ) in the brain is the initiating event in a cascade ultimately leading to neuronal degeneration, dementia and death (Hardy and Selkoe, 2002). Therapies influencing Aβ production/degradation/clearance are all being developed and there is hope that these therapies can slow or halt the progress of AD once diagnosed. With ongoing research into new therapies, animal models are required to test efficacy before clinical trials. The object of this study is one such mouse, the TASTPM mouse.

In this study the transgenic mouse TASTPM, which overexpresses both a mutant form of the amyloid precursor protein (hAPP695swe) and a mutant

presenilin-1 variant (M146V) (Howlett et al., 2004) was investigated. TASTPM mice first show amyloid deposits at 3 months and cognitive impairment is seen from 6 months (Howlett et al., 2004). Here, the aim was to investigate metabolic changes occurring over time in the brains of TASTPM mice compared to their base strain (C57/BL6). In order to accomplish this, chloroform-methanol extractions of the brains were performed and *in vitro* ^{1}H MRS was performed on the resulting extracts. *In vivo* studies of different AD transgenic mice have shown a decrease in NAA and glutamate, and increases in MI and taurine (Dedeoglu et al., 2004; Marjanska et al., 2005; von Kienlin et al., 2005). A greater number of metabolites can be investigated *in vitro* and other metabolites which are of interest included markers of energy usage and neurotransmission, such as succinate and glutamate.

2.2. Methods

Chloroform-methanol extractions (Le Belle et al., 2002) were performed on frozen whole brains of both strains of mice at 3, 6, 9, 12, 15 and 18 months of age, with 5 - 9 mice in each group (Table.1).

	Strain	
Age Group	Wild Type	TASTPM
3	5	7
6	9	8
9	5	7
12	9	8
15	7	8
18	5	8

Table.1 *Group sizes for TASTPM and wild type mice*

Mice were killed by cervical dislocation, brains were removed immediately and flash frozen in liquid N_2. Brains were kept at -80^{0}C until use. During the extraction procedure, the whole frozen brains were kept under liquid nitrogen, adding chloroform and methanol (4^{o}C) in a ratio of 1:2 (v/v; 3 ml/g tissue) and grinding the frozen reagents and brain tissue to a fine powder with a pestle and mortar. The tissue-solvent mixture was then allowed to thaw before being transferred to Teflon centrifuge tubes and sonicated. After 15 mins in contact with the first solvent mix, a 1:1 mix of chloroform and distilled water was added

(1ml/g tissue) to form an emulsion. This was followed by centrifugation at 13000rpm for 20 min. The upper (aqueous) phase was then separated from the lower (organic) phase and both fractions were dried under a stream of nitrogen gas. The aqueous fraction was then redissolved in 650µl D_2O (GOSS Scientific, UK) and the organic fraction in deuterated chloroform. The samples were adjusted to pH 7.0 with DCl and/or NaOD. A known concentration of deuterated trimethylsilylproprionate (TSP) was then added to each aqueous sample as an internal standard. Except where specified, reagents were obtained from Sigma, Aldrich UK.

^{1}H MRS was performed at 25^{o}C with a 9.4T Bruker Avance vertical bore magnet. 80-90% relaxed, one-dimensional spectra with a spectral width of 20.55ppm were acquired with water presaturation using a pulse-acquire sequence with the following parameters: repetition time = 6.4s, central frequency = 400MHz, number of averages = 128, sweep width = 8223.7Hz, number of data points = 32768, dwell time 60.8µs, flip angle 30^o**.** Resonance assignments were based on published chemical shifts and coupling patterns of known compounds. Peak areas were integrated using NUTS NMR Utility Transform Software (Acorn NMR, California, USA) with baseline flattening around each integration region (Fig.8). Water suppressed spectra were used for integration due to the flatter baseline.

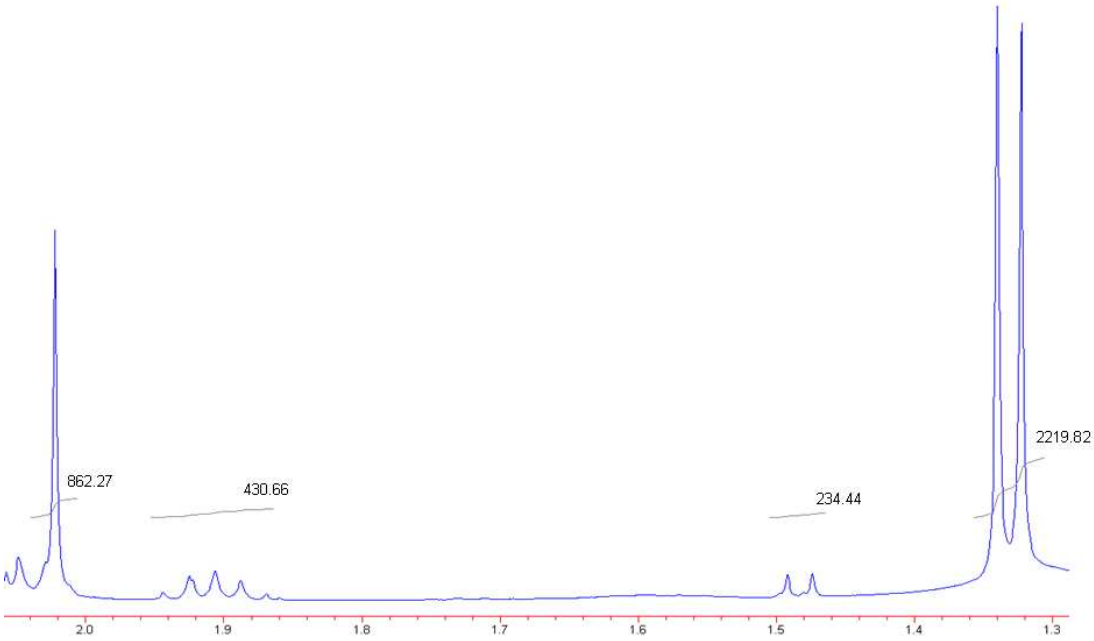

Fig.8 *Example of integration of spectrum, integrated peaks, from left to right: NAA, GABA, alanine, lactate*

Absolute quantification of metabolite levels was achieved by using a known concentration of the internal standard (157mg TSP dissolved in 10ml D_2O, 10µl added to each sample = 0.912 µmoles in each sample) in each sample. Metabolite integrals were converted to concentrations by comparison to the TSP integral, taking into account numbers of equivalent protons making up the integral in question. Prior to statistical analysis, all values were normalised to individual brain weights to prevent brain size being a contributory factor.

2-way ANOVA (age by genotype) was performed on the metabolite integrals using Graphpad Prism version 3.00 for Windows (GraphPad Software, San Diego, California, USA). Metabolites investigated were acetate, aspartate, alanine, choline, creatine, γ-aminobutyric acid (GABA), glutamate, glutamine, glycerophosphocholine (GPC), MI, lactate, NAA, phosphocholine, succinate and taurine.

2.3. Results

High quality spectra, with good signal-to-noise (>10000:1 for the NAA resonance) were acquired from all samples, examples of which are given in Fig. 9 and 10, together with the assignments of the analysed peaks. All metabolite data are summarised in Table.3.

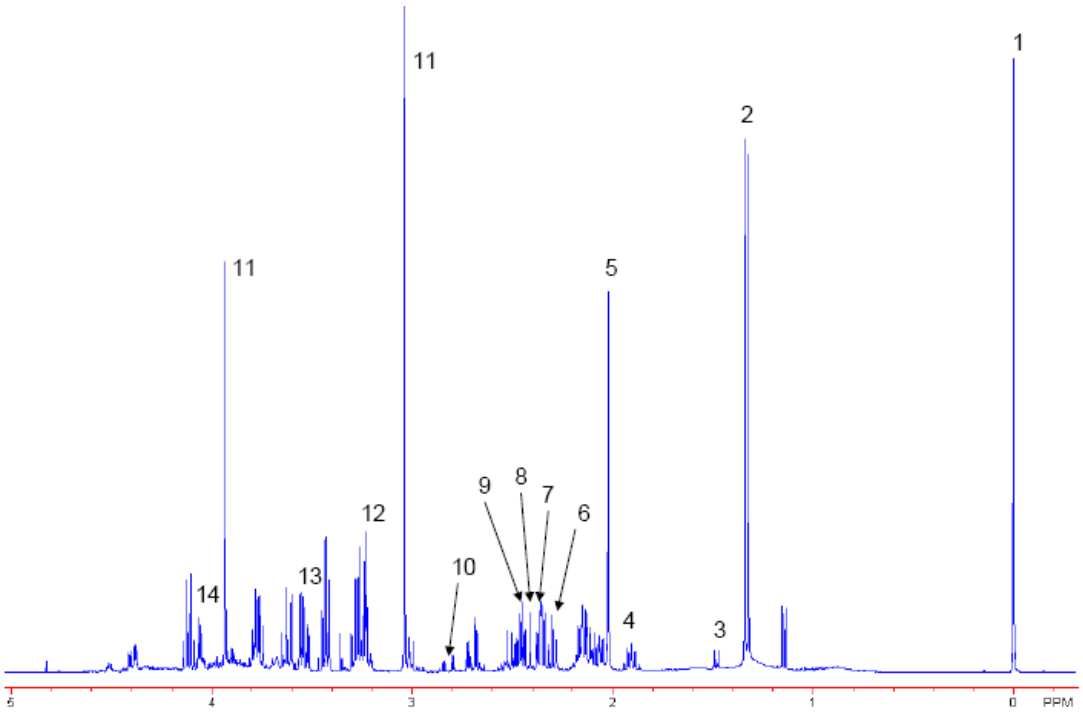

Fig.9 *Example spectrum obtained from an extract of an 18 month old wild type mouse brain. 1 – TSP, 2 – lactate, 3 – alanine, 4 – GABA, 5 – NAA, 6 – GABA, 7 – glutamate, 8 – succinate, 9 – glutamine, 10 – aspartate, 11 – creatine, 12 – choline containing compounds, 13 – taurine, 14 – MI*

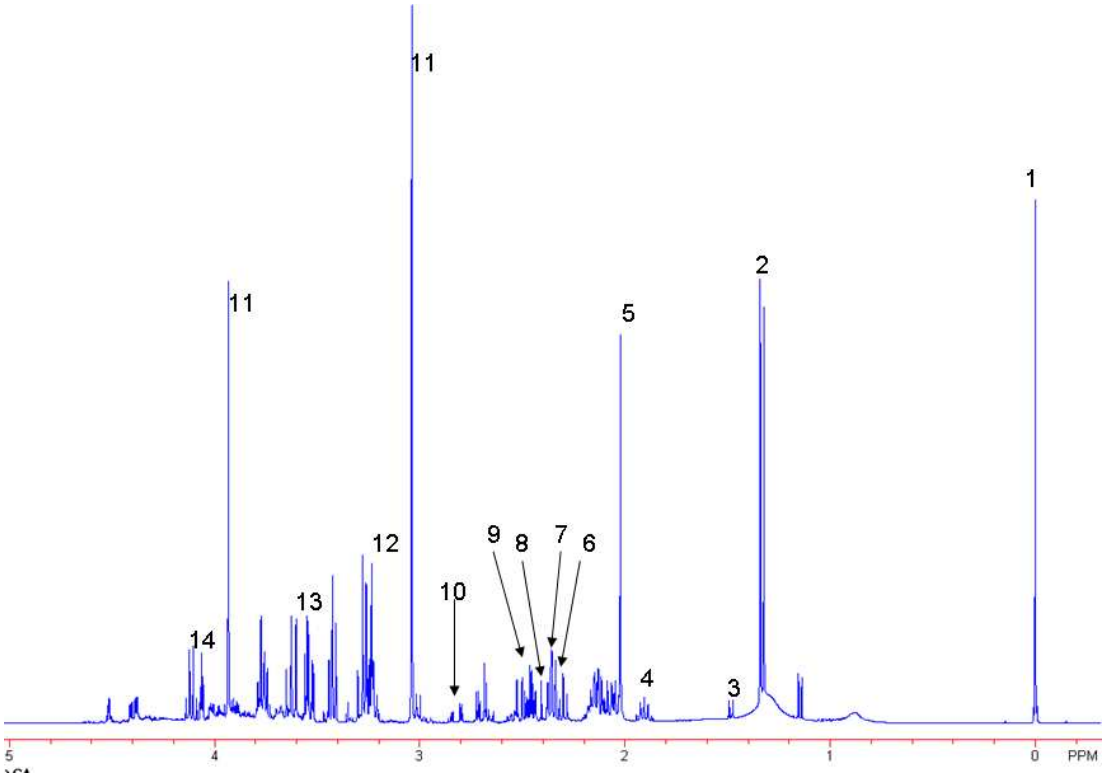

Fig.10 *Example spectrum obtained from an extract of an 18 month old TASTPM mouse brain. 1 – TSP, 2 – lactate, 3 – alanine, 4 – GABA, 5 – NAA, 6 – GABA, 7 – glutamate, 8 – succinate, 9 – glutamine, 10 – aspartate, 11 – creatine, 12 – choline containing compounds, 13 – taurine, 14 - MI*

15 metabolites were quantified and analyzed by a 2-way ANOVA (age and genotype). Due to the high number of variables being compared, a Bonferroni correction was performed on the standard significance level of $p<0.05$, as 15 variables were tested a final significance level of $p<0.0033$ was used. Significant effects of age alone were identified for creatine ($p<0.001$), glutamine ($p<0.0001$) and total choline-containing compounds (the sum of glycerophosphocholine (GPC), phosphocholine and choline levels - $p<0.0001$). Creatine was fairly stable and at similar levels in both groups until 15 months, when there was a marked increase in the TASTPM mice (Fig.11). Despite this change, there was neither an overall effect nor an interaction of genotype on creatine concentration. A significant effect of genotype alone was only identified for *myo*-inositol (Fig.12), which was generally higher in TASTPM mice at all timepoints (Fig. 18). Though the difference appeared greater in the older age-

groups there was no significant interaction with, or main effect of, age. Succinate, GPC and choline all showed significant effects of both age and genotype. Succinate concentration fell continuously from a lower starting point in the TASTPM mice (Fig. 17), whereas it increased in wild type mice up until a fall at 15 months. Succinate was lower in TASTPM mice at all time points (Fig.13). Choline levels fluctuated over time, but this was much more pronounced in the TASTPM mice, with choline much lower than in the wild type at 6 – 12 months (Fig.14 + 19). GPC increased over time in both strains, but was slightly higher in TASTPM mice (Fig.15). No significant effect of age or strain was seen on NAA levels (Fig.16)

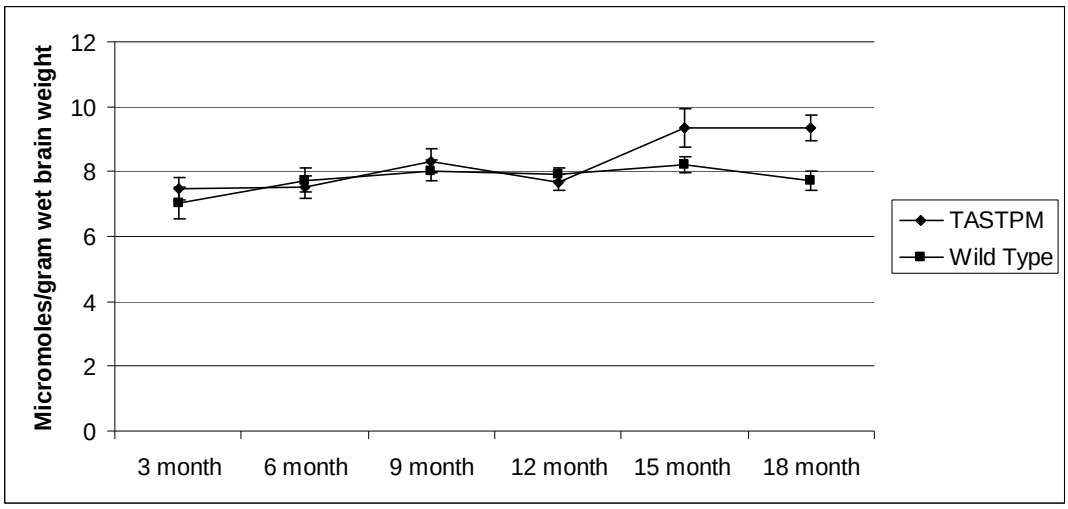

Fig.11 *Creatine levels in TASTPM and wild type mice. Values shown are mean ± S.E.M.*

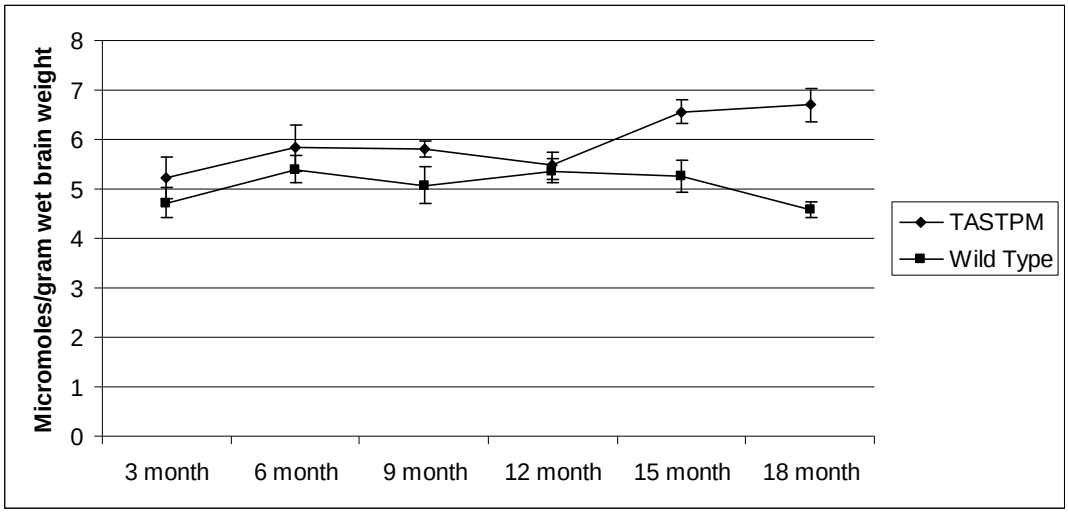

Fig.12 *MI levels in TASTPM and wild type mice. Values shown are mean ± S.E.M.*

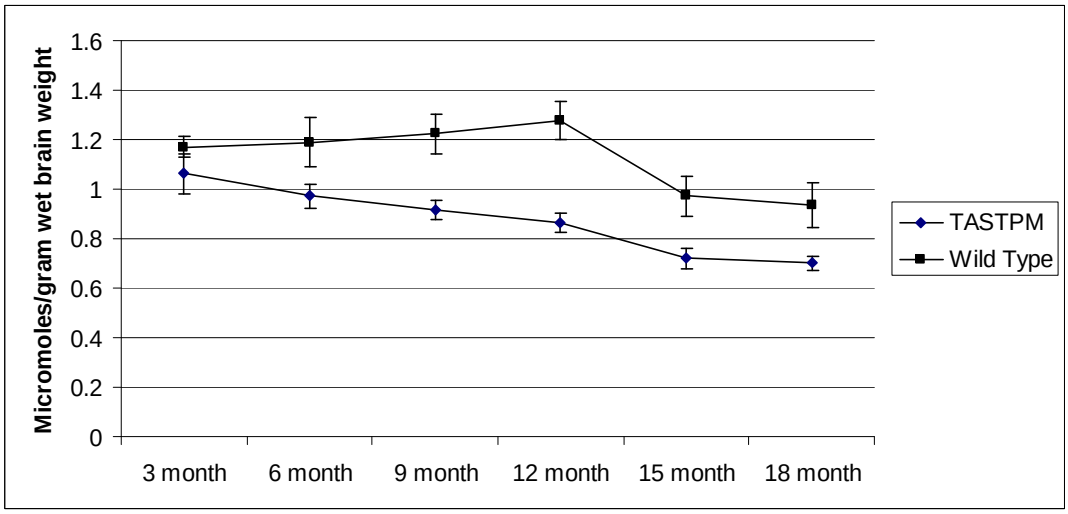

Fig.13 *Succinate levels in TASTPM and wild type mice. Values shown are mean ± S.E.M.*

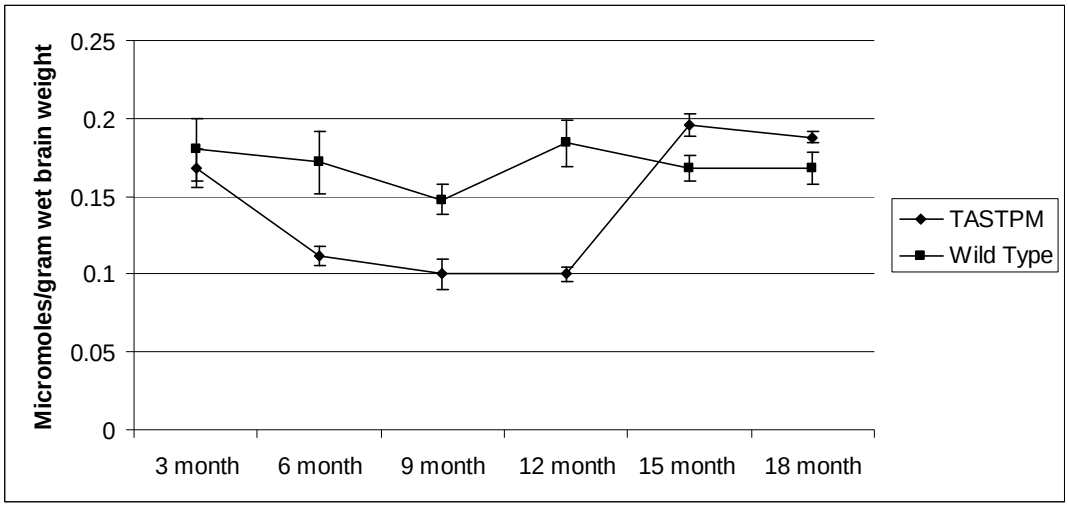

Fig.14 *Choline levels in TASTPM and wild type mice. Values shown are mean ± S.E.M*

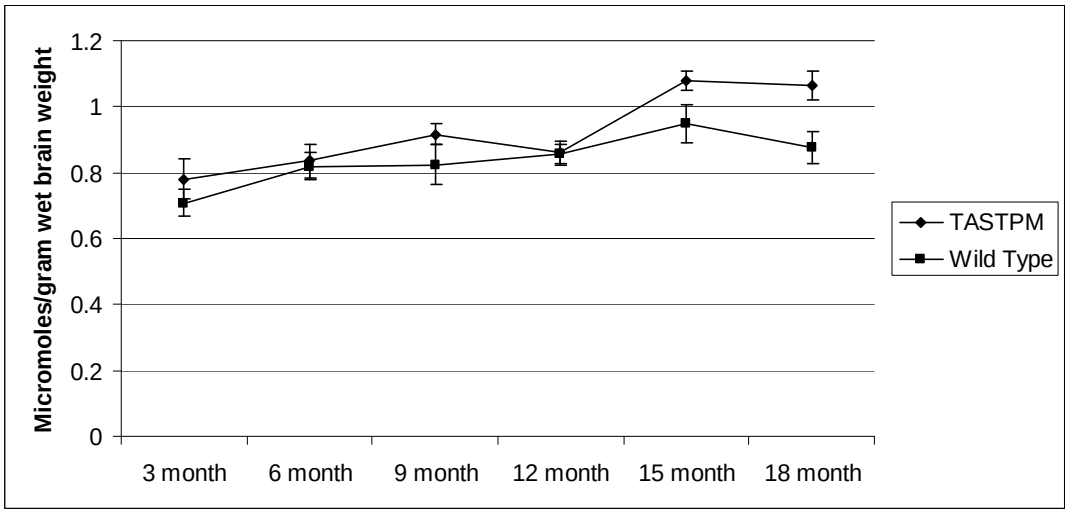

Fig.15 *GPC levels in TASTPM and wild type mice. Values shown are mean ± S.E.M*

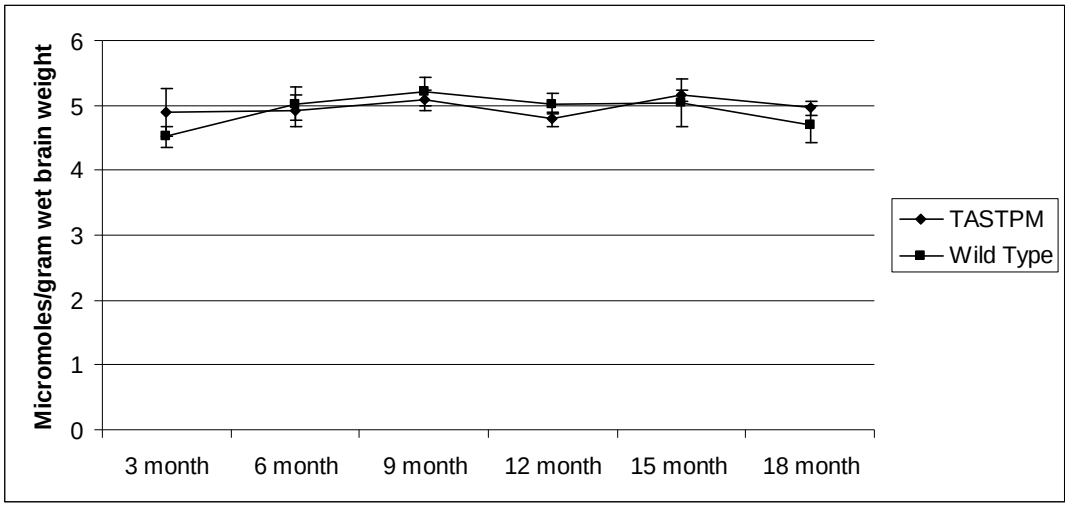

Fig.16 *NAA levels in TASTPM and wild type mice. Values shown are mean ± S.E.M*

Metabolite	Age	Genotype	Interaction
Succinate	<0.0001	<0.0001	ns
Choline	<0.0001	0.0007	<0.0001
MI	ns	<0.0001	ns
GPC	<0.0001	0.0030	ns
Creatine	0.0008	ns	ns
Glutamine	<0.0001	ns	ns
Total Choline	<0.0001	ns	ns

Table.2 *Table showing ANOVA probabilities of significance for metabolites where p<0.005. All other metabolite comparisons did not reach statistical significance.*

	3 months			6 months		
Metabolite	Mean	S.D.	CoV	Mean	S.D	CoV
Inositol Wild Type	4.72	0.70	14.90	5.42	0.86	15.95
Inositol TASTPM	5.21	1.09	20.99	5.82	1.34	23.08
Cr2 Wild Type	5.04	0.50	9.82	5.82	0.94	16.21
Cr2 TASTPM	5.49	0.94	17.10	5.53	0.79	14.26
Taurine Wild Type	6.63	0.91	13.80	7.34	1.10	14.95
Taurine TASTPM	7.02	1.43	20.30	7.28	1.22	16.72
GPC Wild Type	0.71	0.09	12.92	0.82	0.14	16.77
GPC TASTPM	0.78	0.17	21.84	0.83	0.13	16.15
PC Wild Type	0.44	0.04	9.29	0.51	0.07	14.54
PC TASTPM	0.46	0.09	20.42	0.44	0.07	15.44
Choline Wild Type	0.18	0.05	26.38	0.17	0.06	35.13
Choline TASTPM	0.17	0.03	19.71	0.11	0.02	16.29
Cr1 Wild Type	7.05	0.80	11.34	7.74	1.01	13.04
Cr1 TASTPM	7.47	1.28	17.13	7.53	1.09	14.44
Aspartate Wild Type	2.64	0.38	14.58	2.82	0.51	18.11
Aspartate TASTPM	2.60	0.45	17.29	2.46	0.45	18.32
Glutamine Wild Type	4.01	0.74	18.51	4.86	1.40	28.85
Glutamine TASTPM	4.05	0.78	19.38	4.12	0.64	15.56
Succinate Wild Type	0.58	0.05	9.19	0.59	0.15	25.58
Succinate TASTPM	0.53	0.10	18.90	0.48	0.07	14.53
Glutamate Wild Type	7.23	0.65	9.02	7.67	1.22	15.85
Glutamate TASTPM	7.07	1.41	19.87	7.09	1.13	15.99
GABA Wild Type	2.84	0.26	9.07	3.18	0.59	18.41
GABA TASTPM	3.06	0.56	18.18	2.86	0.45	15.56
NAA Wild Type	4.52	0.38	8.36	5.02	0.80	15.91
NAA TASTPM	4.88	0.99	20.33	4.92	0.70	14.20
Acetate Wild Type	0.29	0.08	28.43	0.28	0.05	19.33
Acetate TASTPM	0.83	1.52	182.77	0.25	0.06	23.95
Alanine Wild Type	0.86	0.09	10.22	1.06	0.18	17.16
Alanine TASTPM	0.95	0.39	41.56	0.92	0.10	10.88
Lactate Wild Type	10.77	1.13	10.48	13.59	2.03	14.93
Lactate TASTPM	12.91	3.69	28.59	11.18	1.30	11.67

	9 months			12 months		
Metabolite	Mean	S.D	CoV	Mean	S.D	CoV
Inositol Wild Type	5.07	0.83	16.30	5.37	0.74	13.72
Inositol TASTPM	5.79	0.44	7.54	5.48	0.77	14.10
Cr2 Wild Type	5.79	0.59	10.24	5.75	0.56	9.77
Cr2 TASTPM	6.07	0.64	10.61	5.64	0.42	7.45
Taurine Wild Type	7.25	1.11	15.31	7.57	0.73	9.70
Taurine TASTPM	7.62	0.91	11.93	6.76	0.69	10.22
GPC Wild Type	0.82	0.14	16.57	0.86	0.09	10.09
GPC TASTPM	0.92	0.08	8.67	0.86	0.11	12.21
PC Wild Type	0.55	0.06	10.13	0.50	0.06	12.35
PC TASTPM	0.49	0.04	8.61	0.46	0.04	9.66
Choline Wild Type	0.15	0.02	16.65	0.18	0.05	26.51
Choline TASTPM	0.10	0.03	27.16	0.10	0.02	14.92
Cr1 Wild Type	8.04	0.83	10.28	7.93	0.74	9.28
Cr1 TASTPM	8.31	0.84	10.05	7.66	0.54	7.08
Aspartate Wild Type	2.75	0.22	7.83	2.67	0.24	9.04
Aspartate TASTPM	2.70	0.19	7.20	2.64	0.19	7.07
Glutamine Wild Type	5.86	1.39	23.69	4.22	0.52	12.36
Glutamine TASTPM	4.42	0.46	10.37	5.15	1.30	25.26
Succinate Wild Type	0.61	0.09	15.17	0.64	0.12	18.28
Succinate TASTPM	0.45	0.05	12.01	0.43	0.05	12.17
Glutamate Wild Type	7.80	0.62	7.99	7.55	0.78	10.33
Glutamate TASTPM	7.77	0.74	9.53	7.24	0.42	5.76
GABA Wild Type	3.27	0.46	14.11	3.11	0.39	12.48
GABA TASTPM	2.87	0.32	11.32	2.69	0.15	5.55
NAA Wild Type	5.21	0.50	9.52	5.03	0.53	10.48
NAA TASTPM	5.09	0.45	8.89	4.79	0.31	6.50
Acetate Wild Type	0.28	0.05	16.58	0.28	0.04	13.22
Acetate TASTPM	0.22	0.04	18.75	0.20	0.02	10.87
Alanine Wild Type	1.04	0.10	9.34	1.03	0.14	13.67
Alanine TASTPM	0.92	0.12	13.27	0.88	0.08	8.60
Lactate Wild Type	12.95	1.10	8.47	13.57	1.73	12.75
Lactate TASTPM	11.90	1.66	13.96	11.11	0.94	8.49

	15 months			18 months		
Metabolite	Mean	S.D	CoV	Mean	S.D	CoV
Inositol Wild Type	5.29	0.89	16.88	4.58	0.33	7.26
Inositol TASTPM	6.57	0.69	10.56	6.70	0.99	14.70
Cr2 Wild Type	6.05	1.10	18.12	5.60	0.59	10.55
Cr2 TASTPM	6.84	0.50	7.32	6.91	0.64	9.20
Taurine Wild Type	7.70	1.48	19.25	7.05	0.48	6.84
Taurine TASTPM	8.76	0.74	8.40	8.47	0.63	7.47
GPC Wild Type	0.95	0.16	17.33	0.87	0.10	11.63
GPC TASTPM	1.08	0.09	8.51	1.07	0.13	12.50
PC Wild Type	0.51	0.08	15.22	0.47	0.07	14.23
PC TASTPM	0.53	0.05	8.70	0.53	0.05	8.56
Choline Wild Type	0.17	0.02	13.92	0.17	0.02	11.62
Choline TASTPM	0.20	0.02	10.04	0.19	0.01	6.23
Cr1 Wild Type	8.22	1.53	18.61	7.72	0.82	10.65
Cr1 TASTPM	9.34	0.66	7.06	9.35	0.89	9.48
Aspartate Wild Type	2.83	0.61	21.53	2.54	0.26	10.31
Aspartate TASTPM	3.15	0.17	5.43	2.88	0.24	8.48
Glutamine Wild Type	5.02	0.89	17.66	6.10	1.98	32.49
Glutamine TASTPM	6.06	1.13	18.60	6.45	1.25	19.38
Succinate Wild Type	0.48	0.10	20.12	0.47	0.10	20.53
Succinate TASTPM	0.36	0.05	14.29	0.35	0.05	13.22
Glutamate Wild Type	7.63	1.43	18.77	7.10	0.94	13.18
Glutamate TASTPM	8.45	0.50	5.90	8.18	0.64	7.85
GABA Wild Type	2.90	0.55	19.00	2.76	0.40	14.51
GABA TASTPM	3.07	0.20	6.54	2.99	0.23	7.84
NAA Wild Type	5.04	1.00	19.80	4.70	0.59	12.62
NAA TASTPM	5.15	0.26	4.97	4.96	0.33	6.71
Acetate Wild Type	0.68	0.12	17.98	0.65	0.11	17.04
Acetate TASTPM	0.76	0.05	6.88	0.74	0.05	6.42
Alanine Wild Type	0.90	0.19	21.10	0.72	0.09	12.79
Alanine TASTPM	0.91	0.10	11.09	0.94	0.09	9.71
Lactate Wild Type	12.26	2.85	23.21	10.59	1.10	10.40
Lactate TASTPM	11.36	1.41	12.40	12.12	1.21	9.97

Table.3 *Table of mean, standard deviation and coefficient of variance for all metabolites at all time points*

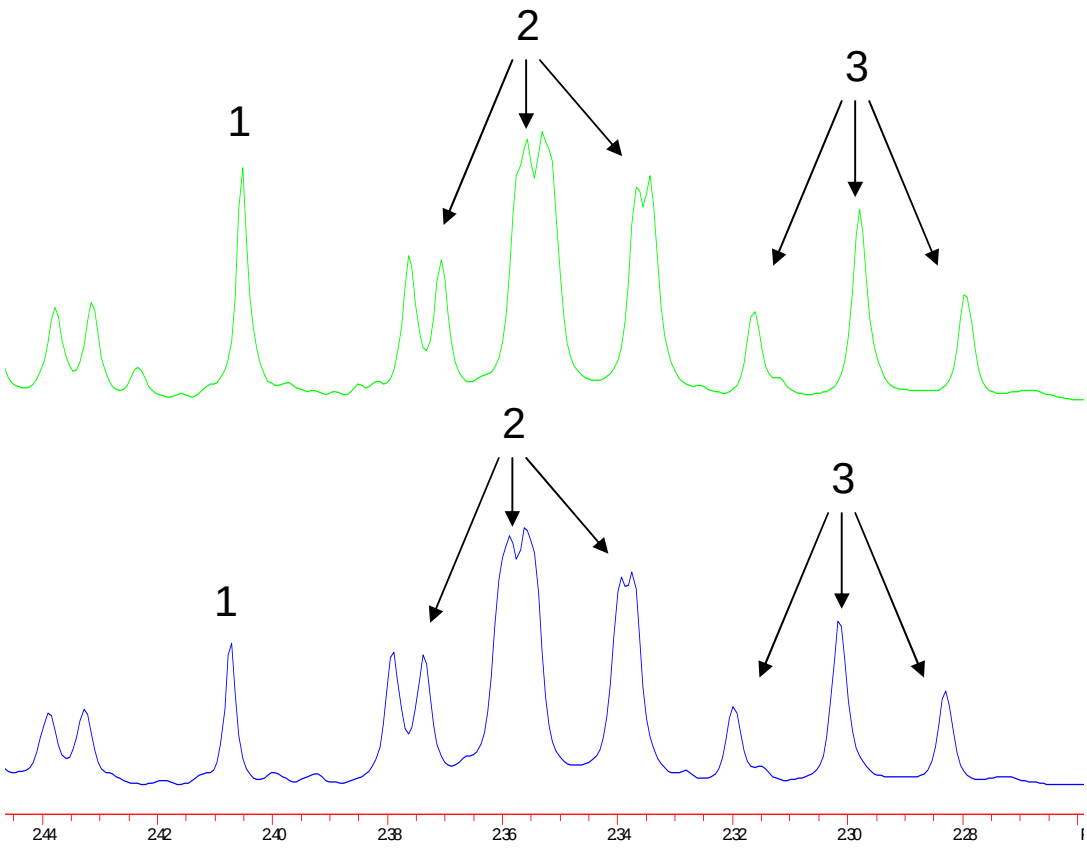

Fig.17 *Comparison of spectra from 18 month wild type (top) and TASTPM mice showing differences in succinate signal (1) at 2.41ppm, also showing the glutamate C4 pseudo triplet (2) and a GABA triplet (3)*

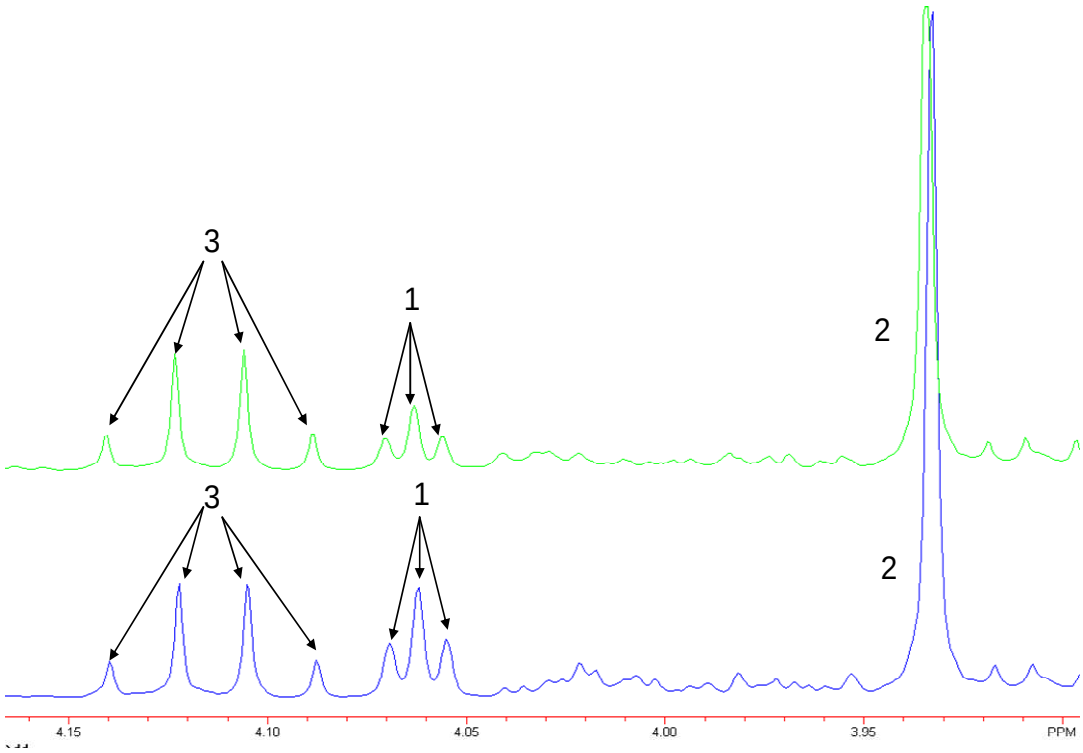

Fig.18 *Comparison of spectra from 18 month wild type (top) and TASTPM mice showing differences in MI signal (1) at 4.06ppm, also showing the creatine peak at 3.93ppm (2) and lactate quartet at 4.12ppm (3)*

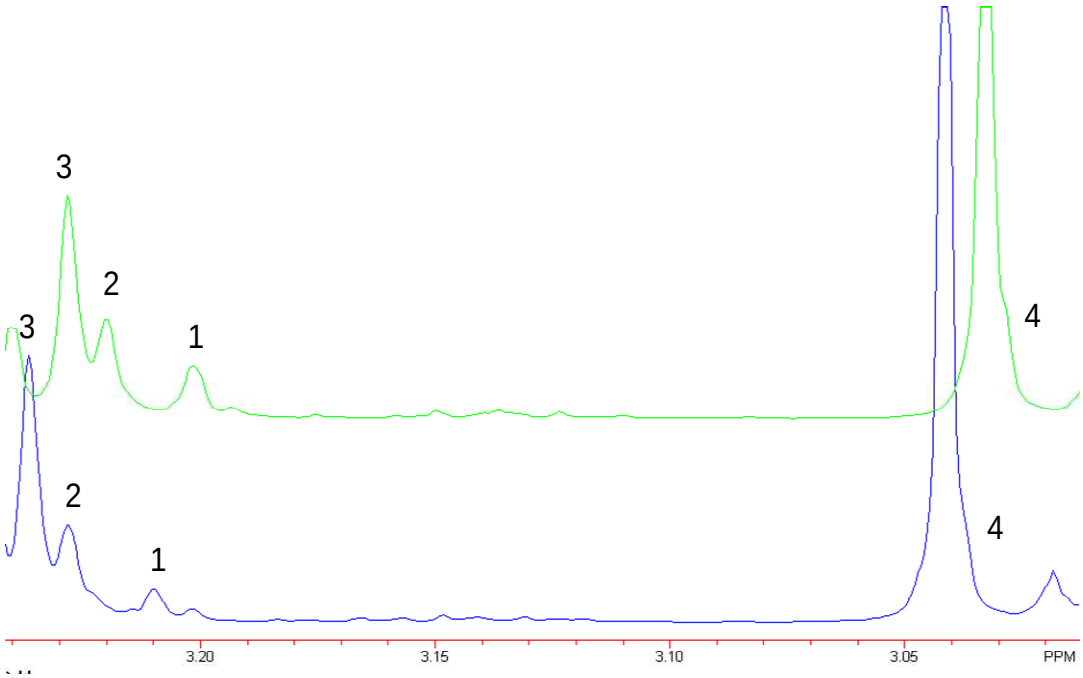

Fig.19 *Comparison of spectra from 12 month wild type (top) and TASTPM mice showing differences in choline signal (1) at 3.20ppm, also showing the phosphocholine peak at 3.23ppm (2), the glycerophosphocholine peak at 3.24ppm (3) and the creatine peak at 3.03ppm (4). These spectra have been offset in frequency for clarity*

2.4. Discussion

Metabolite concentrations are comparable to other studies using *in vitro* ^{1}H MRS on mouse and rat brain extracts (Agrawal et al., 1968; Cerdan et al., 1985; Arvin et al., 1994; Florian et al., 1996; Chassain et al., 2008). Good comparability to studies using HPLC was also achieved (Murai et al., 2001; Bogen et al., 2008). The coefficients of variance indicate good reproducibility in the results for the most part (Table.3).

The higher levels of MI observed in TASTPM mice are a genotype effect. The presence of higher MI in younger TASTPM mice suggests that MI levels are independent of amyloid plaque formation. The greater difference at 15 and 18 months age groups could however, be linked to amyloid deposition. The

elevated levels of MI observed in TASTPM mice are in agreement with a previous *in vivo* study showing increased MI in transgenic (APP-PS1) AD mice (Marjanska et al., 2005). However, in two other studies of transgenic AD mice by ^{1}H MRS, no increase in MI was reported (Dedeoglu et al., 2004; von Kienlin et al., 2005). One study found an increase in taurine levels and postulated that this may be the equivalent of the MI increase seen in human AD (Dedeoglu et al., 2004). The increase in MI could be indicative of glial cell proliferation or microglial activation in these mice. Activated microglia have been found to be associated with the amyloid plaques in TASTPM mice (Howlett et al., 2004). The TASTPM mice and APP-PS1 mice contain the same double mutant APP_{swe} (K671N; M671L) mutation (Richardson et al., 2003; Marjanska et al., 2005). The PS1 mutations incorporated are slightly different, the TASTPM contains the M146V variant (Howlett et al., 2004), the APP-PS1 contains the M146L variant (Marjanska et al., 2005). The functions of MI in osmoregulation and membrane metabolism mean that higher MI levels may cause disruption of normal function (Beacher et al., 2005). MI is also a precursor in the formation inositol trisphosphate and therefore can affect neuronal calcium signalling (Berridge, 1993). Calcium signalling modulates aspects of brain development and function, including neurotransmission, learning and memory (Berridge et al., 2000). The presence of elevated MI may be causing some of the problems, as opposed to being merely a marker. However, the fact that there was no age-dependence of the difference in MI suggests that it may be a disease marker but would not act as a biomarker of disease progression in this model.

Consistently lower levels of succinate in TASTPM mice could be indicative of impaired neuronal energy production or of mitochondrial dysfunction in these mice. The effect appears to be a genotype effect, as succinate is lower in TASTPM mice at all time points. As amyloid plaques are not detectable at 3 months, it would appear that lower succinate is independent of amyloid plaque formation. There is evidence that intraneuronal Aβ accumulation could be responsible for early pathological changes, prior to amyloid plaque formation

(Bayer et al., 2008). Mitochondrial dysfunction and impaired neuronal energy production have also been observed in human AD (Valla et al., 2001; Zhu et al., 2004; Moreira et al., 2007). Data from frozen tissue samples has shown that the posterior cingulate cortex in AD patients has reduced cytochrome oxidase (CO) activity (Valla et al., 2001). CO is a mitochondrial enzyme essential for aerobic energy metabolism. This reduction appears to be linked to disease duration (Valla et al., 2001). Another study found increased CO and lipoic acid in the cytoplasm of neurons of AD sufferers, lipoic acid was also found in autophagic vacuoles. This suggests that mitochondria undergo increased autophagic degradation in AD sufferers (Moreira et al., 2007). Positron emission tomography (PET) has shown reduced cerebral glucose metabolism in AD patients as well as patients thought to be at risk of developing AD (Drzezga et al., 2003).

Glutamate and glutamine levels were not significantly different between the two strains, this does not agree with the *in vivo* studies, all of which found reduced glutamate levels (compared with total creatine) in older mice (Dedeoglu et al., 2004; Marjanska et al., 2005; von Kienlin et al., 2005). The signal from succinate combines with the glutamate signal *in vivo* due to the broad linewidths of *in vivo* MRS. It is possible that these studies were detecting reduced succinate and interpreting this as reduced glutamate levels. It is also possible that the specific brain regions observed had reduced glutamate, which was masked in this study by whole brain usage.

The slightly higher levels of GPC in the TASTPM mice may indicate differences in cell membrane composition. Decreased choline levels in the 6-12 month TASTPM mice could indicate problems with acetylcholine neurotransmission, or perturbation of phospholipid metabolism or cell membrane changes. Altered phospholipid metabolism has been observed in human AD (Kuo et al., 1998; Notkola et al., 1998; Roher et al., 1999; Sparks et al., 2000).

We did not observe decreased NAA levels in older TASTPM mice, though this might be expected on the basis of human data. Although it is possible a difference may be masked by the fact that we used whole brains in this study, amyloid deposition is extensive throughout the brains of TASTPM mice (Howlett et al., 2008). Pathology directly related to amyloid deposition would, therefore be expected to occur throughout the brain. Specific brain areas were targeted in the *in vivo* studies which showed a decrease (Dedeoglu et al., 2004; Marjanska et al., 2005; von Kienlin et al., 2005). All these studies used creatine as the reference metabolite. If creatine is used as the reference metabolite in this study, a decrease in NAA is detected in older TASTPM mice and a significant effect of strain, age and a strain x age interaction ($p<0.0001$) are detected by ANOVA. As the *in vivo* studies used creatine as a reference metabolite, believing it to be stable across age and strain, there is potential this could lead to detection of changes in NAA which may have been influenced by increased creatine signal. The sensitivity of the study to detect changes in NAA would have produced a significant result given ~20% decrease in TASTPM NAA in the 15 and 18 month groups. As the mean NAA actually increased, it is safe to say no decrease in NAA occurs in the TASTPM mice with age.

Increased creatine levels in older TASTPM mice were not expected. Although if there is extensive glial cell proliferation the relatively higher levels of creatine in astrocytes (Urenjak et al., 1993) could be a factor. Increasing creatine levels have also been linked with cognitive decline in elderly humans (Ferguson et al., 2002). A possible reason for the apparent increase could be osmotic stress in these mice (Lien et al., 1990). It is possible that, as plaque load increases in older TASTPM mice, the huge amount of Aβ interferes with normal osmoregulation in the brain. The observed increase indicates that care should be taken when using creatine as a reference metabolite. If creatine ratios were used in this case the results would have indicated a decrease in NAA in the TASTPM mice in the older age group, which could lead to misinterpretation.

The potential for this whole brain study to have masked localised changes in metabolic levels is highlighted by another *in vitro* study carried out on dissected brains of AD transgenic mice (Salek et al., 2010). In this study, decreases in NAA, glutamate, glutamine, taurine, GABA, creatine, choline and succinate were observed in the hippocampus, cortex, frontal cortex and midbrain of TgCRND8 AD transgenic mice. These results indicate the possibility of neurodegeneration as well as disrupted neuronal metabolism in the affected areas.

The brains of mice increase in size with age, in contrast to humans (Maheswaran et al., 2009). Brain growth over time has been shown to be greater in TASTPM mice than their wild type counterparts (Maheswaran et al., 2009). This is especially evident in grey matter rich areas such as the hippocampus and thalamus, in wild type mice there is little or no growth in these areas, with white matter and ventricular enlargement being responsible for the overall increase in size. As different brain regions contain varying concentrations of metabolites, the differential growth of these regions may cause some inaccuracy in this study. However, the brain regions displaying altered growth show marked amyloidosis and astrogliosis (Maheswaran et al., 2009). The increased size does not necessarily indicate altered functionality, but appears to be an inflammatory response to increasing amyloidosis. Additionally, though we observed increasing brain weights right up to the 18 month time point, there was no significant difference between the brain weight of wild type and TASTPM mice. Finally, normalising results to brain weight before analysis removes this as a confounding factor. Therefore I do not believe the differential brain growth between the two strains has a significant effect on the results of this study.

In this study, evidence for a specific disease responsive biomarker was sought. Although some findings were encouraging, with succinate levels being the most promising, the search for conclusive proof of such a biomarker goes on.

Chapter 3. A Comparison of the lipid content of TASTPM and normal mouse brain by ^{1}H MRS of chloroform-methanol extracts

3.1. Introduction

There is strong evidence linking phospholipid, and particularly cholesterol metabolism and handling to AD which prompted the following study of phospholipid profiles in normal and TASTPM mice. This evidence is summarised below.

The apolipoprotein E (ApoE) ε4 allele is a genetic risk factor for late onset AD (LOAD) (Strittmatter et al., 1993). The major function of ApoE is to redistribute lipids and to maintain lipid and cholesterol homeostasis. ApoE mRNA has been found at significantly higher levels in the brains of AD patients (Yamagata et al., 2001). ApoE has been localised by immunohistochemistry to amyloid plaques (Harr et al., 1996). Carriers of the ε4 allele have been found to have consistently higher serum levels of triglycerides and cholesterol compared to peers who carry a different allele (Davignon et al., 1988a). Cholesterol uptake, when bound to ApoE4 was found to be less efficient than with other isoforms (E2 and E3) in cultured neurons *in vitro* (Rapp et al., 2006). ApoE4 also appears to be the least efficient of the three isoforms in promoting cholesterol efflux from neurons in culture (Michikawa et al., 2000).ε4 allele carriers are also thought to be at higher risk of coronary artery disease and atherosclerosis (Davignon et al., 1988b).

High serum total cholesterol and LDL cholesterol have been found to correlate positively with prevalence of AD and amount of Aβ42 in the brain (Kuo et al., 1998; Notkola et al., 1998).AD patients have been found to have higher total and LDL cholesterol, as well as lower HDL levels compared to age-matched controls (Roher et al., 1999; Sparks et al., 2000). In cholesterol-fed experimental animals, increased production and build up of Aβ has been shown

in the brain (Sparks et al., 2000). In humans, use of 3-hydroxy-3-methylglutaryl coenzyme A reductase inhibitors, which lower serum cholesterol have been associated with decreased prevalence of AD (Wolozin et al., 2000).

Alterations in cholesterol homeostasis have been implicated as having a direct role in the pathogenesis of AD, interference with cholesterol transfer between astrocytes and synapses is thought to cause synaptic loss and, eventually neurodegeneration (Pfrieger, 2003). In AD brains a reduction in membrane cholesterol:phospholipid ratios has been discovered (Shobab et al., 2005; Stefani and Liguri, 2009). It is possible that alterations to the structure of the lipid membrane bilayer are involved in the pathogenesis of AD. Changes to the membrane could have a knock on effect on the activity and catabolism of any membrane-bound proteins, including APP.

It is possible that the increased risk of AD associated with ApoE4 is due, in part or in full, to inefficient lipid homeostasis. Perturbations of lipid homeostasis have the potential to damage synapses and neurons and, if serious enough, lead to neurodegeneration. For more detail see (Martins et al., 2009).

Choline, PC and GPC are better reporters of phospholipid metabolism than stationary phospholipids. Choline and its related compounds are essential in formation of the membrane lipid phosphatidylcholine. They are also released when phosphatidylcholine is metabolised. Differences were seen in choline and GPC levels between TASTPM and wild type mice in the aqueous fraction of the brain extracts. Thus there is potential for differences in lipid metabolism between the two strains.

For these reasons, examination of the lipid content of the brains of TASTPM AD mice was instigated. Any changes in lipid content could be markers of altered membrane composition or lipid homeostasis. If either or both of these

effects are present then it would mean the TASTPM model is expressing further hallmarks of human AD, further validating it as an AD model.

3.2. Methods

Chloroform-methanol extractions (Le Belle et al., 2002) were performed on frozen whole brains of TASTPM and wild type mice at 3, 6, 9, and 12 months of age, with 5 - 9 mice in each group. The whole frozen brains were kept under liquid nitrogen, adding chloroform and methanol (4^oC) in a ratio of 1:2 (v/v; 3 ml/g tissue) and grinding the frozen reagents and brain tissue to a fine powder with a pestle and mortar. The tissue-solvent mixture was then allowed to thaw before being transferred to Teflon centrifuge tubes and sonicated. After 15 mins in contact with the first solvent mix, a 1:1 mix of chloroform and distilled water was added (1ml/g tissue) to form an emulsion. This was followed by centrifugation at 13000rpm for 20 min. The upper (aqueous) phase was then separated from the lower (organic) phase and both fractions were dried under a stream of nitrogen gas. The aqueous fraction was then redissolved in 650µl D_2O (GOSS Scientific, UK) and the organic fraction in deuterated chloroform. The samples were pH adjusted to pH 7.0 with DCl and/or NaOD. Except where specified, reagents were obtained from Sigma, Aldrich UK.

^1H MRS was performed at 25^oC with a 9.4T Bruker Avance vertical bore magnet. Fully relaxed, one-dimensional spectra with a spectral width of 20.55ppm were acquired using a pulse-acquire sequence with the following parameters: repetition time = 6.4s, central frequency = 400MHz, sweep width = 8223.7Hz, number of data points = 32768, dwell time 121.6µs, flip angle 30^o**.** Resonance assignments were based on published chemical shifts and coupling patterns of known compounds. Peak areas were integrated using NUTS NMR Utility Transform Software (Acorn NMR) with baseline flattening around each integration region (Fig.20). Peak assignments were performed based on results published in literature (Gunstone, 1995; Kostara et al., 2010).

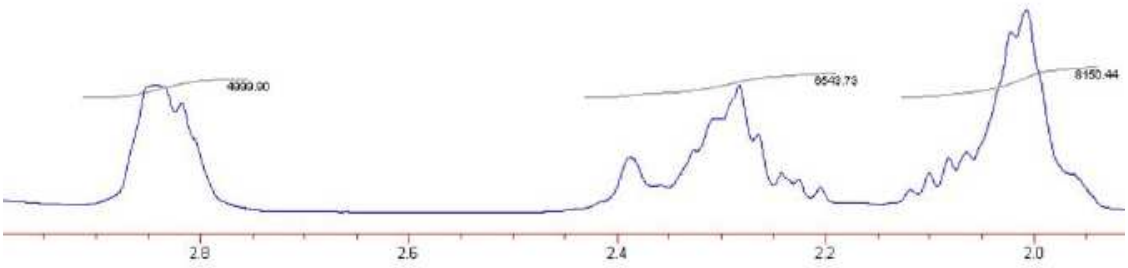

Fig.20 *Example of integration of spectrum, integrated peaks, functional groups represented from left to right: $C{=}CCH_2C{=}C$, CH_2CO and $CH_2C{=}C$*

2 way ANOVA was performed on the lipid integrals using Graphpad Prism version 3.00 for Windows (GraphPad Software, San Diego California USA). Functional groups investigated were CH=CH, CH_2OCOR, $CH_2OPO_2^-$, $(CH_3)_3$, CH_2OR, $N^+(CH_3)_3$, $CH_2NH_3^+$, CH_2CH_2CO, $CH{=}CH\text{-}CH_2\text{-}CH{=}C$, CH_2CO, $CH_2C{=}C$, $(CH_2)_n$, CH_3, Triglyceride terminal methyls and C18/19 cholesterol methyls. The $(CH_2)_n$ peak at 1.3ppm was used as a reference peak as it remained fairly constant in all spectra.

3.3. Results

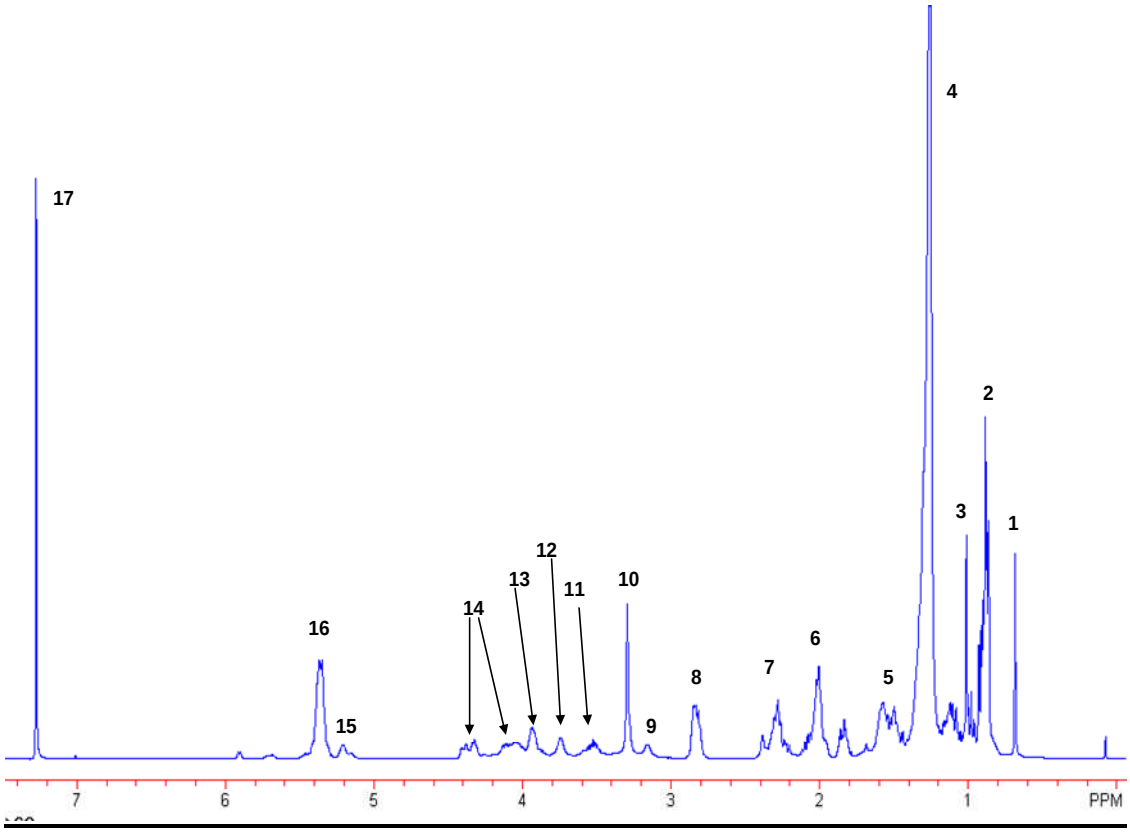

Fig.21 *Peak assignments for lipid integrals. 1 – C18/19 cholesterol methyls, 2 – triglyceride terminal methyls, 3 – CH_3, 4 – $(CH_2)_n$(used as reference peak), 5 - CH_2CH_2CO, 6 - $CH_2C{=}C$, 7 - CH_2CO, 8 – $CH{=}CH\text{-}CH_2\text{-}CH{=}CH$, 9 - $CH_2NH_3^+$, 10 - $N^+(CH_3)_3$, 11 - CH_2OR, 12 - $(CH_3)_3$, 13 - $CH_2OPO_2^-$, 14 - CH_2OCOR, 15 - CH_2OCOR, 16 - $CH{=}CH$, 17 – chloroform (undeuterated)*

The biggest resonance detected was from the methylene backbones of the lipids. We also detected cholesterol and triglyceride methyl groups, as well as phosphorylated, alkylglycerol, ketone and N-methyl head groups. Unsaturated groups were also in evidence.

14 functional groups in all were quantified and analyzed by a 2-way ANOVA (age and genotype). To reduce the likelihood of false positive results, a bonferroni correction was used, giving a significance level of $p<0.0035$. Of all

functional groups investigated, only two approached significance. In the case of CH=CH-CH_2-CH=C there was an almost significant (p=0.0069) effect of genotype, levels were consistently higher in TASTPM mice than wild type (Fig.22). Also for CH_2OR there was an almost significant (p=0.0044) effect of genotype, levels were again consistently higher in TASTPM mice than wild type, though the variance was quite high in the TASTPM groups (Fig.23). Two other lipid groups showed potential mild genotype effects, $(CH_3)_3$ and CH_2CO both appeared to be higher in 12 month old TASTPM mice compared with wild type, the significance level in both cases was p =0.01.

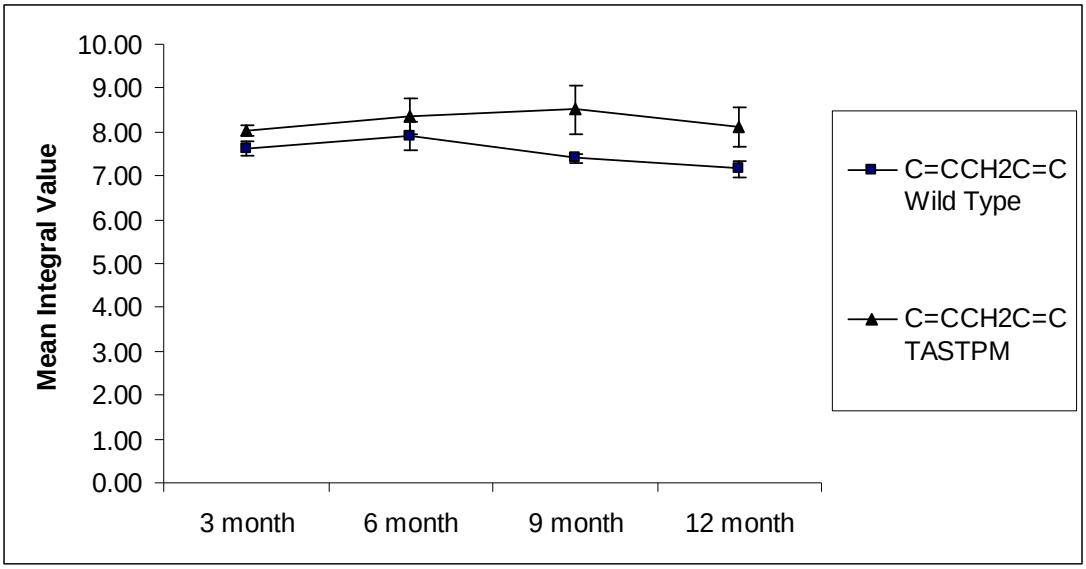

Fig.22 *CH=CH-CH_2-CH=C levels in TASTPM and wild type mice, error bars represent S.E.M.*

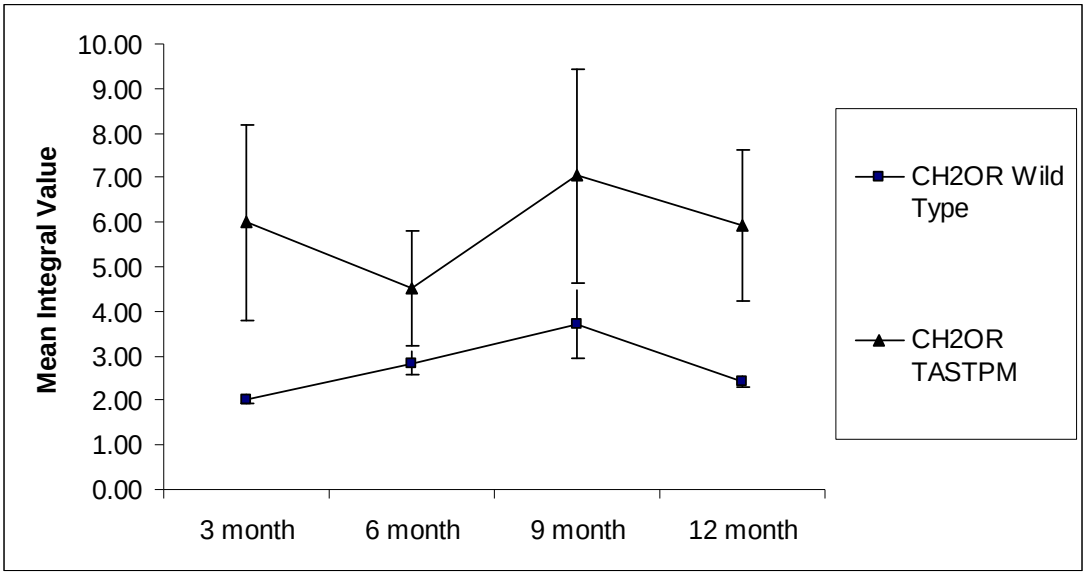

Fig.23 *CH_2OR levels in TASTPM and wild type mice, error bars represent S.E.M.*

		3 month			6 month		
Lipid	Chemical Shift	Mean	S.D	CoV	Mean	S.D	CoV
Chloroform WT	7.34-7.20	4671	3174	67.9	1829	1530	83.6
Chloroform T	7.34-7.20	1643	1013	61.6	1626	874	53.7
CH=CH WT	5.49-5.28	8331	2088	25	7958	1483	18.6
CH=CH T	5.49-5.28	7916	1444	18.2	8024	865	10.8
CH2OCOR WT	5.25-5.11	1170	301	25.6	1127	221	19.6
CH2OCOR T	5.25-5.11	1197	191	15.9	1240	195	15.6
CH2OCOR WT	4.45-4.01	4818	1203	24.9	5471	978	17.9
CH2OCOR T	4.45-4.01	5046	1083	21.4	5298	573	10.8
CH2OPO2- WT	3.99-3.89	2465	589	23.9	2519	445	17.7
CH2OPO2- T	3.99-3.89	2594	495	19.1	2745	504	18.3
(CH3)3 WT	3.8-3.7	1432	332	23.1	1569	279	17.7
(CH3)3 T	3.8-3.7	1667	399	23.9	1750	452	25.8
CH2OR WT	3.59-3.46	1307	292	22.4	1776	563	31.7
CH2OR T	3.59-3.46	3991	4222	105.7	3019	2794	92.5
N+(CH3)3 WT	3.34-3.26	4290	935	21.8	4173	746	17.9
N+(CH3)3 T	3.34-3.26	4439	915	20.6	4303	628	14.6
CH2NH3+ WT	3.2-3.11	1482	394	26.6	1344	213	15.9
CH2NH3+ T	3.2-3.11	1337	243	18.1	1408	273	19.3
C=CCH2C=C WT	2.92-2.75	4976	1455	29.2	4939	1276	25.8
C=CCH2C=C T	2.92-2.75	5014	724	14.4	5497	1295	23.5
CH2CO WT	2.42-2.18	6210	1521	24.5	5942	1125	18.9
CH2CO T	2.42-2.18	6126	1041	17	6173	856	13.9
CH2C=C WT	2.13-1.93	7390	1836	24.8	7295	1453	19.9
CH2C=C T	2.13-1.93	7245	1198	16.5	7515	1100	14.6
CH2*CH2CO WT	1.64-1.43	8674	1917	22.1	8717	1824	20.9
CH2*CH2CO T	1.64-1.43	8803	1379	15.7	8895	1421	16
CH3 WT	1.04-0.97	4180	831	19.9	4198	964	22.1
CH3 T	1.04-0.97	4122	755	18.3	4107	553	13.4
Triglyceride terminal methyls WT	0.95-0.83	15175	3118	20.5	14686	3064	20.9
Triglyceride terminal methyls T	0.95-0.83	14450	2453	17	14665	1853	12.6
C18/19 cholesterol methyls WT	0.71-0.65	1986	446	22.5	2120	551	26
C18/19 cholesterol methyls T	0.71-0.65	1983	454	22.8	1939	346	17.8

		9 month			12 month		
Lipid	Chemical Shift	Mean	S.D	CoV	Mean	S.D	CoV
Chloroform WT	7.34-7.20	1088	384	35.3	2563	2122	82.8
Chloroform T	7.34-7.20	1639	459	28	2175	786	36.1
CH=CH WT	5.49-5.28	7361	2301	31.3	7423	1714	23.1
CH=CH T	5.49-5.28	7551	1304	17.3	6677	1822	27.3
CH2OCOR WT	5.25-5.11	1114	310	27.8	1077	219	20.4
CH2OCOR T	5.25-5.11	1171	173	14.8	1015	257	25.2
CH2OCOR WT	4.45-4.01	5043	2006	39.8	4814	1134	23.6
CH2OCOR T	4.45-4.01	4829	1091	22.6	4563	1103	24.1
CH2OPO2- WT	3.99-3.89	2453	808	32.9	2345	490	20.9
CH2OPO2- T	3.99-3.89	2521	424	16.8	2277	408	17.9
(CH3)3 WT	3.8-3.7	1558	550	35.2	1446	304	21
(CH3)3 T	3.8-3.7	1613	352	21.7	1450	256	17.7
CH2OR WT	3.59-3.46	2254	1143	50.7	1479	418	28.2
CH2OR T	3.59-3.46	4674	4536	97.1	3041	2780	91.4
N+(CH3)3 WT	3.34-3.26	4086	1272	31.1	3995	922	23.1
N+(CH3)3 T	3.34-3.26	4155	786	18.9	3317	1113	33.6
CH2NH3+ WT	3.2-3.11	1417	304	21.5	1289	359	27.9
CH2NH3+ T	3.2-3.11	1448	389	26.8	1093	269	24.5
C=CCH2C=C WT	2.92-2.75	4424	1121	25.3	4315	783	18.1
C=CCH2C=C T	2.92-2.75	5397	1197	22.2	4327	897	20.7
CH2CO WT	2.42-2.18	5562	1431	25.7	5622	1213	21.6
CH2CO T	2.42-2.18	6129	1043	17	5589	1374	24.6
CH2C=C WT	2.13-1.93	6934	1788	25.8	7033	1506	21.4
CH2C=C T	2.13-1.93	7575	1230	16.2	6511	1585	24.3
CH2*CH2CO WT	1.64-1.43	8168	1787	21.9	8359	1819	21.7
CH2*CH2CO T	1.64-1.43	9359	1639	17.5	7635	2140	28
CH3 WT	1.04-0.97	3748	943	25.1	3955	1064	26.9
CH3 T	1.04-0.97	4135	765	18.5	3763	1101	29.3
Triglyceride terminal methyls WT	0.95-0.83	13369	3514	26.3	14160	3460	24.4
Triglyceride terminal methyls T	0.95-0.83	14498	2279	15.7	13030	3461	26.6
C18/19 cholesterol methyls WT	0.71-0.65	1773	540	30.5	1918	609	31.7
C18/19 cholesterol methyls T	0.71-0.65	1900	450	23.6	1904	580	30.5

Table 4. *Mean Integral values, along with standard deviation and coefficient of variance for all measured lipid functional groups at all time points. T – TASTPM mice, WT – Wild type mice*

3.4. Discussion

The use of the methylene peak as a reference appears to compensate well for spectrometer variability between spectra. The coefficients of variance for the functional groups are, for the most part very good (Table.4), with one notable exception, the CH_2OR group, this may be an artefact. The detection accuracy for most of the functional groups appears to be excellent.

Although no significant differences were found in brain lipid content between the two strains of mice, all the groups which approached significance had one thing in common. In all cases the lipid signal was higher in the TASTPM mouse brains than their wild type counterparts.

The apparent increased lipid signal for unsaturated lipid, alkylglycerol, triglyceride methyl groups and ketone groups indicates the possibility of alterations either lipid homeostasis or membrane composition, especially in older TASTPM mice. If this is the case then the TASTPM mice are displaying another of the factors in AD pathology.

A problem arises in that, while appearing to display a trend, the data are not significant. There may be several reasons for this.

One reason is that the entire lipid content of the brain was extracted and analysed. It is quite possible that any perturbations in membrane composition or lipid metabolism would be localised to specific areas such as the hippocampus or thalamus. If this is the case then larger, compartmentalized changes might not be detected due having been combined with less affected areas.

As we can only detect lipid functional groups, rather than whole lipid molecules using this technique, it is possible that there are differences which are disguised by this shortcoming. HPLC analysis of the samples may yield more

useful information. The fact remains that there were differences in choline and its related compounds between the two strains. Thus there remains the potential for differences to be found in lipid metabolism, along with the potential for lipid metabolism being responsible for the pathogenic changes observed in the TASTPM mice.

Potential future work could include HPLC analysis of organic samples from extracts to determine precise lipid content, as well as isolating more specific brain regions to look for regional differences.

Chapter 4. Longitudinal ^{1}H MRS of TASTPM and wild type mice *in vivo* with concurrent T1 measurement and behavioural analysis

4.1. Introduction

There is a need to develop a biomarker for AD, to aid in drug development, treatment monitoring, diagnosis and patient management. An ideal biomarker must be easy to measure non-invasively, related to disease progression and specific for AD. There is currently no such definitive biomarker for AD. Magnetic resonance imaging (MRI) observation of AD patients has found atrophy, increasing in severity with disease progression (Frisoni et al., 2010), however brain atrophy is not specific to AD. A proton magnetic resonance spectroscopy (^{1}H MRS) scan could be performed during the same session as an MRI scan, only adding approximately 10 mins to scan time. If a ^{1}H MRS biomarker could be found, a more robust diagnosis could potentially be made. Disease progression could also be monitored more closely. A metabolic biomarker for AD could also be invaluable in treatment monitoring. If therapeutic intervention caused normalisation of the ^{1}H MRS spectrum from an AD patient this could give an early, non-invasive indication of drug efficacy.

Decreased N-acetylaspartate (NAA) and increased myo-inositol (MI) has been noted in the brains of AD patients (Shonk et al., 1995; Dixon et al., 2002; Ackl et al., 2005). NAA is thought to be a neuronal marker (Urenjak et al., 1992), MI is thought to be a marker of gliosis or microglial activation (Lazeyras et al., 1998), based on observations on cultured glial tumour cells (Brand et al., 1993). Some of these results have suggested ^{1}H MRS might be used for both diagnosis of AD and distinguishing between different dementias. AD was differentiated from frontotemporal dementia (FTD) by analysing spectra acquired from midfrontal grey matter, decreased NAA was found in FTD but not AD (Ernst et al., 1997). This regional differentiation may be present in the early stages of neurodegeneration, but may be lost as the disease progresses and neurodegeneration spreads throughout the brain (Kantarci et al., 2004; Garrard

et al., 2006). NAA/Creatine was found to be lower in white matter of patients with vascular dementia than AD (Kattapong et al., 1996). Several studies have shown positive correlation between neuropsychological cognitive test scores and NAA/Cr, MI/Cr and NAA/MI ratios (Rose et al., 1999; Jessen et al., 2000; Huang et al., 2001; Kantarci et al., 2002), suggesting ^{1}H MRS could be used to monitor disease progression. Decreased NAA can be seen in many neurological disorders, especially those involving neurodegeneration. Differentiation has been achieved by examining different regions. This may only be useful in early stage disese, before neurodegeneration becomes widespread. If another metabolic marker for AD could be discovered it could make differentiation using ^{1}H MRS easier and more accurate.

While the *in vitro* extract chapter of this thesis dealt with changes in cerebral metabolites over time in both TASTPM and wild type mice, it had two drawbacks compared with MRS *in vivo*. The first drawback is the necessary death of the animal in order to perform the extract, obviously this has limited use in human medicine other than at the post mortem stage. The second is related to this, as the animal is killed, cerebral metabolite levels over time in the same animal may not be measured. In this study, as the mice recover following anaesthesia and scanning, cerebral metabolite shifts in each mouse over time may be monitored. Previous studies *in vivo* of different AD transgenic mice have shown a decrease in NAA and glutamate, and increases in MI and taurine (Dedeoglu et al., 2004; Marjanska et al., 2005; von Kienlin et al., 2005).

We chose a 3x3x3mm voxel centred on the hippocampus and thalamus for the spectroscopy, as the hippocampus is one of the first areas affected in human AD, and because of the thalamic lesions present in older TASTPM mice (Evans et al., 2007).

Behavioural differences have been reported in both TASTPM mice (Howlett et al., 2004) and other transgenic AD mice (Holcomb et al., 1998). These

behavioural differences have never been studied along with MRS at the same time. We postulate that any behavioural changes may be mirrored by cerebral metabolite changes measured by MRS. If this were the case it would lend more credence to the link between altered behaviour and metabolic changes in AD.

In our study on brain extracts *in vitro* from TASTPM mice we found apparently increased levels of creatine, along with other metabolites in older TASTPM mice. As creatine levels are thought to be stable over time and are often used as a reference metabolite for MRS *in vivo*, this was of some concern as this increase might not be detected *in vivo*. We postulated that a reason for this apparent increase might be osmotic stress in the brains of the older mice. It is possible that in the brains of the oldest TASTPM mice, the accumulation of amyloid may interfere with normal brain osmoregulation. Metabolite levels detected by MRS have been found to increase under osmotic stress (Lien et al., 1990). As T1 is related to the water content of tissue (Fatouros and Marmarou, 1999), T1 measurements of all the brains of the mice at all age groups were also undertaken in order to determine if osmotic stress is indeed a factor.

During the course of the experiments, it was noted that the amino acid alpha proton peak at 3.74 ppm, which usually mostly represents glutamate (Govindaraju et al., 2000) was larger than would be expected if just caused by glutamate (Fig. 25 and 26). This effect has also been observed in previous MRS studies of transgenic AD mice (Marjanska et al., 2005; Oberg et al., 2007). In order to investigate this, scans using variable repetition times were performed to check saturation factors of metabolite peaks.

4.2. Methods

4.2.1. MR Spectroscopy and T1/T2 Mapping Scans

TASTPM and wild type mice in 3 age groups were used. Initial ages were 3 months, 9 months and 15 months. MRS was performed on all groups at 0, 2

and 4 month time points, meaning mice in 3 – 19 month age groups were scanned at 2 month intervals. Initial group sizes were 8 mice per group, but some of the TASTPM mice died over the time so group sizes for the 17 and 19 month TASTPM were down to 5.

Mice were anaesthetised using a mixture of oxygen and isoflurane. For induction the mixture was 5% isoflurane, for maintenance the mixture was 1.5-2.5% isoflurane. Induction of anaesthesia was carried out in a sealed box with tubing delivering and removing the anaesthetic mixture at 1l/min. Once anaesthetised the mice were placed on the scanner animal bed in supine position with the heads within a nosecone for delivery of anaesthetic within the scanner. Respiration rate was monitored constantly using a Graseby Medical MR10 respiration monitor (Graseby Medical Ltd, UK). Body temperature was monitored constantly throughout scan time using an RS 206-3722 RS Components Ltd. UK) temperature monitor, with an RS K coupling and a filter built in-house connected to an anally-inserted temperature probe.

MRS was performed on a 7T Magnex 7T/160/AS magnet with a horizontal bore (Magnex Scientific Ltd, Oxfordshire, UK) equipped with a 90mm (BGA9-S) internal diameter gradient set (maximum gradient strength 740mT/m). A volume coil was used for excitation and a rat brain surface coil for signal detection. The whole system was run from a Bruker Avance III console (Bruker, Karlsruhe, Germany).

Initially a scout was performed to confirm the position of the animal in the magnet. This was followed by a FLASH (Fast Low Angle Shot) gradient-echo sequence oriented for a series of coronal slices in order to obtain images for accurate voxel positioning. The parameters of this sequence were: slice thickness 1mm, interslice distance 1mm, No. of slices 9, flip angle 40^0, TR 350ms, TE 5.4ms, FOV 3cmx3cm, bandwidth 44642.9Hz. A 3x3x3mm voxel was placed so as to be over the hippocampus and thalamus (Fig.24), this voxel

was then shimmed using Bruker FASTMAP (Gruetter, 2005), which performs a linear shim, followed by a 2nd order shim, then a second linear shim. Shim quality was tested by water peak linewidth estimation in a non-water suppressed spectrum, any value over 14Hz was re-shimmed.

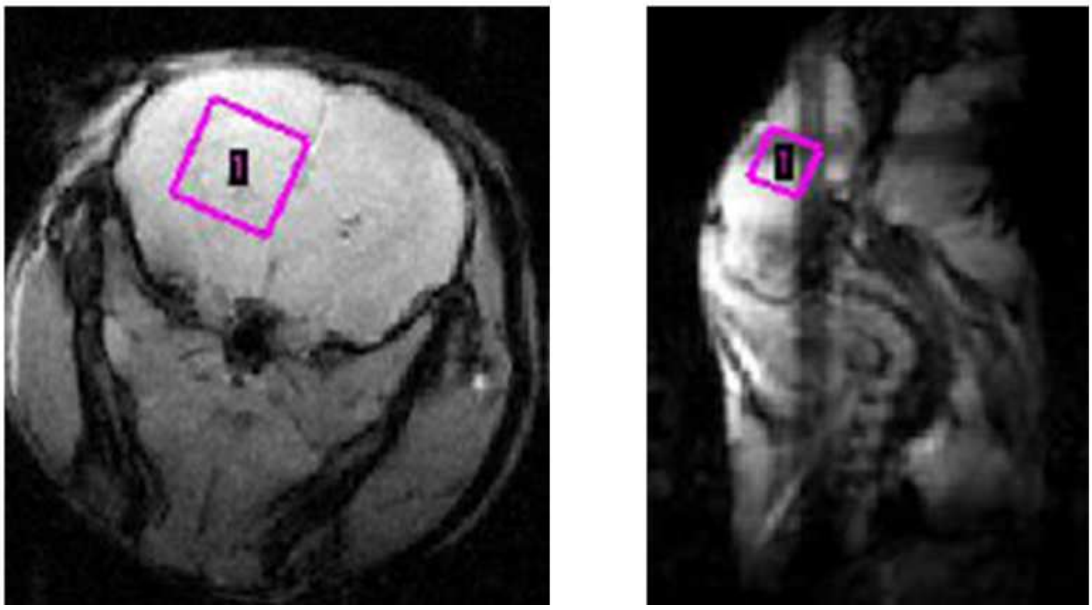

Fig.24 *Example images showing voxel placement. Left image shows coronal slice, right image shows axial slice*

Following this PRESS was performed with the following parameters: TR 2500ms, TE 20ms, No. of averages 512, flip angle 90^0, No. of data points 2048, spectral width 13.35ppm, dwell time 124.8μs, bandwidth 4006.41Hz. Water presaturation was achieved using VAPOR. The total acquisition time for one spectrum was 21'20".

For T1/T2 mapping a single coronal slice T1/T2 map was obtained centred on the hippocampus and thalamus. To obtain this map a RARE sequence was used with the following parameters: effective TE values 11, 33, 55, 77 and 99ms, TR 5000, 3000, 1500, 800, 400 and 200ms, RARE factor 2, No. of repetitions 1, No. of echo images 5, refocusing flip angle 180^0, effective bandwidth 44642.9Hz, FOV 20mmx20mm, spatial resolution 0.156mm/pixel, matrix size 128x128, slice thickness 1mm.

The saturation factor experiments used 4 mice and performed PRESS in the same way as described above, but used TR values of 2500, 5000, 10000 and 20000 ms to check saturation factors.

4.2.2. MRS Quantitation

Analyisis of the spectroscopic data was performed using QUEST (Ratiney et al., 2005), part of the jMRUI software package (Stefan et al., 2009). An initial metabolite basis set was obtained using the routine NMRSCOPE which uses quantum mechanics to simulate time domain signals from metabolites under the pulse sequence conditions *in vivo*. The following metabolite signals were simulated - NAA, MI, phosphocholine (to represent choline-containing compounds), glutamate, glutamine, taurine and creatine. Additional peaks at 1.3 and 0.9 ppm were added to the basis set, these were simulated using simple lorentzian lineshapes to represent the macromolecule resonances at 1.3 and 0.9 ppm to aid with spectral fitting. Spectra were phased prior to analysis and any residual water peak was manually removed using the HLSVD routine in jMRUI. Background estimation was carried out as part of the analysis. Three different references were used for quantification - creatine, water and the sum of a selection of metabolites (creatine, MI, NAA, glutamate, phosphocholine and taurine).

4.2.3. T1/T2 mapping Analysis

Using ParaVision 5 (Bruker, Karlsruhe, Germany), the images acquired from the RARE T1/T2 sequence were used to generate T1 and T2 parametric maps. Areas in the hippocampus, thalamus and cortex were selected and T1 and T2 values were obtained from each region (Fig.25)

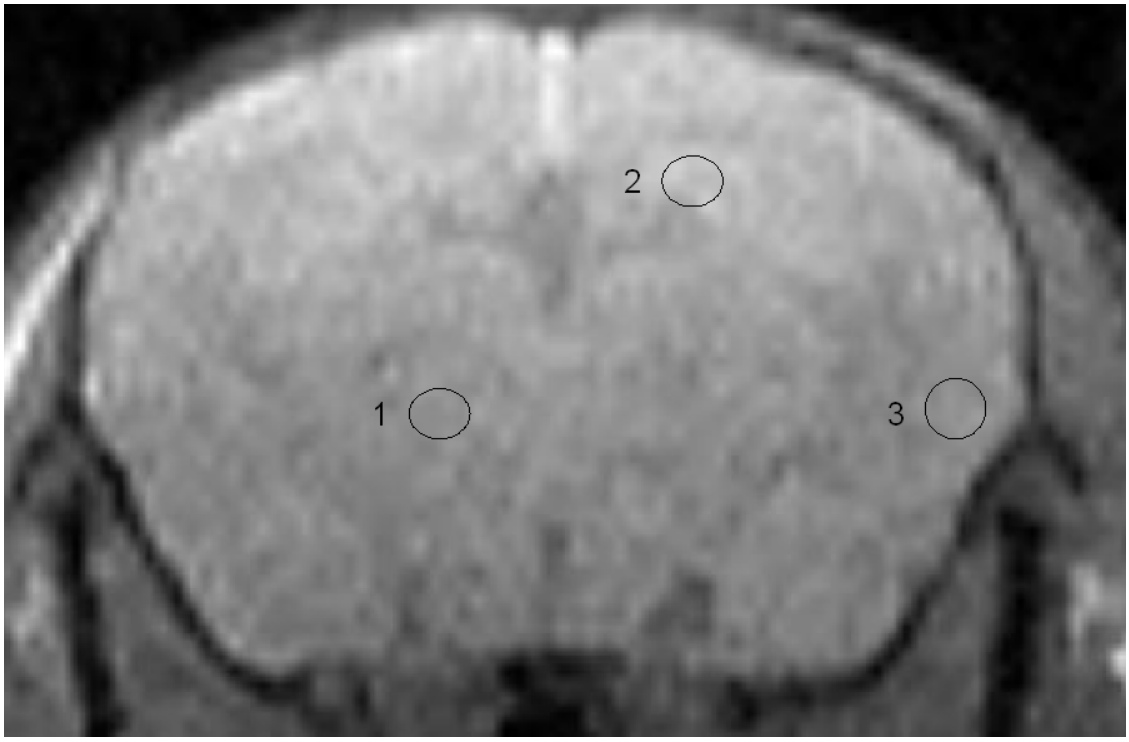

Fig.25 *Image from RARE T1/T2 sequence showing areas from which T1 and T2 values were obtained. 1 – thalamus, 2 – hippocampus, 3 - cortex*

4.2.4. Y Maze

TASTPM and wild type mice in 3 age groups were used. Initial ages were 3 months, 9 months and 15 months. Y maze testing was performed on all groups at 0, 2 and 4 month time points, meaning mice in 3 – 19 month age groups were tested at 2 month intervals. There were 4 mice per group and these animals were not used for MRI, as repeated anaesthesia could potentially have affected behaviour in the maze.

Mice were placed in the centre of the Y maze and their movements were tracked for 8 minutes. Each arm of the maze was marked internally for recognition purposes. Entry into each arm of the Y maze was noted and counted, only full entry into an arm was counted. Exploratory behaviour was investigated by observing how well the mice appeared to remember where they had already been. In other words if a mouse had just been in arm B, then arm

C then logically next it should explore arm A, if the mouse does this, it is known as a repeating triplet.

4.2.5. Statistical analysis

2-way ANOVA (age x genotype) was carried out on all metabolite amplitudes, T1 and T2 values from the hippocampus, thalamus and cortex, and number of moves and repeating triplets from the Y maze. Analysis was performed using Graphpad Prism version 3.00 for Windows (GraphPad Software, San Diego, California, USA).

ANOVA was performed on all age groups combined, but the groups were split to contain groups of mice of the same age tested repeatedly (3 – 7, 9 – 13 and 15 – 19 months).

4.3. Results

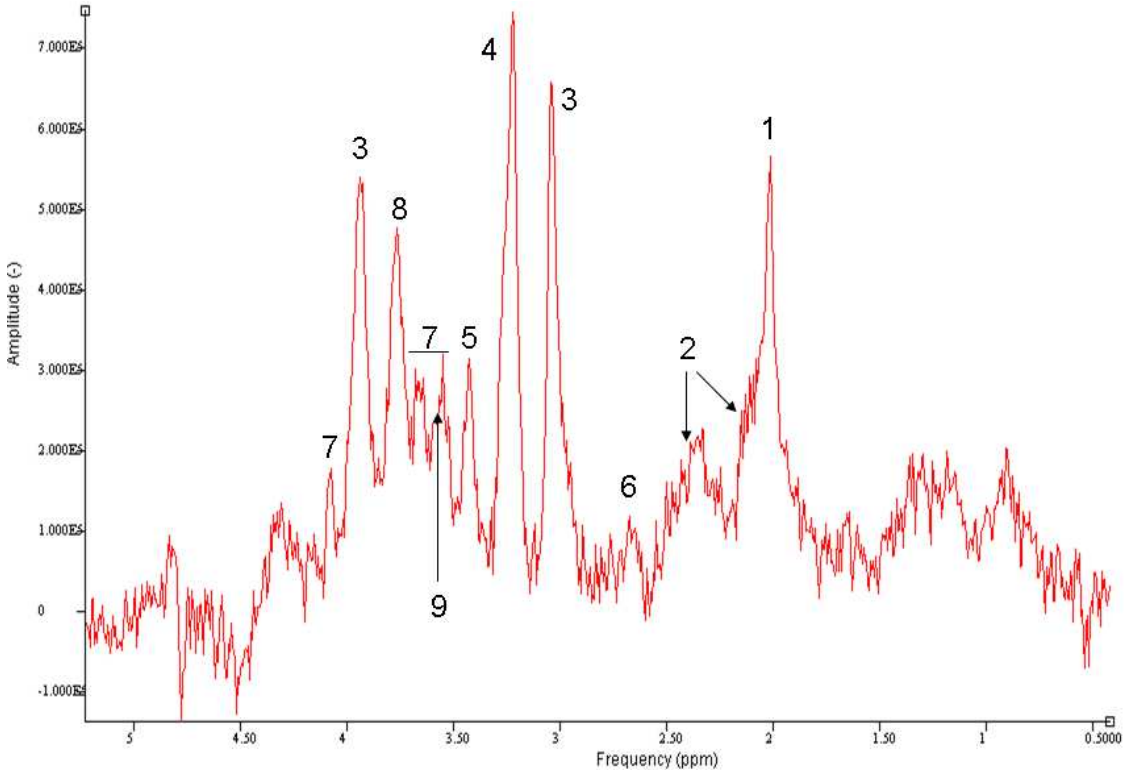

Fig.26 *Example spectrum from a 13 month old TASTPM mouse with peak assignments. 1 – NAA, 2 – Glx, 3 – Creatine, 4 – Choline containing compouns, 5 – Taurine, 6 - NAA aspartyl protons, 7 – MI, 8 – amino acid alpha protons, 9 – glycine coresonates with MI at 3.55ppm. Example has 3Hz line broadening*

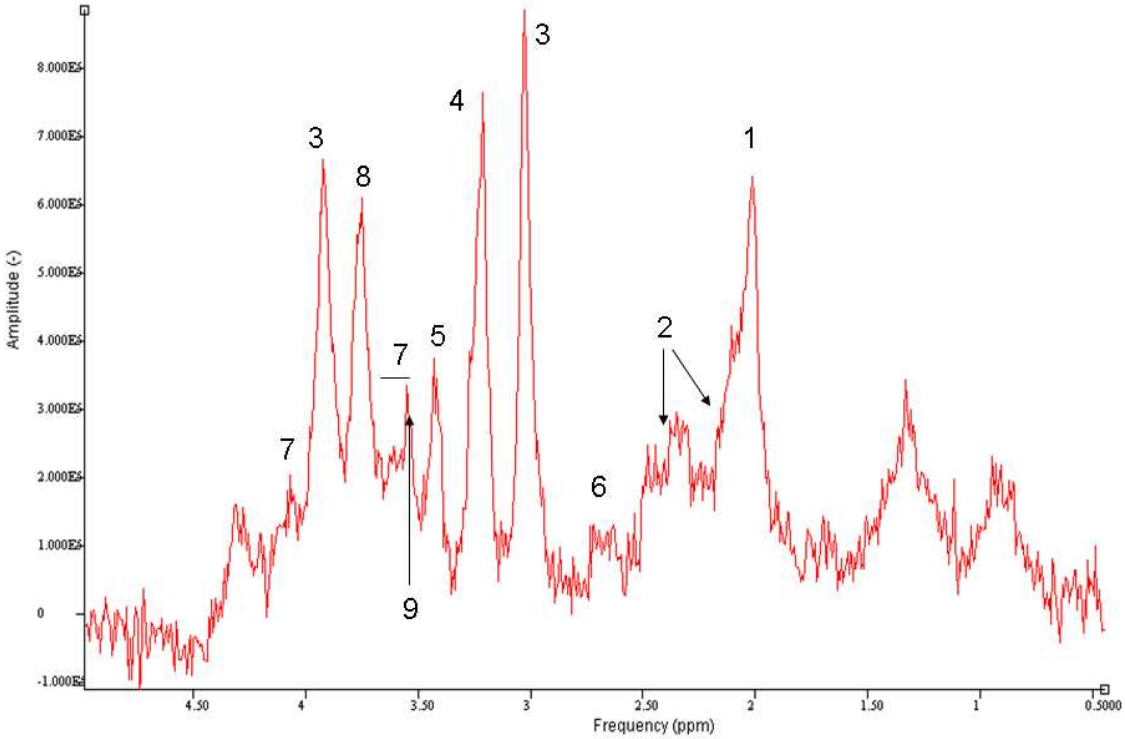

Fig.27 *Example spectrum from a 13 month old wild type mouse with peak assignments. 1 – NAA, 2 – Glx, 3 – Creatine, 4 – Choline containing compouns, 5 – Taurine, 6 - NAA aspartyl protons, 7 – MI, 8 – amino acid alpha protons, 9 – glycine coresonates with MI at 3.55ppm. Example has 3Hz line broadening*

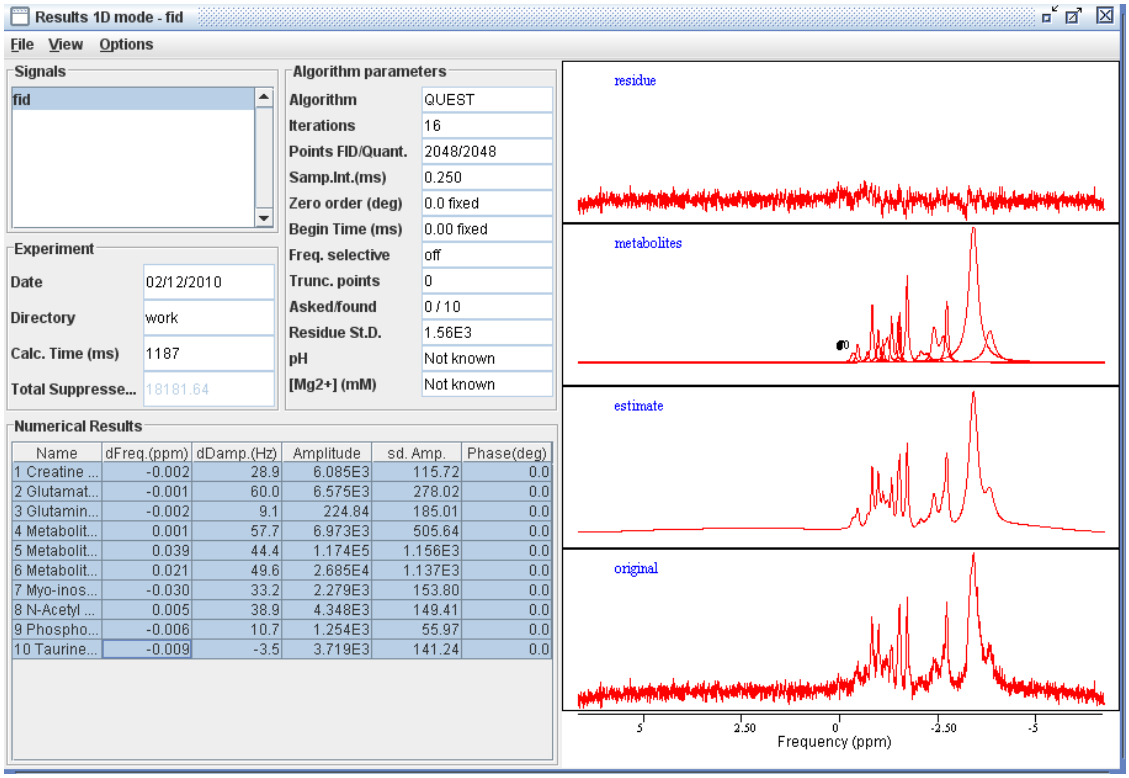

Fig.28 *Example of the fit obtained using QUEST to quantify a spectrum from a 17 month TASTPM mouse*

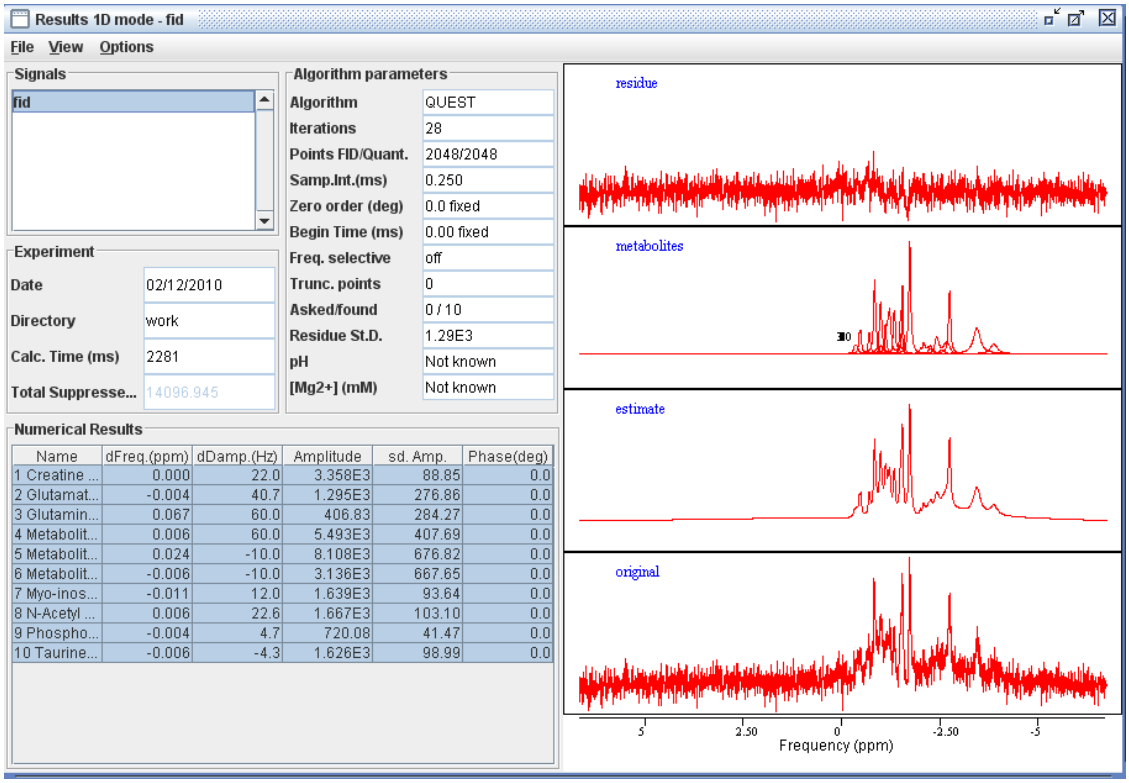

Fig.29 *Example of the fit obtained using QUEST to quantify a spectrum from a 19 month wild type mouse*

Good quality spectra, suitable for quantitative analysis were acquired in all cases except one spectrum which showed low signal-to-noise for unexplained reasons. Examples of spectra from mice of different strains are shown in Fig.26 and 27 A good indication of spectral quality and consistency is the metabolite linewidth which has been estimated for the creatine resonance in a representative set of 6 spectra. The linewidth at half height was 17.1 +/- 5.2 Hz, equivelent to 0.056 ppm. Linewidths of less than 0.1 ppm are considered essential for *in vivo* ^{1}H MRS. The resolution to baseline between choline and creatine is also indicative of good spectral quality (Kreis, 2004). Though it is unwise to place too much emphasis on the amount of signal left in the residual as an indicator of quality of fit, it can be seen that the residual is featureless with very little structure (Fig. 28 and 29). It is easy to generate a flat residual by

incorporating more features into the model, but in this case we have used known metabolites plus two macromolecule peaks.

4.3.1. Reference Selection for Spectroscopy

The three different references that were used for quantification - creatine, water and a selection of metabolites (creatine, MI, NAA, glutamate, phosphocholine and taurine) were compared and contrasted, with their comparative coefficients of variation (Table.5)(Fig.29 and 30)

	Creatine Ratio					
	3 - 7 months		**9 - 13 months**		**15 - 19 months**	
	Mean	**SD**	**Mean**	**SD**	**Mean**	**SD**
Wild Type	16.07	5.53	18.16	5.52	22.40	8.13
TASTPM	12.89	4.50	17.21	5.62	18.54	8.56

	Water Ref					
	3 - 7 months		**9 - 13 months**		**15 - 19 months**	
	Mean	**SD**	**Mean**	**SD**	**Mean**	**SD**
Wild Type	16.97	7.01	19.67	5.75	20.86	8.87
TASTPM	13.13	5.20	20.68	9.12	18.16	9.47

	Selected Metabolites					
	3 - 7 months		**9 - 13 months**		**15 - 19 months**	
	Mean	**SD**	**Mean**	**SD**	**Mean**	**SD**
Wild Type	12.75	5.44	15.26	5.97	18.47	7.68
TASTPM	11.43	6.01	14.51	6.23	15.37	8.50

Table.5 *Mean and standard deviation of coefficients of variation for different quantitation references. The table shows the mean CoV across all metabolites*

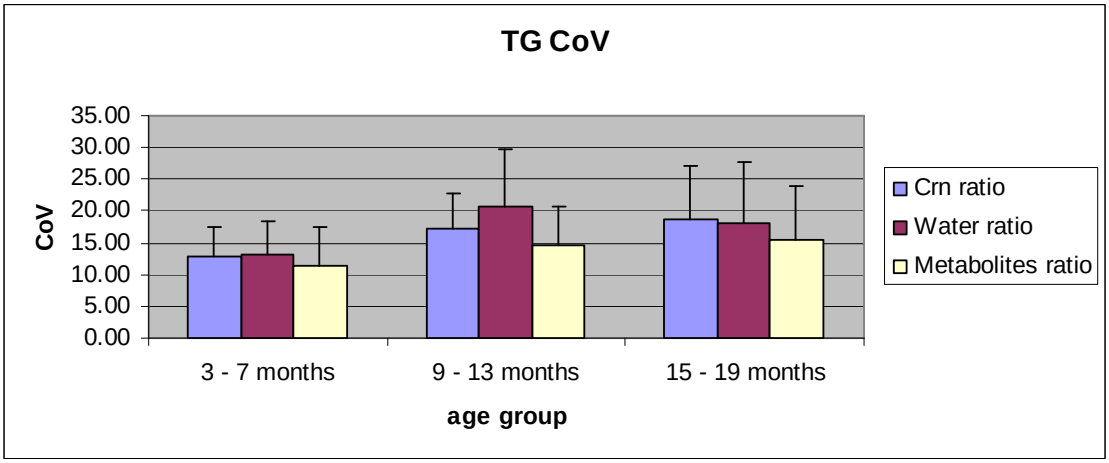

Fig.30 *Average coefficients of variation for the different age groups in TASTPM mice*

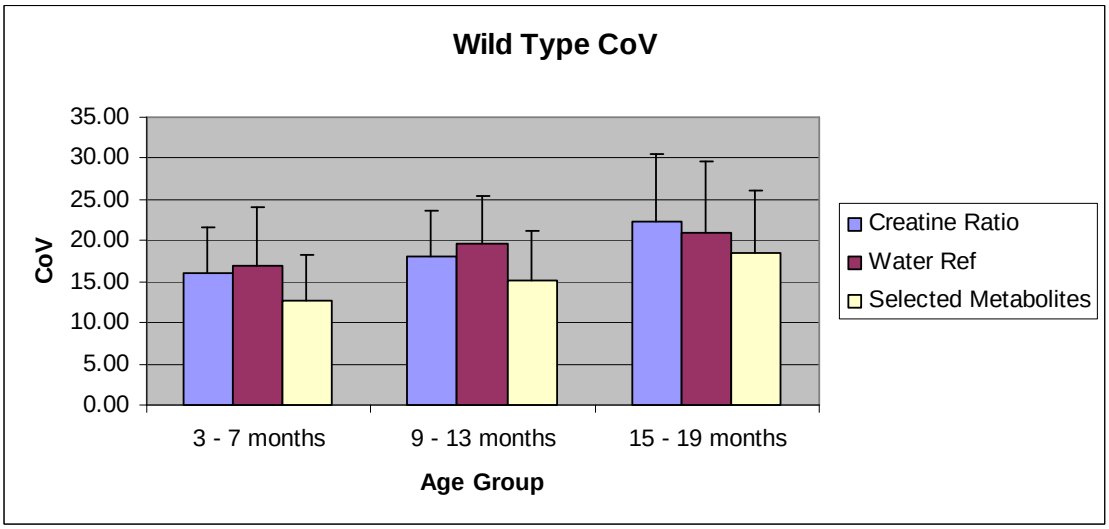

Fig.31 *Average coefficients of variation for the different age groups in wild type mice*

All the results give similar reproducibility, the preferred reference in this case is the selected metabolites because it avoids problems associated with using a separate scan for quantification referencing (as would be the case for the water reference), and allows estimation of all metabolites, including creatine. In addition the selected metabolites reference gives the lowest CoV in nearly all cases, although this is not statistically significant in any individual case (Fig. 30 and 31).

4.3.2. Spectroscopy Results

Creatine levels were higher in older TASTPM mice in our extract study (see *in vitro* chapter). So the results we obtained from this study are of particular importance. A significant effect of genotype was observed overall for creatine ($P<0.005$), as well as in the 3 – 7 ($P<0.01$) and 9 – 13 ($P<0.05$) month groups (Fig.32). Creatine is at a higher level in TASTPM mice, but this difference is most pronounced in the younger age groups, with levels being similar in middle age groups (13 and 15 months) and levels in TASTPM mice higher again in the oldest mice.

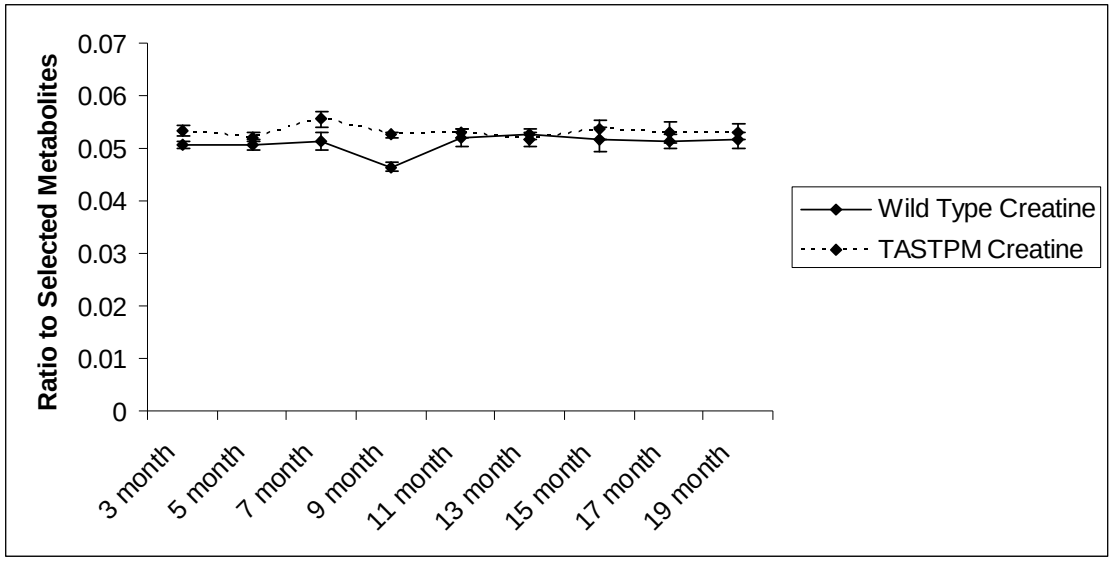

Fig.32 *Creatine ratios to selected metabolites for all age groups, values are given ± S.E.M.*

There was no difference in glutamate signal between wild type and TASTPM mice in our extract study. In this study, overall there was a significant effect of genotype ($P<0.0001$), age ($P<0.001$) and an age x genotype interaction ($P<0.05$). Glutamate levels were higher in wild type mice at all but the 13 month time point (Fig.33). In the 3 – 7 month group, there were significant effects of age ($P<0.05$) and genotype ($P<0.0001$), glutamate levels being higher in wild type mice. In the 9 – 13 month group there were significant effects of age ($P<0.01$), genotype ($P<0.01$) and an age x genotype interaction ($P<0.005$), glutamate levels appeared to be falling over time in wild type mice. In the 15 – 19 month group there was a significant effect of genotype ($P<0.001$), glutamate levels were again higher in TASTPM mice.

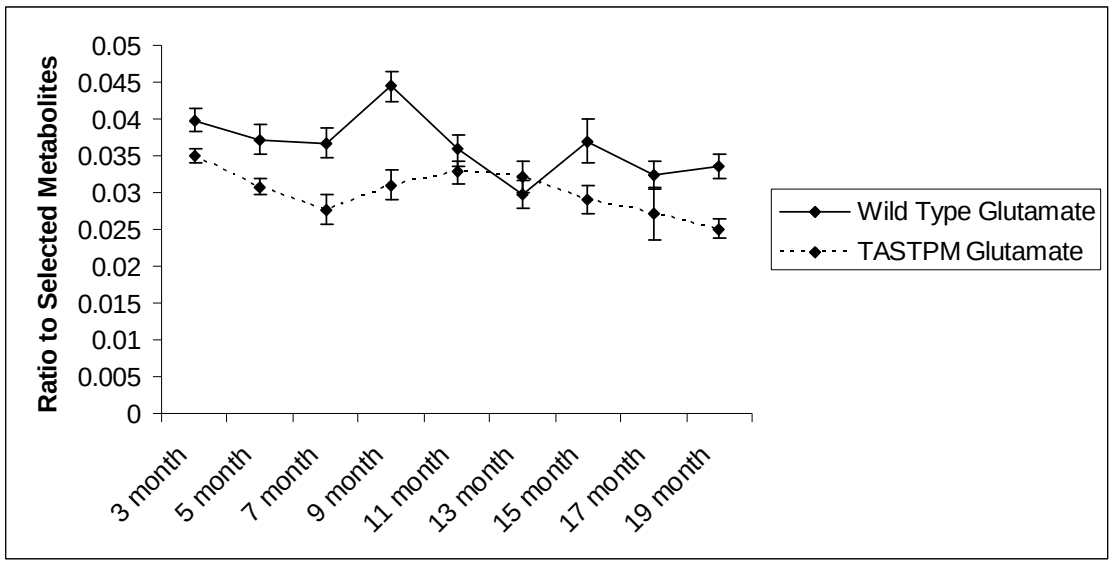

Fig.33 *Glutamate ratios to selected metabolites for all age groups, values are given ± S.E.M.*

The quantification of glutamine as a separate resonance to glutamate produce results with poor reproducibility, coefficients of variation were very high and there were no statistically significant differences found (Fig.34). In some cases, a high glutamine signal corresponded to a low glutamate signal, whereas non-detection of glutamine returned a high glutamate signal. For this reason it was decided to combine the glutamate and glutamine signals, for a combined Glx signal.

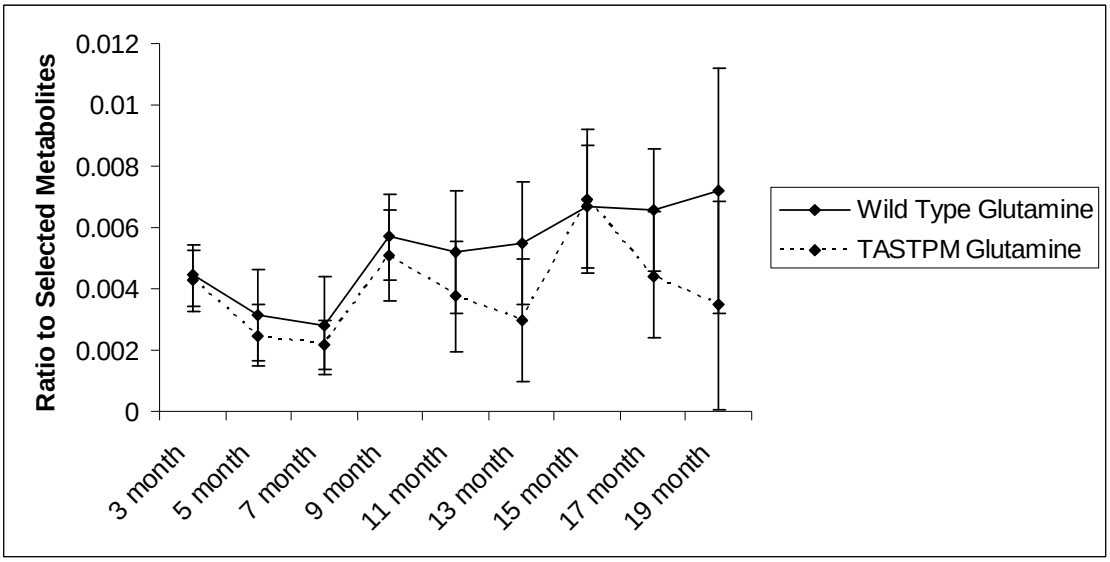

Fig.34 *Glutamine ratios to selected metabolites for all age groups, values are given ± S.E.M.*

Overall, there were significant effects of age (P<0.001) and genotype (P<0.0001) on Glx levels, with combined Glx signal higher in wild type mice at all but the 13 month time point (Fig.35). In the 3 – 7 month group, there were significant effects of age (P<0.005) and genotype (P<0.0001), Glx levels were higher in wild type mice at all time points. In the 9 – 13 month group there were significant effects of age (P<0.05), genotype (P<0.005) and an age x genotype interaction (P<0.05), Glx levels fell over time in the wild type mice. In the 15 – 19 month group there was a significant effect of genotype (P<0.0005), with Glx levels higher in wild type mice.

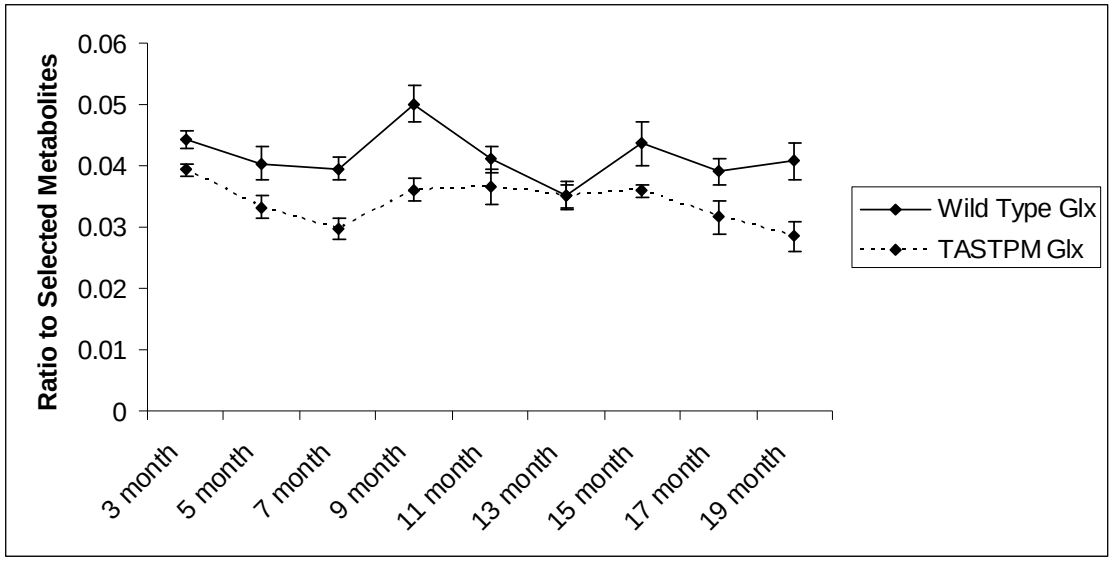

Fig.35 *Glx ratios to selected metabolites for all age groups, values are given ± S.E.M.*

Overall there was a significant effect of genotype on MI levels (P<0.0001), with MI higher in TASTPM mice at all but the 13 month time point (Fig.36). There were also significant effects of genotype in the 3 – 7 and 15 – 19 month groups (P<0.001), MI levels in both groups were higher in TASTPM mice. There were no significant differences in the 9 – 13 month group, with MI levels in TASTPM and wild type mice getting closer with age.

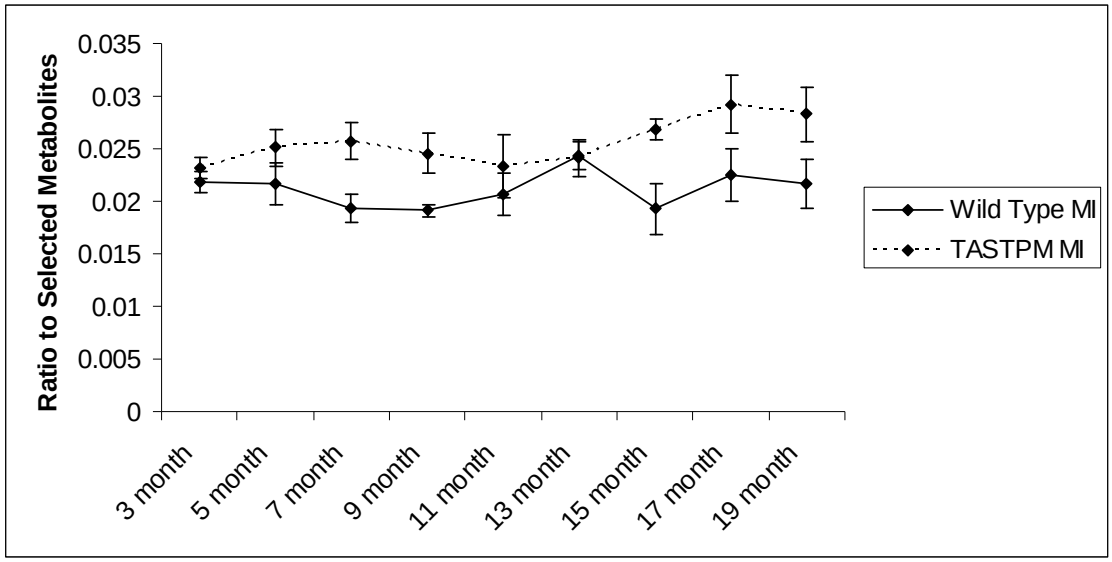

Fig.36 *MI ratios to selected metabolites for all age groups, values are given ± S.E.M.*

In our extract study, we found no significant differences in the NAA levels between TASTPM and wild type mice, this was not in agreement with other MRS studies of transgenic AD mice. Overall in this study there was a significant effect of genotype on NAA levels ($P<0.0001$), with higher levels of NAA in wild type mice (Fig.37). In the 3 – 7 month group, there were significant effects of age ($P<0.005$) and genotype ($P<0.05$), with NAA levels increasing with age steadily in wild type mice, but climbing and then falling in TASTPM mice. In the 9 – 13 month group there were significant effects of genotype ($P<0.05$) and an age x genotype interaction ($P<0.05$), with NAA levels increasing with age in TASTPM mice, and decreasing with age in wild type mice. In the 15 – 19 month group there was a significant effect of genotype ($P<0.05$), with NAA levels consistently higher in wild type mice.

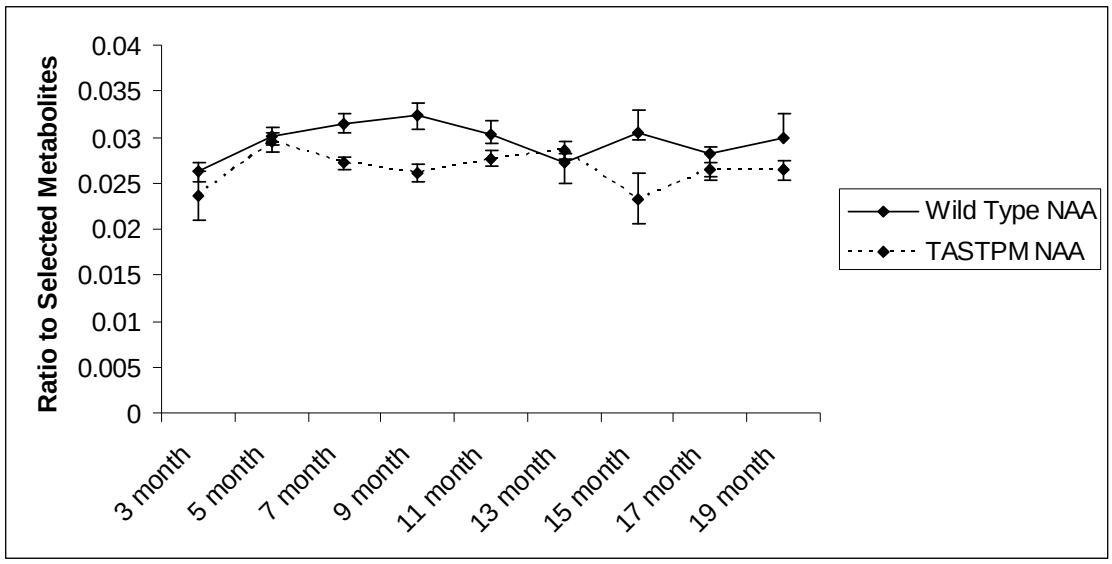

Fig.37 *NAA ratios to selected metabolites for all age groups, values are given ± S.E.M.*

Overall there were significant effects of both age and genotype (P<0.0001) on Cho levels (Fig.38), with generally higher and more stable levels of PC in TASTPM mice and lower, fluctuating levels in wild type mice. In the 3 – 7 month group there were significant effects of age (P<0.0001), genotype (P<0.01) and an age x genotype interaction (P<0.05), Cho levels increased and then leveled off in TASTPM mice, whereas there was a steady increase but at a lower level in wild type mice. In the 9 – 13 month group there were significant effects of age (P<0.05) and genotype (P<0.001), Cho levels were stable at a higher level in TASTPM mice, whereas levels increased but at lower levels in wild type mice. In the 15 – 19 month group there was a significant effect of genotype (P<0.005), with consistently higher levels in TASTPM mice.

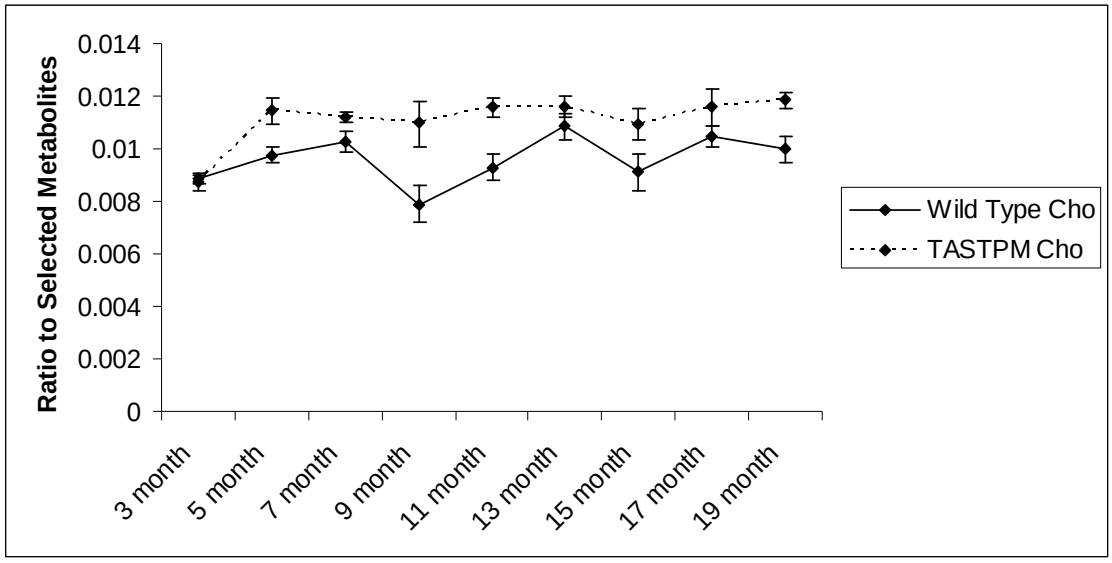

Fig.38 *Cho ratios to selected metabolites for all age groups, values are given ± S.E.M.*

Overall there was a significant effect of age ($P<0.05$) on taurine levels, with a decline over time in both strains (Fig.39). The only other significant difference observed was an effect of age in the 3 – 7 month group ($P<0.001$), with an apparent decline over time.

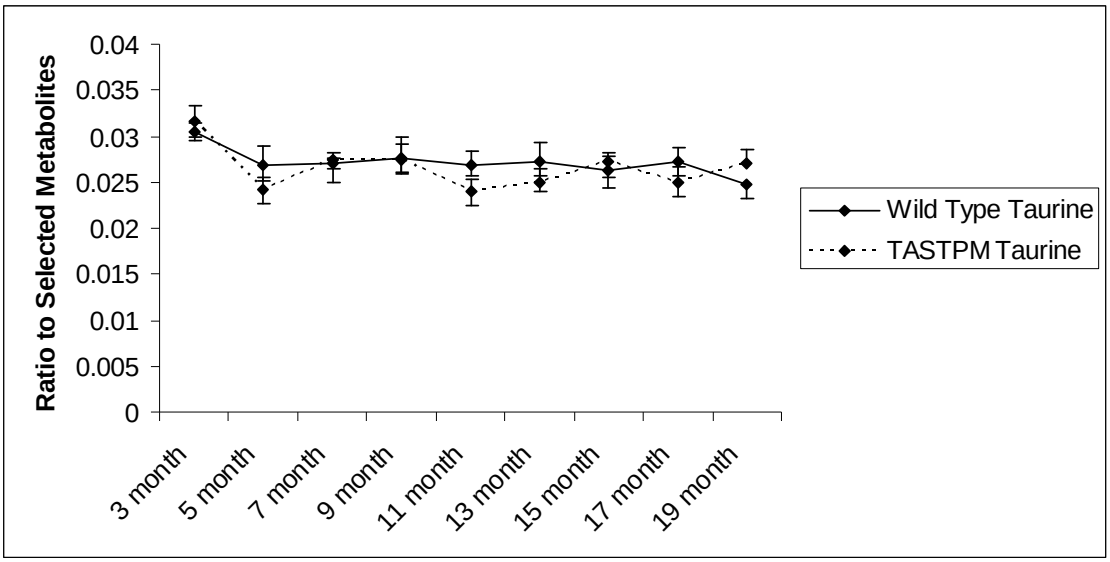

Fig.39 *Taurine ratios to selected metabolites for all age groups, values are given ± S.E.M.*

	3 months			5 months		
	Mean	**S.D.**	**CoV**	**Mean**	**S.D.**	**CoV**
Selected Metabolites						
Creatine Wild Type	0.0507	0.0020	3.9	0.0507	0.0031	6.1
Creatine TASTPM	0.0534	0.0023	4.3	0.0522	0.0022	4.3
Glutamate Wild Type	0.0398	0.0045	11.2	0.0372	0.0056	15.1
Glutamate TASTPM	0.0350	0.0028	7.9	0.0308	0.0034	11.0
Glutamine Wild Type	0.0044	0.0031	70.1	0.0032	0.0045	143.2
Glutamine TASTPM	0.0043	0.0029	67.5	0.0025	0.0033	134.4
Glx Wild Type	0.0443	0.0041	9.3	0.0404	0.0080	19.8
Glx TASTPM	0.0393	0.0027	6.9	0.0333	0.0051	15.5
MI Wild Type	0.0218	0.0028	12.8	0.0217	0.0058	26.5
MI TASTPM	0.0231	0.0026	11.2	0.0251	0.0023	9.3
NAA Wild Type	0.0262	0.0026	10.0	0.0301	0.0033	10.9
NAA TASTPM	0.0237	0.0073	30.7	0.0295	0.0031	10.6
Cho Wild Type	0.0089	0.0008	8.7	0.0097	0.0009	9.0
Cho TASTPM	0.0087	0.0008	8.7	0.0115	0.0014	11.9
Taurine Wild Type	0.0304	0.0029	9.6	0.0269	0.0050	18.4
Taurine TASTPM	0.0317	0.0047	14.8	0.0242	0.0042	17.3
	7 months			**9 months**		
	Mean	**S.D.**	**CoV**	**Mean**	**S.D.**	**CoV**
Selected Metabolites						
Creatine Wild Type	0.0512	0.0047	9.2	0.0464	0.0023	5.0
Creatine TASTPM	0.0557	0.0041	7.4	0.0526	0.0018	3.5
Glutamate Wild Type	0.0367	0.0058	15.8	0.0444	0.0065	14.6
Glutamate TASTPM	0.0277	0.0058	20.9	0.0310	0.0060	19.3
Glutamine Wild Type	0.0028	0.0048	170.9	0.0057	0.0040	71.0
Glutamine TASTPM	0.0022	0.0023	104.2	0.0051	0.0043	85.3
Glx Wild Type	0.0395	0.0055	13.8	0.0501	0.0088	17.5
Glx TASTPM	0.0298	0.0049	16.4	0.0361	0.0055	15.3
MI Wild Type	0.0193	0.0037	19.3	0.0192	0.0017	8.8
MI TASTPM	0.0258	0.0027	10.7	0.0246	0.0060	24.4
NAA Wild Type	0.0315	0.0033	10.5	0.0323	0.0040	12.2
NAA TASTPM	0.0272	0.0021	7.6	0.0261	0.0036	13.9
Cho Wild Type	0.0103	0.0012	11.5	0.0079	0.0019	23.5
Cho TASTPM	0.0112	0.0006	5.6	0.0110	0.0024	22.3
Taurine Wild Type	0.0270	0.0019	7.0	0.0275	0.0050	18.1
Taurine TASTPM	0.0274	0.0023	8.5	0.0274	0.0071	26.0

	11 months			13 months		
	Mean	**S.D.**	**CoV**	**Mean**	**S.D.**	**CoV**
Selected Metabolites						
Creatine Wild Type	0.0521	0.0050	9.6	0.0528	0.0028	5.3
Creatine TASTPM	0.0529	0.0022	4.2	0.0516	0.0034	6.6
Glutamate Wild Type	0.0359	0.0065	18.2	0.0298	0.0052	17.4
Glutamate TASTPM	0.0328	0.0043	13.0	0.0321	0.0056	17.4
Glutamine Wild Type	0.0052	0.0063	120.9	0.0055	0.0059	107.0
Glutamine TASTPM	0.0038	0.0047	126.4	0.0030	0.0049	165.8
Glx Wild Type	0.0411	0.0063	15.4	0.0353	0.0067	18.9
Glx TASTPM	0.0365	0.0078	21.3	0.0351	0.0046	13.0
MI Wild Type	0.0207	0.0060	29.0	0.0243	0.0037	15.1
MI TASTPM	0.0233	0.0051	22.1	0.0241	0.0041	17.0
NAA Wild Type	0.0304	0.0040	13.2	0.0272	0.0034	12.6
NAA TASTPM	0.0277	0.0020	7.3	0.0286	0.0029	10.2
Cho Wild Type	0.0093	0.0016	17.2	0.0109	0.0014	13.2
Cho TASTPM	0.0116	0.0010	8.2	0.0116	0.0010	8.4
Taurine Wild Type	0.0268	0.0036	13.4	0.0273	0.0048	17.6
Taurine TASTPM	0.0240	0.0036	15.1	0.0250	0.0037	14.8
	15 months			**17 months**		
	Mean	**S.D.**	**CoV**	**Mean**	**S.D.**	**CoV**
Selected Metabolites						
Creatine Wild Type	0.0518	0.0067	12.9	0.0512	0.0037	7.3
Creatine TASTPM	0.0536	0.0053	9.9	0.0530	0.0048	9.0
Glutamate Wild Type	0.0370	0.0088	23.8	0.0325	0.0055	16.9
Glutamate TASTPM	0.0291	0.0057	19.7	0.0272	0.0082	30.2
Glutamine Wild Type	0.0067	0.0055	82.8	0.0066	0.0061	93.2
Glutamine TASTPM	0.0069	0.0067	96.5	0.0044	0.0047	107.1
Glx Wild Type	0.0437	0.0104	23.8	0.0390	0.0063	16.1
Glx TASTPM	0.0360	0.0029	8.2	0.0316	0.0062	19.7
MI Wild Type	0.0193	0.0069	35.7	0.0225	0.0073	32.4
MI TASTPM	0.0269	0.0042	15.7	0.0292	0.0019	6.6
NAA Wild Type	0.0306	0.0067	21.9	0.0281	0.0022	7.8
NAA TASTPM	0.0233	0.0079	33.8	0.0265	0.0017	6.6
Cho Wild Type	0.0091	0.0022	24.1	0.0105	0.0012	11.9
Cho TASTPM	0.0109	0.0018	16.3	0.0116	0.0017	14.4
Taurine Wild Type	0.0263	0.0066	25.1	0.0273	0.0045	16.5
Taurine TASTPM	0.0272	0.0031	11.4	0.0249	0.0040	16.1

	19 months		
	Mean	**S.D.**	**CoV**
Selected Metabolites			
Creatine Wild Type	0.0516	0.0038	7.5
Creatine TASTPM	0.0531	0.0034	6.4
Glutamate Wild Type	0.0336	0.0046	13.7
Glutamate TASTPM	0.0250	0.0029	11.6
Glutamine Wild Type	0.0072	0.0118	163.5
Glutamine TASTPM	0.0035	0.0078	223.6
Glx Wild Type	0.0408	0.0081	19.9
Glx TASTPM	0.0285	0.0058	20.2
MI Wild Type	0.0217	0.0062	28.8
MI TASTPM	0.0283	0.0050	17.8
NAA Wild Type	0.0298	0.0072	24.1
NAA TASTPM	0.0264	0.0028	10.7
Cho Wild Type	0.0100	0.0012	12.0
Cho TASTPM	0.0118	0.0006	4.8
Taurine Wild Type	0.0247	0.0037	14.9
Taurine TASTPM	0.0271	0.0033	12.1

Table.6 *Mean, standard deviation and coefficients of variance for all metabolites at all time points*

4.3.3. T1 mapping

Overall, there was a significant effect of genotype on T1 in the cortex ($P<0.0001$), hippocampus ($P<0.0001$) (Fig.40) and thalamus (Fig.41) ($P<0.05$). In all cases, the T1 times from the brains of the TASTPM mice were shorter than the wild type mice. There was also a significant effect of age in the hippocampus ($P<0.05$). In the 3 – 7 month group there was a significant effect of genotype in the cortex and the hippocampus ($P<0.05$) but not in the thalamus, again, where significant effects were seen, TASTPM T1 times were shorter.

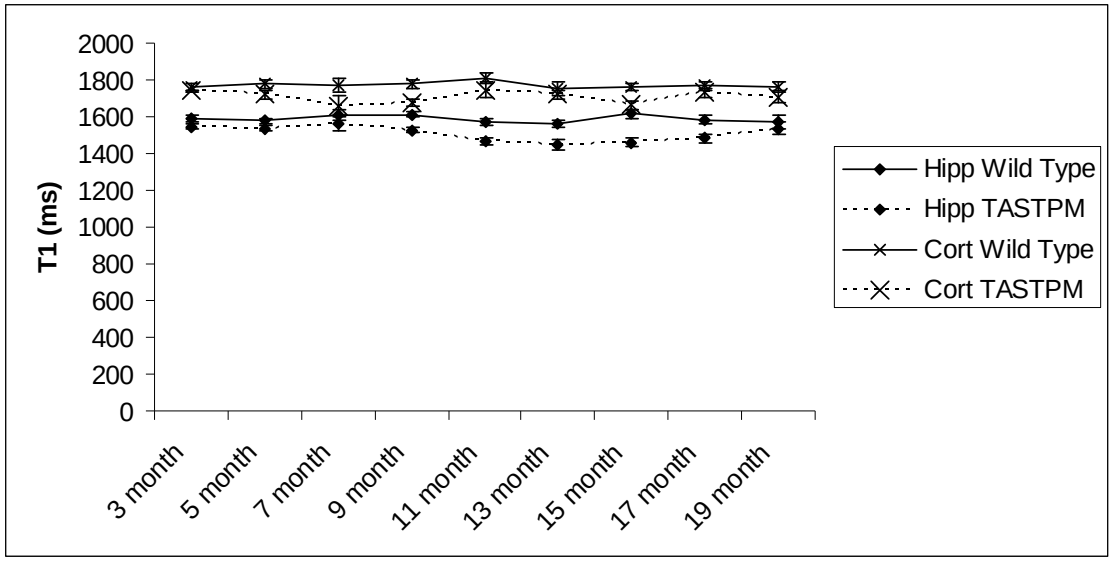

Fig.40 *T1 values in the hippocampus and cortex for mice of both strains and all age groups, values are mean ± S.E.M.*

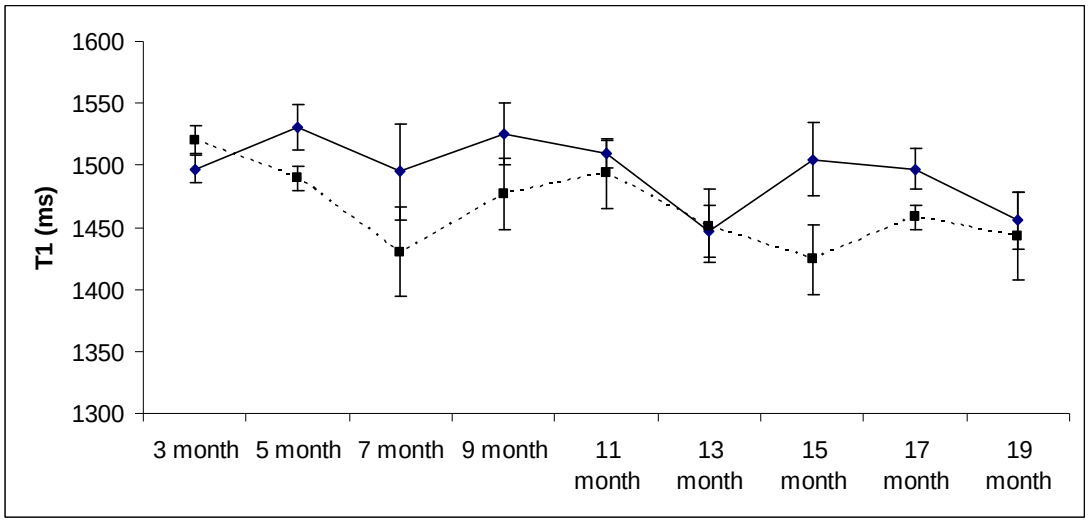

Fig.41 *T1 values in the thalamus for mice of both strains and all age groups, values are mean ± S.E.M.*

In the 9 – 13 month group there was a significant effect of genotype in the hippocampus (P<0.0001) with TASTPM T1 times again shorter. No other significant effects were observed. In the 15 – 19 month group there was a significant effect of genotype in the cortex (P<0.01), hippocampus (P<0.0005) and thalamus (P<0.05), TASTPM T1 times were once again shorter.

T1 has an almost linear dependence on the water content of tissue (Fatouros and Marmarou, 1999), so these data could be interpreted as showing a slight reduction in brain water in TASTPM mice.

4.3.4. T2 mapping

Overall there was a significant effect of genotype on T2 in the hippocampus (P<0.01) and cortex (P<0.001), with TASTPM values slightly lower (Fig.42). There was also a significant effect of age in the thalamus (Fig.43) (P<0.001), with T2 decreasing over time, and a significant age x genotype interaction in the hippocampus (P<0.05).

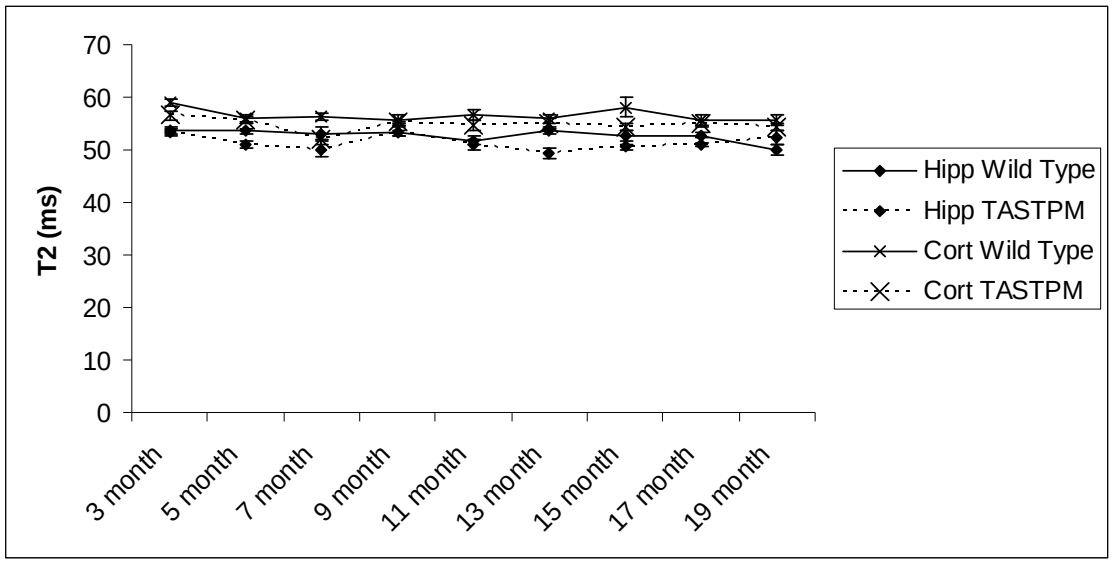

Fig.42 *T2 values in the hippocampus and cortex for mice of both strains and all age groups, values are mean ± S.E.M.*

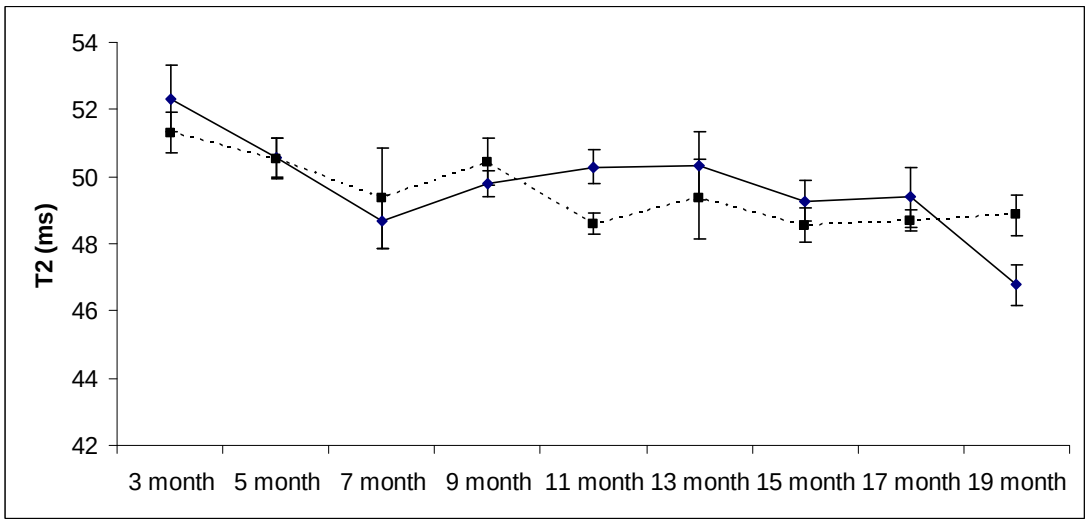

Fig.43 *T2 values in the thalamus for mice of both strains and all age groups, values are mean ± S.E.M.*

In the 3 – 7 month group there was a significant effect of age ($P<0.001$), genotype ($P<0.001$) and an age x genotype ($P<0.05$) interaction in the cortex, where T2 times fell with age, but to a greater degree in the TASTPM mice. There was a significant effect of genotype in the hippocampus ($P<0.05$), with

T2 times shorter in TASTPM. In the thalamus, age was a significant factor ($P<0.05$), again showing a decline with age.

In the 9 – 13 month group there were significant effects of age and genotype, as well as a age x genotype interaction on T2 times in the hippocampus ($P<0.05$), T2 times appeared stable in the wild type mice, whereas T2 values decreased with age in the TASTPM mice. No significant effects were seen in the cortex or thalamus.

In the 15 – 19 month group there was a significant age x genotype interaction in the hippocampus ($P<0.05$), with T2 times decreasing slightly with age in the wild type mice, and increasing in the TASTPM mice. No significant effects were seen in the cortex or thalamus.

4.3.5. Y maze

Overall, Y maze testing showed a significant effect of genotype ($P<0.0001$), with older TASTPM making fewer repeating triplets than wild type (Fig.44), as well as a significant effect of age ($P<0.01$). In the case of total number of moves in the maze, a significant effect of age was seen overall ($P<0.01$)

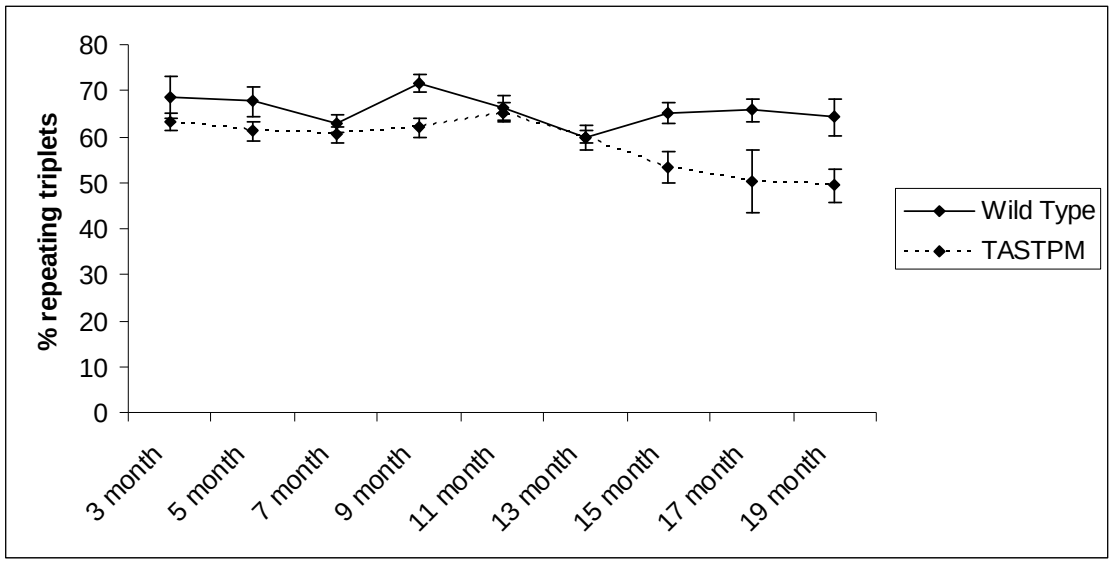

Fig.44 *Graph showing repeating triplet percentages for both strains of mice of all age groups, values shown are ± S.E.M*

In the 3 – 7 month age group there was a significant effect of genotype on repeating triplets ($P<0.05$), with TASTPM again having fewer. There was a significant effect of age on total moves ($P<0.05$)

In the 9 – 13 month age group there was a significant effect of age ($P<0.05$). There was no significant difference detected in total moves.

In the 15 – 19 month age group there was a significant effect of genotype ($P<0.001$), with TASTPM again having fewer repeating triplets. There was no significant difference detected in total moves.

4.3.6 Saturation Factors

With the exception of NAA, at TR 2500 ms all metabolites are over 85% relaxed (Table.7). The difference between spectra at TR 2500 and 20000 ms is not great for any metabolite resonance (Fig.45)

Metabolite	Mean	S.E.M.
NAA	0.74	0.082
Glx	0.98	0.228
Cr1	0.87	0.029
Cho	0.86	0.029
Taurine	0.93	0.132
Alpha	0.90	0.128
Cr2	1.07	0.057

Table.7 *Mean and S.E.M. of saturation factors between 2500 and 20000 ms TR for major metabolites*

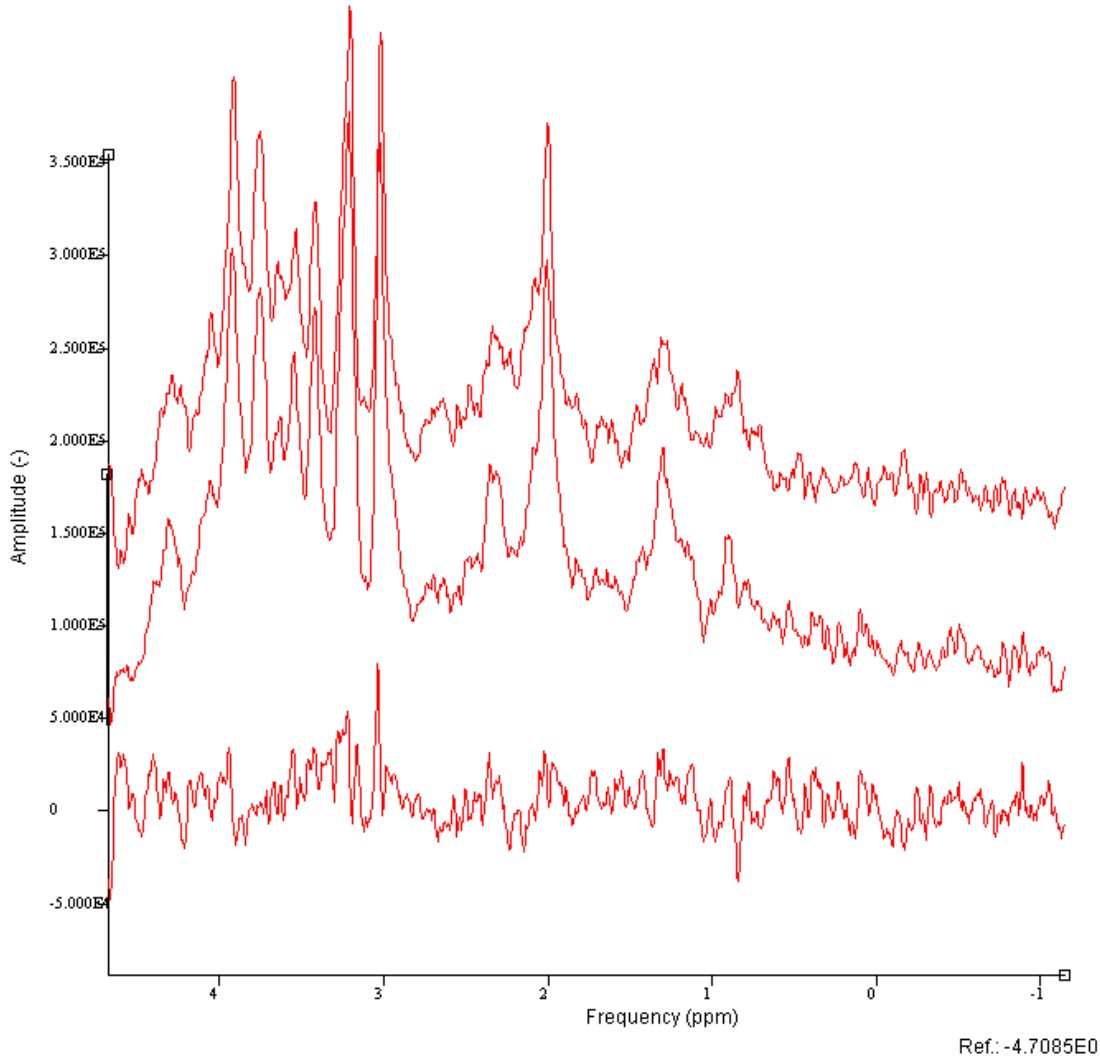

Fig.45 *Comparison of spectra of TR 2500 ms (top), 20000 ms (middle) and the difference between the two*

4.4. Discussion

Firstly, we saw a significant difference in NAA levels between TASTPM and wild type mice. NAA concentration was lower in TASTPM mice at all but the 13 month time point. This is in agreement with other *in vivo* studies on transgenic AD mice (Dedeoglu et al., 2004; Marjanska et al., 2005; von Kienlin et al., 2005), all of which observed decreased NAA/Cr ratios in AD mice compared to their wild type base strain. The lower level of NAA observed indicates that there is disruption, dysfunction or loss of neurons occurring (Demougeot et al., 2004). There is known to be some neurodegeneration in TASTPM mice in the form of the thalamic lesions, but this only occurs after 7 months. It is at 7 months that the difference in NAA concentration between the two strains starts to become most apparent. This may be a consequence of the formation of the thalamic lesions. It is also possible that the difference is caused by neuronal disruption, as opposed to frank neurodegeneration. Normal neuronal function may be affected by Aβ accumulation, without detectable neuronal death, reduced NAA has been observed in similar situations (Demougeot et al., 2004). As there is a difference in NAA in mice of different age groups which appears independent of amyloid deposition, the difference observed may be a marker of disease, without being a marker for disease progression in this model.

The NAA differences observed are not in agreement with the data from our extract study. We saw no difference in NAA between TASTPM and wild type in the extract study. A possible reason for this difference is that we used whole brains in our extract study, whereas a specific voxel was centred over specific regions of interest in this study. The use of the whole brain may have masked regional metabolic differences which this study has picked up due to the more focused area of interest.

Creatine levels were significantly different between the two strains of mice, being slightly higher in TASTPM mice. In our extract study the creatine concentration was higher only in older TASTPM mice, however in this study

creatine concentrations are higher in younger TASTPM mice as well. The difference does not appear as pronounced as in the extract study. The reason for this discrepancy may be the same as for NAA, in this case a whole brain creatine increase may occur which is less pronounced in the regions scanned in this study. The significant difference would still indicate that care must be taken when using creatine as a reference metabolite in these (and possibly other transgenic AD) mice.

Reduced glutamate and Glx concentrations were observed in TASTPM mice at all except the 13 month time point. This is in agreement with other *in vivo* studies of transgenic AD mice (Dedeoglu et al., 2004; Marjanska et al., 2005; von Kienlin et al., 2005). All these studies observed reduced glutamate/Cr ratios. As glutamate is a metabolic indicator, the reduced levels in TASTPM mice are likely a marker of neuronal hypometabolism in these mice, a symptom that has also been observed in human AD (Valla et al., 2001; Zhu et al., 2004; Moreira et al., 2007). As reduced glutamate levels can be observed at 3 months, when amyloid plaques are barely detectable, this effect is likely independent of amyloid deposition. There is a weak age x genotype interaction for glutamate (not Glx) signal, this may be more due to the levels intersecting at 13 months, as the difference appears fairly uniform other than at this time point. It is likely that glutamate and Glx are markers of the presence of amyloid in TASTPM mice, without being sensitive to increasing amyloid deposition.

In our extract study we found no difference in glutamate signal between TASTPM and wild type mice. We did find a decrease in succinate concentration in the brains of TASTPM mice, as succinate coresonates with glutamate *in vivo*, it is possible that this partially explains the difference observed *in vivo*. Again, the more focused nature of this study may be detecting locally decreased glutamate signal which is not detectable by whole brain measurement. It is also possible that there is a difference in glutamate storage between the two strains, since not all of the cerebral glutamate pool is detectable *in vivo* (Kauppinen and

Williams, 1991; Kauppinen et al., 1994), thus it is possible that more glutamate is being stored intracellularly in the TASTPM mice, making it undetectable by *in vivo* spectroscopy, but detectable by *in vitro* spectroscopy on extracts.

Higher MI concentration was observed in TASTPM mice at all except the 13 month time point. This study found increased MI/Cr ratio in APP-PS1 mice. The presence of higher MI in younger TASTPM mice (before extensive amyloid deposition) suggests that MI levels are independent of amyloid plaque formation. The elevated levels of MI observed in TASTPM mice are in agreement with a previous *in vivo* study showing increased MI in transgenic (APP-PS1) AD mice (Marjanska et al., 2005). However, in two other studies of transgenic AD mice by ^{1}H MRS, no increase in MI was reported (Dedeoglu et al., 2004; von Kienlin et al., 2005). One study found an increase in taurine levels and postulated that this may be the equivalent of the MI increase seen in human AD (Dedeoglu et al., 2004). The increase in MI could be indicative of glial cell proliferation or microglial activation in these mice. Activated microglia have been found to be associated with the amyloid plaques in TASTPM mice (Howlett et al., 2004). The TASTPM mice and APP-PS1 mice contain the same double mutant APP_{swe} (K671N; M671L) mutation (Richardson et al., 2003; Marjanska et al., 2005). The PS1 mutations incorporated are slightly different, the TASTPM contains the M146V variant (Howlett et al., 2004), the APP-PS1 contains the M146L variant (Marjanska et al., 2005). The functions of MI in osmoregulation and membrane metabolism mean that higher MI levels may cause disruption of normal function (Beacher et al., 2005). MI is also a precursor in the formation inositol trisphosphate and therefore can affect neuronal calcium signalling (Berridge, 1993). Calcium signalling modulates aspects of brain development and function, including neurotransmission, learning and memory (Berridge et al., 2000). The presence of elevated MI may be causing some of the problems, as opposed to being merely a marker. However, the fact that there was no age-dependence of the difference in MI

suggests that it may be a disease marker but would not act as a biomarker of disease progression in this model.

In the case of MI, the results of the *in vivo* and *in vitro* studies are very similar, thus the increased MI may be present throughout the whole brain, as opposed to areas specifically affected by AD.

Higher levels of Cho were observed in TASTPM mice compared to wild type. Cho levels were also more stable over time in TASTPM mice. This could be indicative of differences in phospholipid metabolism or cell membrane composition between the two strains. Perturbations in phospholipid metabolism have also been observed in human AD (Kuo et al., 1998; Notkola et al., 1998; Roher et al., 1999; Sparks et al., 2000). Differences in lipid functional groups were observed in the organic extract section of this thesis.

The differences in taurine levels between the two strains are minimal and not significant, the only significant factor is age, with taurine levels at 3 months being high in both strains and then declining slightly.

The saturation factors that we obtained showed that most metabolites were over 85% fully relaxed at TR 2500 ms, thus any change in T1 with disease or age will not have a great effect on metabolite signal intensity and T1 can be ruled out as underlying any apparent metabolite changes.

The T1 data indicate slightly shorter T1 times in TASTPM mice, the difference is only about 100ms, but it is significant. It is therefore possible that the presence of amyloid in the brains of TASTPM mice is disrupting normal osmotic function. The effect is present in younger mice but becomes more pronounced in older mice so may be linked to increasing amyloid deposition. Our hypothesis that osmotic changes in the older TASTPM mice may lead to overestimation of

some metabolites does not appear to be true, as the T1 values are reduced at a much earlier time point than the point at which we saw increased metabolite levels *in vitro*. T1 has an almost linear dependence on the water content of tissue (Fatouros and Marmarou, 1999), so these data could be interpreted as showing a slight reduction in brain water in TASTPM mice. T2 shows proportionally similar effects to T1, which is likely also to reflect a similar dependency on total water content.

The Y maze data show the most significant difference in exploratory behaviour to be in the oldest age group (15 – 19 months) when amyloid deposition is extensive. The metabolites showing significant differences do not become more significant over time, so cannot be said to be dependent upon amyloid deposition. The behavioural differences may be dependent upon amyloid deposition and thus may be a marker of disease progression.

In this study several metabolitic differences have been observed between TASTPM and wild type mice (NAA, glutamate, MI, Cho and creatine), these may be markers of pathology but do not appear sensitive to disease progression or amyloid deposition. The behavioural differences may be sensitive to disease progression, more extensive study is needed, using different behavioural tests to confirm this. If there is sensitivity to disease progression behavioral differences may be useful in testing amyloid-lowering therapies in this mouse model.

Chapter 5. Pilot Study for Evaluation of TASTPM and Wild Type Brain Sections using MALDI MS Imaging and Laser Capture Microscopy

5.1. Introduction

TASTPM mice are known to have increasing deposits of Aβ in the brain from 6 months onward (Howlett et al., 2004). MALDI MS Imaging is a useful tool for profiling protein expression in tissues, and is also used widely for analysis of small molecules and peptides. The ability to observe protein profiles in the brains of TASTPM mice and their wild type base strain could be used to identify potential protein biomarkers in the TASTPM mice, as well as Aβ. Such biomarkers could be invaluable in furthering our understanding of the pathogenesis of AD, as well as having uses in preclinical efficacy trials.

This chapter will focus on several aspects of MALDI MS Imaging. The first aspect will be development of a protocol for the analysis of formalin-fixed tissue sections by MALDI MS Imaging, using TASTPM brain sections.

The second aspect will describe the optimisation of the matrix application procedure, comparing manual spraying with automated matrix application using an ImagePrep device.

The final section will focus on the use of MALDI MS Imaging to look for differences in regional protein expression between TASTPM and wild type mouse brains, followed by isolation of any differences and attempted identification.

Efforts are being made to enable the use of MALDI MS imaging on formalin-fixed tissue sections (Lemaire et al., 2007; Stauber et al., 2008). Alternatives to formalin-fixation for long term storage are also being investigated (Chaurand et al., 2008). If a method could be found to obtain useful information on protein profiles from formalin-fixed paraffin-embedded tissue sections, this could be

useful to histologists as the extensive libraries of fixed tissues could be analysed in a completely different way than is currently available.

The initial work carried out was to attempt to develop a protocol for analysing fixed sections using MALDI MS Imaging.

Before embarking on method development with fixed tissue, experiments were performed on frozen tissue sections. Firstly, MALDI imaging of amyloid peptide solutions that had been spotted onto tissue sections and allowed to dry was undertaken to confirm their detection and provide estimates of the limits of detection. This was followed by tryptic digests of these spots to confirm the detection of amyloid fragments. MALDI MS imaging of endogenous TASTPM amyloid deposits was then undertaken, followed by trypsin digests of TASTPM brain sections and subsequent MALDI MS imaging. These proof of concept experiments on frozen tissue sections were successful following four repeats and so the attention was then transferred to fixed tissue sections.

Formalin fixed TASTPM brain sections were dewaxed and trypsin digests performed in order to break the protein crosslinks formed during the fixing process. MALDI MS imaging was then performed to look for amyloid fragments in the dewaxed brain sections. The successful detection of any amyloid fragments by this approach would indicate that further study of other formalin-fixed tissues might be carried out in ways not previously thought possible, looking for individual peptide signals previously invisible to MS due to protein crosslinks.

Matrix can be manually applied using a spray device, or in an automated system, one example an automated device is the ImagePrep (Bruker Daltonics). Matrix thickness and tissue wetness are both crucial factors in the preparation of samples for MALDI MS analysis. A comparison of the two

methods of matrix application was carried out to determine the optimum conditions for sample preparation.

Coronal sections of frozen TASTPM and wild type mouse brains were used as test samples. The areas chosen for study contain the hippocampus and the thalamus. The hippocampus was selected as it is one of the first areas affected in human AD, the thalamus was included due to the presence of thalamic hypointensities (THIs) in TASTPM mice (Evans et al., 2007). THI regions have been observed in other transgenic AD mice, such as APP/PS1 (Dhenain et al., 2009). The images obtained are presented and discussed below.

During the course of matrix application comparison an unknown peptide ion of apparent molecular weight (m/z) 4811 Daltons was detected localised to the THI regions. Identification of this unknown peptide may provide insight into the underlying pathology causing the formation of the THIs. Further study was carried out using laser capture microscopy (LCM) to dissect out the THI regions and attempt to isolate and identify the unknown peptide using MALDI and liquid chromatography-MS

5.2. Methods

5.2.1. Section Preparation for MALDI Imaging

Frozen mouse brains were mounted onto a cryostat sample disc using carboxymethylcellulose (2%w/v) medium. After wiping down all surfaces in the cryostat with ethanol to remove any contamination, 12µm sections of brain were cut and thaw mounted onto indium tin oxide (ITO) coated glass slides (Bruker Daltonics) which had been kept inside the cryostat at -20^{o}C whilst the sectioning was taking place. The tissue section was touched onto the ITO coated surface of the slide and then from underneath the slide the finger is touched onto the slide to gently warm up the slide and aid the mounting

process. Any sections unused on the day of sectioning were stored in a slide container in the freezer at approx. -20^{o}C.

5.2.2. Amyloid Spots on Tissue

In all cases 1µl of amyloid solution (dissolved in deionised water) was spotted onto the tissue, at varying concentrations, concentrations are indicated in the images for the different experiments.

5.2.3. Tissue Washing

Mouse brain sections were each pipette washed five times with 1ml 70% ethanol, followed by five washes with 1ml 100% ethanol to remove lipids. The sections were then allowed to dry in the fume cupboard.

5.2.4. Tissue Dewaxing

Formalin-fixed paraffin-embedded sections were cut onto ITO coated slides. Each slide was then immersed for 5 minutes in Histoclear (x2), 100% methylated spirit (x2), 90% methylated spirit, 70% methylated spirit and finally distilled water to remove the paraffin wax.

5.2.5. Trypsin Digests

Trypsin dilutions were made up in 100mM ammonium bicarbonate to 500ng/µl. Trypsin solution was spotted onto brain sections, sections were then placed in an incubator at 37^{o}C and 100% humidity for the desired time (either 1 hour or 24 hours). In cases of digestion of applied Aβ 1-40, a 1µl spot of trypsin solution was applied on top of the Aβ spot after it had been allowed to dry, in cases of trypsin digest without applied amyloid, trypsin solution was applied to the entire brain section in question.

5.2.6. Matrix Application

The matrix used was 7mg/ml alpha-cyano-4hydroxycinnamic acid in 50% acetonitrile and 0.2% trifluoroacetic acid (TFA). This solution was prepared and sonicated for 30 minutes to ensure the matrix was fully dissolved

The manual spray application (performed in a fume cupboard) involved spraying small amounts of the matrix onto the tissue multiple times. Care was taken during each application of matrix to not allow the tissue to get too wet. Otherwise this could lead to delocalisation of the components of interest. The sections were allowed to air dry between each application of matrix. Matrix application continued until an even coating on the tissue was achieved.

For automated matrix application, the slide with sections mounted onto it was placed in the ImagePrep (Bruker Daltonics) matrix application device, ensuring that the light sensor was not covered. The matrix was loaded into the machine and the sequence was started, spray was automated and tissue wetness/matrix thickness was monitored by passage of light through the slide onto the light sensor beneath. This sensor allowed the machine to sense when matrix was to be reapplied and when sufficient matrix had been applied.

5.2.7. MALDI Imaging

Before matrix application, very small droplets of liquid paper were placed onto the glass slide containing the sections of interest to act as “teach marks” as part of the sample alignment procedure for the mass spectrometer. An optical image of the contents of the slide was obtained using a scanner. After matrix application, the slide was mounted in a specially designed slide holder, the location of the teach marks was then recorded to be referenced to a grid for sample alignment. The sample was then placed in a Bruker Ultraflex III MALDI TOF/TOF mass spectrometer, software used was Compass 1.2 which includes FlexControl v3.0., FlexImaging v1.1.9.0 and FlexAnalysis v3.0.5.

FlexImaging was used to align the slide with the optical image using the teach marks. This software allows us to observe the slide containing the sections to be analysed at magnification (x20 – x40). The software also contains a grid system which can be compared to the recorded locations of the teach marks. The teach marks are used to triangulate the exact location of the sections on the slide, so that the MALDI image obtained will be properly aligned with the optical image.

The preferred method for imaging the tissue sections used the following parameters; mass range 3000-20000Da, laser power 51%, detector gain 6.5x, Ion source 1 voltage 25kV, Ion source 2 voltage 23.3kV, lens voltage 6.5kV, pulsed ion extraction delay 100ms. The desired areas required for analysis were selected using the FlexImaging software. This software allows observation of the optical image and selection of areas of interest to acquire MALDI data to construct an image. Ahead of the automated data acquisition by the mass spectrometer, the method was tested and adjustments to laser power and attenuation were made in order to get good resolution of mass peaks without the noise associated with too much laser power. The refined method was then saved in the FlexControl software prior to commencement of the analysis. The method was refined before each data acquisition from each new sample. Data was acquired in a dot matrix fashion from the sample, individual points were 200μm in diameter. Sample analysis and data acquisition took between 1 and 24 hours depending on the size and number of sections being imaged.

Spectral analysis of the captured images was done using the FlexAnalysis software. This software takes the mass spectra gathered from each point and overlays them on the optical image, creating a MALDI image. We can then refine the image to pick out a particular mass or a range of masses in order to investigate the distribution of molecules of interest. We can also use the software to search for molecules, as we can highlight an area and get the

overall mass spectrum from that area, then look at the distribution of any major peaks we find. The MALDI Images shown in this thesis are created using mass ranges, from the mass of interest ±1 Dalton.

Other studies of peptides specific to TASTPM mice performed as part of the investigation consisted of the isolation of areas of interest from selected brain sections using LCM. Captured areas were then analysed, first by MALDI, then using other analytical techniques (e.g. nanoLC-MS) in an attempt to identify the peptide(s) of interest.

5.2.8. Laser Capture Microscopy – Slide Preparation

Frozen mouse brains were mounted onto a cryostat mounting disc using carboxymethylcellulose (2%w/v) medium. After wiping down all surfaces in the cryostat with ethanol to minimise contamination, 8µm sections were cut and mounted onto room temperature uncoated glass slides, a maximum of 2 sections were collected per slide. The slides were immediately placed in a slide box on dry ice and not allowed to air dry. Four slides at a time were removed from the dry ice and allowed to thaw on a kimwipe for no more than 30 seconds. The slides were then immersed for 30 seconds in 75% ethanol, 2x distilled water, 75% ethanol, 95% ethanol, 100% ethanol and finally placed in xylene for 5 minutes. Slides were then placed in a dessicator containing fresh silica gel dessicant until ready for LCM. All washing solutions were changed after each wash.

5.2.9. Manual Laser Capture Microscopy

The slide containing the sample was placed on the laser capture microscope and the area containing the desired region was located. A fresh cap was placed on the arm and lowered onto the sample. The desired area was collected onto the cap by LCM, manoeuvring the table to allow collection. Once the desired area from one slide was collected, a fresh slide was put in place and the process repeated. Caps were stored in a -20^{o}C freezer until ready to use.

5.2.10. Automated Laser Capture Microscopy

Slides were loaded into a Veritas Microdissection Instrument (Arcturus Bioscience Inc.), 3 at a time. The areas of interest were located and highlighted using the Veritas software (Fig.46). The laser was focused using pulse length, laser power and intensity in order to maximise capture. Following laser focussing, capture of desired areas was initiated. Between each section, laser focus was adjusted to retain optimum tissue adhesion to caps. No more than 6 sections worth of sample was collected onto each cap, again to maximise adhesion. Caps were stored in the -20^{o}C freezer until ready to use.

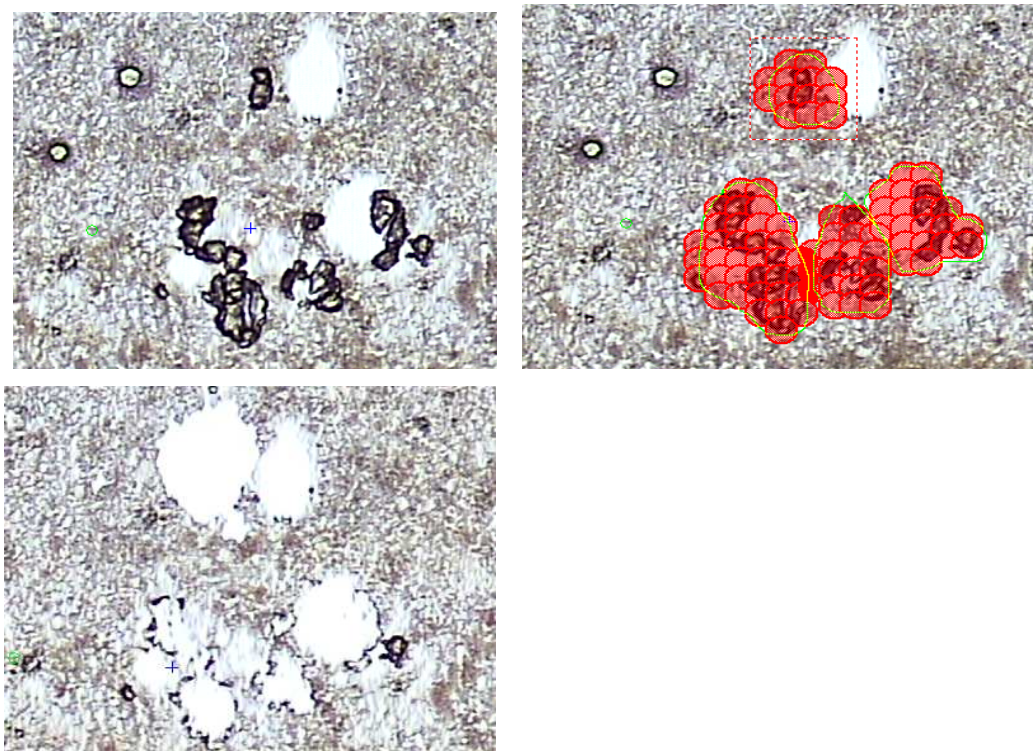

Fig.46 *Optical image of THI regions in the LCM instrument, before capture, marked for capture, after capture. Magnification x100*

5.2.11. Preparation For Analysis

To the surface of the LCM caps containing the sample, 1µl of a solution of formic acid:water:isopropanol (1:3:2) was added, agitated around the surface and then immediately removed into a vial prior to analysis. For MALDI analysis

1µl was added to 1µl of matrix (7mg/ml alpha-cyano-4hydroxycinnamic acid in 50% acetonitrile and 0.2% trifluoroacetic acid), mixed and spotted onto a MALDI target. Analysis was carried out once the spot was dry.

5.2.12. Nano-LC/MS

An Orbitrap XL mass spectrometer (Thermo Fisher Scientific, San Jose, CA), coupled to a nanoAcquity uPLC system (Waters) was used for the analysis. Nano-LC was performed using a 0.1 mm X 150 mm Cadenza C18 (Imtakt) analytical column maintained at 40C, along with a Symmetry C18 5um 180um X 20mm trapping column (Waters). The sample was injected in 5µl aliquots. Buffer A consisted of 0.1% formic acid (Aristar grade) in Water (Optima LC/MS grade) (Fisher), buffer B consisted of 0.1% formic acid (Aristar grade) in Acetonitrile (Optima LC/MS grade) (Fisher). Vented column trapping was carried out using buffer A for 5 minutes at 4µl/min following sample loading. The flow rate was then adjusted to 0.3 ul/min. A series of nano-flow gradients were used, the profile of which was (i) 5 minutes at 98% A; (ii) 40 minutes at 60% A; (iii) 2 minutes at 5% A; (iv) 3 minutes at 5% A; (v) 2 minutes at 98% A, and finally (vi) 18 minutes at 98% A. A blank run was performed between each sample using buffer A and the data were searched in the same manner as the sample runs, with no proteins found in any blanks.

For the mass spectrometry, one scan cycle included an initial scan (m/z 300-1800) at a resolution of 60000 followed by 5 collision-induced dissociation (CID) scans at resolution 15000 to perform MS/MS on the 5 most intense ion signals from the first scan. The activation time was 30ms, the isolation width was 2amu, the normalised activation energy was 30% and the activation *q* was 0.25.

Data analysis was performed using MASCOT. RAW files were searched using MASCOT running in Thermo Proteome Discoverer 1.0 processing software. MS data was searched using MASCOT against the psr_all non-redundant

database, taxonomy Rodentia. Max number missed cleavages 3, 15ppm precursor mass tolerance, 0.8 Da fragment mass tolerance. carbamidomethyl ysteine as a fixed modification and N-term acetylation and oxidised methionine were used as dynamic modifications. Resulting protein hits were filtered to remove any protein containing only 1 peptide hit and any keratin related proteins.

5.3. Results

Detection of amyloid fragments was based on mass from fragments observed previously from trypsin digestion (Kheterpal et al., 2001). Fragments observed were 17-40, 17-28, 1-16 and 6-16.

5.3.1. Protocol development for analysis of formalin-fixed tissues

5.3.1.1. Aβ 1-40 spotted on to frozen sections, followed by 1 hour trypsin digest (500ng/µl)

Following trypsin digest, Aβ peptide 1-40 and fragments 17-40 (Fig.47) along with 17-28, 1-16 and 6-16 were observed on tissue sections.

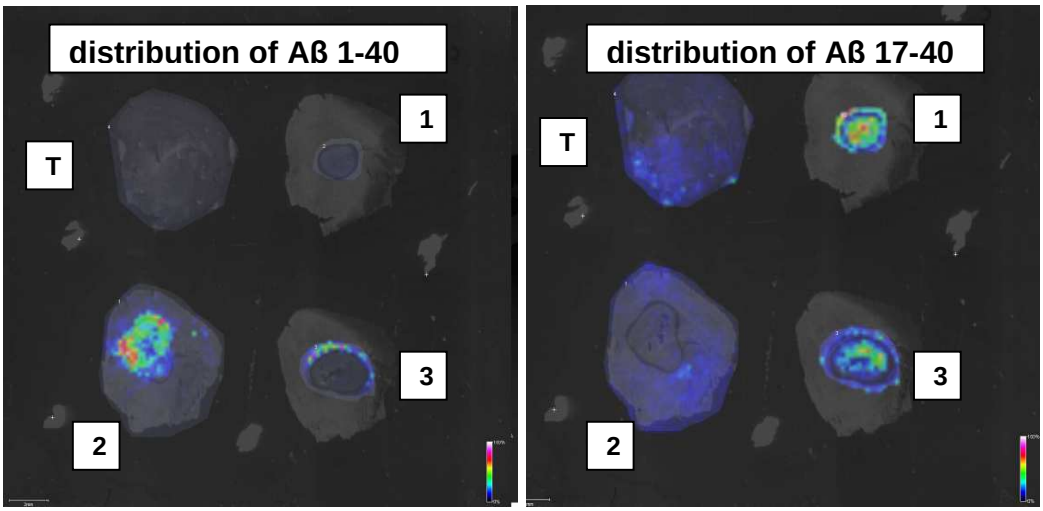

Fig.47 *MALDI Imaging results from frozen brain sections from TASTPM mice. Treatment of sections:* ***T*** *– trypsin (500ng/µl) only,* ***1*** *- 100µg/ml Aβ 1-40 + trypsin (500ng/µl) ,* ***2*** *– 1mg/ml Aβ 1-40 only,* ***3*** *– 1mg/ml Aβ 1-40 + trypsin (500ng/µl). Scaling bars indicate intensity of signal, from low intensity (blue) to high intensity (white). Magnification x 5*

From these images Aβ 1-40 was detected when spotted onto the section at 1mg/ml in the absence of trypsin. Aβ 17-40 can be detected following 1 hour trypsin digest of both 1mg/ml and 100µg/ml Aβ 1-40. Where some Aβ 1-40 can be seen around the edges of the trypsin digest at 1mg/ml, all Aβ 1-40 was digested by the trypsin at 100µg/ml. Aβ 17-40 can also be detected on the section where only trypsin was added, indicating that endogenous amyloid is being digested in this case.

5.3.1.2. Aβ 1-40 spotted on to frozen sections, followed by 24 hour trypsin digest (500ng/µl)

Aβ peptide fragments 1-40, 17-40, 17-28, and 1-16 were observed on tissue sections following digest (Fig.48).

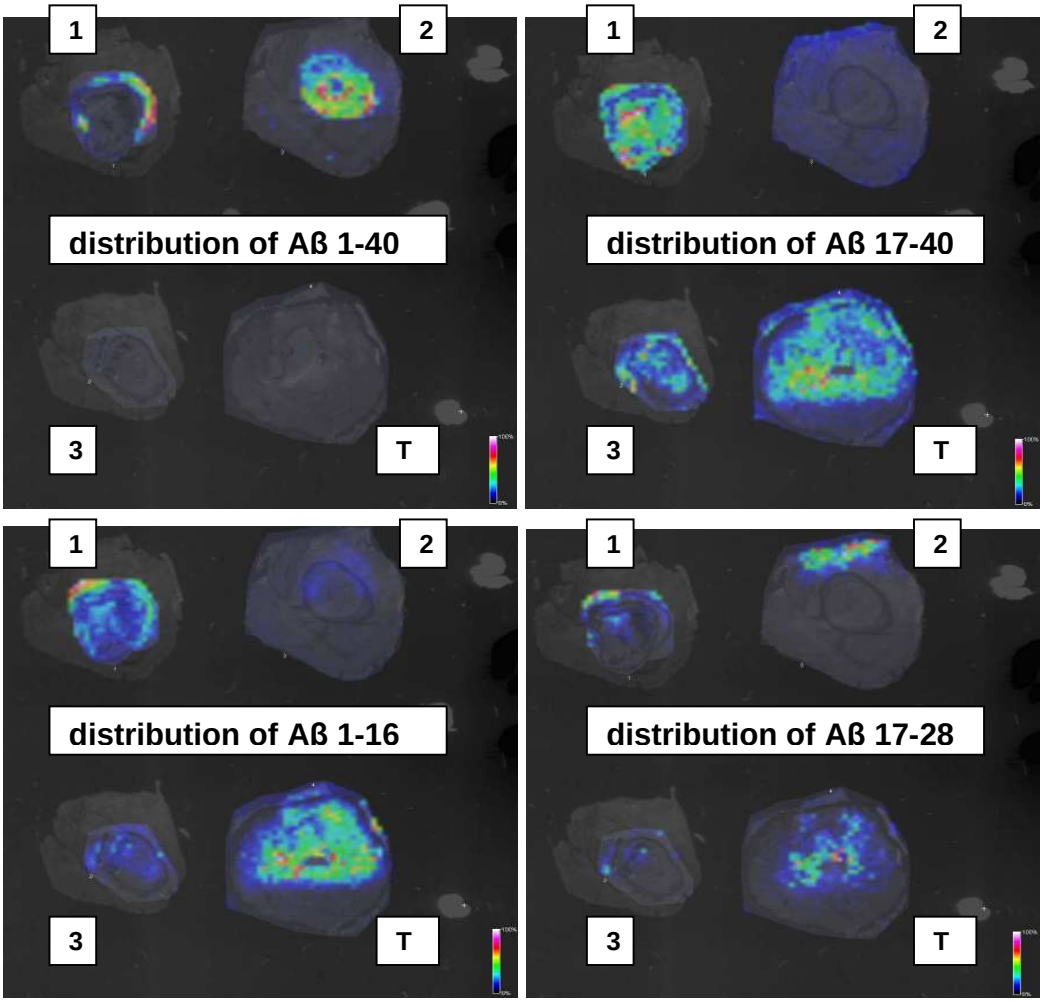

Fig.48 *MALDI Imaging results from frozen brain sections from TASTPM mice. Treatment of sections:* ***1*** *- 1mg/ml Aβ 1-40 + trypsin (500ng/µl),* ***2*** *- 1mg/ml Aβ 1-40 only,* ***3*** *– 100µg/ml Aβ 1-40 + trypsin (500ng/µl),* ***T*** *– trypsin only (500ng/µl). Scaling bars indicate intensity of signal, from low intensity (blue) to high intensity (white). Magnification x 5*

From these images Aβ 1-40 was almost completely digested at 1mg/ml and 100µg/ml in a 24 hour trypsin digest. On section 1 where Aβ 1-40 is present

around the edges of the spot, this is likely where the trypsin spot did not entirely cover the spot of applied Aβ 1-40. Aβ 17-40 is present in all the sections where trypsin was added, whereas Aβ 1-16 is only weakly detected on the 100µg/ml Aβ1-40 section, indicating that it has been further digested by the trypsin over 24 hours. Aβ 17-28 was observed in the images, including the section to which no trypsin was added, overall signal in this case was weak, so this may be an artefact. Aβ 1-16 and 17-40 were strongly detected on the sections with just trypsin added, indicating digestion of endogenous amyloid.

Following this work, the aim was to show that Aβ peptide and fragments can be observed by MALDI on dewaxed formalin-fixed tissue sections, as well as performing trypsin digests on the dewaxed sections without adding Aβ.

5.3.1.3. Aβ 1-40 spotted on to dewaxed sections, followed by 1 hour trypsin digest (500ng/µl)

Aβ peptide fragments 1-40, 17-40, 1-16 and 6-16 were observed on tissue sections following digest (Fig.49).

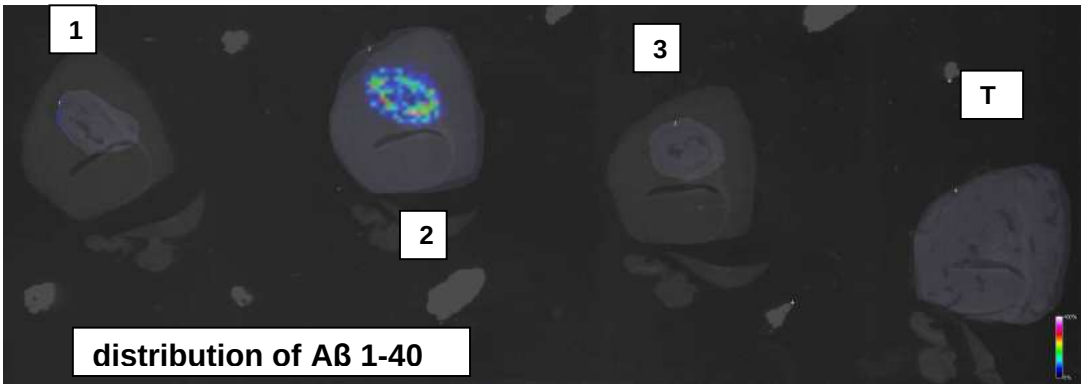
1
2
3
T
distribution of Aß 1-40

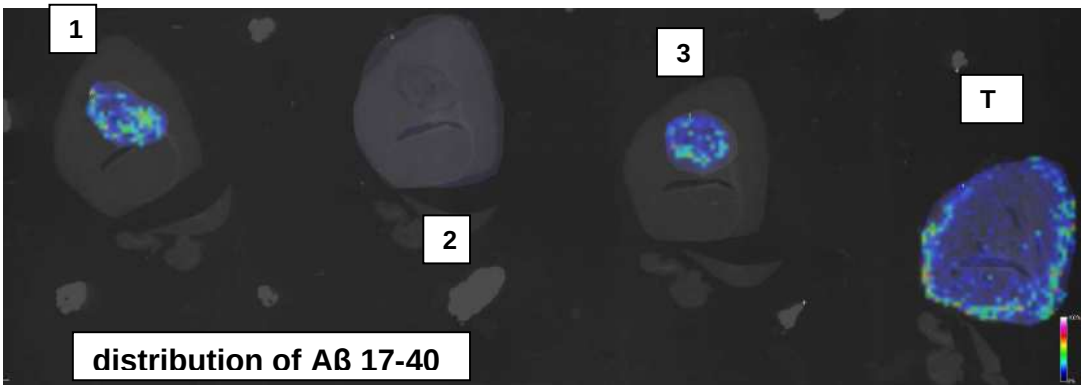
1
2
3
T
distribution of Aß 17-40

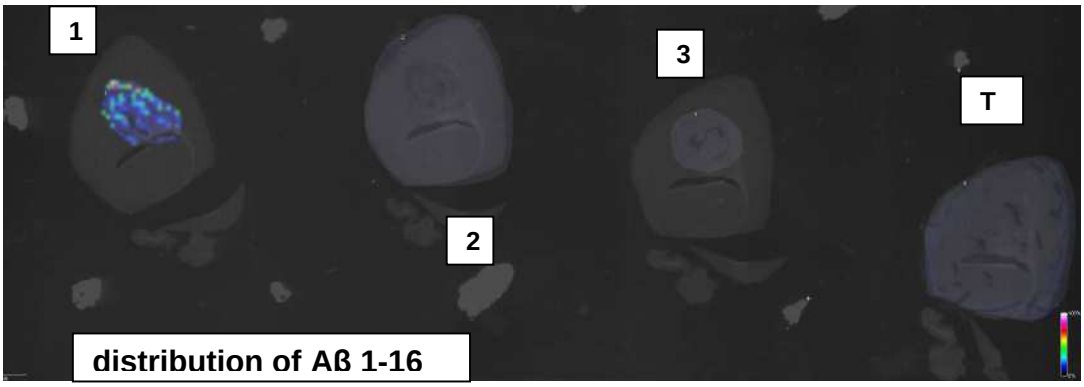
1
2
3
T
distribution of Aß 1-16

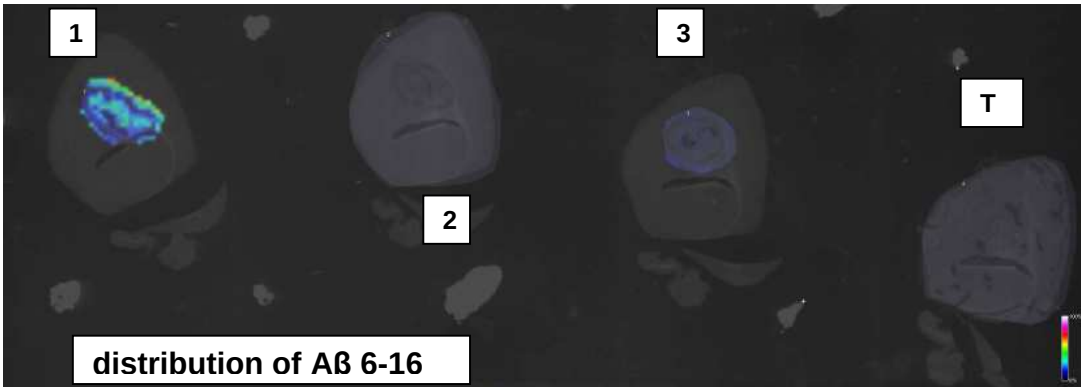
1
2
3
T
distribution of Aß 6-16

Fig.49 *MALDI Imaging results from dewaxed formalin-fixed TASTPM brain sections. Treatment of sections:* ***1*** *- 1mg/ml Aβ 1-40 + trypsin (500ng/µl),* ***2*** *- 1mg/ml Aβ 1-40 only,* ***3*** *- 100µg/ml Aβ 1-40 + trypsin (500ng/µl),* ***T*** *- trypsin (500ng/µl) only. Scaling bars indicate intensity of signal, from low intensity (blue) to high intensity (white). Magnification x 5*

From these sections it can be seen that Aβ 1-40 is only detectable on the section where no trypsin was added, indicating that all Aβ 1-40 was digested on the other sections. Aβ 17-40, 1-16 and 6-16 were all detected on the section with the 1mg/ml Aβ solution added, with just 17-40 detectable with the 100µg/ml Aβ solution. Encouragingly, it appears that Aβ 17-40 was detected on the section treated with trypsin only, indicating that crosslinked Aβ has been digested by the trypsin, allowing it's detection by MALDI.

5.3.1.4. Aβ 1-40 spotted on to dewaxed sections, followed by 24 hour trypsin digest (500ng/µl)

Aβ peptide fragments 1-40, 17-40 and 1-16 were observed on tissue sections following digest (Fig.50).

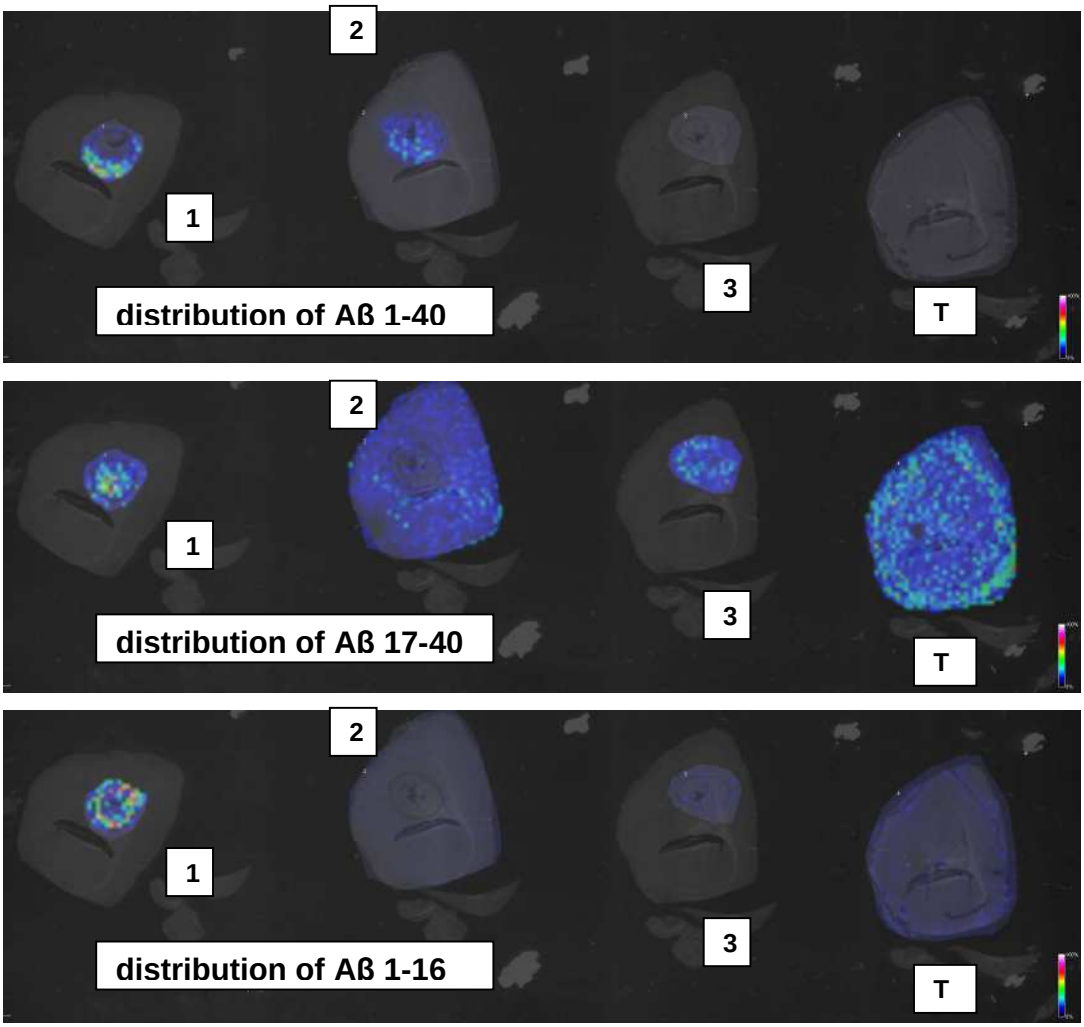

Fig.50 *MALDI Imaging results from dewaxed formalin-fixed TASTPM brain sections. Treatment of sections:* ***1*** *- 1mg/ml Aβ 1-40 + trypsin,* ***2*** *- 1mg/ml Aβ 1-40 only,* ***3*** *- 100µg/ml Aβ 1-40 + trypsin,* ***T*** *- trypsin, trypsin only. Scaling bars indicate intensity of signal, from low intensity (blue) to high intensity (white). Magnification x 5*

From these sections it can be seen that Aβ 1-40, as well as 17-40 and 1-16 were detected on the section treated with 1mg/ml Aβ solution plus trypsin, the Aβ 1-40 detected is likely as a result of the trypsin solution spot not entirely covering the spot of applied Aβ 1-40. Aβ 17-40 is the only fragment detected on the section treated with 100µg/ml Aβ solution plus trypsin, indicating Aβ 1-16 may have been further digested. Aβ 17-40 has been detected in large amounts

on the section only treated with trypsin, suggesting digestion of endogenous Aβ within the tissue.

The detection of Aβ fragments on dewaxed sections treated with trypsin in these experiments indicates that there is potential in this method for digesting protein crosslinks in formalin-fixed tissues, allowing proteomic analysis by MALDI MS Imaging. The following sections describe our attempts to refine these methods.

5.3.2. Refinement of protocol, optimisation of trypsin concentrations and limits of amyloid detection

5.3.2.1. Aβ 1-40 (1mg/ml) spotted on to frozen TASTPM brain sections sections, followed by 1 hour trypsin digest

1 mg/ml Aβ was spotted on to frozen TASTPM brain sections, followed by digestion with varying concentrations of trypsin. Aβ peptide fragments 1-40, 17-40 and 1-16 were observed on tissue sections following digest (Fig.51).

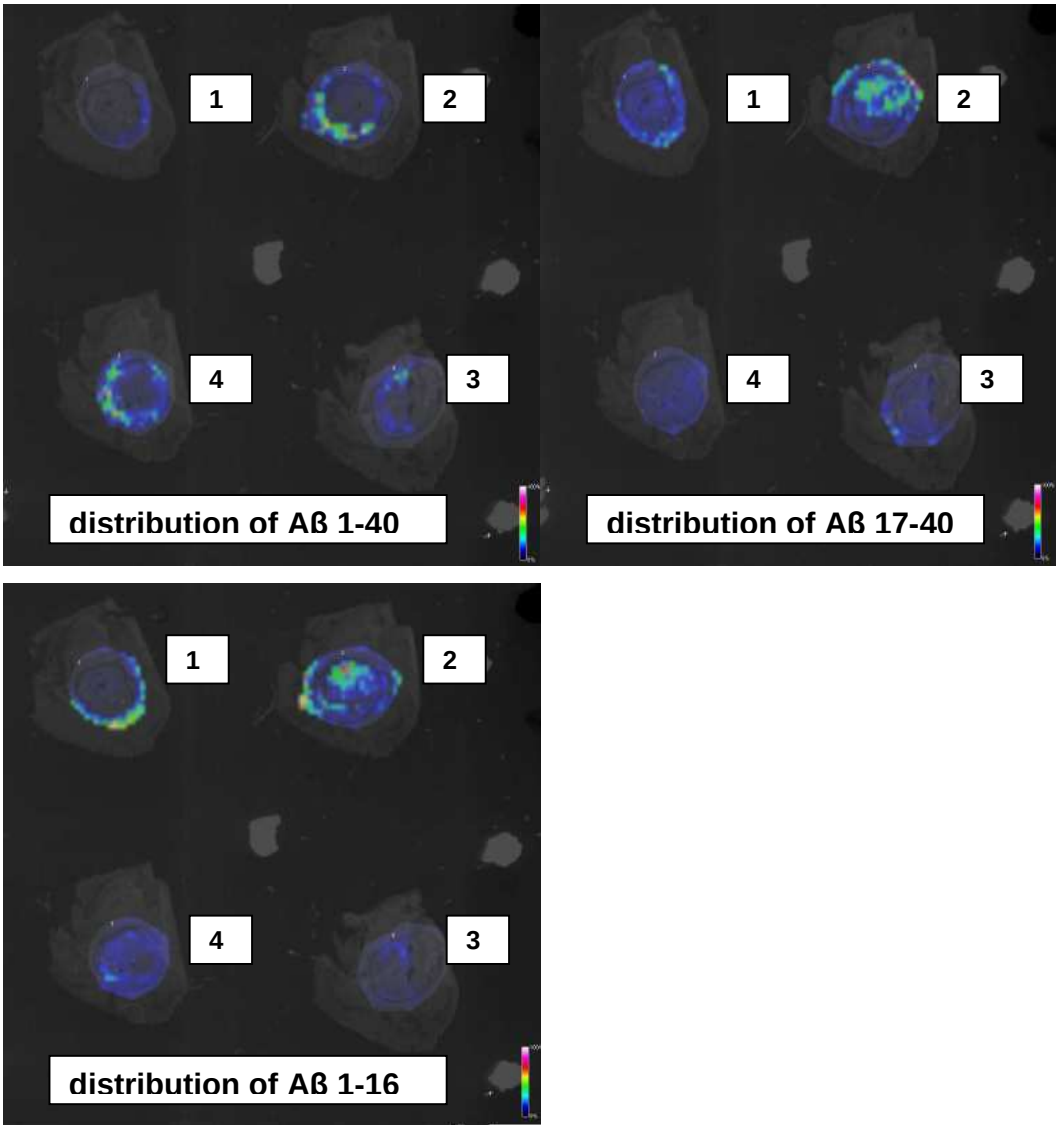

Fig.51 *MALDI Imaging results from frozen brain sections from TASTPM mice. Trypsin concentrations on sections **1** - 500ng/µl, **2** - 50ng/µl, **3** - 500pg/µl, **4** - 5ng/µl. Scaling bars indicate intensity of signal, from low intensity (blue) to high intensity (white). Magnification x 5*

From these images, the only trypsin concentration where both Aβ 17-40 and 1-16 can be detected is 50ng/ml, in which the original peptide is also detected, but it appears that this is due to the trypsin spot not fully covering the applied Aβ 1-40 spot. The 500ng/ml trypsin appears to have fully digested the applied Aβ 1-40 and digested the endogenous amyloid around the spot, causing

detection of Aβ 1-16 from endogenous amyloid. Due to detection of Aβ 17-40 1-16 it appears that for 1 hour trypsin digests 50ng/ml trypsin solution is the optimum concentration of the four tested.

5.3.2.2. Different Aβ 1-40 concentrations spotted onto frozen TASTPM brain sections along with trypsin digests

Aβ concentrations of 1mg/ml, 200µg/ml, 40µg/ml and 8µg/ml were spotted onto frozen TASTPM brain sections, on the same slide, 24 hour trypsin digests were carried out using trypsin at 20ng/µl. Aβ 1-40 was detectable at 200µg/ml, but not at 40µg/ml. On trypsin digests of the 1mg/ml spot, fragments 1-40, 6-16, 17-28 were visible. Thus the limit of detection in a spot approximately 1mm in diameter is 200ng (1µl of 200µg/ml in the spot). For trypsin digests it seems more than this amount is needed for subsequent fragment detection.

5.3.2.3. Aβ 1-40 spotted on to dewaxed sections, followed by both 1 hour and 24 hour trypsin digests

In the 1 hour digest, Aβ 1-40, as well as fragments 17-40, 17-28, 1-16 and 6-16 were observed on tissue sections (Fig.52)

In the 24 hour digest, Aβ 1-40, as well as fragments 17-40, 17-28, 1-16 and 6-16 were observed on tissue sections (Fig.53)

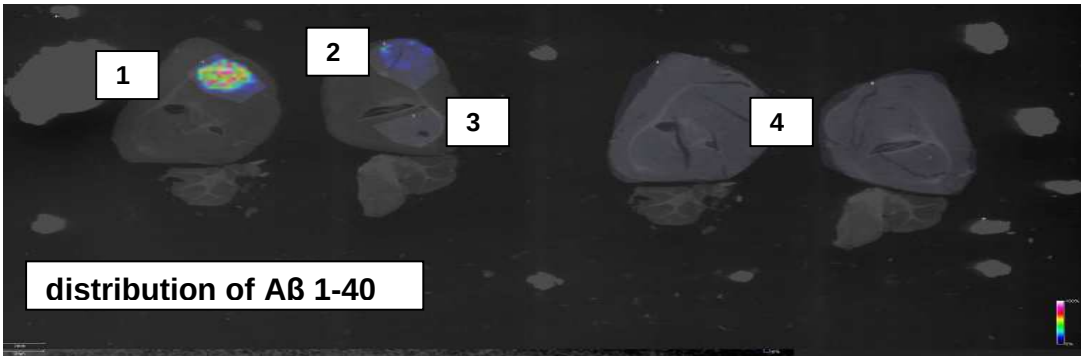
1
2
3
4
distribution of Aß 1-40

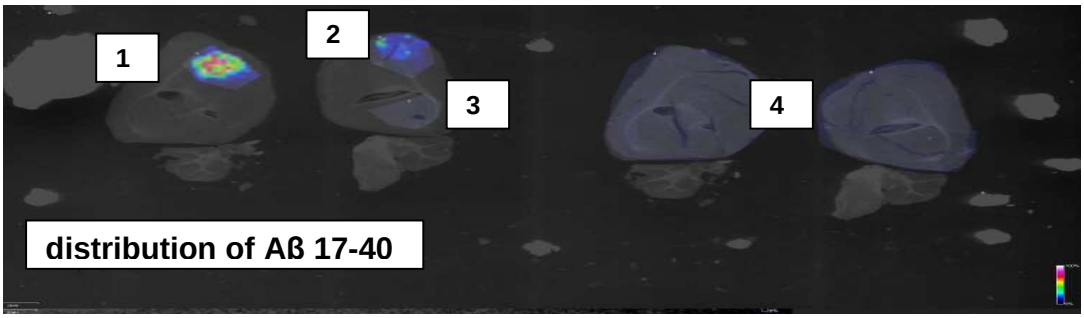
1
2
3
4
distribution of Aß 17-40

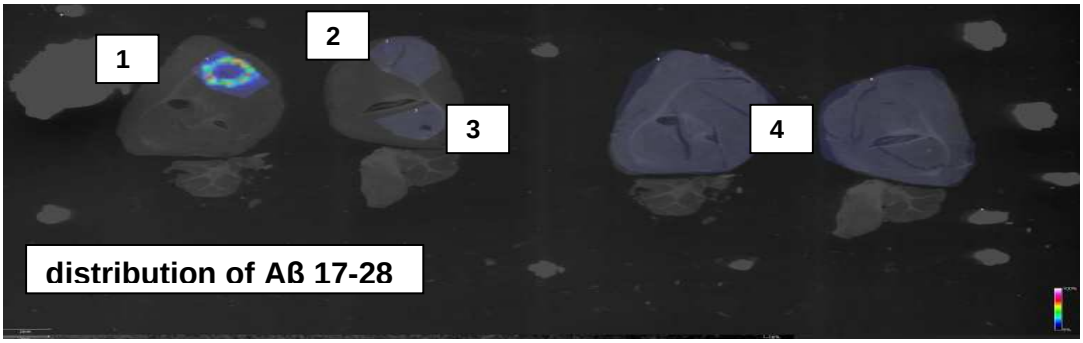
1
2
3
4
distribution of Aß 17-28

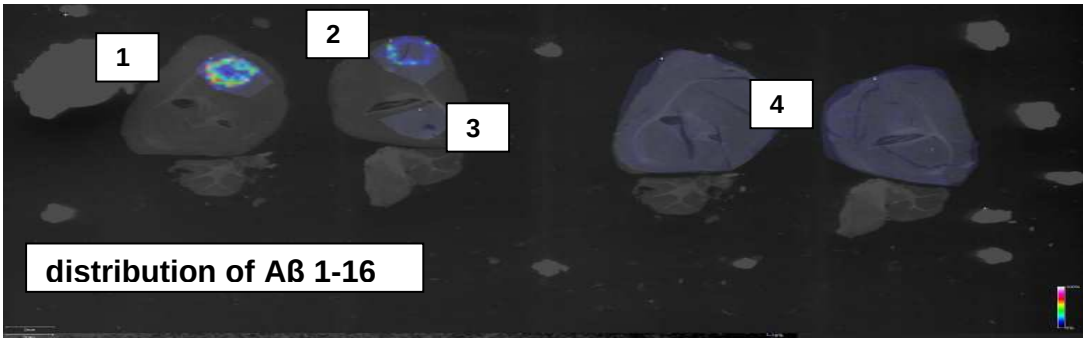
1
2
3
4
distribution of Aß 1-16

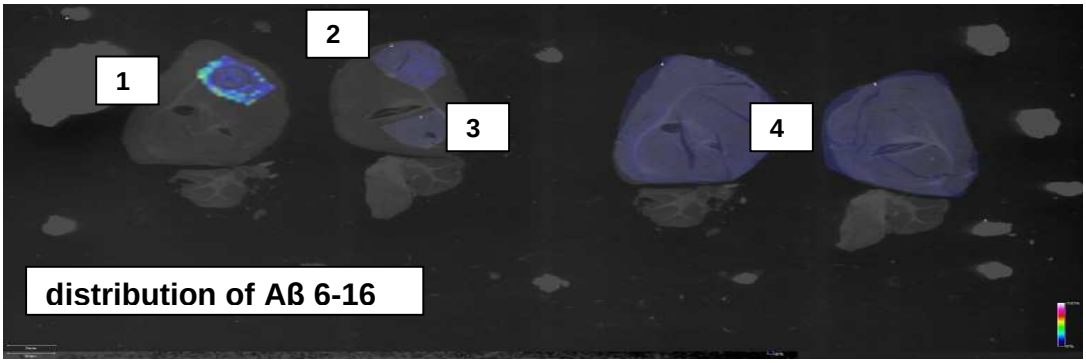

Fig.52 *MALDI Imaging results from dewaxed formalin-fixed TASTPM brain sections, 1 hour trypsin digest. Treatment of sections* ***1*** *- 1mg/ml Aβ 1-40 + trypsin (40ng/µl),* ***2 (top spot, second section from the left)*** *- 200µg/ml Aβ 1-40 + trypsin (40ng/µl),* ***3 (bottom spot, second section from the left)*** *– 40µg/ml Aβ 1-40 + trypsin (40ng/µl),* ***4 (Both right hand sections)*** *– trypsin (40ng/µl) only. Scaling bars indicate intensity of signal, from low intensity (blue) to high intensity (white). Magnification x 5*

From these images, after 1 hour trypsin digests, all the Aβ fragments mentioned above are detectable on the 1 mg/ml Aβ spot. Aβ 1-40, 17-40 and 1-16 can just be detected on the 200µg/ml Aβ spot. Nothing can be detected on the 40µg/ml Aβ spot, unfortunately the same is the case for the two sections which just had trypsin added to them, indicating digestion of endogenous, crosslinked Aβ has not occurred.

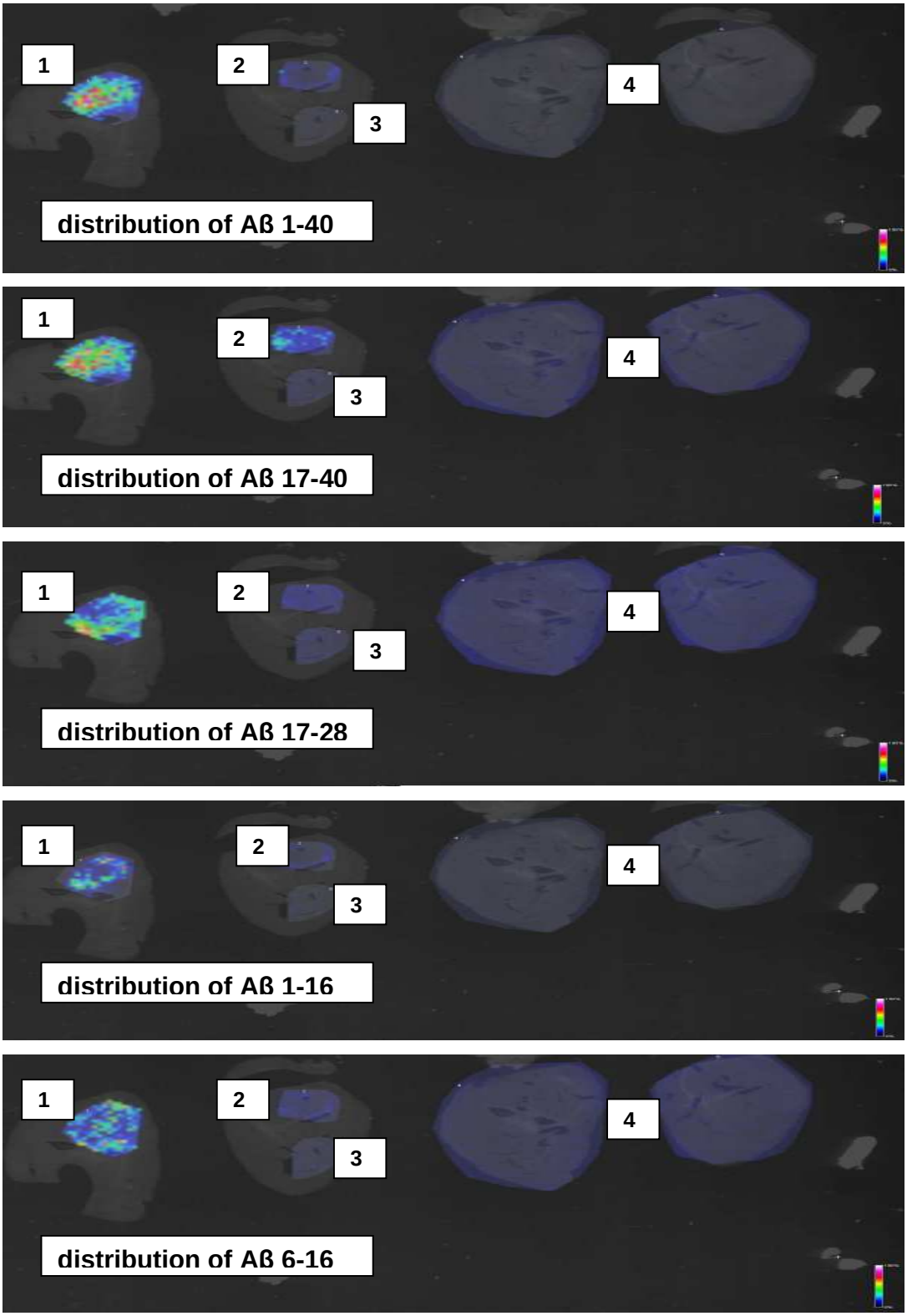

Fig.53 *MALDI Imaging results from dewaxed formalin-fixed TASTPM brain sections, 24 hour trypsin digest. Treatment of sections **1** - 1mg/ml Aβ 1-40 +*

trypsin (40ng/µl), ***2 (top spot, second section from the left)*** *- 200µg/ml Aβ 1-40 + trypsin (40ng/µl),* ***3 (bottom spot, second section from the left)*** *– 40µg/ml Aβ 1-40 + trypsin (40ng/µl),* ***4 (Both right hand sections)*** *– trypsin (40ng/µl) only. Scaling bars indicate intensity of signal, from low intensity (blue) to high intensity (white). Magnification x 5*

From these sections it can be seen that after 24 hour trypsin digests, all the amyloid fragments mentioned are detectable on the 1mg/ml Aβ 1-40 spot. Aβ 1-40 and17-40 can just be detected on the 200µg/ml Aβ 1-40 spot. Nothing can be detected on the 40µg/ml Aβ 1-40 spot, unfortunately the same is the case for the two sections which just had trypsin added to them, again indicating digestion of endogenous, crosslinked Aβ has not occurred.

5.3.3. Matrix application comparison

Manual spray was compared to automated (ImagePrep) matrix application. During this experiment the initial detection of the unknown ion m/z 4811 in THI regions of TASTPM brains was made. In the case of the unknown peptide, the ImagePrep was found to give better signal localisation (Fig.54) but less overall signal (Fig.52). Maximum intensity of the unknown peptide was found to be 4800 for ImagePrep matrix application, whereas the maximum intensity for manual matrix application was 15000 (Fig.55).

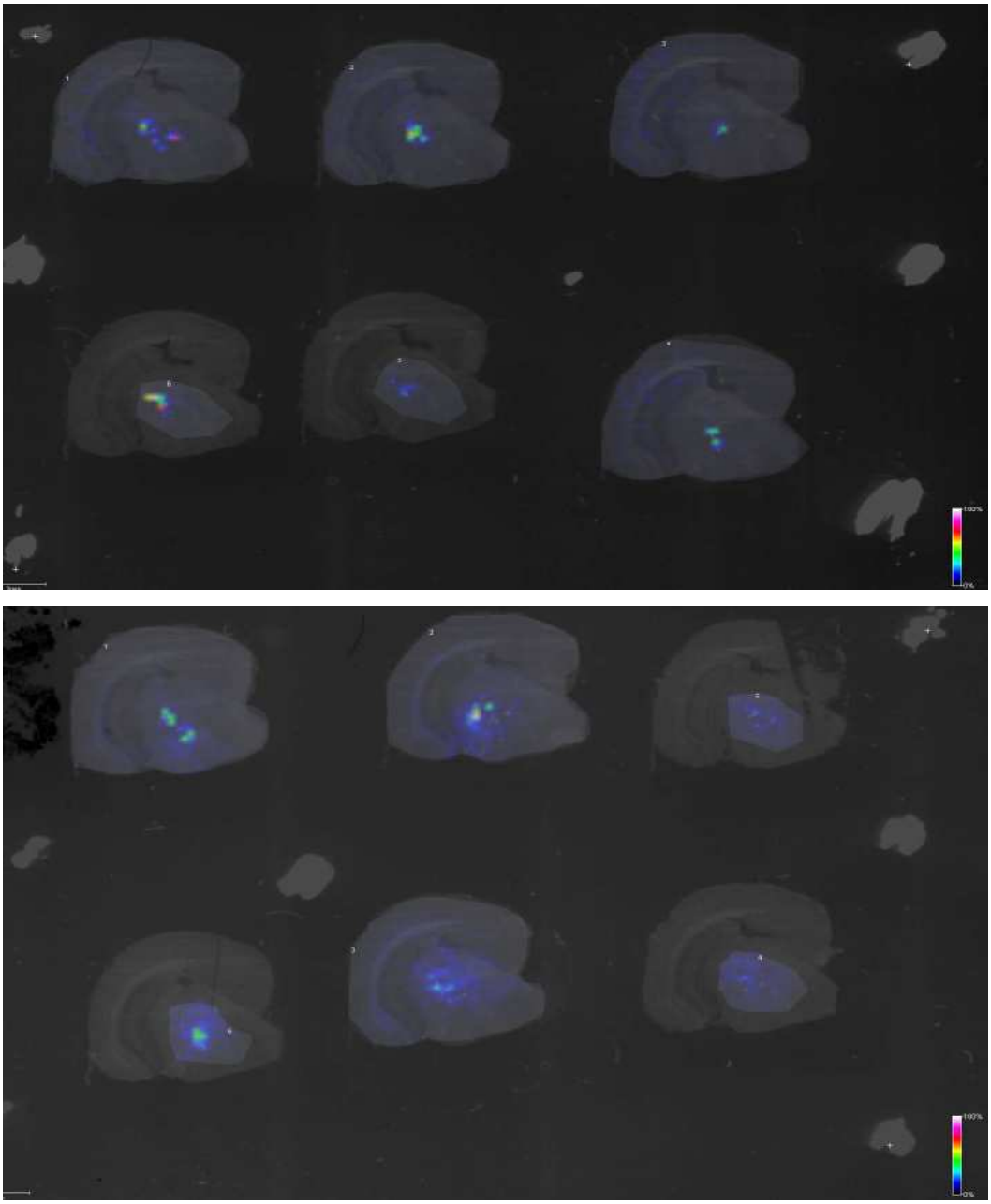

Fig.54 *Images showing distribution of unknown ion m/z 4811 in TASTPM brain sections containing thalamic hypointensity regions. ImagePrep (top), manual spray (bottom). Scaling bars indicate intensity of signal, from low intensity (blue) to high intensity (white). Magnification x 5*

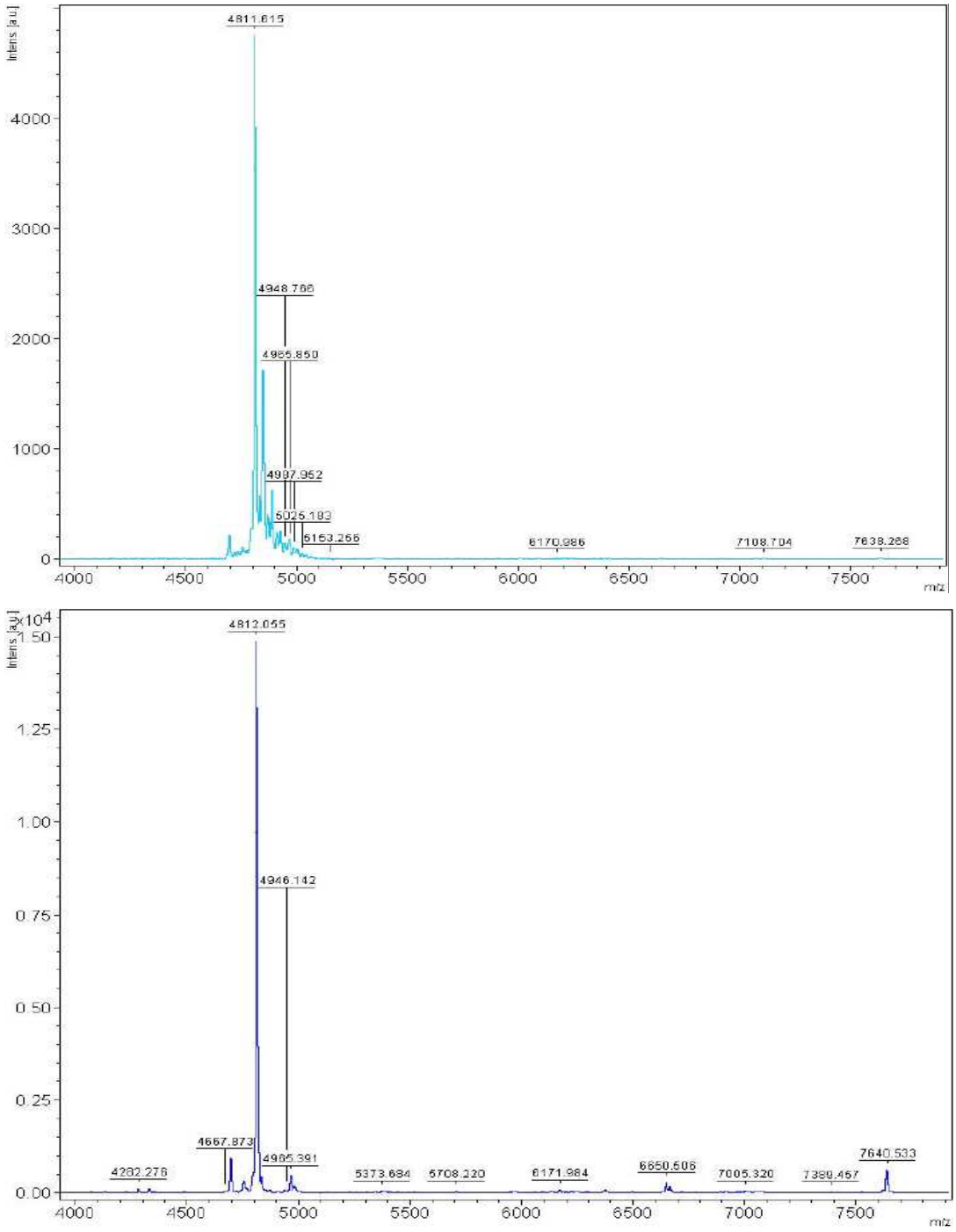

Fig.55 *Mass spectra from THI regions showing intensity of signal for unknown peptide 4811. ImagePrep (top), manual spray (bottom).*

From these images and spectra, it appears that manual spraying has allowed for stronger detection of the peptide in question, whereas the ImagePrep

seems to suffer from less delocalisation, with the peptide signal confined to smaller areas.

When the overall spectra from the experiments are examined (Fig.56), the situation is very different, while no information is available about localisation of molecules, it can be clearly seen that, in this instance, not only can many more different molecules be detected by the manual spray technique, but overall signal strength is also better.

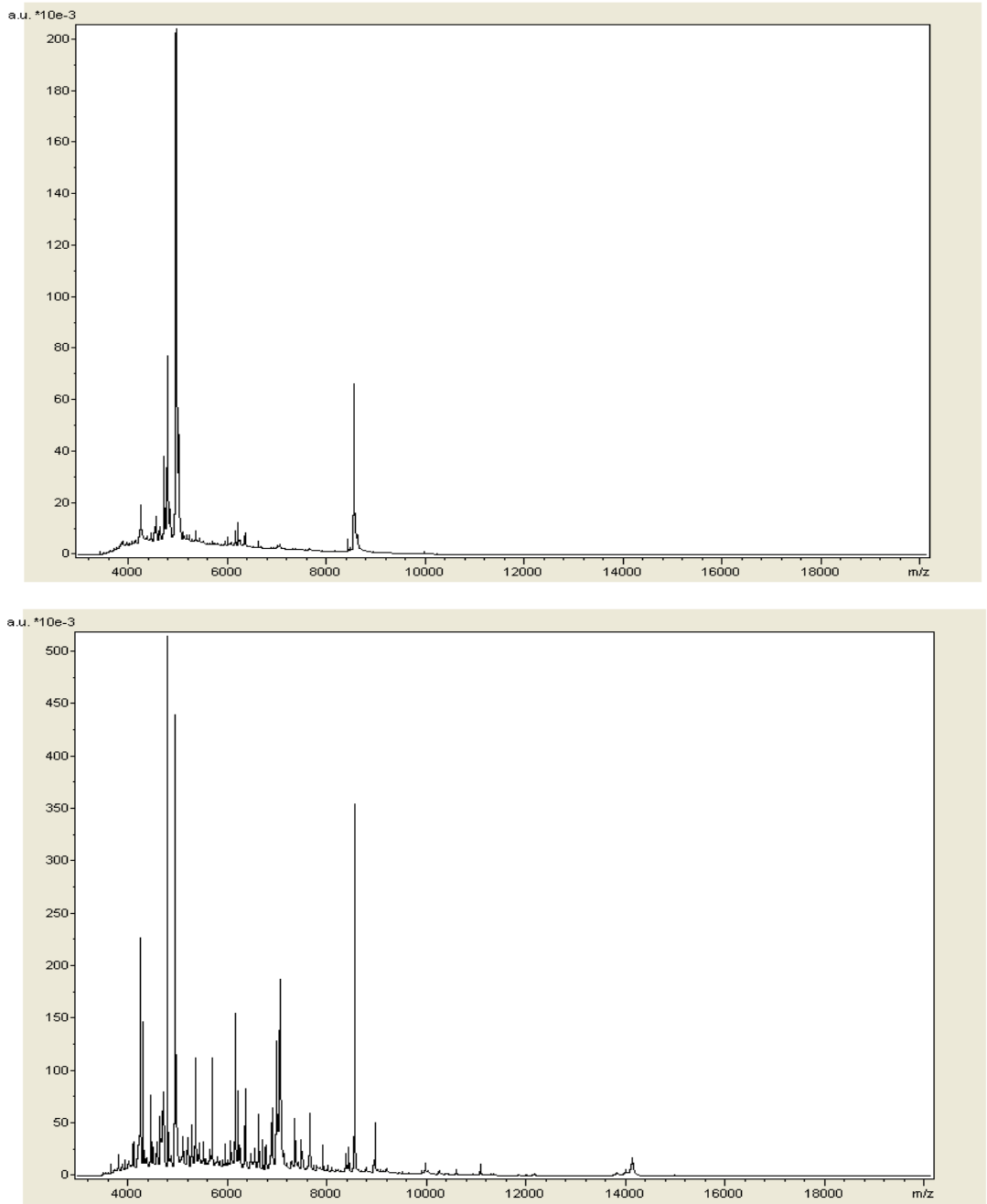

Fig.56 *Overall spectra from ImagePrep (top) and manual spray (bottom) comparison*

Following this experiment, focus shifted to analysis of the distribution and signal intensity of the unknown peptide m/z 4811 in TASTPM and wild type mouse brains.

5.3.4. Analysis of TASTPM and Wild Type brain sections in order to image the distribution of the unknown peptide identified above

5.3.4.1. 12 month TASTPM brain sections imaged to look for distribution of unknown ion

The unknown ion 4811 was found to be localised to the THIs, another ion m/z 7635 was also found localised to the THIs (Fig 57). The highest intensity peak of the 4811 ion was 14000 (Fig.58), the highest intensity of the 7636 peak was 400.

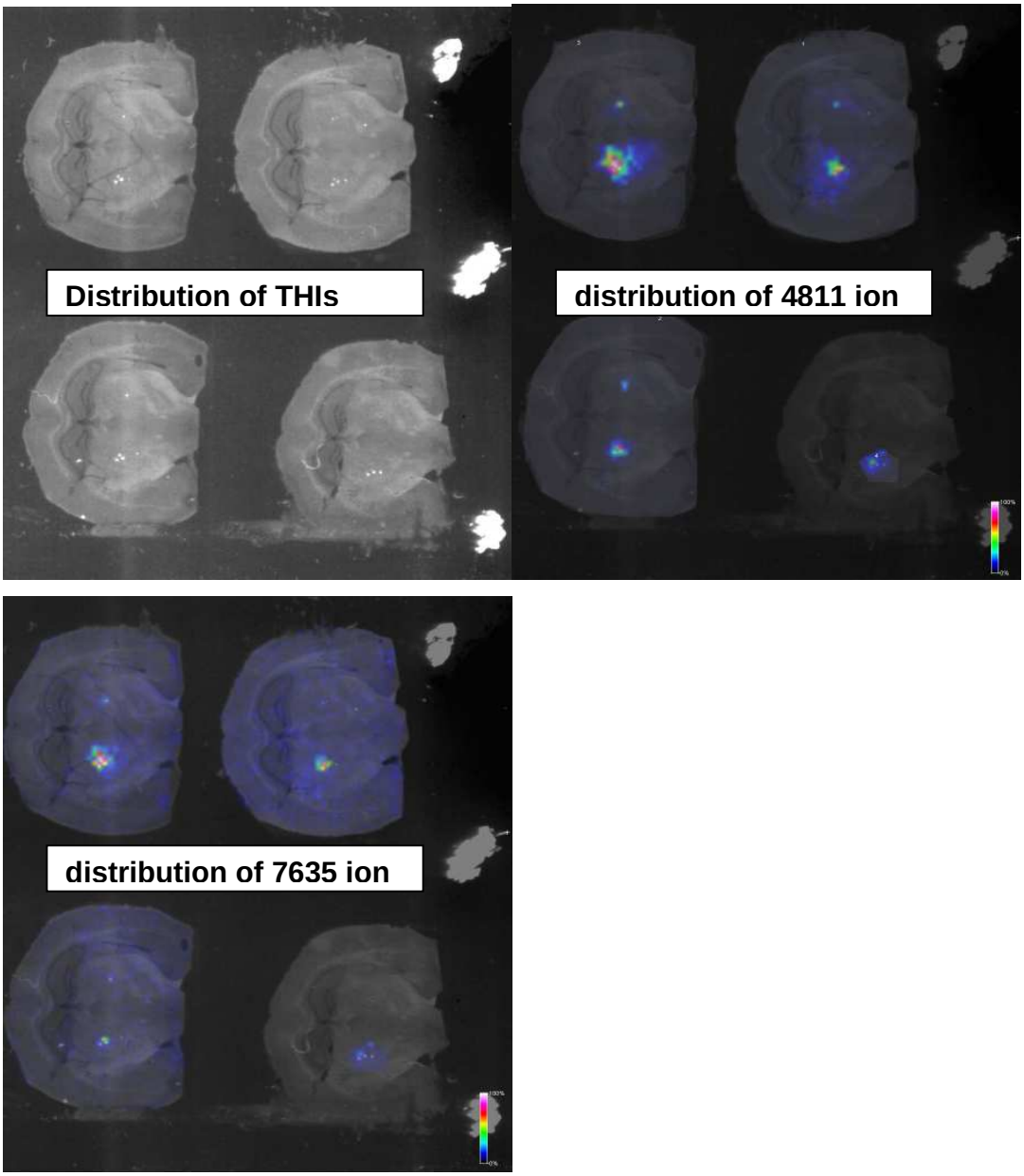

Fig.57 *MALDI Images of 12 month old TASTPM brain sections showing an optical image with the THIs depicted as white spots, and the distribution of the 4811 ion (coloured spots) and its localisation to the THI regions. Another ion found localised to the THI regions, though apparently in much lesser concentration, m/z 7635 is also shown. Scaling bars indicate intensity of signal, from low intensity (blue) to high intensity (white). Magnification x 5*

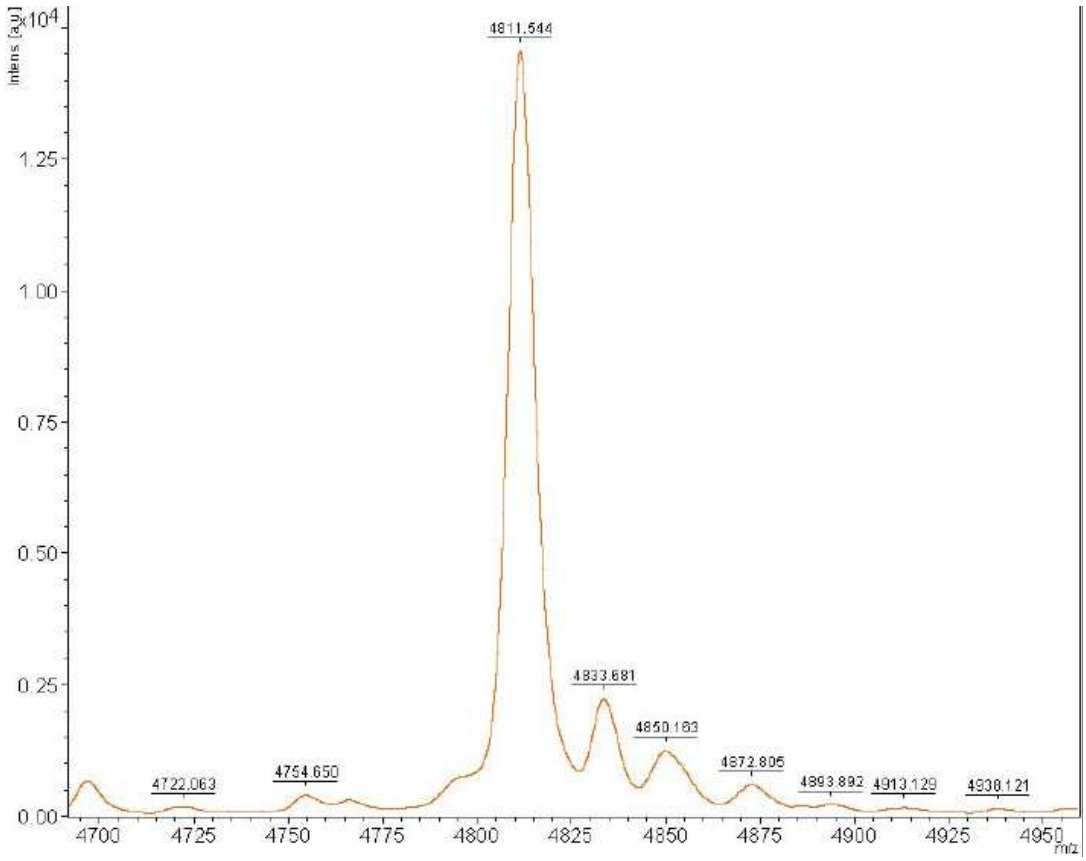

Fig.58 *Zoom of relevant section of mass spectrum showing highest intensity of unknown ion 4811*

5.3.4.2. 18 month TASTPM brain sections Imaged to look for distribution of unknown ion

The unknown ion 4811 was found to be localised to the THIs, another ion m/z 7635 was also found localised to the THIs (Fig 59). The highest intensity peak of the 4811 ion was 20000 (Fig.60), the highest intensity of the 7636 peak was 750

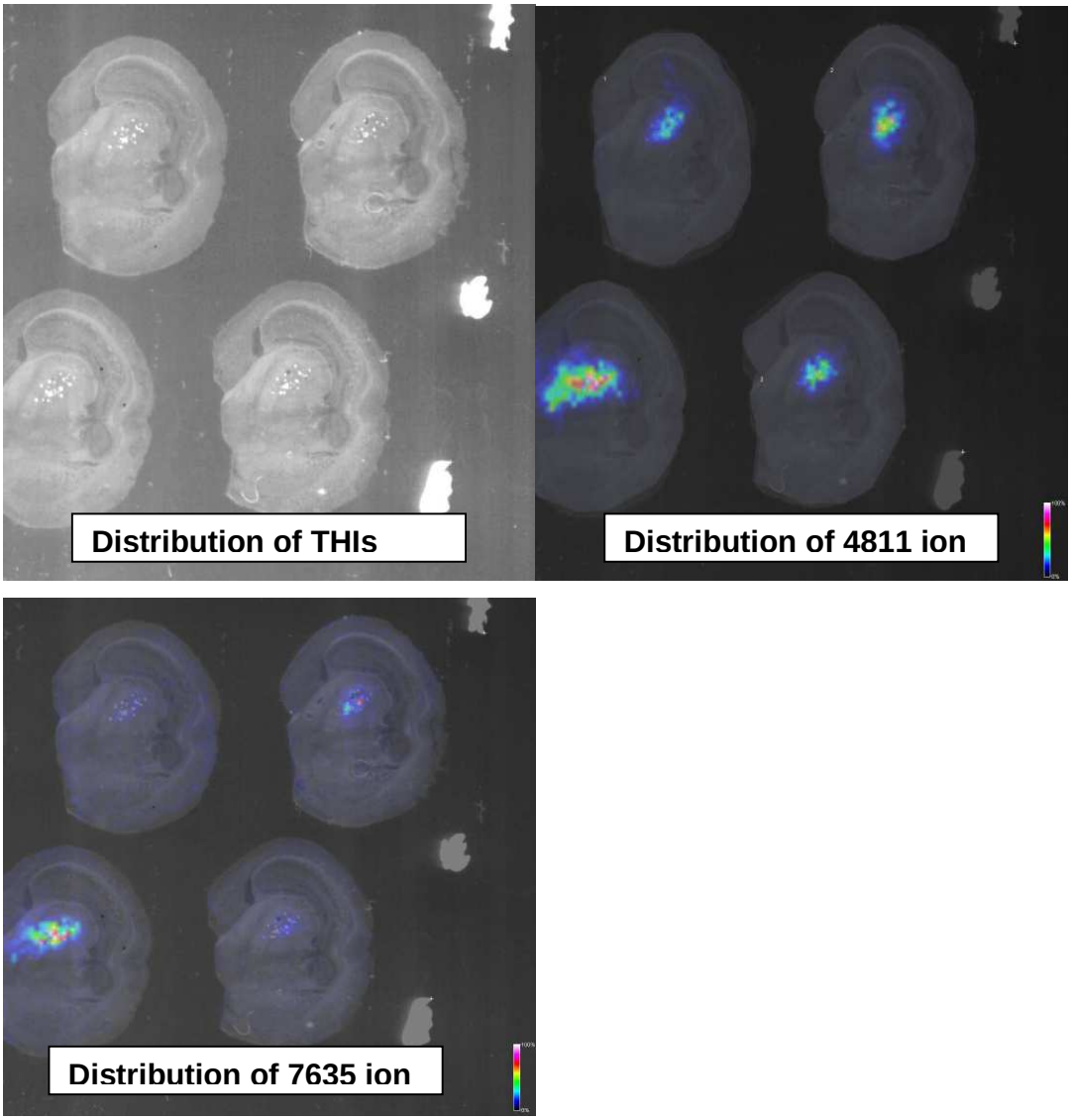

Fig.59 *MALDI Images of 18 month old TASTPM brain sections showing an optical image with the THIs depicted as white spots, also the distribution of the 4811 and 7635 ions and their localisation to the THI regions. Scaling bars indicate intensity of signal, from low intensity (blue) to high intensity (white). Magnification x 5*

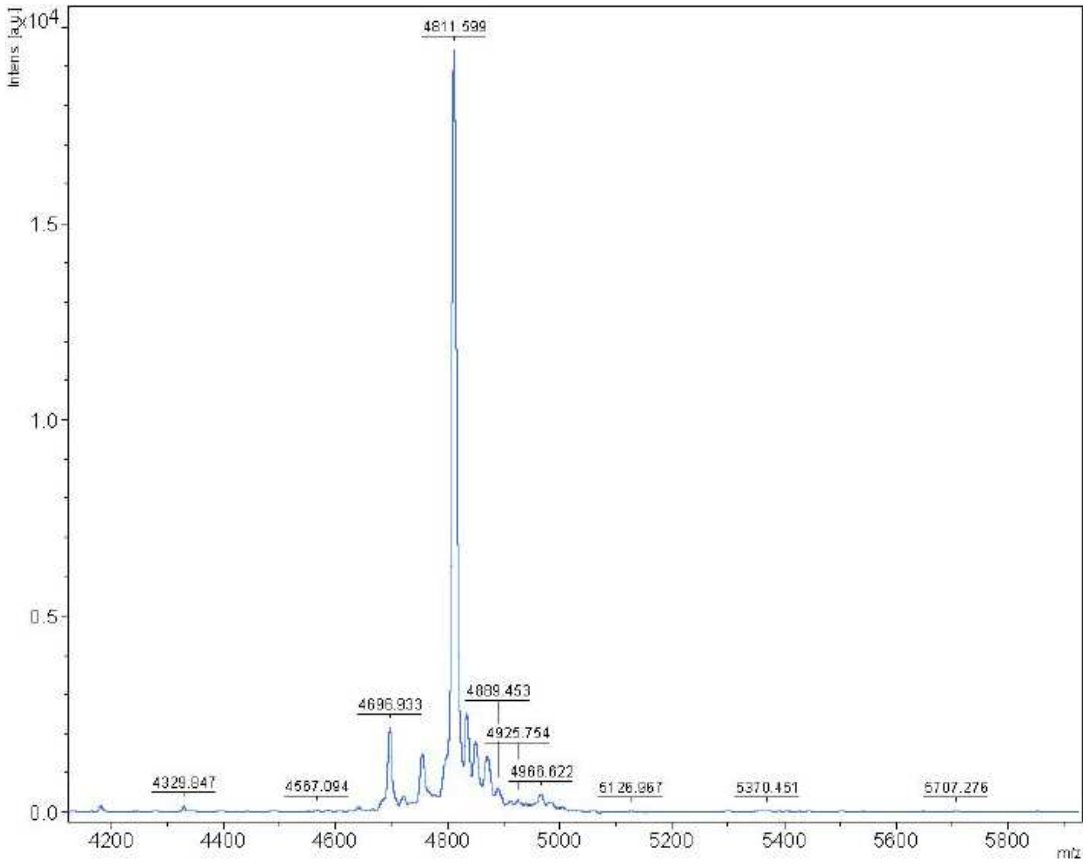

Fig.60 *Zoom of relevant section of mass spectrum showing highest intensity of unknown ion 4811*

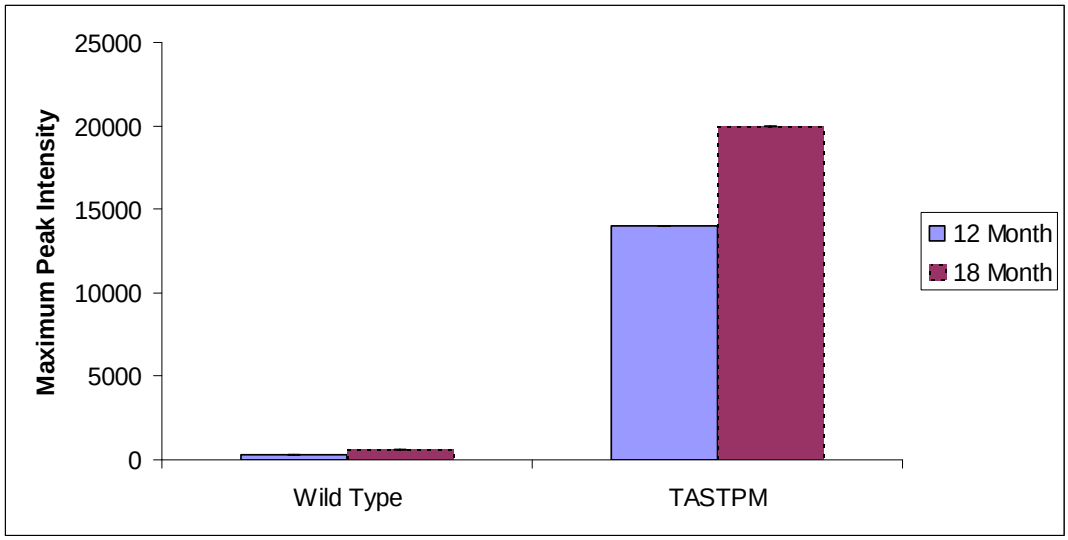

Fig.61 *Graph showing maximum peak intensities for detection of 4811 peptide in TASTPM and wild type mice*

5.3.4.3. 12 month Wild Type brain sections Imaged to look for distribution of unknown ion

Small THIs were found in the thalamus, 4811 peptide was found to be present (Fig. 62), the highest intensity peak was 300 (Fig. 63).

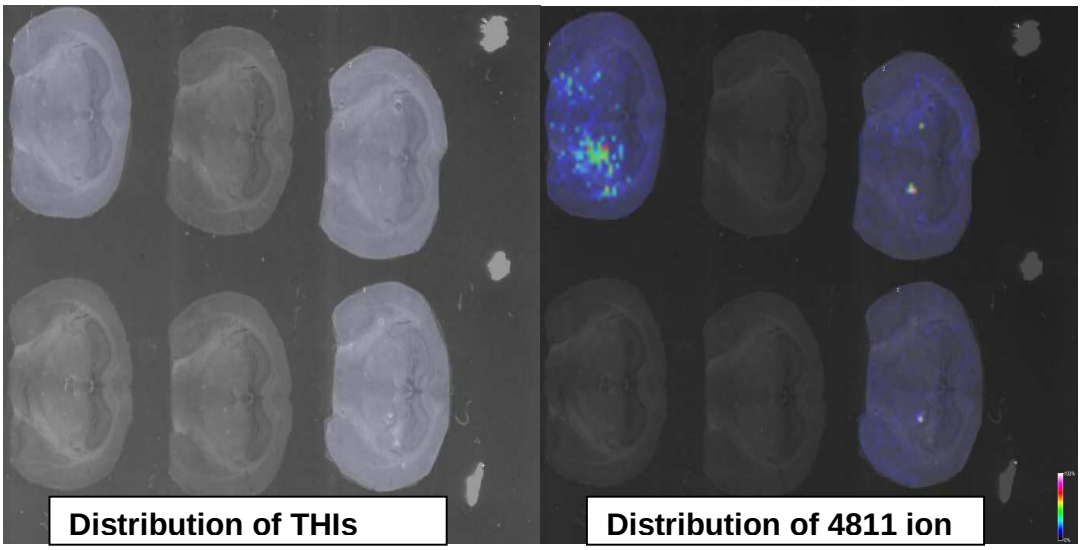

Fig.62 *MALDI Images of 12 month old wild type brain sections showing an optical image with the small THIs depicted as white spots, also the distribution of the 4811 ion and its localisation to the THI regions. Scaling bars indicate intensity of signal, from low intensity (blue) to high intensity (white). Magnification x 5*

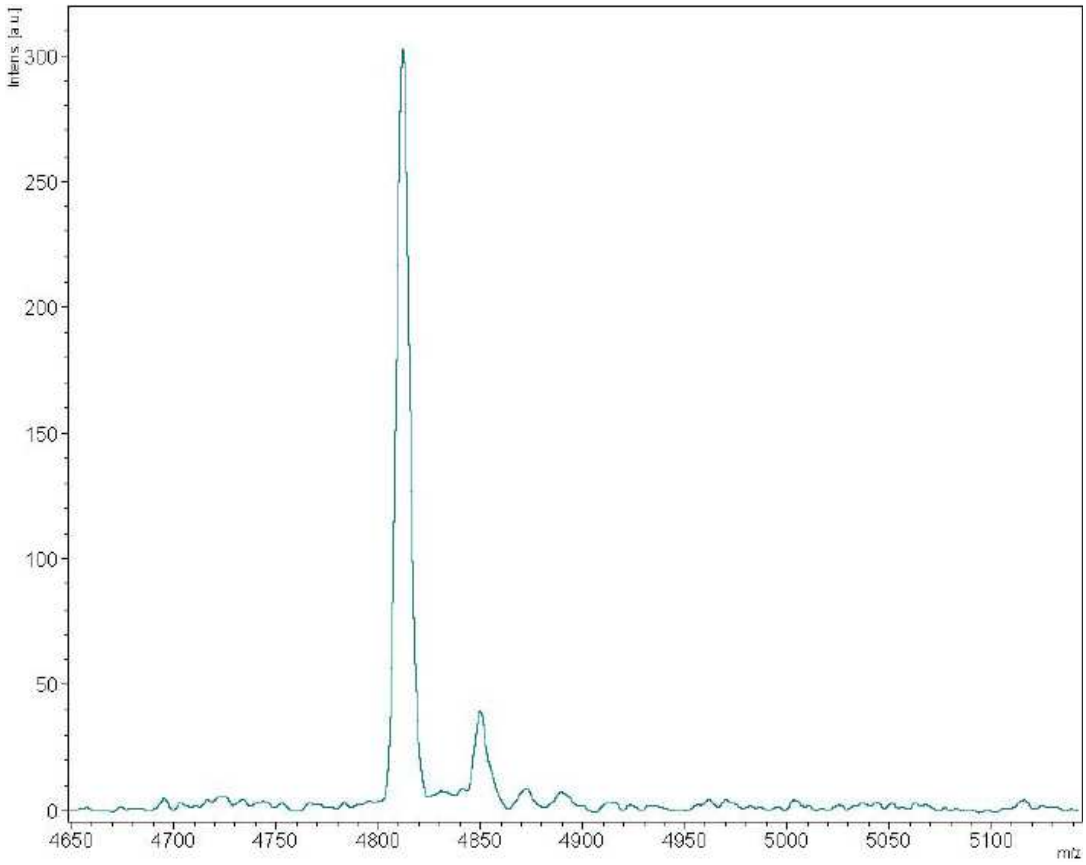

Fig.63 *Zoom of relevant section of mass spectrum showing highest intensity of unknown ion 4811*

5.3.4.4. 18 month Wild Type brain sections Imaged to look for distribution of unknown ion

Small THIs were found in the thalamus, 4811 peptide was found to be present (Fig.64), the highest intensity peak was 600 (Fig.65).

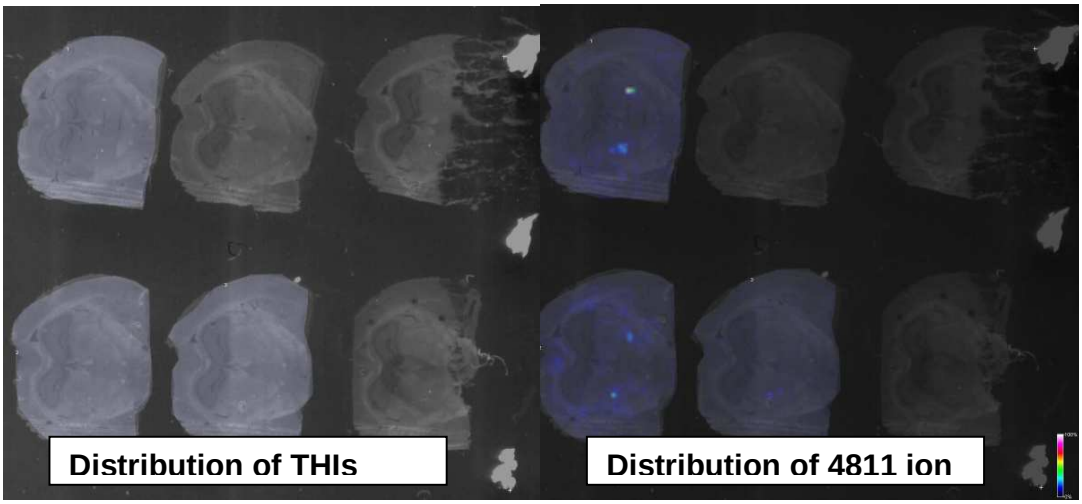

Fig.64 *MALDI Images of 18 month old wild type brain sections showing an optical image with the small THIs depicted as white spots, also the distribution of the 4811 ion and its localisation to the THI regions. Scaling bars indicate intensity of signal, from low intensity (blue) to high intensity (white). Magnification x 5*

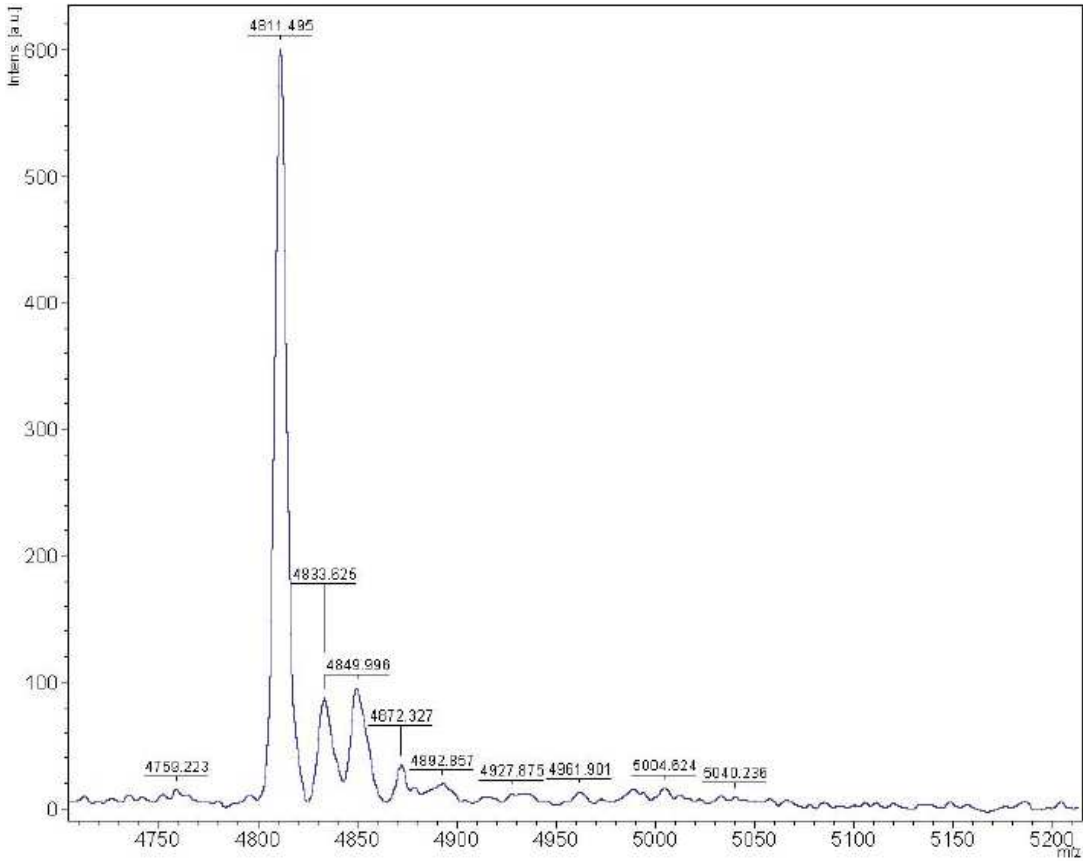

Fig.65 *Zoom of relevant section of mass spectrum showing highest intensity of unknown ion 4811*

5.3.5. Direct comparison of TASTPM and wild type brain sections on the same slide

5.3.5.1. 12 month TASTPM and Wild Type sections on same slide for comparison

Coronal sections of brains from both TASTPM and wild type mice were MALDI imaged on the same slide for direct comparison. Both the 4811 and 7635 peptides were seen in TASTPM sections, neither was detected in wild type sections (Fig.66)

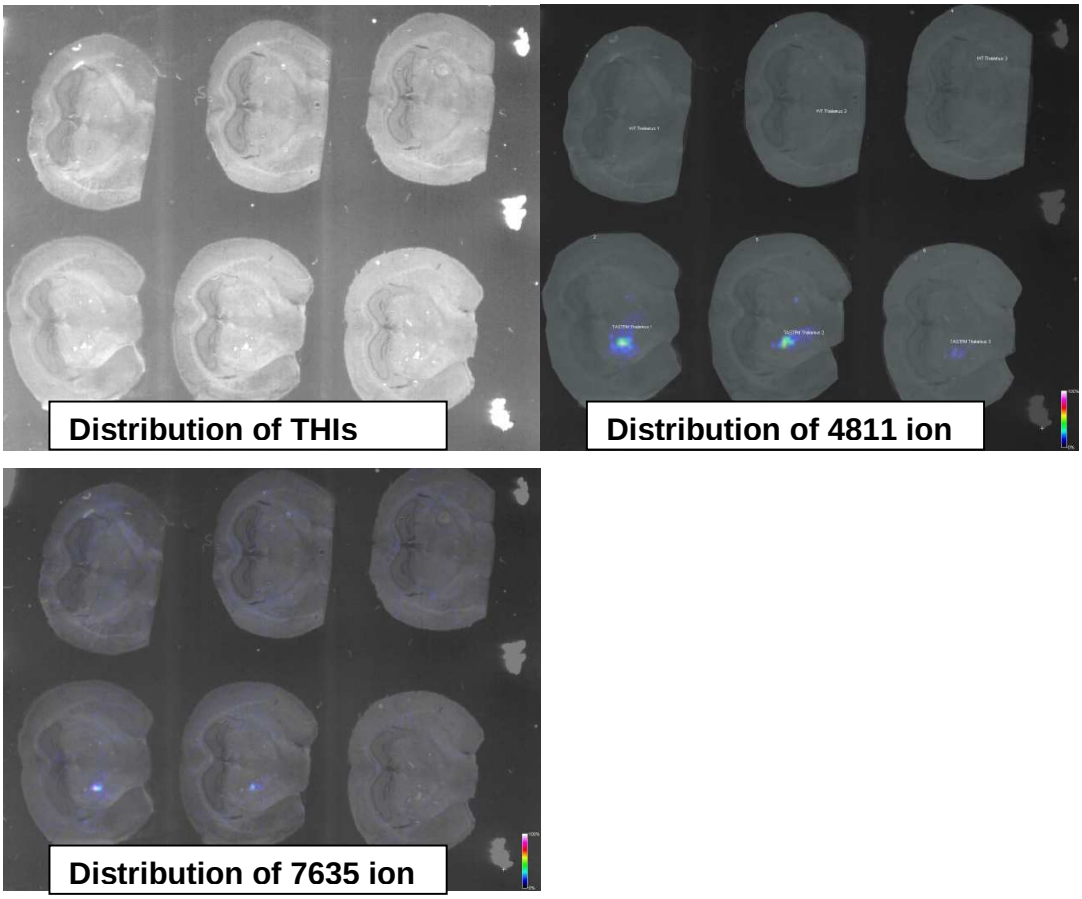

Fig.66 *MALDI Images of 12 month old TASTPM (bottom 3) and wild type (top 3) brain sections showing an optical image with the THIs (where present)*

depicted as white spots, also the distribution of the 4811 and 7635 ions and their localisation to the THI regions. Scaling bars indicate intensity of signal, from low intensity (blue) to high intensity (white). Magnification x 5

5.3.5.2. 18 month TASTPM and Wild Type sections on same slide for comparison

Coronal sections of brains from both TASTPM and wild type mice were MALDI imaged on the same slide for direct comparison. Both the 4811 and 7635 peptides were seen in TASTPM sections, neither were detected in wild type sections (Fig.67)

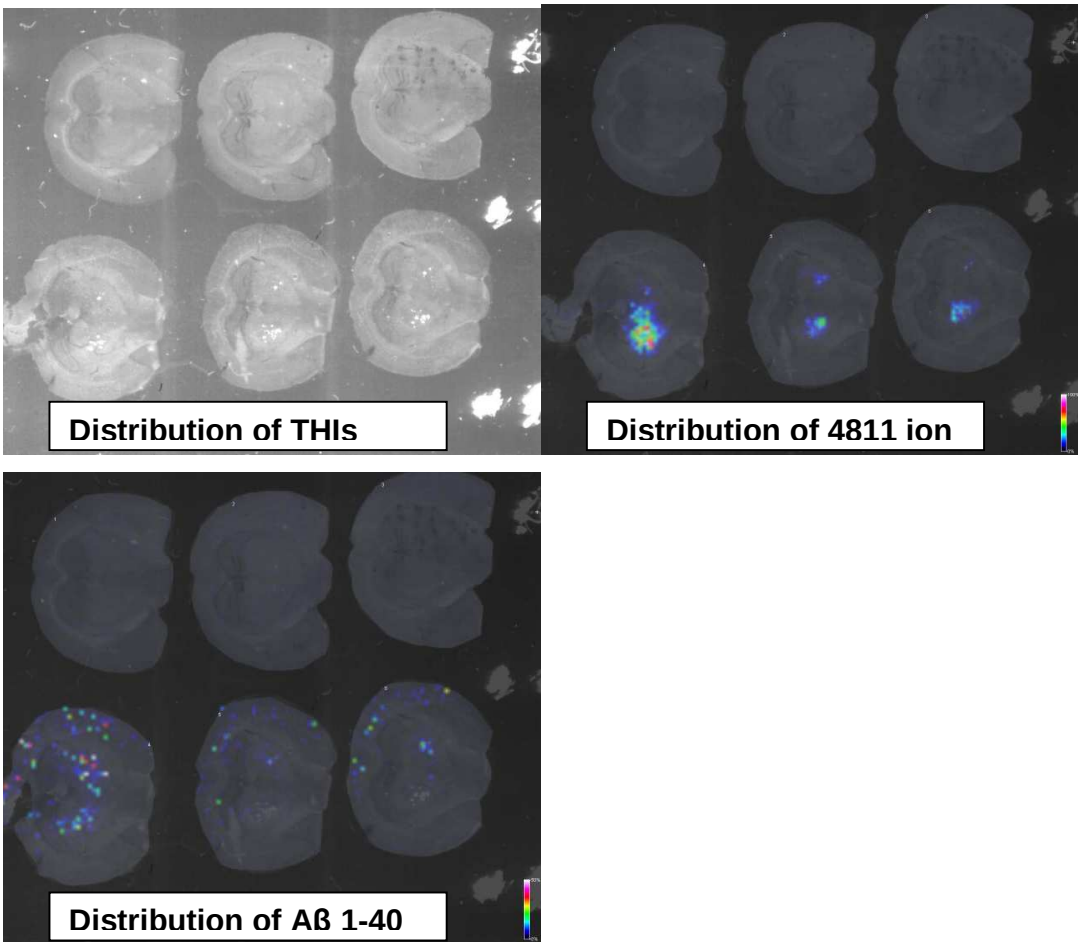

Fig.67 *MALDI Images of 18 month old TASTPM (bottom 3) and wild type (top 3) brain sections showing an optical image with the THIs (where present)*

depicted as white spots, also the distribution of the 4811 ion and its localisation to the THI regions. Also shown is a visualisation of amyloid plaques detected by the presence of Aβ 1-40 in the TASTPM sections. Scaling bars indicate intensity of signal, from low intensity (blue) to high intensity (white). Magnification x 5

From the findings above, the 4811 peptide (and the 7635) are well localised to the THI regions, as well as giving a stronger signal the more developed the THI regions are. It is possible that one or both are linked to the underlying processes which cause the development of these lesions. Identification of the unknown peptides could provide valuable information about not only the THI regions, but of amyloid pathology in general.

In an effort to identify the 4811 and 7635 peptides, LCM was used to isolate and dissect out the THI regions, extraction procedures were then used to dissolve the contents and LC-MS was performed to attempt to identify the components. LC-MS was used as it is much more sensitive than MALDI so the chances of identifying a very small amount of a molecule are much greater.

5.3.6. Further analysis of components of THI regions isolated by LCM

5.3.6.1. MALDI Analysis of LCM samples

MALDI analysis of the THI regions isolated by LCM was able to identify Aβ 1-38, 1-40 and 1-42 along with the unknown peptide 4811. MS/MS was attempted on the 4811 fragment but no signal was detected. A tryptic digest of the sample was performed and whilst fragments of the amyloid peptides were observed and identified, nothing was observed or identified as a fragment of the 4811 peptide.

5.3.6.2. LC/MS Analysis of LCM samples

LC/MS analysis of THI regions isolated from TASTPM brain sections by LCM allowed identification of a number of proteins localised within the THI regions. These were APP, Glial fibrillary acidic protein, myelin basic protein apolipoprotein E precursor and secretogranin. The unknown peptide 4811 was found to be doubly charged and thus have an actual mass of 9622Da, however it could not be identified. The unknown peptide with mass 7635Da could not be identified either.

5.4. Discussion

The visualisation of amyloid plaques in brain sections from transgenic AD mice by MALDI MS Imaging has been reported before (Rohner et al., 2005; Stoeckli et al., 2006), but this is the first report in TASTPM mice. One of the aims of this research was to visualise the distribution of Aβ 1-40 and Aβ 1-42 in plaques in transgenic mouse brains. One finding of previous studies was that Aβ 1-40 was diffusely spread in different areas of the brain, whereas Aβ 1-42 was more confined to the centre of the denser plaques.

Tryptic digests of applied and endogenous amyloid peptides followed by MALDI MS Imaging has not been reported before. It was also observed that, in the case of frozen sections with applied amyloid peptide the endogenous amyloid peptide is detectable but because it is present at lower concentrations than the applied amyloid peptide, it is difficult to visualise in an image. However, following trypsin digestion, (especially for 24 hours), endogenous amyloid fragments were easily observable on tissue sections treated with trypsin only, in some cases overall signal was stronger than on sections where amyloid had been applied. The trypsin digestion thus appears to make more amyloid fragments available for detection by MALDI than undigested amyloid on untreated sections. It is possible that, due to the aggregated nature of amyloid plaques, not all amyloid peptides are available for ionisation by the MALDI

laser. Thus, when the aggregated structure is broken down by the trypsin digest, the resulting fragments are much more easily ionised, resulting in a much stronger MALDI signal.

In the case of the dewaxed formalin-fixed sections, it was observed that following dewaxing, ions were generated and detected from the tissues. Applied amyloid peptide was detected, along with amyloid fragments following tryptic digests. The tryptic digests of the dewaxed sections without any amyloid applied showed some encouraging results. In the initial 1 and 24 hour trypsin digests (Figs.46 and 47), Aβ 17-40 fragment could be detected on the dewaxed sections. However this was not found when the experiment was repeated. The initial detection of Aβ 17-40 from the tryptic digests of the dewaxed sections suggests that the method could be used to generate information from fixed sections. Further refinement of the techniques is required to ensure reproducibility. Varying the trypsin concentration, the solutes used, the method of application and incubation are all parameters that need refining. Several pilot studies have been carried out (Lemaire et al., 2007; Ronci et al., 2008). Attaining a suitable, reliable and robust method would allow the analysis of extensive libraries of tissue samples, which are a source of vast quantities of clinical and biological information for proteomic investigation.

In the comparison between manual spray matrix application and the ImagePrep automated system, results from the 4811 peptide indicated that overall signal intensity was better with the manual spray method. A potential problem with manual spray can be delocalisation of peptides/proteins of interest, caused by over-wetting of the tissue during matrix application. This gives rise to apparent signal from areas where none of the detected molecule is present. In the same example, the ImagePrep gave much less compound delocalisation than manual spraying. Looking at the overall picture showed that as well as better overall signal strength, many different compounds were detected with the manual spray method than with the ImagePrep. Thus, according to our data, if signal

detection is more important than exact location, manual spray matrix application is preferable. Whereas, if exact localisation of signal is paramount, ImagePrep application is the preferred.

It was during this comparison, that the initial discovery took place of the unknown peptide which was highly localised in the THI regions.
Further study of THI regions from TASTPM and wild type animals of different ages confirmed the co-localisation of the THIs and the unknown peptide. Furthermore, as THI size and number increased, so did the intensity of the MS peak for the unknown peptide. In older wild type mice, where THIs (if present) were small, the intensity of the peak for the unknown peptide was between 300 and 600. In the TASTPM mice at 12 months, where THIs were larger and more numerous, peak intensity reached 14000. In the 18 month TASTPM mice, where THIs were even more developed and numerous, maximum peak intensity reached 20000 (Fig.58).

The importance and role of this unknown peptide is of significant interest, as the THIs represent a neurodegenerative process which involves amyloid plaques, neuroinflammatory mediators (astrocytes and macrophages) and iron accumulation (Evans et al., 2007; Howlett et al., 2008), all of which occur in human AD. Many mouse models of AD do not show any neurodegeneration, thus any data from this model on the underlying pathology could be valuable in furthering our understanding of human AD. It should be noted that, although the pathology has similarities with human AD, it is by no means identical. Human AD is much more complex than simply amyloid plaques, as outlined in the introduction to this thesis, there are many other factors which have an effect. The human mutant genes which are expressed in the TASTPM mouse cause early onset AD, which can be very different to sporadic AD and only causes less than 1% of cases. Due to this any information gleaned from studying the THIs should be interpreted with caution.

Following THI isolation using LCM, LC/MS revealed the identities of several different proteins present in the THI regions. These included APP and the different Aβ peptides as expected, as the THIs are associated with amyloid plaques. Glial fibrillary acidic protein is a glial cell marker and may be increased as a consequence of glial cell proliferation due to neurodegeneration. Myelin basic protein is also to be expected, as some neurons will be contained in the THI regions, despite the overall neurodegeneration. The presence of apolipoprotein E precursor is interesting, as the ε4 allele is known to be a risk factor for late onset AD in humans (Strittmatter et al., 1993). The fact that we see this protein may mean that some perturbation of lipid metabolism is involved in the formation of the THIs, as apolipoprotein E is known to be involved in triglyceride and cholesterol homeostasis (Davignon et al., 1988a). The detection of secretogranin is likely not significant as it performs multiple roles throughout the CNS.

In summary, this study has shown several potential applications of MALDI MS Imaging in proteomics research which may become increasingly prevalent as the technology becomes more widely available. Whether the study is to determine the distribution of endogenous components, investigating old tissue libraries in novel ways or for the discovery of novel biomarkers of pathology, MALDI Imaging has the potential to be a very useful tool in years to come.

Chapter 6. Final Discussion

During the course of this thesis, the brain of the TASTPM mouse has been investigated using 1H MRS and MALDI Imaging. The experiments undertaken were carried out with several aims in mind.

The first was to continue the search for a reliable biomarker of disease progression in AD (or at least the TASTPM mouse), which, if found could be useful in the diagnosis and monitoring of the disease.

The second was to evaluate the TASTPM mouse as a model for AD, and to compare MRS results with results from other models of AD. Any reproducible differences observed could potentially be exploited in preclinical testing, aiding the drug discovery process.

The third was to investigate any regional proteomic differences in TASTPM mice using MALDI Imaging. Any differences would have the potential to further our understanding of the underlying pathology behind AD.

In the search for a biomarker, a marker of disease progression was elusive. We found age x genotype interactions *in vitro* with choline and *in vivo* with glutamate, but neither of these interactions was present in both studies. It is possible they might be used to plot disease progression in association with other measurable factors, but levels fluctuated over time in both cases, meaning using them separately to accurately map what stage of pathology a TASTPM mouse is in would be impossible. Thus, though we found parallels both with human AD and previous animal studies, the search for an AD specific biomarker goes on.

In our evaluation of the suitability of TASTPM mice as a model of AD we found a number of cerebral metabolic differences between TASTPM mice and the wild type base strain. These might be used as biomarkers of pathology in further study of the TASTPM mice.

In vitro we found whole brain differences in levels of MI, succinate, choline, creatine and several lipid functional groups. In all cases except choline there was no statistically significant change with age in the disease group during the time when amyloid plaques are being formed. Therefore MI, succinate, creatine and the observed lipid functional groups may be markers of AD in this model, without being linked to disease progression. It is possible choline levels are related to disease progression, but the fluctuating levels observed would make it difficult to accurately estimate disease progression from choline levels alone. There were possible similarities with human AD, where increased MI has also been observed (Kantarci et al., 2000; Dixon et al., 2002; Ackl et al., 2005; Zhu et al., 2006) and linked with gliosis and membrane dysfunction (Lazeyras et al., 1998). Decreased succinate may be indicative of impaired neuronal energy metabolism, another effect seen in human AD (Valla et al., 2001; Zhu et al., 2004; Moreira et al., 2007). The increased creatine levels observed, while not linked with human AD, have been shown to correlate with cognitive decline in older humans (Ferguson et al., 2002). The cholinergic differences, along with differences in lipid functional groups could indicate perturbation of phospholipid metabolism or membrane changes, altered phospholipid metabolism has also been observed in human AD (Kuo et al., 1998; Roher et al., 1999; Sparks et al., 2000).

In vivo we observed differences in NAA, glutamate, Glx, MI, PC, T1 values and exploratory behaviour. Differences were compared with previous *in vivo* work in other transgenic AD mice, along with our own *in vitro* work. Lower NAA levels in TASTPM mice are indicative of neuronal damage/death (Demougeot et al.,

2004), possibly a consequence of the formation of THIs. Lower NAA levels have been linked to neurodegeneration and have been observed in many cases in human AD (Kantarci et al., 2000; Dixon et al., 2002; Chantal et al., 2004; Ackl et al., 2005). Decreased glutamate and Glx may indicate neuronal metabolic deficiency, a symptom of AD (Valla et al., 2001; Zhu et al., 2004; Moreira et al., 2007). Changes in MI levels and choline containing compounds were discussed above.

The observed changes in NAA, glutamate and MI are in agreement with other *in vivo* studies on different transgenic AD mice (Dedeoglu et al., 2004; Marjanska et al., 2005; von Kienlin et al., 2005), with all in agreement regarding reduced NAA and glutamate, but only one of these other mouse models showed increasing MI (the APP-PS1 mouse),- (Marjanska et al., 2005). The differences observed with choline levels were not seen in other studies, the possible link to altered lipid homeostasis (along with evidence from *in vitro* changes in lipid functional groups) shows TASTPM mice may exhibit another hallmark of human AD not exhibited by the other mouse models.

The metabolic differences observed *in vitro* and *in vivo* showed similarities, such as MI and choline differences, but also several differences, such as no changes in glutamate or NAA *in vitro*. A possible explanation for this lies in the use of whole brain extracts for the *in vitro* study, as opposed to a voxel focused on areas known to suffer pathological changes. Localised metabolic differences may have been masked by the use of whole brains in the extract study.

Shorter T1 values in TASTPM mice may be due to alterations in brain water content (Bell et al., 1987; Besson et al., 1989). The alterations may be due to large amounts of amyloid disrupting normal brain osmoregulation, the effect becomes more pronounced with age, so may be linked to increasing amyloid deposition.

The changes in exploratory behaviour observed became most pronounced in older mice, meaning this effect may be in some way dependent on amyloid deposition. It may also be due to the increasing size of the THI regions, meaning administration of an amyloid lowering agent would have no effect on behaviour.

The most striking findings of the MALDI investigation are the presence of the two unknown peptides localised to the THI regions in the TASTPM (and older wild type) mice. Efforts to identify these peptides are ongoing and, if identification can be achieved it may provide valuable information concerning the underlying pathology behind these lesions,

Thus, we have advanced our knowledge of the TASTPM mouse and shown parallels between the TASTPM mouse other transgenic mouse models and human AD. The differences observed in vivo are most promising, as they would allow repeat investigation of the same mouse over a course of therapeutic intervention. Further study using amyloid lowering agents would allow observation of whether normalisation back to wild type values occurs in any of the metabolites, T1 or behavioural differences. If this was to occur then the TASTPM may be a useful tool in preclinical screening of amyloid-lowering agents.

The comparison of in vivo MRS data between TASTPM and other strains of transgenic AD model must be done carefully, as in all the mice tested the protocols used varied, as did the MR scanners and peripheral equipment, as well as the ages of the mice. MRS voxel placement and size was different in all mice, for example. Thus the only way to be fully confident of comparisons would be to use the same equipment and the same protocols to obtain data from mice from the different strains, all of the same age, something which was beyond the scope of this thesis.

Another limitation of the study is that we found quite large discrepancies between the MRS data from *in vitro* and in vivo scans from brains of the same strains of mice. While this may be due to the more focused nature of the in vivo scans, it may also be that these mice do not have fully stable or predictable levels of the various metabolites investigated over their lifespans. If this were the case then attempting to observe brain metabolites by MRS as a way of measuring the action of amyloid-lowering agents would be problematic at best. One way to test this would be to carry out further extract studies on dissected brains of TASTPM mice to see if we detect regional differences, as have been performed on other transgenic AD mice (Salek et al., 2010). If we see similar changes to the in vivo work in areas such as the hippocampus and thalamus then we can be more confident of the robustness of the TASTPM mouse as a model for preclinical testing.

7. Reference List

Ackl N, Ising M, Schreiber YA, Atiya M, Sonntag A, Auer DP (2005) Hippocampal metabolic abnormalities in mild cognitive impairment and Alzheimer's disease. Neurosci Lett 384:23-28.

Agrawal HC, Glisson SN, Himwich WA (1968) Developmental changes in monoamines of mouse brain. Int J Neuropharmacol 7:97-101.

Akiyama H, Arai T, Kondo H, Tanno E, Haga C, Ikeda K (2000a) Cell mediators of inflammation in the Alzheimer disease brain. Alzheimer Dis Assoc Disord 14 Suppl 1:S47-53.

Akiyama H, Barger S, Barnum S, Bradt B, Bauer J, Cole GM, Cooper NR, Eikelenboom P, Emmerling M, Fiebich BL, Finch CE, Frautschy S, Griffin WS, Hampel H, Hull M, Landreth G, Lue L, Mrak R, Mackenzie IR, McGeer PL, O'Banion MK, Pachter J, Pasinetti G, Plata-Salaman C, Rogers J, Rydel R, Shen Y, Streit W, Strohmeyer R, Tooyoma I, Van Muiswinkel FL, Veerhuis R, Walker D, Webster S, Wegrzyniak B, Wenk G, Wyss-Coray T (2000b) Inflammation and Alzheimer's disease. Neurobiol Aging 21:383-421.

Alonso AC, Grundke-Iqbal I, Iqbal K (1996) Alzheimer's disease hyperphosphorylated tau sequesters normal tau into tangles of filaments and disassembles microtubules. Nat Med 2:783-787.

Alonso AC, Zaidi T, Grundke-Iqbal I, Iqbal K (1994) Role of abnormally phosphorylated tau in the breakdown of microtubules in Alzheimer disease. Proc Natl Acad Sci U S A 91:5562-5566.

Alonso AD, Grundke-Iqbal I, Barra HS, Iqbal K (1997) Abnormal phosphorylation of tau and the mechanism of Alzheimer neurofibrillary degeneration: sequestration of microtubule-associated proteins 1 and 2 and the disassembly of microtubules by the abnormal tau. Proc Natl Acad Sci U S A 94:298-303.

Antuono PG, Jones JL, Wang Y, Li SJ (2001) Decreased glutamate + glutamine in Alzheimer's disease detected in vivo with (1)H-MRS at 0.5 T. Neurology 56:737-742.

Areosa SA, Sherriff F, McShane R (2005) Memantine for dementia. Cochrane Database Syst Rev:CD003154.

Arvin B, Lekieffre D, Graham JL, Moncada C, Chapman AG, Meldrum BS (1994) Effect of the non-NMDA receptor antagonist GYKI 52466 on the microdialysate and tissue concentrations of amino acids following transient forebrain ischaemia. J Neurochem 62:1458-1467.

Bayer TA, Wirths O (2008) Review on the APP/PS1KI mouse model: intraneuronal Abeta accumulation triggers axonopathy, neuron loss and working memory impairment. Genes Brain Behav 7 Suppl 1:6-11.

Bayer TA, Breyhan H, Duan K, Rettig J, Wirths O (2008) Intraneuronal beta-amyloid is a major risk factor--novel evidence from the APP/PS1KI mouse model. Neurodegener Dis 5:140-142.

Beacher F, Simmons A, Daly E, Prasher V, Adams C, Margallo-Lana ML, Morris R, Lovestone S, Murphy K, Murphy DG (2005) Hippocampal myo-inositol and cognitive ability in adults with Down syndrome: an in vivo proton magnetic resonance spectroscopy study. Arch Gen Psychiatry 62:1360-1365.

Bell BA, Smith MA, Kean DM, McGhee CN, MacDonald HL, Miller JD, Barnett GH, Tocher JL, Douglas RH, Best JJ (1987) Brain water measured by magnetic resonance imaging. Correlation with direct estimation and changes after mannitol and dexamethasone. Lancet 1:66-69.

Benveniste H, Einstein G, Kim KR, Hulette C, Johnson GA (1999) Detection of neuritic plaques in Alzheimer's disease by magnetic resonance microscopy. Proc Natl Acad Sci U S A 96:14079-14084.

Berridge MJ (1993) Inositol trisphosphate and calcium signalling. Nature 361:315-325.

Berridge MJ, Lipp P, Bootman MD (2000) The versatility and universality of calcium signalling. Nat Rev Mol Cell Biol 1:11-21.

Besson JA, Greentree SG, Foster MA, Rimmington JE (1989) Regional variation in rat brain proton relaxation times and water content. Magn Reson Imaging 7:141-143.

Bhakoo KK, Pearce D (2000) In vitro expression of N-acetyl aspartate by oligodendrocytes: implications for proton magnetic resonance spectroscopy signal in vivo. J Neurochem 74:254-262.

Birks J (2006) Cholinesterase inhibitors for Alzheimer's disease. Cochrane Database Syst Rev:CD005593.

Black S, Wilcock GK, Haworth J, Hendrix S, Zavitz K, Christensen D, Binger MH, Bass S, Laughlin M, Swabb E (2006) Efficacy and safety of MPC-7869 (R-flurbiprofen), a selective ab42-lowering agent, in mild Alzheimer's disease (AD): Results of a 12-month Phase 2 trial and 1-year follow-on study. Neurology 66:A347-A347.

Blennow K, de Leon MJ, Zetterberg H (2006) Alzheimer's disease. Lancet 368:387-403.

Bogen IL, Risa O, Haug KH, Sonnewald U, Fonnum F, Walaas SI (2008) Distinct changes in neuronal and astrocytic amino acid neurotransmitter metabolism in mice with reduced numbers of synaptic vesicles. J Neurochem.

Bottomley PA (1987) Spatial localization in NMR spectroscopy in vivo. Ann N Y Acad Sci 508:333-348.

Braak E, Griffing K, Arai K, Bohl J, Bratzke H, Braak H (1999) Neuropathology of Alzheimer's disease: what is new since A. Alzheimer? Eur Arch Psychiatry Clin Neurosci 249 Suppl 3:14-22.

Braak H, Braak E (1991) Neuropathological stageing of Alzheimer-related changes. Acta Neuropathol (Berl) 82:239-259.

Brand A, Richter-Landsberg C, Leibfritz D (1993) Multinuclear NMR studies on the energy metabolism of glial and neuronal cells. Dev Neurosci 15:289-298.

Brooks WM, Friedman SD, Stidley CA (1999) Reproducibility of 1H-MRS in vivo. Magn Reson Med 41:193-197.

Burri R, Bigler P, Straehl P, Posse S, Colombo JP, Herschkowitz N (1990) Brain development: 1H magnetic resonance spectroscopy of rat brain extracts compared with chromatographic methods. Neurochem Res 15:1009-1016.

Buxbaum JD, Liu KN, Luo Y, Slack JL, Stocking KL, Peschon JJ, Johnson RS, Castner BJ, Cerretti DP, Black RA (1998) Evidence that tumor necrosis factor alpha converting enzyme is involved in regulated alpha-secretase cleavage of the Alzheimer amyloid protein precursor. J Biol Chem 273:27765-27767.

Cai H, Wang Y, McCarthy D, Wen H, Borchelt DR, Price DL, Wong PC (2001) BACE1 is the major beta-secretase for generation of Abeta peptides by neurons. Nat Neurosci 4:233-234.

Casas C, Sergeant N, Itier JM, Blanchard V, Wirths O, van der Kolk N, Vingtdeux V, van de Steeg E, Ret G, Canton T, Drobecq H, Clark A, Bonici B, Delacourte A, Benavides J, Schmitz C, Tremp G, Bayer TA, Benoit P, Pradier L (2004) Massive CA1/2 neuronal loss with intraneuronal and N-terminal truncated Abeta42 accumulation in a novel Alzheimer transgenic model. Am J Pathol 165:1289-1300.

Catani M, Cherubini A, Howard R, Tarducci R, Pelliccioli GP, Piccirilli M, Gobbi G, Senin U, Mecocci P (2001) (1)H-MR spectroscopy differentiates mild cognitive impairment from normal brain aging. Neuroreport 12:2315-2317.

Cerdan S, Parrilla R, Santoro J, Rico M (1985) 1H NMR detection of cerebral myo-inositol. FEBS Lett 187:167-172.

Chang L, Ernst T, Poland RE, Jenden DJ (1996) In vivo proton magnetic resonance spectroscopy of the normal aging human brain. Life Sci 58:2049-2056.

Chantal S, Braun CM, Bouchard RW, Labelle M, Boulanger Y (2004) Similar 1H magnetic resonance spectroscopic metabolic pattern in the medial temporal lobes of patients with mild cognitive impairment and Alzheimer disease. Brain Res 1003:26-35.

Chassain C, Bielicki G, Durand E, Lolignier S, Essafi F, Traore A, Durif F (2008) Metabolic changes detected by proton magnetic resonance spectroscopy in vivo and in vitro in a murin model of Parkinson's disease, the MPTP-intoxicated mouse. J Neurochem 105:874-882.

Chaurand P, Latham JC, Lane KB, Mobley JA, Polosukhin VV, Wirth PS, Nanney LB, Caprioli RM (2008) Imaging mass spectrometry of intact proteins from alcohol-preserved tissue specimens: bypassing formalin fixation. J Proteome Res 7:3543-3555.

Chyung JH, Raper DM, Selkoe DJ (2005) Gamma-secretase exists on the plasma membrane as an intact complex that accepts substrates and effects intramembrane cleavage. J Biol Chem 280:4383-4392.

Cottrell DA, Blakely EL, Johnson MA, Ince PG, Turnbull DM (2001) Mitochondrial enzyme-deficient hippocampal neurons and choroidal cells in AD. Neurology 57:260-264.

Crouch PJ, White AR, Bush AI (2007) The modulation of metal bio-availability as a therapeutic strategy for the treatment of Alzheimer's disease. Febs J 274:3775-3783.

Cuajungco MP, Goldstein LE, Nunomura A, Smith MA, Lim JT, Atwood CS, Huang X, Farrag YW, Perry G, Bush AI (2000) Evidence that the beta-amyloid plaques of Alzheimer's disease represent the redox-silencing and entombment of abeta by zinc. J Biol Chem 275:19439-19442.

Dahlgren KN, Manelli AM, Stine WB, Jr., Baker LK, Krafft GA, LaDu MJ (2002) Oligomeric and fibrillar species of amyloid-beta peptides differentially affect neuronal viability. J Biol Chem 277:32046-32053.

Davanipour Z, Tseng CC, Lee PJ, Sobel E (2007) A case-control study of occupational magnetic field exposure and Alzheimer's disease: results from the California Alzheimer's Disease Diagnosis and Treatment Centers. BMC Neurol 7:13.

Davignon J, Gregg RE, Sing CF (1988a) Apolipoprotein E polymorphism and atherosclerosis. Arteriosclerosis 8:1-21.

Davignon J, Bouthillier D, Nestruck AC, Sing CF (1988b) Apolipoprotein E polymorphism and atherosclerosis: insight from a study in octogenarians. Trans Am Clin Climatol Assoc 99:100-110.

de Beer R, van den Boogaart A, van Ormondt D, Pijnappel WW, den Hollander JA, Marien AJ, Luyten PR (1992) Application of time-domain fitting in the quantification of in vivo 1H spectroscopic imaging data sets. NMR Biomed 5:171-178.

de Graaf RA (1998) In Vivo NMR Spectroscopy Principles And Techniques, 1st Edition. Chichester: John Wiley & Sons Ltd.

de Leon MJ, Convit A, Wolf OT, Tarshish CY, DeSanti S, Rusinek H, Tsui W, Kandil E, Scherer AJ, Roche A, Imossi A, Thorn E, Bobinski M, Caraos C, Lesbre P, Schlyer D, Poirier J, Reisberg B, Fowler J (2001) Prediction of cognitive decline in normal elderly subjects with 2-[(18)F]fluoro-2-deoxy-D-glucose/poitron-emission tomography (FDG/PET). Proc Natl Acad Sci U S A 98:10966-10971.

De Strooper B, Annaert W, Cupers P, Saftig P, Craessaerts K, Mumm JS, Schroeter EH, Schrijvers V, Wolfe MS, Ray WJ, Goate A, Kopan R (1999) A presenilin-1-dependent gamma-secretase-like protease mediates release of Notch intracellular domain. Nature 398:518-522.

Dedeoglu A, Choi JK, Cormier K, Kowall NW, Jenkins BG (2004) Magnetic resonance spectroscopic analysis of Alzheimer's disease mouse brain that express mutant human APP shows altered neurochemical profile. Brain Res 1012:60-65.

Demougeot C, Marie C, Giroud M, Beley A (2004) N-acetylaspartate: a literature review of animal research on brain ischaemia. J Neurochem 90:776-783.

Dhenain M, El Tannir El Tayara N, Wu TD, Guegan M, Volk A, Quintana C, Delatour B (2009) Characterization of in vivo MRI detectable thalamic amyloid plaques from APP/PS1 mice. Neurobiol Aging 30:41-53.

Dixon RM, Bradley KM, Budge MM, Styles P, Smith AD (2002) Longitudinal quantitative proton magnetic resonance spectroscopy of the hippocampus in Alzheimer's disease. Brain 125:2332-2341.

Dodart JC, Mathis C, Bales KR, Paul SM, Ungerer A (1999) Early regional cerebral glucose hypometabolism in transgenic mice overexpressing the V717F beta-amyloid precursor protein. Neurosci Lett 277:49-52.

Dominguez D, Tournoy J, Hartmann D, Huth T, Cryns K, Deforce S, Serneels L, Camacho IE, Marjaux E, Craessaerts K, Roebroek AJ, Schwake M, D'Hooge R, Bach P, Kalinke U, Moechars D, Alzheimer C, Reiss K, Saftig P, De Strooper B (2005) Phenotypic and biochemical analyses of BACE1- and BACE2-deficient mice. J Biol Chem 280:30797-30806.

Doraiswamy PM, Charles HC, Krishnan KR (1998) Prediction of cognitive decline in early Alzheimer's disease. Lancet 352:1678.

Doraiswamy PM, Chen JG, Charles HC (2000) Brain magnetic resonance spectroscopy - Role in assessing outcomes in Alzheimer's disease CNS Drugs 14:457-472.
Drzezga A, Lautenschlager N, Siebner H, Riemenschneider M, Willoch F, Minoshima S, Schwaiger M, Kurz A (2003) Cerebral metabolic changes accompanying conversion of mild cognitive impairment into Alzheimer's disease: a PET follow-up study. Eur J Nucl Med Mol Imaging 30:1104-1113.
Eckman EA, Eckman CB (2005) Abeta-degrading enzymes: modulators of Alzheimer's disease pathogenesis and targets for therapeutic intervention. Biochem Soc Trans 33:1101-1105.
Eikelenboom P, Veerhuis R (1996) The role of complement and activated microglia in the pathogenesis of Alzheimer's disease. Neurobiol Aging 17:673-680.
Ernst T, Chang L, Melchor R, Mehringer CM (1997) Frontotemporal dementia and early Alzheimer disease: differentiation with frontal lobe H-1 MR spectroscopy. Radiology 203:829-836.
Esler WP, Kimberly WT, Ostaszewski BL, Diehl TS, Moore CL, Tsai JY, Rahmati T, Xia W, Selkoe DJ, Wolfe MS (2000) Transition-state analogue inhibitors of gamma-secretase bind directly to presenilin-1. Nat Cell Biol 2:428-434.
Evans SC, Barjat H, Pohlmann A, Tilling L, Vidgeon-Hart M, Hayes BP, Upton N, James MF (2007) Pathologies in the thalamus of TASTPM transgenic mouse model of Alzheimer's disease - characterisation by MRI, micro-CT and histology. British Neurosci Assoc Abstr 19:145.
Fagan AM, Mintun MA, Mach RH, Lee SY, Dence CS, Shah AR, LaRossa GN, Spinner ML, Klunk WE, Mathis CA, DeKosky ST, Morris JC, Holtzman DM (2006) Inverse relation between in vivo amyloid imaging load and cerebrospinal fluid Abeta42 in humans. Ann Neurol 59:512-519.
Fahrenholz F, Gilbert S, Kojro E, Lammich S, Postina R (2000) Alpha-secretase activity of the disintegrin metalloprotease ADAM 10. Influences of domain structure. Ann N Y Acad Sci 920:215-222.
Falini A, Bozzali M, Magnani G, Pero G, Gambini A, Benedetti B, Mossini R, Franceschi M, Comi G, Scotti G, Filippi M (2005) A whole brain MR spectroscopy study from patients with Alzheimer's disease and mild cognitive impairment. Neuroimage 26:1159-1163.
Fatouros PP, Marmarou A (1999) Use of magnetic resonance imaging for in vivo measurements of water content in human brain: method and normal values. J Neurosurg 90:109-115.
Fearing MA, Bigler ED, Norton M, Tschanz JA, Hulette C, Leslie C, Welsh-Bohmer K (2007) Autopsy-confirmed Alzheimer's disease versus clinically diagnosed Alzheimer's disease in the Cache County Study on Memory and Aging: a comparison of quantitative MRI and neuropsychological findings. J Clin Exp Neuropsychol 29:553-560.
Ferguson KJ, MacLullich AM, Marshall I, Deary IJ, Starr JM, Seckl JR, Wardlaw JM (2002) Magnetic resonance spectroscopy and cognitive function in healthy elderly men. Brain 125:2743-2749.
Florian CL, Williams SR, Bhakoo KK, Noble MD (1996) Regional and developmental variations in metabolite concentration in the rat brain and eye: a study using 1H

NMR spectroscopy and high performance liquid chromatography. Neurochem Res 21:1065-1074.
Fox NC, Freeborough PA, Rossor MN (1996a) Visualisation and quantification of rates of atrophy in Alzheimer's disease. Lancet 348:94-97.
Fox NC, Crum WR, Scahill RI, Stevens JM, Janssen JC, Rossor MN (2001) Imaging of onset and progression of Alzheimer's disease with voxel-compression mapping of serial magnetic resonance images. Lancet 358:201-205.
Fox NC, Warrington EK, Freeborough PA, Hartikainen P, Kennedy AM, Stevens JM, Rossor MN (1996b) Presymptomatic hippocampal atrophy in Alzheimer's disease. A longitudinal MRI study. Brain 119 (Pt 6):2001-2007.
Fox NC, Black RS, Gilman S, Rossor MN, Griffith SG, Jenkins L, Koller M (2005) Effects of Abeta immunization (AN1792) on MRI measures of cerebral volume in Alzheimer disease. Neurology 64:1563-1572.
Fratiglioni L, Paillard-Borg S, Winblad B (2004) An active and socially integrated lifestyle in late life might protect against dementia. Lancet Neurol 3:343-353.
Frederick BD, Lyoo IK, Satlin A, Ahn KH, Kim MJ, Yurgelun-Todd DA, Cohen BM, Renshaw PF (2004) In vivo proton magnetic resonance spectroscopy of the temporal lobe in Alzheimer's disease. Prog Neuropsychopharmacol Biol Psychiatry 28:1313-1322.
Frisoni GB, Fox NC, Jack CR, Jr., Scheltens P, Thompson PM (2010) The clinical use of structural MRI in Alzheimer disease. Nat Rev Neurol 6:67-77.
Gadian DG (1995) NMR and its applications to living systems, 2nd Edition. Oxford: Oxford University Press.
Garrard P, Schott JM, MacManus DG, Hodges JR, Fox NC, Waldman AD (2006) Posterior cingulate neurometabolite profiles and clinical phenotype in frontotemporal dementia. Cogn Behav Neurol 19:185-189.
Gauthier S, Reisberg B, Zaudig M, Petersen RC, Ritchie K, Broich K, Belleville S, Brodaty H, Bennett D, Chertkow H, Cummings JL, de Leon M, Feldman H, Ganguli M, Hampel H, Scheltens P, Tierney MC, Whitehouse P, Winblad B (2006) Mild cognitive impairment. Lancet 367:1262-1270.
Gibson GE, Sheu KF, Blass JP (1998) Abnormalities of mitochondrial enzymes in Alzheimer disease. J Neural Transm 105:855-870.
Goate A, Chartier-Harlin MC, Mullan M, Brown J, Crawford F, Fidani L, Giuffra L, Haynes A, Irving N, James L, et al. (1991) Segregation of a missense mutation in the amyloid precursor protein gene with familial Alzheimer's disease. Nature 349:704-706.
Golde TE (2003) Alzheimer disease therapy: can the amyloid cascade be halted? J Clin Invest 111:11-18.
Golde TE (2006) Disease modifying therapy for AD? J Neurochem 99:689-707.
Govindaraju V, Young K, Maudsley AA (2000) Proton NMR chemical shifts and coupling constants for brain metabolites. NMR Biomed 13:129-153.
Graveron-Demilly D, Diop A, Briguet A, Fenet B (1993) Product-operator algebra for strongly coupled spin systems. J Magn Reson A101:233-239.
Griffey RH, Flamig DP (1990) VAPOR for Solvent-Suppressed, Short-Echo, Volume-Localized Proton Spectroscopy. Journal of Magnetic Resonance 88:161-166.

Gruetter R (2005) Automatic, localized in Vivo adjustment of all first-and second-order shim coils. Magn Reson Med 29:804-811.
Grundke-Iqbal I, Iqbal K, Tung YC, Quinlan M, Wisniewski HM, Binder LI (1986) Abnormal phosphorylation of the microtubule-associated protein tau (tau) in Alzheimer cytoskeletal pathology. Proc Natl Acad Sci U S A 83:4913-4917.
Gsell W, Conrad R, Hickethier M, Sofic E, Frolich L, Wichart I, Jellinger K, Moll G, Ransmayr G, Beckmann H, et al. (1995) Decreased catalase activity but unchanged superoxide dismutase activity in brains of patients with dementia of Alzheimer type. J Neurochem 64:1216-1223.
Gunstone FD (1995) The Lipid Handbook, 2nd Edition. London: Chapman & Hall.
Haase A, Frahm J, Hanicke W, Matthaei D (1985) 1H NMR chemical shift selective (CHESS) imaging. Phys Med Biol 30:341-344.
Harada A, Oguchi K, Okabe S, Kuno J, Terada S, Ohshima T, Sato-Yoshitake R, Takei Y, Noda T, Hirokawa N (1994) Altered microtubule organization in small-calibre axons of mice lacking tau protein. Nature 369:488-491.
Hardy J, Selkoe DJ (2002) The amyloid hypothesis of Alzheimer's disease: progress and problems on the road to therapeutics. Science 297:353-356.
Harr SD, Uint L, Hollister R, Hyman BT, Mendez AJ (1996) Brain expression of apolipoproteins E, J, and A-I in Alzheimer's disease. J Neurochem 66:2429-2435.
Hellstrom-Lindahl E, Ravid R, Nordberg A (2006) Age-dependent decline of neprilysin in Alzheimer's disease and normal brain: Inverse correlation with Abeta levels. Neurobiol Aging.
Hensley K, Hall N, Subramaniam R, Cole P, Harris M, Aksenov M, Aksenova M, Gabbita SP, Wu JF, Carney JM, et al. (1995) Brain regional correspondence between Alzheimer's disease histopathology and biomarkers of protein oxidation. J Neurochem 65:2146-2156.
Herholz K, Carter SF, Jones M (2007) Positron emission tomography imaging in dementia. Br J Radiol 80 Spec No 2:S160-167.
Herminghaus S, Frolich L, Gorriz C, Pilatus U, Dierks T, Wittsack HJ, Lanfermann H, Maurer K, Zanella FE (2003) Brain metabolism in Alzheimer disease and vascular dementia assessed by in vivo proton magnetic resonance spectroscopy. Psychiatry Res 123:183-190.
Heun R, Schlegel S, Graf-Morgenstern M, Tintera J, Gawehn J, Stoeter P (1997) Proton magnetic resonance spectroscopy in dementia of Alzheimer type. Int J Geriatr Psychiatry 12:349-358.
Higgins GA, Jacobsen H (2003) Transgenic mouse models of Alzheimer's disease: phenotype and application. Behav Pharmacol 14:419-438.
Higinbotham J, Marshall I (2001) NMR lineshapes and lineshape fitting. A Rep NMR Spectrosc 43:59-120.
Hock C, Konietzko U, Streffer JR, Tracy J, Signorell A, Muller-Tillmanns B, Lemke U, Henke K, Moritz E, Garcia E, Wollmer MA, Umbricht D, de Quervain DJ, Hofmann M, Maddalena A, Papassotiropoulos A, Nitsch RM (2003) Antibodies against beta-amyloid slow cognitive decline in Alzheimer's disease. Neuron 38:547-554.

Holcomb L, Gordon MN, McGowan E, Yu X, Benkovic S, Jantzen P, Wright K, Saad I, Mueller R, Morgan D, Sanders S, Zehr C, O'Campo K, Hardy J, Prada CM, Eckman C, Younkin S, Hsiao K, Duff K (1998) Accelerated Alzheimer-type phenotype in transgenic mice carrying both mutant amyloid precursor protein and presenilin 1 transgenes. Nat Med 4:97-100.

Howlett DR, Richardson JC, Austin A, Parsons AA, Bate ST, Davies DC, Gonzalez MI (2004) Cognitive correlates of Abeta deposition in male and female mice bearing amyloid precursor protein and presenilin-1 mutant transgenes. Brain Res 1017:130-136.

Howlett DR, Bowler K, Soden PE, Riddell D, Davis JB, Richardson JC, Burbidge SA, Gonzalez MI, Irving EA, Lawman A, Miglio G, Dawson EL, Howlett ER, Hussain I (2008) Abeta deposition and related pathology in an APP x PS1 transgenic mouse model of Alzheimer's disease. Histol Histopathol 23:67-76.

Hsia AY, Masliah E, McConlogue L, Yu GQ, Tatsuno G, Hu K, Kholodenko D, Malenka RC, Nicoll RA, Mucke L (1999) Plaque-independent disruption of neural circuits in Alzheimer's disease mouse models. Proc Natl Acad Sci U S A 96:3228-3233.

Huang W, Alexander GE, Chang L, Shetty HU, Krasuski JS, Rapoport SI, Schapiro MB (2001) Brain metabolite concentration and dementia severity in Alzheimer's disease: a (1)H MRS study. Neurology 57:626-632.

Huang X, Atwood CS, Hartshorn MA, Multhaup G, Goldstein LE, Scarpa RC, Cuajungco MP, Gray DN, Lim J, Moir RD, Tanzi RE, Bush AI (1999) The A beta peptide of Alzheimer's disease directly produces hydrogen peroxide through metal ion reduction. Biochemistry 38:7609-7616.

Hussain I, Powell D, Howlett DR, Tew DG, Meek TD, Chapman C, Gloger IS, Murphy KE, Southan CD, Ryan DM, Smith TS, Simmons DL, Walsh FS, Dingwall C, Christie G (1999) Identification of a novel aspartic protease (Asp 2) as beta-secretase. Mol Cell Neurosci 14:419-427.

Iqbal K, Grundke-Iqbal I, Zaidi T, Merz PA, Wen GY, Shaikh SS, Wisniewski HM, Alafuzoff I, Winblad B (1986) Defective brain microtubule assembly in Alzheimer's disease. Lancet 2:421-426.

Iqbal K, Alonso Adel C, Chen S, Chohan MO, El-Akkad E, Gong CX, Khatoon S, Li B, Liu F, Rahman A, Tanimukai H, Grundke-Iqbal I (2005) Tau pathology in Alzheimer disease and other tauopathies. Biochim Biophys Acta 1739:198-210.

Jack CR, Jr., Petersen RC, Xu YC, Waring SC, O'Brien PC, Tangalos EG, Smith GE, Ivnik RJ, Kokmen E (1997) Medial temporal atrophy on MRI in normal aging and very mild Alzheimer's disease. Neurology 49:786-794.

James MF, Maheswaran S, Barjat H, Rueckert D, Bate ST, Howlett DR, Tilling L, Smart SC, Pohlmann A, Hill DL, Hajnal JV, Upton N (2007) Effects of Abeta42 deposition in Alzheimer's APPxPS1 mice: Inflammatory response and regional MRI voulmetry. British Neurosci Assoc Abstr 19:145.

Jarrett JT, Berger EP, Lansbury PT, Jr. (1993) The carboxy terminus of the beta amyloid protein is critical for the seeding of amyloid formation: implications for the pathogenesis of Alzheimer's disease. Biochemistry 32:4693-4697.

Jessen F, Traeber F, Freymann K, Maier W, Schild HH, Block W (2006) Treatment monitoring and response prediction with proton MR spectroscopy in AD. Neurology 67:528-530.

Jessen F, Block W, Traber F, Keller E, Flacke S, Papassotiropoulos A, Lamerichs R, Heun R, Schild HH (2000) Proton MR spectroscopy detects a relative decrease of N-acetylaspartate in the medial temporal lobe of patients with AD. Neurology 55:684-688.

Jessen F, Gur O, Block W, Ende G, Frolich L, Hammen T, Wiltfang J, Kucinski T, Jahn H, Heun R, Maier W, Kolsch H, Kornhuber J, Traber F (2009) A multicenter (1)H-MRS study of the medial temporal lobe in AD and MCI. Neurology 72:1735-1740.

Jones RS, Waldman AD (2004) 1H-MRS evaluation of metabolism in Alzheimer's disease and vascular dementia. Neurol Res 26:488-495.

Jung RE, Brooks WM, Yeo RA, Chiulli SJ, Weers DC, Sibbitt WL, Jr. (1999a) Biochemical markers of intelligence: a proton MR spectroscopy study of normal human brain. Proc Biol Sci 266:1375-1379.

Jung RE, Yeo RA, Chiulli SJ, Sibbitt WL, Jr., Weers DC, Hart BL, Brooks WM (1999b) Biochemical markers of cognition: a proton MR spectroscopy study of normal human brain. Neuroreport 10:3327-3331.

Kanfer JN, Sorrentino G, Sitar DS (1998) Phospholipases as mediators of amyloid beta peptide neurotoxicity: an early event contributing to neurodegeneration characteristic of Alzheimer's disease. Neurosci Lett 257:93-96.

Kang J, Lemaire HG, Unterbeck A, Salbaum JM, Masters CL, Grzeschik KH, Multhaup G, Beyreuther K, Muller-Hill B (1987) The precursor of Alzheimer's disease amyloid A4 protein resembles a cell-surface receptor. Nature 325:733-736.

Kantarci K, Smith GE, Ivnik RJ, Petersen RC, Boeve BF, Knopman DS, Tangalos EG, Jack CR, Jr. (2002) 1H magnetic resonance spectroscopy, cognitive function, and apolipoprotein E genotype in normal aging, mild cognitive impairment and Alzheimer's disease. J Int Neuropsychol Soc 8:934-942.

Kantarci K, Jack CR, Jr., Xu YC, Campeau NG, O'Brien PC, Smith GE, Ivnik RJ, Boeve BF, Kokmen E, Tangalos EG, Petersen RC (2000) Regional metabolic patterns in mild cognitive impairment and Alzheimer's disease: A 1H MRS study. Neurology 55:210-217.

Kantarci K, Petersen RC, Boeve BF, Knopman DS, Tang-Wai DF, O'Brien PC, Weigand SD, Edland SD, Smith GE, Ivnik RJ, Ferman TJ, Tangalos EG, Jack CR, Jr. (2004) 1H MR spectroscopy in common dementias. Neurology 63:1393-1398.

Kantarci K, Weigand SD, Petersen RC, Boeve BF, Knopman DS, Gunter J, Reyes D, Shiung M, O'Brien P C, Smith GE, Ivnik RJ, Tangalos EG, Jack CR, Jr. (2006) Longitudinal (1)H MRS changes in mild cognitive impairment and Alzheimer's disease. Neurobiol Aging.

Karas M, Hillenkamp F (1988) Laser desorption ionization of proteins with molecular masses exceeding 10,000 daltons. Anal Chem 60:2299-2301.

Karas M, Bachmann D, Bahr U, Hillenkamp F (1987) Matrix-Assisted Ultraviolet-Laser Desorption of Nonvolatile Compounds. Int J Mass Spectrom Ion Processes 78:53-68.
Karp A, Kareholt I, Qiu C, Bellander T, Winblad B, Fratiglioni L (2004) Relation of education and occupation-based socioeconomic status to incident Alzheimer's disease. Am J Epidemiol 159:175-183.
Kattapong VJ, Brooks WM, Wesley MH, Kodituwakku PW, Rosenberg GA (1996) Proton magnetic resonance spectroscopy of vascular- and Alzheimer-type dementia. Arch Neurol 53:678-680.
Katzov H (2007) SORL1 adds another piece to the complex puzzle of Alzheimer disease genetics. Clin Genet 72:183-184.
Kauppinen RA, Williams SR (1991) Nondestructive detection of glutamate by 1H nuclear magnetic resonance spectroscopy in cortical brain slices from the guinea pig: evidence for changes in detectability during severe anoxic insults. J Neurochem 57:1136-1144.
Kauppinen RA, Pirttila TR, Auriola SO, Williams SR (1994) Compartmentation of cerebral glutamate in situ as detected by 1H/13C n.m.r. Biochem J 298 (Pt 1):121-127.
Khan A, Dobson JP, Exley C (2006) Redox cycling of iron by Abeta42. Free Radic Biol Med 40:557-569.
Khatoon S, Grundke-Iqbal I, Iqbal K (1992) Brain levels of microtubule-associated protein tau are elevated in Alzheimer's disease: a radioimmuno-slot-blot assay for nanograms of the protein. J Neurochem 59:750-753.
Kheterpal I, Williams A, Murphy C, Bledsoe B, Wetzel R (2001) Structural features of the Abeta amyloid fibril elucidated by limited proteolysis. Biochemistry 40:11757-11767.
Kimberly WT, LaVoie MJ, Ostaszewski BL, Ye W, Wolfe MS, Selkoe DJ (2003) Gamma-secretase is a membrane protein complex comprised of presenilin, nicastrin, Aph-1, and Pen-2. Proc Natl Acad Sci U S A 100:6382-6387.
Klegeris A, McGeer PL (1997) beta-amyloid protein enhances macrophage production of oxygen free radicals and glutamate. J Neurosci Res 49:229-235.
Klunk WE, Xu C, Panchalingam K, McClure RJ, Pettegrew JW (1996) Quantitative 1H and 31P MRS of PCA extracts of postmortem Alzheimer's disease brain. Neurobiol Aging 17:349-357.
Knobloch M, Konietzko U, Krebs DC, Nitsch RM (2007) Intracellular Abeta and cognitive deficits precede beta-amyloid deposition in transgenic arcAbeta mice. Neurobiol Aging 28:1297-1306.
Kojro E, Fahrenholz F (2005) The non-amyloidogenic pathway: structure and function of alpha-secretases. Subcell Biochem 38:105-127.
Koller KJ, Zaczek R, Coyle JT (1984) N-acetyl-aspartyl-glutamate: regional levels in rat brain and the effects of brain lesions as determined by a new HPLC method. J Neurochem 43:1136-1142.
Kopke E, Tung YC, Shaikh S, Alonso AC, Iqbal K, Grundke-Iqbal I (1993) Microtubule-associated protein tau. Abnormal phosphorylation of a non-paired helical filament pool in Alzheimer disease. J Biol Chem 268:24374-24384.

Kostara CE, Papathanasiou A, Cung MT, Elisaf MS, Goudevenos J, Bairaktari ET (2010) Evaluation of established coronary heart disease on the basis of HDL and non-HDL NMR lipid profiling. J Proteome Res 9:897-911.

Kreis R (2004) Issues of spectral quality in clinical 1H-magnetic resonance spectroscopy and a gallery of artifacts. NMR Biomed 17:361-381.

Kreis R, Ross BD (1992) Cerebral metabolic disturbances in patients with subacute and chronic diabetes mellitus: detection with proton MR spectroscopy. Radiology 184:123-130.

Kreis R, Ross BD, Farrow NA, Ackerman Z (1992) Metabolic disorders of the brain in chronic hepatic encephalopathy detected with H-1 MR spectroscopy. Radiology 182:19-27.

Kruse B, Hanefeld F, Christen HJ, Bruhn H, Michaelis T, Hanicke W, Frahm J (1993) Alterations of brain metabolites in metachromatic leukodystrophy as detected by localized proton magnetic resonance spectroscopy in vivo. J Neurol 241:68-74.

Kuo YM, Emmerling MR, Bisgaier CL, Essenburg AD, Lampert HC, Drumm D, Roher AE (1998) Elevated low-density lipoprotein in Alzheimer's disease correlates with brain abeta 1-42 levels. Biochem Biophys Res Commun 252:711-715.

Laird FM, Cai H, Savonenko AV, Farah MH, He K, Melnikova T, Wen H, Chiang HC, Xu G, Koliatsos VE, Borchelt DR, Price DL, Lee HK, Wong PC (2005) BACE1, a major determinant of selective vulnerability of the brain to amyloid-beta amyloidogenesis, is essential for cognitive, emotional, and synaptic functions. J Neurosci 25:11693-11709.

Lam FC, Liu R, Lu P, Shapiro AB, Renoir JM, Sharom FJ, Reiner PB (2001) beta-Amyloid efflux mediated by p-glycoprotein. J Neurochem 76:1121-1128.

Lammich S, Kojro E, Postina R, Gilbert S, Pfeiffer R, Jasionowski M, Haass C, Fahrenholz F (1999) Constitutive and regulated alpha-secretase cleavage of Alzheimer's amyloid precursor protein by a disintegrin metalloprotease. Proc Natl Acad Sci U S A 96:3922-3927.

Lazeyras F, Charles HC, Tupler LA, Erickson R, Boyko OB, Krishnan KR (1998) Metabolic brain mapping in Alzheimer's disease using proton magnetic resonance spectroscopy. Psychiatry Res 82:95-106.

Le Belle JE, Harris NG, Williams SR, Bhakoo KK (2002) A comparison of cell and tissue extraction techniques using high-resolution 1H-NMR spectroscopy. NMR Biomed 15:37-44.

Le Corre S, Klafki HW, Plesnila N, Hubinger G, Obermeier A, Sahagun H, Monse B, Seneci P, Lewis J, Eriksen J, Zehr C, Yue M, McGowan E, Dickson DW, Hutton M, Roder HM (2006) An inhibitor of tau hyperphosphorylation prevents severe motor impairments in tau transgenic mice. Proc Natl Acad Sci U S A 103:9673-9678.

Ledesma MD, Da Silva JS, Crassaerts K, Delacourte A, De Strooper B, Dotti CG (2000) Brain plasmin enhances APP alpha-cleavage and Abeta degradation and is reduced in Alzheimer's disease brains. EMBO Rep 1:530-535.

Leissring MA, Farris W, Chang AY, Walsh DM, Wu X, Sun X, Frosch MP, Selkoe DJ (2003) Enhanced proteolysis of beta-amyloid in APP transgenic mice prevents

plaque formation, secondary pathology, and premature death. Neuron 40:1087-1093.
Lemaire R, Desmons A, Tabet JC, Day R, Salzet M, Fournier I (2007) Direct analysis and MALDI imaging of formalin-fixed, paraffin-embedded tissue sections. J Proteome Res 6:1295-1305.
Liang WS, Reiman EM, Valla J, Dunckley T, Beach TG, Grover A, Niedzielko TL, Schneider LE, Mastroeni D, Caselli R, Kukull W, Morris JC, Hulette CM, Schmechel D, Rogers J, Stephan DA (2008) Alzheimer's disease is associated with reduced expression of energy metabolism genes in posterior cingulate neurons. Proc Natl Acad Sci U S A 105:4441-4446.
Lien YH, Shapiro JI, Chan L (1990) Effects of hypernatremia on organic brain osmoles. J Clin Invest 85:1427-1435.
Liu F, Shi J, Tanimukai H, Gu J, Gu J, Grundke-Iqbal I, Iqbal K, Gong CX (2009) Reduced O-GlcNAcylation links lower brain glucose metabolism and tau pathology in Alzheimer's disease. Brain 132:1820-1832.
Lovell MA, Ehmann WD, Butler SM, Markesbery WR (1995) Elevated thiobarbituric acid-reactive substances and antioxidant enzyme activity in the brain in Alzheimer's disease. Neurology 45:1594-1601.
Luo Y, Bolon B, Kahn S, Bennett BD, Babu-Khan S, Denis P, Fan W, Kha H, Zhang J, Gong Y, Martin L, Louis JC, Yan Q, Richards WG, Citron M, Vassar R (2001) Mice deficient in BACE1, the Alzheimer's beta-secretase, have normal phenotype and abolished beta-amyloid generation. Nat Neurosci 4:231-232.
Maheswaran S, Barjat H, Rueckert D, Bate ST, Howlett DR, Tilling L, Smart SC, Pohlmann A, Richardson JC, Hartkens T, Hill DL, Upton N, Hajnal JV, James MF (2009) Longitudinal regional brain volume changes quantified in normal aging and Alzheimer's APP x PS1 mice using MRI. Brain Res 1270:19-32.
Marjanska M, Curran GL, Wengenack TM, Henry PG, Bliss RL, Poduslo JF, Jack CR, Jr., Ugurbil K, Garwood M (2005) Monitoring disease progression in transgenic mouse models of Alzheimer's disease with proton magnetic resonance spectroscopy. Proc Natl Acad Sci U S A 102:11906-11910.
Martinez-Bisbal MC, Arana E, Marti-Bonmati L, Molla E, Celda B (2004) Cognitive impairment: classification by 1H magnetic resonance spectroscopy. Eur J Neurol 11:187-193.
Martins IJ, Berger T, Sharman MJ, Verdile G, Fuller SJ, Martins RN (2009) Cholesterol metabolism and transport in the pathogenesis of Alzheimer's disease. J Neurochem 111:1275-1308.
Michikawa M, Fan QW, Isobe I, Yanagisawa K (2000) Apolipoprotein E exhibits isoform-specific promotion of lipid efflux from astrocytes and neurons in culture. J Neurochem 74:1008-1016.
Miller BL (1991) A review of chemical issues in 1H NMR spectroscopy: N-acetyl-L-aspartate, creatine and choline. NMR Biomed 4:47-52.
Miller BL, Moats RA, Shonk T, Ernst T, Woolley S, Ross BD (1993) Alzheimer disease: depiction of increased cerebral myo-inositol with proton MR spectroscopy. Radiology 187:433-437.

Moats RA, Ernst T, Shonk TK, Ross BD (1994) Abnormal cerebral metabolite concentrations in patients with probable Alzheimer disease. Magn Reson Med 32:110-115.

Modrego PJ, Fayed N, Pina MA (2005) Conversion from mild cognitive impairment to probable Alzheimer's disease predicted by brain magnetic resonance spectroscopy. Am J Psychiatry 162:667-675.

Modrego PJ, Pina MA, Fayed N, Diaz M (2006) Changes in metabolite ratios after treatment with rivastigmine in Alzheimer's disease: A nonrandomised controlled trial with magnetic resonance spectroscopy. CNS Drugs 20:867-877.

Moechars D, Dewachter I, Lorent K, Reverse D, Baekelandt V, Naidu A, Tesseur I, Spittaels K, Haute CV, Checler F, Godaux E, Cordell B, Van Leuven F (1999) Early phenotypic changes in transgenic mice that overexpress different mutants of amyloid precursor protein in brain. J Biol Chem 274:6483-6492.

Moffett JR, Namboodiri MA, Cangro CB, Neale JH (1991) Immunohistochemical localization of N-acetylaspartate in rat brain. Neuroreport 2:131-134.

Moreira PI, Siedlak SL, Wang X, Santos MS, Oliveira CR, Tabaton M, Nunomura A, Szweda LI, Aliev G, Smith MA, Zhu X, Perry G (2007) Autophagocytosis of mitochondria is prominent in Alzheimer disease. J Neuropathol Exp Neurol 66:525-532.

Mosconi L, Tsui WH, Herholz K, Pupi A, Drzezga A, Lucignani G, Reiman EM, Holthoff V, Kalbe E, Sorbi S, Diehl-Schmid J, Perneczky R, Clerici F, Caselli R, Beuthien-Baumann B, Kurz A, Minoshima S, de Leon MJ (2008) Multicenter standardized 18F-FDG PET diagnosis of mild cognitive impairment, Alzheimer's disease, and other dementias. J Nucl Med 49:390-398.

Mrak RE, Sheng JG, Griffin WS (1996) Correlation of astrocytic S100 beta expression with dystrophic neurites in amyloid plaques of Alzheimer's disease. J Neuropathol Exp Neurol 55:273-279.

Murai S, Saito H, Shirato R, Kawaguchi T (2001) An improved method for assaying phosphocholine and glycerophosphocholine in mouse tissue. J Pharmacol Toxicol Methods 46:103-109.

Newman M, Musgrave FI, Lardelli M (2006) Alzheimer disease: Amyloidogenesis, the presenilins and animal models. Biochim Biophys Acta.

Nicoll JA, Wilkinson D, Holmes C, Steart P, Markham H, Weller RO (2003) Neuropathology of human Alzheimer disease after immunization with amyloid-beta peptide: a case report. Nat Med 9:448-452.

Noble W, Planel E, Zehr C, Olm V, Meyerson J, Suleman F, Gaynor K, Wang L, LaFrancois J, Feinstein B, Burns M, Krishnamurthy P, Wen Y, Bhat R, Lewis J, Dickson D, Duff K (2005) Inhibition of glycogen synthase kinase-3 by lithium correlates with reduced tauopathy and degeneration in vivo. Proc Natl Acad Sci U S A 102:6990-6995.

Notkola IL, Sulkava R, Pekkanen J, Erkinjuntti T, Ehnholm C, Kivinen P, Tuomilehto J, Nissinen A (1998) Serum total cholesterol, apolipoprotein E epsilon 4 allele, and Alzheimer's disease. Neuroepidemiology 17:14-20.

Nunomura A, Perry G, Aliev G, Hirai K, Takeda A, Balraj EK, Jones PK, Ghanbari H, Wataya T, Shimohama S, Chiba S, Atwood CS, Petersen RB, Smith MA (2001)

Oxidative damage is the earliest event in Alzheimer disease. J Neuropathol Exp Neurol 60:759-767.

Oberg J, Spenger C, Wang FH, Andersson A, Westman E, Skoglund P, Sunnemark D, Norinder U, Klason T, Wahlund LO, Lindberg M (2007) Age related changes in brain metabolites observed by (1)H MRS in APP/PS1 mice. Neurobiol Aging.

Oppenheimer SM, Bryan RN, Conturo TE, Soher BJ, Preziosi TJ, Barker PB (1995) Proton magnetic resonance spectroscopy and gadolinium-DTPA perfusion imaging of asymptomatic MRI white matter lesions. Magn Reson Med 33:61-68.

Orgogozo JM, Gilman S, Dartigues JF, Laurent B, Puel M, Kirby LC, Jouanny P, Dubois B, Eisner L, Flitman S, Michel BF, Boada M, Frank A, Hock C (2003) Subacute meningoencephalitis in a subset of patients with AD after Abeta42 immunization. Neurology 61:46-54.

Pacheco MA, Jope RS (1996) Phosphoinositide signaling in human brain. Prog Neurobiol 50:255-273.

Petersen RC (2004) Mild cognitive impairment as a diagnostic entity. J Intern Med 256:183-194.

Petrella JR, Coleman RE, Doraiswamy PM (2003) Neuroimaging and early diagnosis of Alzheimer disease: a look to the future. Radiology 226:315-336.

Pfrieger FW (2003) Cholesterol homeostasis and function in neurons of the central nervous system. Cell Mol Life Sci 60:1158-1171.

Postina R, Schroeder A, Dewachter I, Bohl J, Schmitt U, Kojro E, Prinzen C, Endres K, Hiemke C, Blessing M, Flamez P, Dequenne A, Godaux E, van Leuven F, Fahrenholz F (2004) A disintegrin-metalloproteinase prevents amyloid plaque formation and hippocampal defects in an Alzheimer disease mouse model. J Clin Invest 113:1456-1464.

Poullet JB, Sima DM, Van Huffel S (2008) MRS signal quantitation: a review of time- and frequency-domain methods. J Magn Reson 195:134-144.

Prohovnik I, Perl DP, Davis KL, Libow L, Lesser G, Haroutunian V (2006) Dissociation of neuropathology from severity of dementia in late-onset Alzheimer disease. Neurology 66:49-55.

Qiu C, De Ronchi D, Fratiglioni L (2007) The epidemiology of the dementias: an update. Curr Opin Psychiatry 20:380-385.

Rapp A, Gmeiner B, Huttinger M (2006) Implication of apoE isoforms in cholesterol metabolism by primary rat hippocampal neurons and astrocytes. Biochimie 88:473-483.

Ratiney H, Sdika M, Coenradie Y, Cavassila S, van Ormondt D, Graveron-Demilly D (2005) Time-domain semi-parametric estimation based on a metabolite basis set. NMR Biomed 18:1-13.

Richardson JC, Kendal CE, Anderson R, Priest F, Gower E, Soden P, Gray R, Topps S, Howlett DR, Lavender D, Clarke NJ, Barnes JC, Haworth R, Stewart MG, Rupniak HT (2003) Ultrastructural and behavioural changes precede amyloid deposition in a transgenic model of Alzheimer's disease. Neuroscience 122:213-228.

Ringman JM, Frautschy SA, Cole GM, Masterman DL, Cummings JL (2005) A potential role of the curry spice curcumin in Alzheimer's disease. Curr Alzheimer Res 2:131-136.

Ritchie K, Touchon J (2000) Mild cognitive impairment: conceptual basis and current nosological status. Lancet 355:225-228.

Roher AE, Kuo YM, Kokjohn KM, Emmerling MR, Gracon S (1999) Amyloid and lipids in the pathology of Alzheimer disease. Amyloid 6:136-145.

Rohner TC, Staab D, Stoeckli M (2005) MALDI mass spectrometric imaging of biological tissue sections. Mech Ageing Dev 126:177-185.

Ronci M, Bonanno E, Colantoni A, Pieroni L, Di Ilio C, Spagnoli LG, Federici G, Urbani A (2008) Protein unlocking procedures of formalin-fixed paraffin-embedded tissues: application to MALDI-TOF imaging MS investigations. Proteomics 8:3702-3714.

Rose SE, de Zubicaray GI, Wang D, Galloway GJ, Chalk JB, Eagle SC, Semple J, Doddrell DM (1999) A 1H MRS study of probable Alzheimer's disease and normal aging: implications for longitudinal monitoring of dementia progression. Magn Reson Imaging 17:291-299.

Ross BD (1991) Biochemical considerations in 1H spectroscopy. Glutamate and glutamine; myo-inositol and related metabolites. NMR Biomed 4:59-63.

Rottkamp CA, Raina AK, Zhu X, Gaier E, Bush AI, Atwood CS, Chevion M, Perry G, Smith MA (2001) Redox-active iron mediates amyloid-beta toxicity. Free Radic Biol Med 30:447-450.

Salek RM, Xia J, Innes A, Sweatman BC, Adalbert R, Randle S, McGowan E, Emson PC, Griffin JL (2010) A metabolomic study of the CRND8 transgenic mouse model of Alzheimer's disease. Neurochem Int 56:937-947.

Santacruz K, Lewis J, Spires T, Paulson J, Kotilinek L, Ingelsson M, Guimaraes A, DeTure M, Ramsden M, McGowan E, Forster C, Yue M, Orne J, Janus C, Mariash A, Kuskowski M, Hyman B, Hutton M, Ashe KH (2005) Tau suppression in a neurodegenerative mouse model improves memory function. Science 309:476-481.

Satlin A, Bodick N, Offen WW, Renshaw PF (1997) Brain proton magnetic resonance spectroscopy (1H-MRS) in Alzheimer's disease: changes after treatment with xanomeline, an M1 selective cholinergic agonist. Am J Psychiatry 154:1459-1461.

Sayre LM, Perry G, Harris PL, Liu Y, Schubert KA, Smith MA (2000) In situ oxidative catalysis by neurofibrillary tangles and senile plaques in Alzheimer's disease: a central role for bound transition metals. J Neurochem 74:270-279.

Schaefer EJ, Bongard V, Beiser AS, Lamon-Fava S, Robins SJ, Au R, Tucker KL, Kyle DJ, Wilson PW, Wolf PA (2006) Plasma phosphatidylcholine docosahexaenoic acid content and risk of dementia and Alzheimer disease: the Framingham Heart Study. Arch Neurol 63:1545-1550.

Schenk D, Barbour R, Dunn W, Gordon G, Grajeda H, Guido T, Hu K, Huang J, Johnson-Wood K, Khan K, Kholodenko D, Lee M, Liao Z, Lieberburg I, Motter R, Mutter L, Soriano F, Shopp G, Vasquez N, Vandevert C, Walker S, Wogulis M, Yednock T, Games D, Seubert P (1999) Immunization with amyloid-beta

attenuates Alzheimer-disease-like pathology in the PDAPP mouse. Nature 400:173-177.

Scheuner D, Eckman C, Jensen M, Song X, Citron M, Suzuki N, Bird TD, Hardy J, Hutton M, Kukull W, Larson E, Levy-Lahad E, Viitanen M, Peskind E, Poorkaj P, Schellenberg G, Tanzi R, Wasco W, Lannfelt L, Selkoe D, Younkin S (1996) Secreted amyloid beta-protein similar to that in the senile plaques of Alzheimer's disease is increased in vivo by the presenilin 1 and 2 and APP mutations linked to familial Alzheimer's disease. Nat Med 2:864-870.

Schuff N, Amend D, Ezekiel F, Steinman SK, Tanabe J, Norman D, Jagust W, Kramer JH, Mastrianni JA, Fein G, Weiner MW (1997) Changes of hippocampal N-acetyl aspartate and volume in Alzheimer's disease. A proton MR spectroscopic imaging and MRI study. Neurology 49:1513-1521.

Schuff N, Capizzano AA, Du AT, Amend DL, O'Neill J, Norman D, Kramer J, Jagust W, Miller B, Wolkowitz OM, Yaffe K, Weiner MW (2002) Selective reduction of N-acetylaspartate in medial temporal and parietal lobes in AD. Neurology 58:928-935.

Selkoe DJ (1994) Cell biology of the amyloid beta-protein precursor and the mechanism of Alzheimer's disease. Annu Rev Cell Biol 10:373-403.

Selkoe DJ (2001) Alzheimer's disease: genes, proteins, and therapy. Physiol Rev 81:741-766.

Shen J, Kelleher RJ, 3rd (2007) The presenilin hypothesis of Alzheimer's disease: evidence for a loss-of-function pathogenic mechanism. Proc Natl Acad Sci U S A 104:403-409.

Shibata M, Yamada S, Kumar SR, Calero M, Bading J, Frangione B, Holtzman DM, Miller CA, Strickland DK, Ghiso J, Zlokovic BV (2000) Clearance of Alzheimer's amyloid-ss(1-40) peptide from brain by LDL receptor-related protein-1 at the blood-brain barrier. J Clin Invest 106:1489-1499.

Shobab LA, Hsiung GY, Feldman HH (2005) Cholesterol in Alzheimer's disease. Lancet Neurol 4:841-852.

Shonk TK, Moats RA, Gifford P, Michaelis T, Mandigo JC, Izumi J, Ross BD (1995) Probable Alzheimer disease: diagnosis with proton MR spectroscopy. Radiology 195:65-72.

Siemers E, Skinner M, Dean RA, Gonzales C, Satterwhite J, Farlow M, Ness D, May PC (2005) Safety, tolerability, and changes in amyloid beta concentrations after administration of a gamma-secretase inhibitor in volunteers. Clin Neuropharmacol 28:126-132.

Smith GE, Pankratz VS, Negash S, Machulda MM, Petersen RC, Boeve BF, Knopman DS, Lucas JA, Ferman TJ, Graff-Radford N, Ivnik RJ (2007) A plateau in pre-Alzheimer memory decline: evidence for compensatory mechanisms? Neurology 69:133-139.

Smith MA, Harris PL, Sayre LM, Perry G (1997) Iron accumulation in Alzheimer disease is a source of redox-generated free radicals. Proc Natl Acad Sci U S A 94:9866-9868.

Sparks DL, Martin TA, Gross DR, Hunsaker JC, 3rd (2000) Link between heart disease, cholesterol, and Alzheimer's disease: a review. Microsc Res Tech 50:287-290.

Stampfer MJ, Kang JH, Chen J, Cherry R, Grodstein F (2005) Effects of moderate alcohol consumption on cognitive function in women. N Engl J Med 352:245-253.

Stauber J, Lemaire R, Franck J, Bonnel D, Croix D, Day R, Wisztorski M, Fournier I, Salzet M (2008) MALDI imaging of formalin-fixed paraffin-embedded tissues: application to model animals of Parkinson disease for biomarker hunting. J Proteome Res 7:969-978.

Stefan D, Di Cesare F, Andrasescu A, Popa E, Lazariev A, Vescovo E, Strbak O, Williams S, Starcuk Z, Cabanas M, van Ormondt D, Graveron-Demilly D (2009) Quantitation of magnetic resonance spectroscopy signals: the jMRUI software package Meas Sci Technol 20:104035.

Stefani M, Liguri G (2009) Cholesterol in Alzheimer's disease: unresolved questions. Curr Alzheimer Res 6:15-29.

Stoeckli M, Knochenmuss R, McCombie G, Mueller D, Rohner T, Staab D, Wiederhold KH (2006) MALDI MS imaging of amyloid. Methods Enzymol 412:94-106.

Stoppe G, Bruhn H, Pouwels PJ, Hanicke W, Frahm J (2000) Alzheimer disease: absolute quantification of cerebral metabolites in vivo using localized proton magnetic resonance spectroscopy. Alzheimer Dis Assoc Disord 14:112-119.

Strittmatter WJ, Saunders AM, Schmechel D, Pericak-Vance M, Enghild J, Salvesen GS, Roses AD (1993) Apolipoprotein E: high-avidity binding to beta-amyloid and increased frequency of type 4 allele in late-onset familial Alzheimer disease. Proc Natl Acad Sci U S A 90:1977-1981.

Strohmeyer R, Kovelowski CJ, Mastroeni D, Leonard B, Grover A, Rogers J (2005) Microglial responses to amyloid beta peptide opsonization and indomethacin treatment. J Neuroinflammation 2:18.

Terry AV, Jr., Buccafusco JJ (2003) The cholinergic hypothesis of age and Alzheimer's disease-related cognitive deficits: recent challenges and their implications for novel drug development. J Pharmacol Exp Ther 306:821-827.

Tkac I, Starcuk Z, Choi IY, Gruetter R (1999) In vivo 1H NMR spectroscopy of rat brain at 1 ms echo time. Magn Reson Med 41:649-656.

Truchot L, Costes SN, Zimmer L, Laurent B, Le Bars D, Thomas-Anterion C, Croisile B, Mercier B, Hermier M, Vighetto A, Krolak-Salmon P (2007) Up-regulation of hippocampal serotonin metabolism in mild cognitive impairment. Neurology 69:1012-1017.

Urenjak J, Williams SR, Gadian DG, Noble M (1992) Specific expression of N-acetylaspartate in neurons, oligodendrocyte-type-2 astrocyte progenitors, and immature oligodendrocytes in vitro. J Neurochem 59:55-61.

Urenjak J, Williams SR, Gadian DG, Noble M (1993) Proton nuclear magnetic resonance spectroscopy unambiguously identifies different neural cell types. J Neurosci 13:981-989.

Valenzuela MJ, Sachdev P (2001) Magnetic resonance spectroscopy in AD. Neurology 56:592-598.

Valla J, Berndt JD, Gonzalez-Lima F (2001) Energy hypometabolism in posterior cingulate cortex of Alzheimer's patients: superficial laminar cytochrome oxidase associated with disease duration. J Neurosci 21:4923-4930.

Van Broeck B, Vanhoutte G, Pirici D, Van Dam D, Wils H, Cuijt I, Vennekens K, Zabielski M, Michalik A, Theuns J, De Deyn PP, Van der Linden A, Van Broeckhoven C, Kumar-Singh S (2008) Intraneuronal amyloid beta and reduced brain volume in a novel APP T714I mouse model for Alzheimer's disease. Neurobiol Aging 29:241-252.

van Groen T, Puurunen K, Maki HM, Sivenius J, Jolkkonen J (2005) Transformation of diffuse beta-amyloid precursor protein and beta-amyloid deposits to plaques in the thalamus after transient occlusion of the middle cerebral artery in rats. Stroke 36:1551-1556.

Vanhamme L, van den Boogaart A, Van Huffel S (1997) Improved method for accurate and efficient quantification of MRS data with use of prior knowledge. J Magn Reson 129:35-43.

Vassar R, Bennett BD, Babu-Khan S, Kahn S, Mendiaz EA, Denis P, Teplow DB, Ross S, Amarante P, Loeloff R, Luo Y, Fisher S, Fuller J, Edenson S, Lile J, Jarosinski MA, Biere AL, Curran E, Burgess T, Louis JC, Collins F, Treanor J, Rogers G, Citron M (1999) Beta-secretase cleavage of Alzheimer's amyloid precursor protein by the transmembrane aspartic protease BACE. Science 286:735-741.

von Kienlin M, Kunnecke B, Metzger F, Steiner G, Richards JG, Ozmen L, Jacobsen H, Loetscher H (2005) Altered metabolic profile in the frontal cortex of PS2APP transgenic mice, monitored throughout their life span. Neurobiol Dis 18:32-39.

Wahlund LO (1996) Magnetic resonance imaging and computed tomography in Alzheimer's disease. Acta Neurol Scand Suppl 168:50-53.

Waldman AD, Rai GS (2003) The relationship between cognitive impairment and in vivo metabolite ratios in patients with clinical Alzheimer's disease and vascular dementia: a proton magnetic resonance spectroscopy study. Neuroradiology 45:507-512.

Walsh DM, Selkoe DJ (2004) Deciphering the molecular basis of memory failure in Alzheimer's disease. Neuron 44:181-193.

Wang YP, Biernat J, Pickhardt M, Mandelkow E, Mandelkow EM (2007) Stepwise proteolysis liberates tau fragments that nucleate the Alzheimer-like aggregation of full-length tau in a neuronal cell model. Proc Natl Acad Sci U S A 104:10252-10257.

Weeraratna AT, Kalehua A, Deleon I, Bertak D, Maher G, Wade MS, Lustig A, Becker KG, Wood W, 3rd, Walker DG, Beach TG, Taub DD (2007) Alterations in immunological and neurological gene expression patterns in Alzheimer's disease tissues. Exp Cell Res 313:450-461.

Weggen S, Eriksen JL, Das P, Sagi SA, Wang R, Pietrzik CU, Findlay KA, Smith TE, Murphy MP, Bulter T, Kang DE, Marquez-Sterling N, Golde TE, Koo EH (2001) A subset of NSAIDs lower amyloidogenic Abeta42 independently of cyclooxygenase activity. Nature 414:212-216.

Weiner HL, Frenkel D (2006) Immunology and immunotherapy of Alzheimer's disease. Nat Rev Immunol 6:404-416.

Wilcock GK (2003) Memantine for the treatment of dementia. Lancet Neurol 2:503-505.

Wolfe MS (2007) When loss is gain: reduced presenilin proteolytic function leads to increased Abeta42/Abeta40. Talking Point on the role of presenilin mutations in Alzheimer disease. EMBO Rep 8:136-140.

Wolozin B, Kellman W, Ruosseau P, Celesia GG, Siegel G (2000) Decreased prevalence of Alzheimer disease associated with 3-hydroxy-3-methyglutaryl coenzyme A reductase inhibitors. Arch Neurol 57:1439-1443.

Woo DC, Lee SH, Lee DW, Kim SY, Kim GY, Rhim HS, Choi CB, Kim HY, Lee CU, Choe BY (2010) Regional metabolic alteration of Alzheimer's disease in mouse brain expressing mutant human APP-PS1 by 1H HR-MAS. Behav Brain Res 211:125-131.

Xanthakos S, Krishnan KR, Kim DM, Charles HC (1996) Magnetic resonance imaging of Alzheimer's disease. Prog Neuropsychopharmacol Biol Psychiatry 20:597-626.

Yamagata K, Urakami K, Ikeda K, Ji Y, Adachi Y, Arai H, Sasaki H, Sato K, Nakashima K (2001) High expression of apolipoprotein E mRNA in the brains with sporadic Alzheimer's disease. Dement Geriatr Cogn Disord 12:57-62.

Yan R, Bienkowski MJ, Shuck ME, Miao H, Tory MC, Pauley AM, Brashier JR, Stratman NC, Mathews WR, Buhl AE, Carter DB, Tomasselli AG, Parodi LA, Heinrikson RL, Gurney ME (1999) Membrane-anchored aspartyl protease with Alzheimer's disease beta-secretase activity. Nature 402:533-537.

Yan SD, Yan SF, Chen X, Fu J, Chen M, Kuppusamy P, Smith MA, Perry G, Godman GC, Nawroth P, et al. (1995) Non-enzymatically glycated tau in Alzheimer's disease induces neuronal oxidant stress resulting in cytokine gene expression and release of amyloid beta-peptide. Nat Med 1:693-699.

Yang F, Lim GP, Begum AN, Ubeda OJ, Simmons MR, Ambegaokar SS, Chen PP, Kayed R, Glabe CG, Frautschy SA, Cole GM (2005) Curcumin inhibits formation of amyloid beta oligomers and fibrils, binds plaques, and reduces amyloid in vivo. J Biol Chem 280:5892-5901.

Zhang B, Maiti A, Shively S, Lakhani F, McDonald-Jones G, Bruce J, Lee EB, Xie SX, Joyce S, Li C, Toleikis PM, Lee VM, Trojanowski JQ (2005) Microtubule-binding drugs offset tau sequestration by stabilizing microtubules and reversing fast axonal transport deficits in a tauopathy model. Proc Natl Acad Sci U S A 102:227-231.

Zhao Z, Xiang Z, Haroutunian V, Buxbaum JD, Stetka B, Pasinetti GM (2007) Insulin degrading enzyme activity selectively decreases in the hippocampal formation of cases at high risk to develop Alzheimer's disease. Neurobiol Aging 28:824-830.

Zhu X, Smith MA, Perry G, Aliev G (2004) Mitochondrial failures in Alzheimer's disease. Am J Alzheimers Dis Other Demen 19:345-352.

Zhu X, Su B, Wang X, Smith MA, Perry G (2007) Causes of oxidative stress in Alzheimer disease. Cell Mol Life Sci 64:2202-2210.

Zhu X, Schuff N, Kornak J, Soher B, Yaffe K, Kramer JH, Ezekiel F, Miller BL, Jagust WJ, Weiner MW (2006) Effects of Alzheimer disease on fronto-parietal brain N-acetyl aspartate and myo-inositol using magnetic resonance spectroscopic imaging. Alzheimer Dis Assoc Disord 20:77-85.